Manipulating T lymphocyte homing and activation for cancer immunotherapy

A thesis submitted to Cardiff University in candidature for the degree of Doctor of Philosophy.

Sophie Catherine Wehenkel

Institute of Infection and Immunity, School of Medicine

Cardiff University

April 2015

DECLARATION

This work has not been submitted in substance for any other degree or award at this or any other university or place of learning, nor is being submitted concurrently in candidature for any degree or other award.

Signed …… (candidate) Date ……

STATEMENT 1

This thesis is being submitted in partial fulfillment of the requirements for the degree of PhD

Signed …… (candidate) Date ……

STATEMENT 2

This thesis is the result of my own independent work/investigation, except where otherwise stated.

Other sources are acknowledged by explicit references. The views expressed are my own.

Signed …… (candidate) Date ……

STATEMENT 3

I hereby give consent for my thesis, if accepted, to be available online in the University's Open Access repository and for inter-library loan, and for the title and summary to be made available to outside organisations.

Signed …… (candidate) Date ……

STATEMENT 4: PREVIOUSLY APPROVED BAR ON ACCESS

I hereby give consent for my thesis, if accepted, to be available online in the University's Open Access repository and for inter-library loans **after expiry of a bar on access previously approved by the Academic Standards & Quality Committee.**

Signed …… (candidate) Date ……

Acknowledgments

This thesis is dedicated to my late auntie ‘Tatgen’ Wehenkel.

I would like to thank both my supervisors, Dr Ann Ager and Dr James Matthews for their endless support during my PhD, both inside and outside of the lab, and for all the delicious food and early morning champagne. Thanks the whole research group for their help, especially with mouse experiments and everybody else who helped me with epxeriments along the way. Thank you, Moe Muhith and Adam Clark, two medic students that helped me with this project. Special thanks go to Dr John Bridgeman, who was my go-to person for all molecular and lentiviral problems. I am grateful to our collaborator Dr Aleksander Ivetic at King’s College London.

Thanks to all Henry Wellcome PhD students (Gabrielle, Diana, Andrea, Johanne, Matthieu, Chris, Flo and co.) and Postdocs for having lunches away from the computer! Thanks to my flatmate Magda for the last 3 years. A Merci to les filles les P. B. du LCE for keeping me updated on life outside of the PhD bubble and thanks to Dragos for keeping up with me during my writing up time.

A villmols Merci go to the most important people, my Mum, Dad, Ani and Nic for always supporting me and keeping me happy!

Summary

The immune system, and in particular $CD8^+$ T cells, have the potential to eliminate tumours and novel immunotherapies are giving encouraging results for cancer patients. This thesis focuses on the improvement of one such therapy, adoptive T cell therapy. The aim of this thesis was to genetically modify human $CD8^+$ T cells to enhance their anti-tumour potential for adoptive T cell therapy. One approach was to mutate the SH2 domain containing protein tyrosine phosphatase (SHP-1) gene to reduce T cell checkpoint inhibition. A second approach was to express a shedding-resistant form of L-selectin in T cells to promote T cell homing.

In this thesis, the rapid shedding of L-selectin within minutes after TCR stimulation was shown to be ADAM17 dependent. Furthermore, new data indicated a second proteolytic cleavage which is γ-secretase dependent. The shedding-resistant L-selectin (ΔM-N) was shown to resist proteolysis by both ADAM17 and γ-secretase.

Previous work by our group and others has shown that the loss of SHP-1 leads to the enhanced entrance of T cells into proliferation and gives better protection against tumour growth in mice. To study the effect of SHP-1 loss in human $CD8^+$ T cells, SHP-1 deficient tumour-specific T cells were generated by lentiviral delivery of a pair of SHP-1 specific zinc finger nucleases in conjunction with the Mel TCR. Populations of melanoma-specific $CD8^+$ T cells containing a small fraction (< 8 %) of SHP-1 mutant cells showed no enhanced Mel526 target cell killing *in vitro* or *in vivo* in Mel526 xenograft bearing NSG mice. However, there was some suggestion of enhanced survival and/or proliferation *in vitro* of melanoma-specific $CD8^+$ T cells containing a population of SHP-1 $CD8^+$ mutant cells. Overall the proof of principle of gene-editing SHP-1 in T cell lines and primary $CD8^+$ T cells was demonstrated which supports further exploitation of this approach for testing in adoptive T cell therapy strategies.

Abbreviations

aa	Amino acid
AAV	Adeno-associated viruses
Ab	Antibody
ACT	Adoptive T cell therapy
ADAM	A disintegrin and metalloproteinase
Ag	Antigen
AICD	Activation induced cell death
AmCyan	*Anemonia Majano* cyan fluorescent protein
APC	Allophycocyanin
Bp	Base pairs
CAR	Chimeric Antigen receptor
CCR7	Chemokine receptor 7
CD	Cluster of differentiation
cDNA	Complementary deoxyribonucleic acid
CEACAM1	Carcinoembryonic antigen related cell adhesion molecule 1
CFSE	Carboxyfluorescein Succinimidyl Ester
cPPT	Central polypurine tract
C-SH2	C-terminal SH2 domain
CTL	Cytotoxic lymphocyte
CTLA-4	Cytotoxic T-lymphocyte-associated protein 4
Ctrl	Control
DC	Dendritic cells
dnLN	Draining lymph node
DSB	Double stranded break
dsDNA	Double stranded deoxyribonucleic acid

DsRed	*Discosoma* species red fluorescent protein
E	Effector
EGF	Epidermal growth factor
ELISA	Enzyme-linked immunosorbent assay
ERM	Ezrin-radixin-moesin
FACS	Fluorescence-activated cell sorting
FASL	FAS ligand
FCS	Foetal calf serum
FMO	Fluorescence minus one
FokI	*Flavobacterium okeanokoites* restriction endonuclease I
FOXO-1	Forkhead box protein O1
FSC	Forward scatter
gDNA	Genomic DNA
GFP	Green fluorescent protein
GLuciferase	Gaussia Luciferase
GRB2	Growth factor receptor-bound protein 2
h	Hour
HEK	Human Embryonic Kidney
HEV	High endothelial venules
HLA	Human leucocyte antigen
HUVEC	Human umbilical vein endothelial cells
IFN	Interferon
IL-2 / IL-15	Interleukin-2 / interleukin-15
IDLV	Integrase-deficient lentiviral vector
indels	Insertions and deletions
ITIM	Immunoreceptor tyrosine-based inhibitory motif
Jak	Janus kinase

KLF-2	Krueppel-like factor 2
LAIR-1	Leukocyte-associated immunoglobulin receptor-1
LAT	Linker for activation of T cells
Lck	Lymphocyte-specific protein tyrosine *kinase*
LFA-1	Lymphocyte function-associated antigen 1
LN	Lymph node
L-selectin	Leukocyte-selectin
LV	Lentiviral vector
MACS	Magnetic-activated cell sorting
me	Motheaten
mev	Motheaten viable
MFI	Geometric mean fluorescent intensity
MHC-I	Major histocompatibility complex I
min	Minute
MMP	Matrix metalloproteinase
MPR	Membrane proximal region
MRF	Membrane-retained fragment
mRNA	Messenger ribonucleic acid
MS	Multiple sclerosis
NHEJ	Non-homologous end joining
NK	Natural killer
N-SH2	N-terminal SH2 domain
p	Probability coefficient
P2A	Porcine teschovirus-1 2A
PBMC	Peripheral blood mononuclear cells
PBS	Phosphate buffered saline
PD-1	Programmed death-1

PE	Phycoerythrin
PCR	Polymerase chain reaction
PHA	Phytohaemagglutinin
PMA	Phorbol-12-mystrate-13-acetate
PNAd	Peripheral node addressin
PSGL-1	P-selectin glycoprotein ligand-1
PTK	Protein tyrosine kinase
PTP	Protein tyrosine phosphatase
PTPN-6	Protein tyrosine phosphatase non-receptor type 6
rCD2	Rat cluster of differentiation 2
RFP	Red fluorescent protein
RIPing	Regulated intramembrane proteolysis
RRE	Rev response element
RT	Room temperature
RFP	Red fluorescent protein
SCID	Severe immunodeficiency
SCR	Short consensus repeat
SDF-1	Stromal derived factor-1
SEM	Standard error of mean
SFK	SRC family kinase
SH-2	Src homology 2
SHP-1	SH-2 domain containing protein tyrosine phosphatase
sLe^x	Sialyl Lewis X
SLO	Secondary lymphoid organs
SLP76	SH2 domain-containing leucocyte protein of 76 kDa
sL-selectin	Soluble L-selectin
SSG	Sodium stibogluconate

ssRNA	Single stranded ribonucleic acid
SSV	Spleen focus-forming virus
STAT	Signal transducer and activator of transcription
T	T cell
T2A	*Thosea asigna* virus 2A
TAA	Tumour associated antigen
TACE	TNF-α converting enzyme
TALEN	transcription activator like nucleases
TCR	T cell receptor
T_{CM}	Central memory T cell
TEM	Transendothelial migration
T_{EM}	Effector memory T cell
TF	Transcription factor
TIL	Tumour infiltrating lymphocyte
T_{reg}	Regulatory T cell
TM	Transmembrane
TNF	Tumour-necrosis factor
TRAIL	TNF-related apoptosis inducing ligand receptors
VSV-G	Vesicular stomatitis virus G glycoprotein
wt	Wild-type
WRPE	Woodchuck post-transcriptional regulatory element
ZAP70	Zeta-associated-70
ZFN	Zinc finger nucleases
ZFP	Zinc finger protein

Table of contents

Table of figures

Chapter 1: Introduction

1.1 The immune system and cancer

1.1.1 The immune system and cancer development

Cancer development is a complicated multifactorial process but put simply, cancer arises due to the accumulation of mutations by cells leading to the dysregulation of the cell cycle and enhanced cell proliferation. Such mutations can lead to the cells becoming resistant to both growth inhibiting and death inducing signals as well as the cancer cells developing a capacity to shape their environment by inducing angiogenesis and by invading new tissues (Hanahan and Weinberg 2011).

Although long ignored by many oncologists and cancer researchers, many studies have now implicated the immune system in the control of tumour establishment and development. There is a striking increase in virally induced malignancies, such as Kaposi's sarcoma and non-Hodgkin's lymphoma, in immunodeficient patients (Boshoff and Weiss 2002). However, one can argue that the immune system would be involved in controlling these cancers as they express foreign antigens (Ags), a key trigger to a robust immune response. An example that shows that the control of tumour growth by the immune system extends to a broader range of cancers is that immunosuppressed transplant recipients have been shown to develop malignancies such as melanoma when organs from seemingly healthy immunocompetent donors are transplanted (Strauss and Thomas 2010). This indicates that the immune system is keeping tumour cells under stringent pressure and thereby maintaining tumours in a dormant state. Additionally, correlations exist between the number of tumour infiltrating cytotoxic immune cells and a favourable prognosis in patients with colon (Galon et al. 2006), ovarian (Sato et al. 2005), melanoma (Clemente et al. 1996) and breast tumours (Loi et al. 2013). Not only is the number of tumour infiltrating lymphocytes (TILs) important but also the type of

immune cell. A high ratio of effector to regulatory T cells (T_{regs}) has been shown to be beneficial, as the latter cell type suppresses the anti-tumour immune response (Curiel et al. 2004; Sato et al. 2005). Furthermore, patients with a mutation in a gene encoding for a protein involved in T cell mediated killing (perforin) have shown an increased frequency of lymphomas (Chia et al. 2009). In addition to correlations between naturally mounted immune responses and cancer control, therapies aimed at enhancing an anti-tumour immune response have shown considerable benefits. Examples of immunotherapies will be given below with special emphasis on adoptive T cell therapy (ACT).

As mentioned above, effector T cells, and more specifically killer $CD8^+$ T cells play a crucial role in killing tumour cells via a range of mechanisms described in section 1.2.2. To stimulate an efficient T cell response, a number of steps need to be followed as shown in figure 1.1. Firstly, antigen presenting cells (APCs) need to take up neo-Ag or tumour-associated Ag (TAA) from tumour cells before Ag-loaded APCs migrate to lymph nodes (LNs). Here T cells survey the environment for cognate Ag presented by APCs and once T cells find the latter, T cells are activated as described in section 1.2.1. Once activated, T cells exit the LNs via the lymphatics, re-enter the blood stream and migrate towards the tumour, where T cells extravasate and enter the tumour mass, if the endothelial cells express the appropriate adhesion molecules. Here T cells will get activated by cognate Ag presented by tumour cells and target cells will be killed (Chen and Mellman 2013).

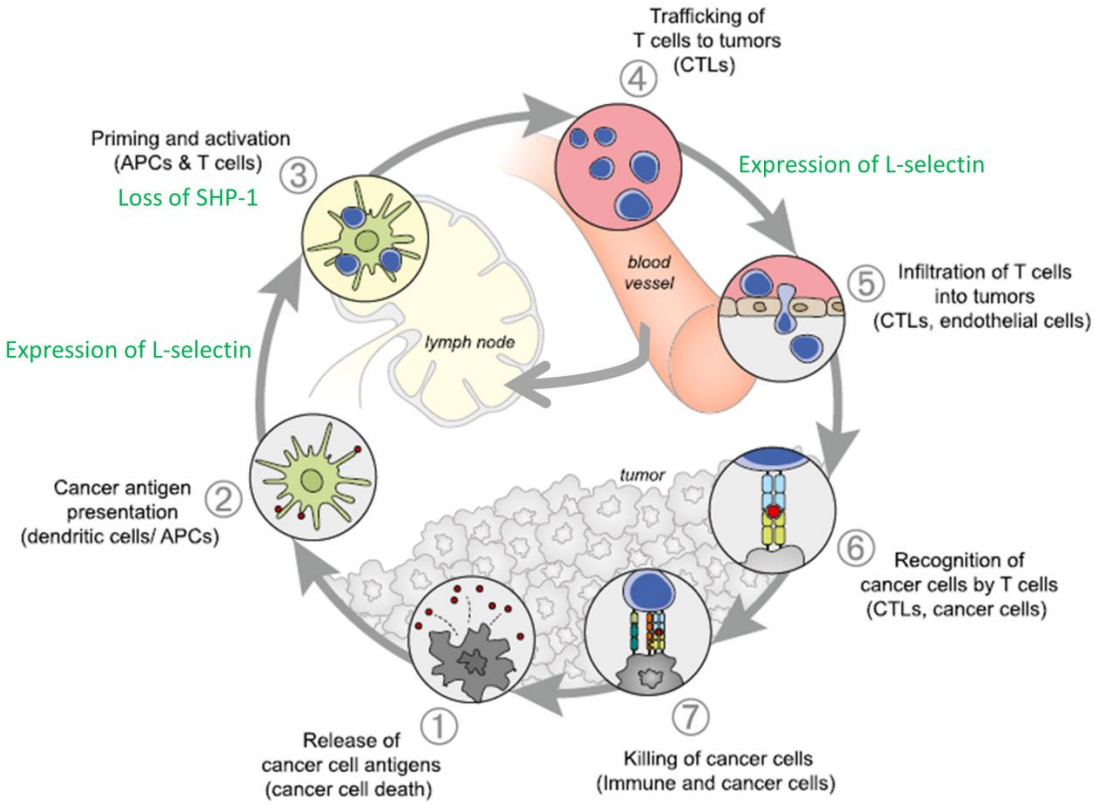

Figure 1.1: The cancer-immunity cycle and approach taken in this thesis to improve the immune response to cancer. The ideal immune response to cancer starts with the release of TAAs from tumour cells which can then be presented by APCs on MHC-I or MHC-II. The third step is the priming of naïve T cells by Ag loaded APCs in LNs. Activated T cells, such as cytotoxic T cells (CTLs), leave the LNs via the blood stream and are recruited to the tumour site if the vasculature provides the right ligands. Finally, T cells will recognise target tumour cells, be activated and kill cancer cells by several cytotoxic mechanisms. Lysis of tumour cells will release more TAA and the cycle will start all over again. However, in patients manifesting with tumours, one or several steps of this cycle are deficient or absent. Therefore the aim of all immunotherapies is it to enhance one or several aspects of this cycle. The two main targets in this thesis are a negative regulator of T cell activation, SHP-1, and the homing molecule, L-selectin. Abrogation of the former and prolonged expression of the latter is hypothesised to enhance the priming of T cells (step 3) and the homing step to LNs and tumours (step 3 and 5), respectively. Figure modified from (Chen and Mellman 2013).

In patients manifesting with tumours, one or multiple of these steps are either faulty, absent or inhibited by tumour derived mechanisms. There are multiple mechanisms of tumour escape from the immune system and only a few will be briefly described here (Zitvogel et al. 2006). Immunoselection of tumour cells expressing low levels of the major histocompatibility complex class–I (MHC-I) and Ag processing molecules as well as selection of cells expressing

weakly immunogenic Ag can occur. Some tumours have also been found to express PI9, a protease inhibitor that can protect against a cytotoxic enzyme called granzyme B (Medema et al. 2001). A more active way of escaping deletion by the immune system is by recruiting T_{regs} or myeloid derived suppressor cells to the tumour via the secretion of cytokines and growth factors. The latter also influence the maturation of dendritic cells (DCs), keeping them in an immature state and thus unable to fully activate $CD4^+$ and $CD8^+$ T cells. Additionally tumour cells can express high levels of programmed death ligand-1 (PD-L1) able to interact with an inhibitory receptor, PD-1, on activated T cells and induce exhaustion of the T cells (Victor et al. 2015).

1.1.2 Cancer immunotherapy

The immune system is an attractive weapon against cancer as it has the ability to form memory cells that can patrol the body for reoccurring tumour cells. Cancer immunotherapy is also often stated as being potentially less toxic than existing chemotherapies and radiotherapies, however this is debatable as some of the most successful therapies, mentioned below, are associated with very severe side effects which are often an early indication of the success of the treatment. One of the first examples of immunotherapy was the injection of bacterial extracts into patients with tumours in 1891 by William B. Coley, the 'father of immunotherapy' (McCarthy 2006). The rationale behind this partially successful therapy, called Coley's toxin, was that the infection caused by this immunogenic mix would lead to the shrinkage of solid tumours.

Currently, a whole range of immunotherapies are being trialled and some have gained USA Food and Drug Administration (FDA) approval. Similarly to Coley's toxin, the aim of the newer therapies is to stimulate the immune response and direct it towards tumour cell killing by

altering one or several steps of the cancer-immune cycle (figure 1.1). Based on successes of vaccinations in protecting against pathogens, cancer vaccines have been studied extensively with limited success (Klebanoff et al. 2011a). Cancer vaccinations aim to stimulate Ag presentation by APCs and thus T cell activation (step 2 and 3) by either directly injecting TAA and adjuvant or using *ex vivo* modified DCs (Palucka and Banchereau 2012). A recent publication showed that identifying tumour-specific mutations and including them into a personalised autologous DC vaccine can induce a robust neo-Ag T cell response in patients (Carreno et al. 2015). However, some key questions remain unanswered such as what the nature of the Ag and adjuvant should be in order to trigger an efficient non-tolerogenic, cytotoxic response.

Even if the initial priming of T cells is enhanced by cancer vaccines, T cells will face a vast array of inhibitory signals within the tumour microenvironment. To overcome this inhibition, vaccinations could be combined with antibody (Ab) therapies that prevent these checkpoint inhibitors (step 7). Two such molecules are cytotoxic T-lymphocyte-associated protein 4 (CTLA-4) and PD-1. Blocking Abs against both molecules (ipilimumab and pembrolizumab, respectively) have been FDA-approved for the treatment of advanced melanoma based on very promising clinical trials (Chen and Mellman 2013; Callahan et al. 2014). The immune system is also crucial in the elimination of cancer cells when Abs targeting molecules expressed on the tumour cells such as CD20 (rituximab) or Her2/*neu* (Trastuzumab) are given therapeutically (Adler and Dimitrov 2012). Additionally, cytokines stimulating an anti-cancer immune response such as IL-2 have been used in patients for 20 years but only yielding modest clinical benefits (Votavova et al. 2014).

It is clear that the most successful therapies will be combinations of two or more approaches, targeting multiple steps of the cancer-immune cycle, together with biomarker analysis. One study showed a dramatic increase in overall response rate from 17% for radiation and anti-

CTLA-4 Ab only to 80% for the combination of radiotherapy, anti-CTLA-4 and anti-PDL-1 Abs (Victor et al. 2015). The three treatments were shown to be non-redundant and complementary with radiation increasing the repertoire of tumour reactive T cells, anti-PD-L1 Ab increasing $CD8^+$ TIL numbers and anti-CTLA-4 Ab reducing T_{reg} numbers.

1.1.3 Adoptive T cell therapy

An immunotherapy aiming to circumvent low frequencies of endogenous tumour-specific T cells and poor *in vivo* priming of T cells is adoptive T cell therapy (ACT). Originally, ACT was done by isolating TILs from excised tumours and expanding them *in vitro* before reinfusing them to patients (figure 1.2). For a second type of ACT, T cells can be isolated from peripheral blood mononuclear cells (PBMCs) from patients' blood, T cells genetically modified to confer tumour specificity and expanded *in vitro* before being reinfused to the patients (figure 1.2). Both types of ACT can generate large numbers of tumour-reactive T cells (up to 10^{11}).

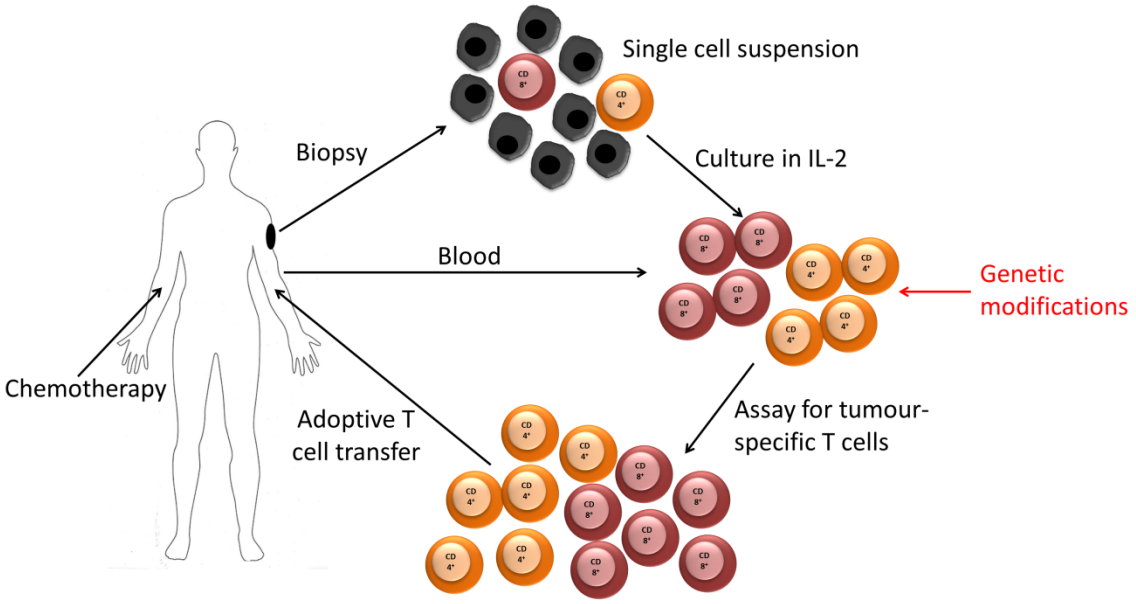

Figure 1.2: Adoptive T cell therapy using TILs or genetically modified PBMCs. Initially ACT trials were based on the excision of patients' tumours and the generation of single cell suspensions from the biopsies. Cells were cultured *in vitro* in conditions favouring T cell growth (i.e.: IL-2) and TILs (red and orange) were assayed for tumour reactivity before being further expanded and reinfused into patients having undergone preconditioning chemotherapy. More recently, PBMCs from patient's blood were isolated and T cells genetically modified *in vitro*, be it to express tumour-specific T cell receptors (TCRs) or chimeric Ag receptors (CARs). As for the TIL therapy, T cells were expanded and reinfused into patients.

One of the earliest ACTs using TIL was done by Rosenberg *et al.*, where 11/20 patients with metastatic melanoma showed objective regression when treated with endogenous TILs and high doses of IL-2 (Rosenberg et al. 1988). However, a problem with ACT was that the transferred T cells engrafted poorly and did not persist in patients and thus the overall clinical outcome was not as good as expected (Rosenberg et al. 1990). It is now believed that lymphodepletion with chemotherapy, prior to the transfer of T cells, enhances T cell engraftment and persistence (Dudley et al. 2002). Lymphodepletion is thought to eliminate local inhibitory cells such as myeloid-derived suppressor cells and T_{regs} and to create 'space' by reducing cellular competition for engrafting T cells. Additionally in a lymphodepleted host, homeostatic cytokine levels are elevated and cytokines such as IL-15 are readily available to transferred T cells (Dudley et al. 2008). ACT has also given encouraging results in clinical trials

such as a phase 2 trial where Epstein-Barr virus (EBV) specific donor cytotoxic T cells (CTLs) were given to patients with EBV-positive post-transplantation lymphoproliferative disease and a response rate of 52% was observed (Haque et al. 2007). However in this trial, the Ag targeted by T cells is of viral origin as opposed to most tumour Ags that arise from normal or mutated self-protein. Overall, TIL therapy has also shown promising results in patients with metastatic melanoma with 38% (Pilon-Thomas et al. 2012) to 55% (Rosenberg and Restifo 2015) objective response rates. Although other tumours also enable the growth of TILs *in vitro*, only melanoma specific TILs have been shown to consistently give beneficial clinical responses (Rosenberg and Restifo 2015).

To overcome the absence of pre-existing tumour-reactive T cells, the lack of accessible tumour and the low success rate of TIL therapy in non-melanoma patients, researchers have been genetically engineering patient T cells to redirect their specificity to TAAs. The first study doing this was done in 2006, where autologous lymphocytes from melanoma patient peripheral blood were isolated and transduced with a retrovirus expressing both the T cell receptor (TCR) α and β chains of a melanoma-specific (MART-1) TCR previously isolated from a patient undergoing TIL ACT (Morgan et al. 2006). This study showed that T cells persisted for at least 2 months *in vivo*, however only 2/15 patients showed a partial response. One of the first trials targeting not only metastatic melanoma but also synovial cell sarcoma utilised a NY-ESO-1 cancer-testis Ag specific TCR and showed response rates of 45% and 67%, respectively (Robbins et al. 2011).

As well as TCRs, chimeric Ag receptors (CARs) have been utilised to confer tumour-specificity to T cells. CARs have the advantage that their extracellular Ab fragment recognises Ag in a human leucocyte Ag (HLA) independent manner while retaining the intracellular signalling of a TCR via the CD3 ζ chain. This HLA-independence circumvents the need to develop HLA-specific receptors for patients with different HLA haplotypes. Furthermore, many tumours have been

shown to have very low to absent HLA expression, in which case TCR expressing T cells will not recognise the tumour cells (Algarra et al. 2004). Additionally, transduced TCR α and β chains can mispair with endogenous TCR, potentially giving rise to new pathogenic auto-reactive T cell specificities (Bendle et al. 2010). On the other hand, TCRs are able to recognise intracellular proteins presented on MHC-I to which CARs will be ignorant. The first generation CARs expressed only the CD3ζ chain, whereas the second generation CARs currently used in clinical trials also express intracellular signalling domains from costimulatory molecules such as CD28. CARs have been developed to recognise the B cell surface Ag CD19, amongst other surface Ags, and clinical trials have shown significant regression of patient B cell lymphomas but CAR expressing T cells have not yet shown clinical responses in solid tumours (Cheadle et al. 2014).

An issue with genetically modifying T cells with TCRs or CARs is the selection of the specificity of the receptor which ideally should recognise only tumour cells and not cells in healthy tissue. Non-mutated self-epitopes, overexpressed in tumour cells, have also been the focus of many studies. The main problem with this is the generation of on-target but off-tumour T cells that kill healthy tissue expressing the Ag to a low degree. Destruction of healthy tissue is acceptable for non-vital tissues, however some studies have shown life-threatening side effects when organs such as the liver (Lamers et al. 2013) or the gut (Parkhurst et al. 2011) are attacked by T cells. Additionally, altering the sequence of TCRs to enhance their intrinsic affinity has been found to have fatal consequences. In a study where an affinity enhanced cancer-testes Ag (MAGE-3) specific TCR was transduced into T cells and these were given to patients, the T cells attacked cardiac muscle cells expressing a cross-reactive epitope from titin, leading to the death of two patients (Linette et al. 2013).

One of the reasons why TIL therapy works best in melanoma could be the high frequency of mutations which is up to 1000 fold more than in other tumours (Lawrence et al. 2013). As self-reactive T cells are eliminated during thymic selection, T cells recognising self-peptide, such as

those proteins upregulated in tumour cells, might simply not exist in the periphery. This might explain the low success rate of non-mutated self-peptide Ag vaccines (Klebanoff et al. 2011a). It was shown that the number of mutational epitopes in tumours correlated with high CTL numbers in the tumour and enhanced survival (Brown et al. 2014). Thus ideally, TCRs specific to each patient's own mutations would be isolated and genetically transferred to T cells for ACT.

Most TCR and CAR gene delivery has been done using retroviral vectors, however lentiviral (LV) delivery has been used successfully to deliver a CD19-specific CAR to T cells and 2/3 patients showed complete remission (Kalos et al. 2011). The use of transposon systems, such as the 'Sleeping Beauty', might be beneficial for the delivery of TCR or CARs as T cells do not need to be activated prior to gene transfer (Huang et al. 2008). This system has now been used to deliver a CD19-specific CAR to T cells in a clinical trial (Kebriaei et al. 2012).

1.1.4 Optimisation of ACT protocols

Ideally, ACT will lead to a large population of effector T cells as well as a considerable number of memory T cells. The latter will provide long-term protection due to the capacity of memory T cells to proliferate and generate additional differentiated effector T cells. It is crucial to optimise the *in vitro* culture of TILs or genetically modified T cells so as to promote T cell differentiation into a memory phenotype and prevent immediate effector phenotypes and T cell exhaustion. Reducing the *in vitro* culture period to produce younger TILs has been trialled in patients and has shown promising results (Besser et al. 2010). As an alternative to reducing the *in vitro* culture times, 'fitter' T cells can potentially be obtained by varying the Abs and cytokines used when activating T cells. One such change, proposed by Gattinoni *et al.*, was to culture T cells in IL-15 rather than IL-2 as they demonstrated that T cells grown in the former

provided better protection against tumour growth in mice (Gattinoni et al. 2005). This finding was supported by a study where genetically modified human T cells showed improved engraftment in immunodeficient mice when grown in the presence of IL-15 and/or IL-7 rather than IL-2 (Alcantar-Orozco et al. 2013).

Contrary to previous thinking, it was found that differentiated effector T cells that showed highly cytotoxic phenotypes *in vitro* were actually poorer at *in vivo* protection when compared to less extensively stimulated T cells (Gattinoni et al. 2005). In a recent study it was also shown that signalling pathways, such as the Akt pathway, associated with the differentiation of T cells into an effector phenotype, can be inhibited during the *in vitro* T cell expansion, leading to an increase in the memory transcription profile in T cells and enhanced tumour protection by these cells in mice (Crompton et al. 2015). This fitted with another study performed in mice where T cells with a more memory-like phenotype were better at protecting than their effector T cell counterparts (Klebanoff et al. 2011b). As well as the differentiation status, it has was shown in mice that the number of transferred T cells is crucial for the success of the treatment, with higher T cell numbers giving better outcomes (Klebanoff et al. 2011b; Alcantar-Orozco et al. 2013). Additionally, *in vivo* Ag restimulation with a vaccine was shown to enhance the anti-tumour effect both in mice (Klebanoff et al. 2011b) and in humans (Smith et al. 2009).

Overall, it is clear that there are many aspects of ACT that may be optimised to generate a maximal clinical impact. As well as conferring Ag specificity, genetic manipulation of T cells *in vitro* can be used to deliver other molecules to enhance their *in vivo* anti-tumour effect. In this thesis, two aspects of T cell biology were addressed by genetic modifications; T cell activation and T cell homing. By genetically deleting a negative regulator of T cell activation, SHP-1, and prolonging expression of a lymphocyte homing molecule, L-selectin, we aimed at enhancing

both the activation of T cells (step 3 in figure 1.1) and the homing of the T cells to LNs and possibly tumour (step 3 and 5 in figure 1.1).

1.2 $CD8^+$ T cells

1.2.1 $CD8^+$ T cells and their role in the immune system

$CD8^+$ T cells are part of the adaptive immune system where their main function it is to kill cells infected with virus or an intracellular pathogen. $CD8^+$ T cells originate from haematopoietic stem cells in the bone marrow and are subjected to positive and negative selection in the thymus; the latter giving T cells their name. The TCR expressed by $CD8^+$ T cells is composed of an α and a β chain and each TCR expressed in naïve T cells is unique due to recombination events occurring during T cell development. $CD8^+$ T cells can recognise and bind to cognate peptide presented in the peptide binding cleft of the MHC-I on cells via the TCR (figure 1.3). Subsequent downstream signalling leading to T cell activation will be described in more detail later (figure 1.5). To stabilise this interaction, CD8αβ, a heterodimeric co-receptor, binds to a conserved region of the MHC-I. MHC-I is expressed on the majority of nucleated cells albeit different tissues have different expression levels. High levels can be found in lymphocytes whereas cells in the brain or kidney have lower levels and non-nucleated red blood cells do not express any MHC-I. The latter observation fits with the inability of red blood cells to support viral replication and the role of $CD8^+$ T cells in detecting and eliminating virally infected cells. (Kenneth Murphy 2008)

Naïve T cells have not encountered Ag recognised by their TCR (cognate Ag) outside of the primary lymphoid organs (bone marrow and thymus) and have consequently not yet been activated. Naïve $CD8^+$ T cells circulate via the blood stream to secondary lymphoid organs such

as the spleen, lymph nodes and mucosal-associated lymphoid tissue. Here they scan the environment for Ag presented by APCs such as DCs. If cells do not encounter cognate Ag, they exit the LNs within 24 h via the lymphatics and recirculate through other secondary lymphoid organs.

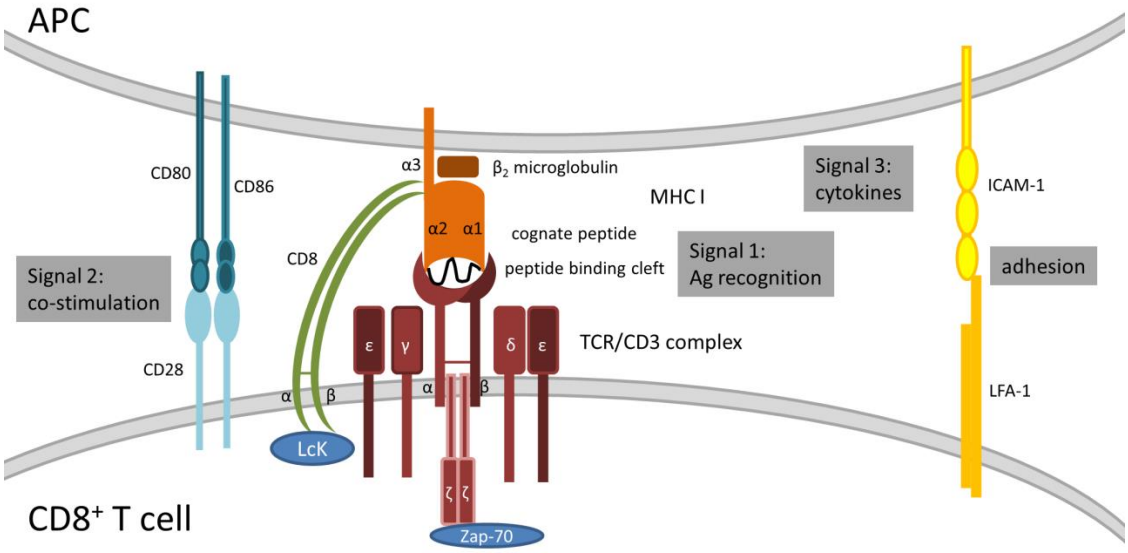

Figure 1.3: CD8$^+$ T cell priming by APCs in secondary lymphoid tissues. CD8$^+$ T cells are primed in secondary lymphoid organs when the TCR (red) encounters cognate peptide (black line) presented within the peptide binding cleft of MHC-I (orange) expressed by APCs. The CD8 co-receptor (green) stabilises this interaction by binding to the α3 domain of the MHC-I. For optimal activation, co-stimulation (e.g.: CD80/86 and CD28) and cytokines provide stimulatory signals 2 and 3. A stable conjugate between the two cells is formed once adhesion molecules interact (e.g.: LFA-1 and ICAM-1). Once these combined signals are provided, the protein tyrosine kinase (PTK), LCK, phosphorylates the ζ-chain of the CD3 receptor enabling the recruitment of the PTK, ZAP70, leading to a signalling cascade resulting in metabolic changes to the cell, proliferation and gene transcription changes.

Peptides presented by MHC-I complex of APCs can originate both from intracellular proteins and extracellular proteins as professional APCs are able to cross-present the latter. Most other cells present exclusively intracellular peptide on MHC-I and the vast majority of these peptides will not trigger any immune response as strongly self-reactive T cells have been negatively selected in the thymus due to a strong response to self-Ag. However, incomplete selection or cross reactivity can give rise to potentially self-reactive CD8$^+$ T cells circulating in the body.

Indeed, autoimmune disorders, graft-versus-host and graft rejection can all be linked to the killing of healthy tissue by self-reactive $CD8^+$ T cells (Barry and Bleackley 2002).

Consequently, $CD8^+$ T cell activation is highly regulated and not only requires cognate peptide presented on MHC-I by APCs but the APCs need to be activated and express co-stimulatory molecules such as CD80/86. For maximal $CD8^+$ T cell activation and expansion, an additional requirement is an inflammatory cytokine environment such as exposure to interleukin-12 (IL-12) and type I interferon (IFN). The overall triggering and maintenance of an adaptive immune response depends on a wide array of different signals such as cytokines and cell to cell contact from different immune and non-immune cells in a variety of locations. Naïve $CD8^+$ T cells will not be activated by non-APC cells unless they are found within a highly inflammatory environment and are activated as bystanders. (Kenneth Murphy 2008)

During an infection with a virus not previously seen by a given individual, a phenotypically and functionally heterogeneous immune response is mounted by a population of distinct naïve $CD8^+$ T cells, expressing a range of TCRs, being activated by DCs. The activation will happen in the subcapsular sinus of the draining LN (dnLN) of the infected tissue. This can be independent from $CD4^+$ T cells as shown for influenza or Listeria infections or it can require help from $CD4^+$ T cells. The latter requires the $CD4^+$ T cells to interact with the APCs and induce their maturation to fully competent APCs. This is needed for non-inflammatory Ags and some infections such as the herpes simplex virus (Zhang and Bevan 2011).

It has been found that a naïve $CD8^+$ T cell activated with a strong Ag stimuli, co-stimulation and an inflammatory cytokine environment can undergo up to 19 divisions within the first week with a maximum rate of cell division of 4-6 h. This expansion is associated with a large change in T cell metabolism. The expansion of $CD8^+$ T cells is in contrast to $CD4^+$ T cells which do not clonally expand to the same degree (Zhang and Bevan 2011).

1.2.2 Cytotoxic T cells and their killing mechanism

It takes 5-8 days for a naïve $CD8^+$ T cell to be primed in a secondary lymphoid organ, differentiate into a CTL and migrate to the site of infection. Each CTL can kill multiple target cells without causing significant bystander pathology. This is due to the requirement of the target cell to express the cognate peptide-MHC complex. Once differentiated, CTLs do not require co-stimulatory signals to kill and the engagement of as few as 3-10 TCRs is enough to trigger a CTL (Purbhoo et al. 2004). Once CTLs enter the affected tissue and localise to a target cell, the latter undergoes apoptosis within 20-30 min. As reviewed elsewhere, apoptosis or necrosis of target cells can be induced via three main mechanisms (figure 1.4), all of which are triggered by TCR activation (Barry and Bleackley 2002; de Saint Basile et al. 2010).

The first mechanism of cytotoxicity used by CTLs is the calcium dependant secretion of granules, containing amongst other proteins, perforin and granzyme B, at the immunological synapse. Perforin is exclusively found in granules of cytolytic cells (CTLs and NK cells) and is thought to form pores in the cytoplasmic membrane or endosomes to release granzymes into the cytoplasm of target cells. Granzymes, such as granzyme B, enter the target cell cytoplasm via perforin pores or by endocytosis and induce caspase-dependant apoptotic cell death. Alternatively, granzyme B can interfere with mitochondrial activity leading to necrotic cell death. Perforin and the granzymes are synthesised *de novo* during the differentiation of a naïve $CD8^+$ T cell into a CTL. Lymphocytes and activated DCs are protected against granzyme B as they express a specific protease inhibitor (PI9). CD107a is a surrogate marker for degranulation of cytotoxic granules (Betts et al. 2003) as CD107a is associated with intracellular lysosomal membranes until degranulation occurs and it is translocated to the cell surface.

A second mechanism by which CTLs induce target cell death is via the contact dependant interaction of death receptors and their ligands. One such interaction is that of FAS on the target cell and FAS ligand (FASL) on the CTL. The former is a member of the TNF receptor (TNFR) family and contains a death domain which leads to downstream activation of caspases and the initiation of apoptosis. Besides FAS, there are other TNFRs and TNF-related apoptosis inducing ligand receptor (TRAIL) contacts. The FAS-FASL interaction limits the survival of repeatedly activated lymphocytes as these cells will start upregulating FASL. Deficiency in the human FAS or FASL genes was shown to cause an autoimmune lymphoproliferative syndrome due to the lack of apoptosis of autoreactive B and T cells (Rieux-Laucat et al. 2003).

Lastly, CTLs can kill target cells by producing cytokines such as interferon-γ (IFN-γ) and tumour-necrosis factor (TNF) which can damage target cells if secreted in close proximity.

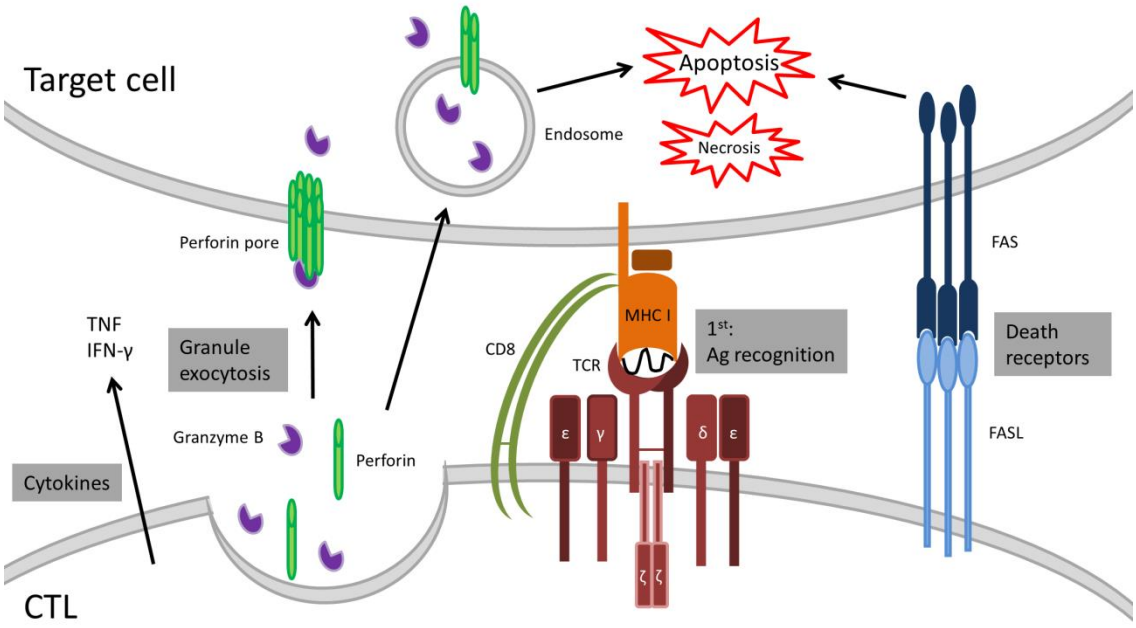

Figure 1.4: Cytotoxic killing of target cells by CD8$^+$ T cells. CD8$^+$ T cells are activated by cognate Ag presented by MHC-I on target cells in the periphery. TCR induced signalling will lead to the exocytosis of granulocytes containing perforin and granzyme. The former will form pores in the target cell cytoplasm through which the granzymes can enter the cell and induce apoptosis. Additionally, CD8$^+$ T cells upregulate the surface expression of the death receptor ligand FASL, which interacts with FAS on the target cell and leads to target cell death. Finally, CD8$^+$ T cells secrete cytokines such as TNF and IFN-γ. These three arms of attack will lead to target cell death by apoptosis or necrosis.

1.2.3 $CD8^+$ T cell differentiation into effector and memory cells

Differentiation of a naïve $CD8^+$ T cell has two goals; clearing the pathogen or malignant cells and establishing immunological memory to protect against secondary Ag encounters. To enable this, $CD8^+$ T cell responses to novel Ag consist of three phases. Firstly, clonal expansion, preceded by the activation of T cells (figure 1.3), yields a large number of effector $CD8^+$ T cells to eliminate the Ag. Short lived effector T cells, expressing high levels of the transcription factor, T-bet, and proteins of the cytotoxic signature, make up the bulk of the response. IL-12 has been implicated to induce terminally differentiated $CD8^+$ T cells via the mTOR pathway and via the upregulation of T-bet. This is followed by a contraction phase where 90-95% of all $CD8^+$ T cells die by apoptosis, once all the Ag has been eliminated. Thirdly, a pool of memory cells is formed, constituted of 5-10% of cells from the initial clonal expansion. (Kaech and Cui 2012)

Several different models have been proposed for the differentiation of $CD8^+$ T cells into effector T cells (T_{EF}), effector memory (T_{EM}) and central memory (T_{CM}) T cells. The favoured models are based on the principle that the duration and/or strength of the T cell stimulation influences the differentiation of the cells. T_{CM} cells are L-selectin $(CD62L)^{high}$ $CCR7^{high}$ cells and are found in bone marrow, LNs, the spleen and blood whereas T_{EM} are L-$selectin^{low}$ $CCR7^{low}$ cells and are found in the spleen, blood and liver. The former show high proliferative potential and secrete large amounts of IL-2 whereas the latter can rapidly upregulate their cytotoxic function when faced with a second challenge. It is important to note that expression of these memory markers is not definitive and that some cells can be $CCR7^+$ but L-$selectin^-$ (Unsoeld and Pircher 2005). A third subset of memory T cells is composed of the tissue-resident memory T cells located in mucosal tissues and the brain and similarly to T_{EM} cells they are able to quickly respond to a local challenge (Kaech and Cui 2012).

There are different requirements, such as cytokines and cell to cell contact, for the maintenance of the different $CD8^+$ T cell subsets (effector and memory). During an immune

response, T cells are activated and start making IL-2 due to signalling via the NFAT pathway and IL-2 acts in an auto- and paracrine manner. There are three different possible IL-2 receptor combinations; the low affinity CD25 (IL-2αR), the intermediate affinity CD132/CD122 (γ_c/β chains) or the high affinity αβγ heterotrimer composed of all three units. CD25 is upregulated during $CD8^+$ T cell activation leading to a selective IL-2 driven expansion of activated $CD8^+$ T cells. IL-2 is required for an optimal $CD8^+$ response generating effector and memory cells. However, continued exposure to IL-2 can lead to activation induced cell death (AICD) which can be inhibited by the presence of IL-15 signalling. IL-15 is another cytokine implicated in $CD8^+$ T cell survival and proliferation. It is produced by type I IFN stimulated cells (non-T cells). IL-15 bound to the IL-15αR act *in trans* with the CD132/CD122 heterodimer expressed on T cells. IL-15 has been shown to be critical for $CD8^+$ memory maintenance (Votavova et al. 2014). Homeostasis of $CD8^+$ T cells requires IL-7 for both naïve and memory $CD8^+$ T cells, but the latter also require IL-15 signalling (Surh and Sprent 2008).

1.3 SHP-1 and $CD8^+$ T cell activation

1.3.1 T cell signalling upon TCR engagement

As reviewed recently (Brownlie and Zamoyska 2013), when $CD8^+$ T cells are activated via the TCR recognising cognate peptide presented on MHC-I, the SRC family kinases (SFKs) LCK and FYN are activated (figure 1.5). LCK is associated with CD8 (Veillette et al. 1988), and the binding of CD8 to MHC-I will bring it in close proximity with its substrates, the immunoreceptor tyrosine-based activation motifs (ITAMs) of the CD3 γ, ε, δ and ζ chains. This phosphorylation depends on a threshold of activation and it is not yet clear how this is controlled. Phosphorylated ITAMs of the CD3 complex recruit the SYK family kinase zeta-associated-70 (ZAP70) to the TCR-CD3 complex and the phosphorylation of activating residues on ZAP70 by LCK occurs. Once in an active conformation, ZAP70 phosphorylates its substrates, the main one being the linker for activation of T cells (LAT). Once the four tyrosines on LAT are phosphorylated, a multitude of molecules aggregate to form the LAT signalosome. The latter complex is composed amongst others of GRB2, SLP76 and VAV1. This in turn leads to further signalling, with the conformational change of integrins (LFA-1), the nuclear translocation of NFAT and NF-κB and actin rearrangements. Overall, changes in T cell adhesion, cell growth and differentiation will occur.

Relatively little is known about the negative signalling involved in controlling the threshold of T cell activation and the termination of signalling. Several protein tyrosine phosphatases (PTPs), such as CD45 and SHP-1, have been implicated in setting the T cell threshold and ending signalling via the TCR by dephosphorylating kinases and molecules in the T cell signalling cascade. PTPs and in particular SHP-1 will be discussed in more detail below.

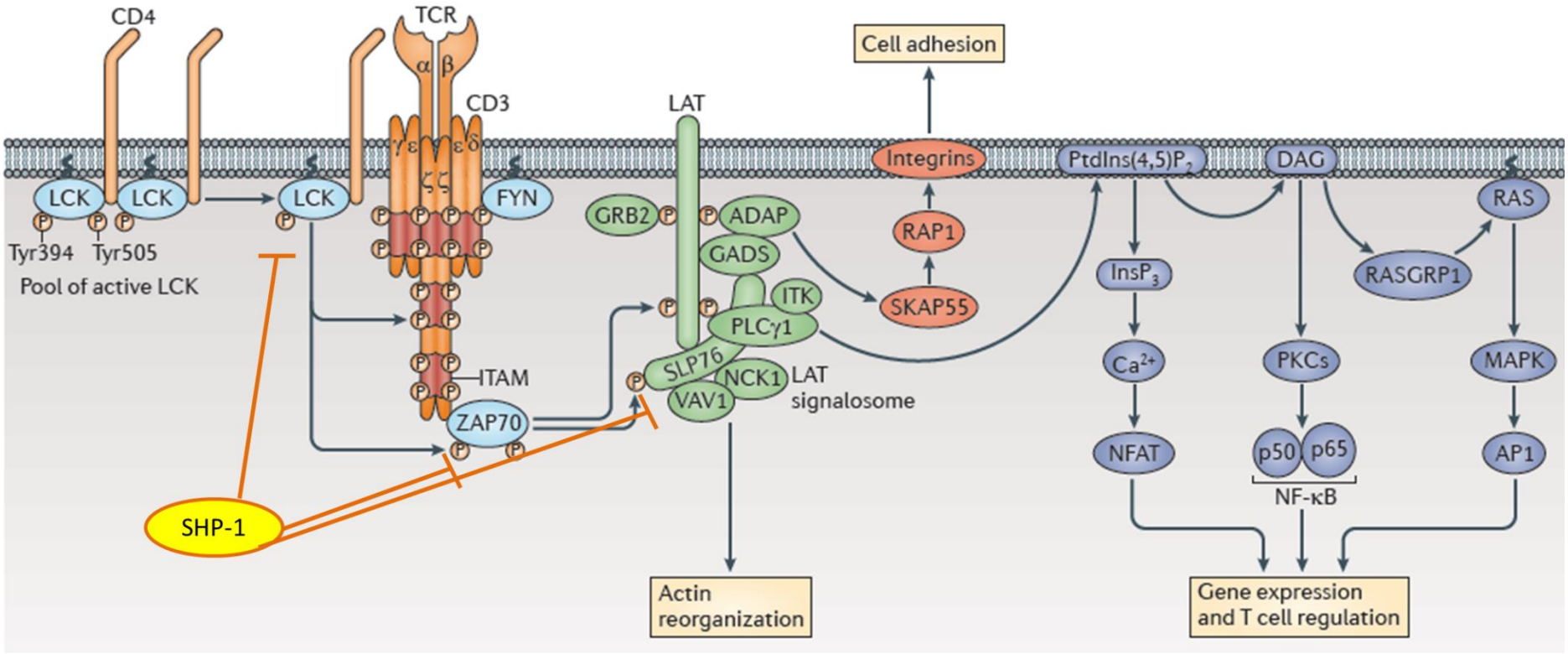

Figure 1.5: T cell signalling following engagement of cognate peptide MHC. When the TCR recognises cognate peptide presented on MHC-I or MHC-II, and CD4 or CD8 engages with MHC, the SRC family kinases FYN and LCK are activated, brought into the proximity of the TCR-CD3 complex and phosphorylate ITAM motifs of the CD3 γ, ε, δ and ζ chains. This enables the recruitment of ZAP70, which is phosphorylated by LCK and can in turn phosphorylate key tyrosines on LAT. Phosphorylated LAT recruits other proteins such as GRB2, SLP76 and VAV1, forming the LAT signalosome. The latter leads to signal propagation down three main pathways; the Ca^{2+} and NFAT, the MAPK and the NF-κB pathway. Overall, this will lead to altered cytoskeletal organisation, gene expression and metabolism. A key negative regulator of this signalling cascade is the protein tyrosine phosphatase, SHP-1 (yellow), possibly dephosphorylating and binding to some key molecules such as LCK, ZAP70 and SLP76. Figure adapted from (Brownlie and Zamoyska 2013).

1.3.2 Protein tyrosine phosphatases and T cell regulation

Protein phosphorylation is a major post-translational modification leading to changes in cellular activity such as proliferation, differentiation and migration. Tyrosine phosphorylation, although only accounting for 0.01-0.05% of all protein phosphorylation (Hunter and Sefton 1980), is essential for the regulation of all immune cells. The dynamic actions of PTKs are counteracted by PTPs and both enzymes are necessary to keep signalling balanced. Whereas PTKs add phosphoryl entities to proteins, PTPs remove them and by doing so potentially alter protein stability, the binding of adaptor proteins and the degree of enzyme activity (Zhang 2002). PTPs have been implicated in both positive and negative regulation of T cell activation.

The PTP family can be divided into four groups, with the two most studied being the classical receptor-type PTPs (e.g. CD45 and CD148) and the nonreceptor-like PTPs (PTPN22, PTPN2 and SHP-1). The latter are located within the cytoplasm as opposed to being membrane-bound. PTPs are characterised by an active site motif (H/V)CXXXXXR(S/T), where X can be any residue, within the conserved catalytic domain (Zhang et al. 1994).

Tightly controlled regulation of T cell activation is crucial in preventing autoimmunity and pathology, both during T cell development in the thymus and in the periphery. The importance of PTPs has been illustrated in a range of patients with immune disorders linked to altered PTP expression. For example, loss of the PTP CD45 has been shown to lead to severe immunodeficiency disease, marked by a decrease in T cell numbers and hyporesponsiveness (Kung et al. 2000) and a functional polymorphism in the PTP, Lyp (PTPN22), has been shown to correlate with the development of different autoimmune disorders (Criswell et al. 2005).

One downside of this tight control of T cell activation is that tumours, originating from self, are poor at activating T cells. Tumour cells express little immunogenic Ag, decreasing the chance of T cells being activated by them. Hence lowering the threshold for T cell activation by such

tumour Ags has been envisioned as a potential component for successful adoptive T cell therapy. One such key negative regulator of T cells is a PTP termed SHP-1, described in more detail below.

1.3.3 SHP-1 structure and regulation

SHP-1, a src homology 2 (SH2) domain containing PTP, has been shown to negatively regulate T cell activation. SHP-1 is thought to dephosphorylate key proteins downstream of immune receptors, cytokine receptors and receptor PTKs and consequently counteract the actions of key PTKs in the T cell signalling cascade. SHP-1 has been implicated in setting the threshold for T cell activation; both during development of T cells in the thymus (Carter et al. 1999; Johnson et al. 1999) and during an immune response (Lorenz 2009) and evidence for this will be discussed here.

In 1992, the cDNAs for mouse and human SHP-1 (PTPN6) were identified by several different groups using reverse genetics, based on the high level of conservation of the PTP domains and it was shown that there is 95% homology between the SHP-1 cDNAs of the two species (Matthews et al. 1992; Plutzky et al. 1992a; Yi et al. 1992). The SHP-1 cDNA from a pre-B-cell line encoded for a 595 aa, 68 kDa protein composed of two distinct N-terminal SH2 domains and a C-terminal PTP catalytic domain (figure 1.6 A) (Matthews et al. 1992). It was shown that the SHP-1 mRNA is primarily found in haematopoietic tissues such as the BM, thymus and LNs. Additional studies showed that SHP-1 is mainly expressed in haematopoietic cells and less strongly in epithelial cells and oligodendrocytes in the brain (Massa and Wu 1996). The human PTPN6 gene encoding for the SHP-1 protein is located on chromosome 12 and composed of 17 exons yielding 4 different isoforms (Plutzky et al. 1992b). The two major SHP-1 transcripts encode for non-haematopoietic and haematopoietic SHP-1 isoforms of 597 and 595 aa

respectively (Banville et al. 1995). Expression of the latter transcript is controlled by a downstream promoter, separated by 7 kb from the first promoter used for the non-haematopoietic transcripts.

The resolution of the crystal structure of a tail-truncated SHP-1 protein in the inactive state confirmed the presence of three main domains, namely the N-terminal SH2 (N-SH2) (residues 1-108), the C-terminal SH2 (C-SH2) (residues 116-208) and the C-terminal catalytic PTP domain (residues 270-532) (Yang et al. 2003). Additionally, it was shown that inactive SHP-1 protein is auto-inhibitory due to a conformation where the N-SH2 domain strongly interacts with the PTP domain thus obstructing the entrance to the PTP active site (figure 1.6 B). This was supported by data showing that the N-SH2 domain was necessary and sufficient for the auto-inhibition of SHP-1 (Pei et al. 1996) and SHP-1 deficient in the N-SH2 domain generated more PTP activity *in vitro* than the intact full length SHP-1 (Brockdorff et al. 1999). It was hypothesised that the flexibility of the C-SH2 domain enables it to search the environment and recruit phosphopeptide ligands. Once bound to ligand, a conformational change occurs and the N-SH2 detaches from the PTP domain and binds a second tyrosine phosphorylated residue (figure 1.6 A). This fitted with findings that optimal phosphatase activity was only observed when both SH2 domains were engaged, as shown by biphosphorylated peptide inducing SHP-1 catalytic activity of up to 4 fold above that of monophosphorylated peptide (Pluskey et al. 1995). Another study showed that mutating crucial arginine residues involved with phosphoprotein binding led to suboptimal activation (Pei et al. 1996). The resolution of the full-length open conformation SHP-1 protein crystal structure confirmed this model (Wang et al. 2011) where upon binding to ligand, the N-SH2 domain flips around and interacts with the opposite side of the PTP domain (figure 1.6 C). These new interactions help to stabilise the active state of SHP-1 and allow substrate to enter the PTP domain active site. This study did not resolve the structure of the C-terminal tail.

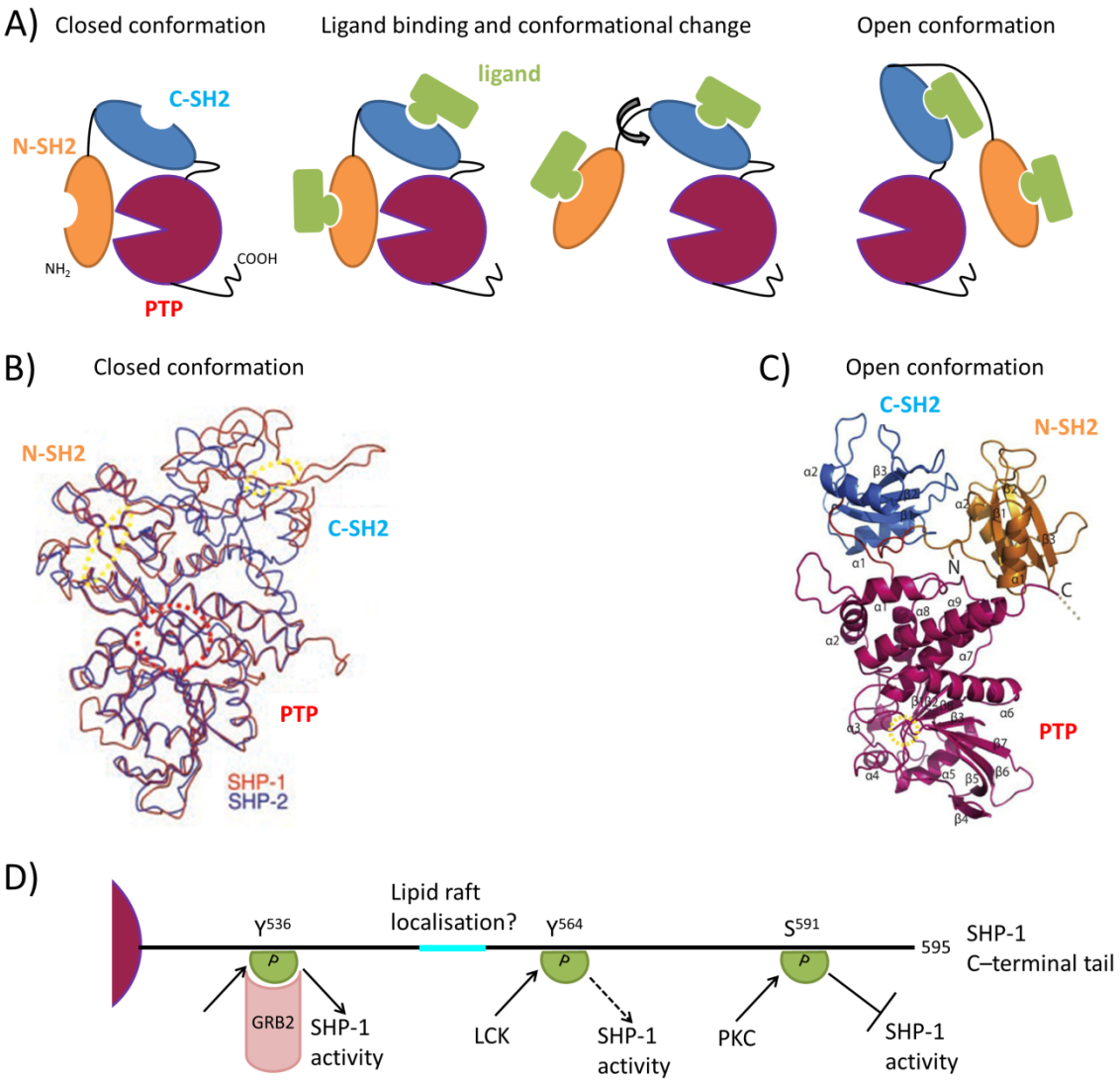

Figure 1.6: Model of the activation of SHP-1 by conformational changes and possible modifications of the C-terminal tail. A) Model of the activation of SHP-1. In the inactive/closed conformation, the N-SH2 domain obstructs the catalytic PTP domain (red) whereas binding of phosphorylated ligand (green) by both the N-SH2 (orange) and the C-SH2 (blue) domains leads to a rotation in the linker between both domains and the relocation of the N-SH2 to the opposite side of the catalytic PTP domain. This results in the stable opening of the catalytic domain and its accessibility to substrate. B) The structure of tail-truncated inactive SHP-1 protein was resolved and showed the obstruction of the active PTP site (red dotted circle) by the N-SH2 domain. The overlay of the SHP-1 and SHP-2 structures are shown and the picture was taken from (Yang et al. 2003). C) The structure of the full-length SHP-1 protein in its active state is shown. As opposed to B), the N-SH2 domain has flipped to the other side of the PTP domain, opening up the catalytic PTP domain (yellow dotted circle) to substrates. The picture was taken from (Wang et al. 2011). D) The C-terminal tail of SHP-1 has three potential phosphorylation sites (green half circle). The kinases potentially involved in phosphorylating Y^{564} and S^{591} are shown. Phosphorylation of tyrosines can lead to the recruitment of SH2-domain containing molecules such as the adaptor GRB2. The potential lipid raft localisation sequence (SKHKED at 557-562) (Sankarshanan et al. 2007) is shown in turquoise.

SHP-1 PTP activity can be regulated not only by the obstruction of the catalytic domain by the N-SH2 domain but also by spatial separation of SHP-1 and its substrates. The SHP-1 C-terminal tail has been implicated in regulating the activity of SHP-1 directly, by recruiting adaptor proteins and by altering the cellular positioning of SHP-1 (figure 1.6 D). The C-terminal tail was shown to have a considerably lower degree of homology with SHP-2 than the rest of the molecule (<15 % versus 60 %), indicating its possibly unique function (Yang et al. 2003). The C-terminal tail also contains a potential nuclear localisation signal (Yang et al. 2002). In non-haematopoietic cells, the tail has been implicated with the redistribution of SHP-1 into the nucleus of cells stimulated with cytokines and growth factors (Yang et al. 2002; He et al. 2005). In T cells this has not been reported, however residues 557-562 of the C-terminal tail have been implicated with localisation of SHP-1 to lipid rafts (figure 1.6 D) (Fawcett and Lorenz 2005). This study showed that in Jurkat cells and primary T cells, 20-30% of SHP-1 is located in lipid rafts. This lipid raft positioning of SHP-1 was shown to be vital for the inhibition of IL-2 production by T cells, as cells expressing mutant SHP-1 lacking the lipid raft targeting motif did not show any inhibition (Sankarshanan et al. 2007).

The C-terminal tail serine residue at position 591 has been shown to be phosphorylated in resting T cells and it is believed that phosphorylated S^{591} negatively regulates SHP-1 activity (Lorenz et al. 1994; Poole and Jones 2005). Two tyrosines, Y^{536} and Y^{564}, have been shown to be phosphorylated and LCK was implicated in the phosphorylation of Y^{564} in activated T cells (Lorenz et al. 1994). Reports showed that the phosphorylation of Y^{536} and to a lesser extent Y^{564} enhances SHP-1 activity; however these studies were done with non-haematopoietic SHP-1 (Uchida et al. 1994; Frank et al. 2004). Phosphorylated Y^{536} has been proposed to recruit the SH2 domain containing adaptor protein GRB2 and possibly other SH2 domain containing molecules such as VAV1 and mSos1 (Kon-Kozlowski et al. 1996; Minoo et al. 2004). Auto-dephosphorylation of the two tyrosine residues by SHP-1 has been shown, however not in T cells (Bouchard et al. 1994).

1.3.4 Possible SHP-1 ligands and substrates

It is clear that SHP-1 needs to bind phospho-proteins with both SH2 domains to enable access of the substrate to the active site of the catalytic domain. Such ligands are found on members of the inhibitory-receptor superfamily (IRS) expressing immunoreceptor tyrosine-based inhibitory motifs (ITIMs) (V/L/IXpYXXL/V) within their cytoplasmic tails (Long 1999). Proteins from the IRS family inhibit activation receptors in *trans* by recruiting PTPs such as SHP-1 and bringing them into proximity of substrates. IRS members in T cells often express multiple ITIM motifs, enabling both SHP-1 SH2 domains to engage, resulting in a stable activation of the PTP (Burshtyn et al. 1997; Vely et al. 1997). SHP-1 has been shown to constitutively interact with leucocyte-associated immunoglobulin receptor-1 (LAIR-1), an ITIM containing inhibitory receptor (Sathish et al. 2001a). Recruitment of SHP-1 to these receptors might contribute to basal inhibitory signalling and thereby keep T cells in an inactive state. The carcinoembryonic antigen related cell adhesion molecule 1 (CEACAM1) is upregulated in activated T cells and possibly inhibits T cell activation via the recruitment of SHP-1 and the subsequent dephosphorylation of ZAP70 and the TCR ζ chain (Nagaishi et al. 2006; Chen et al. 2008).

Considering the growing use of anti-CTLA-4 and anti-PD1 Abs in cancer immunotherapy, it is of interest to know whether SHP-1 interacts with either of the two molecules. CTLA-4 does not express any ITIMs but contains two tyrosines to which the SHP-1 SH2 domains could potentially bind. An association between SHP-1 and CTLA-4 has been reported (Guntermann and Alexander 2002) however there is no direct evidence of SHP-1 binding to CTLA-4 (Yokosuka et al. 2010). As for PD-1, it was shown that SHP-1 and SHP-2 could potentially bind to the ITIM of PD-1 (Sathish et al. 2001a; Chemnitz et al. 2004), however only SHP-2 seems to interact with PD-1 in TCR activated T cells (Yokosuka et al. 2012).

Many potential substrates for SHP-1 have been identified in leucocytes, ranging from ZAP70, SFKs and activatory tyrosines on receptors expressing ITAMs to adaptors such as LAT, SH2

domain-containing leucocyte protein (SLP-76) and VAV1 (figure 1.5) (Rhee and Veillette 2012). However, no direct binding partner for SHP-1 has been established in T cells. Multiple possible binding partners and substrates have been proposed and will be discussed below, however many studies have not been reproducible due to a variety of experimental settings and cell types used. As mentioned previously, SHP-1 is proposed to interact with GRB2 and VAV1 via the binding of the SH2 domains of the latter to phosphorylated tyrosines of the SHP-1 C-terminus (Kon-Kozlowski et al. 1996). One study showed that ZAP70 interacts with SHP-1 in Jurkat cells transduced with both proteins and activated via TCR cross-linking. It was proposed that this interaction was via the binding of the SHP-1 SH2 domains to phosphorylated tyrosine on ZAP70 (Plas et al. 1996). This would lead to the dephosphorylation of the activating tyrosine on ZAP70 by SHP-1 (Brockdorff et al. 1999). Another co-expression experiment, using LCK and SHP-1 indicated a possible interaction between the LCK SH2 domain and the phosphorylated tyrosine of SHP-1, however this was done in unstimulated HEK293T cells and another study stated that SHP-1 did not dephosphorylate LCK (Brockdorff et al. 1999; Stefanova et al. 2003). As well as ZAP70 and LCK, SLP-76 has been proposed as a substrate (Binstadt et al. 1998).

1.3.5 Functional implications of SHP-1 deficiency

No individuals have been identified with mutations in the SHP-1 locus, possibly due to the predicted severity of such mutations and early death of the foetus. However there are a number of diseases where altered levels of SHP-1 have been identified. A study in multiple sclerosis patients showed that the haematopoietic SHP-1 promoter 2 transcript was expressed less in patient PBMCs when compared to healthy controls and consequently more phosphorylated Signal Transducer and Activator of Transcription 6 (STAT6) and STAT1 molecules were observed (Christophi et al. 2008). This report fits in with findings in SHP-1 deficient mice that show enhanced disease severity due to myelin basic protein degradation in

the central nervous system mediated by T cells (Deng et al. 2002). Low levels of SHP-1 protein have also been observed in some leukaemias and lymphomas in humans, probably due to epigenetic modifications (Zhang et al. 2000; Oka et al. 2001). Elevated SHP-1 activity was observed in T cells from elderly donors and downregulation of SHP-1 activity in these T cells enhanced T cell responsiveness, thus linking SHP-1 to the impaired activation of T cells from aged people (Le Page et al. 2014).

The discovery of a natural mutation in the SHP-1 gene in mice greatly advanced the understanding of SHP-1 and its role in the immune system. In 1965 a recessive mutation in the SHP-1 gene was discovered in a mouse colony at the Jackson Laboratory (Bar Harbor, Main, USA) (Dickie et al. 1969). These mice were characterised by a patchy appearance of the coat that provides them the name of *motheaten* (*me*) (Green and Shultz 1975). As well as skin and foot lesions, *motheaten* mice manifest with, amongst other symptoms, slower growth, splenomegaly and premature thymic involution. These mice die at approximately of 2-4 weeks due to severe pneumonitis caused by a large infiltration of macrophages and neutrophils (Jiao et al. 1997). The *me* mutation, causing this lethal phenotype, is a point mutation within the sequence encoding for the N-SH2 domain that introduces a new splice-donor site leading to a premature truncation of the mRNA and a complete loss-of-function mutation. A less severe mutation in the SHP-1 locus is called *motheaten* viable (me^v) and its mutation gives SHP-1 protein levels of approximately 20% of that of wt mice. Hence, me^v mice survive up to 3 times longer than the *me* mice (Shultz et al. 1984; Shultz et al. 1993). When me^v mice were crossed with Rag-1 knockout mice it was found that the observed pathology in these mice is T and B cell independent (Yu et al. 1996). A third phenotype linked to a mutation in the SHP-1 locus was induced by exposure of mice to a mutagenic compound and this genotype was called *spin* (spontaneous inflammation) (Croker et al. 2008). The pathology associated with the *spin* genotype is less pronounced than that of me^v mice. Crucially, this study showed that if these mice were house in a germ-free environment, no inflammation or autoimmunity was

observed, hence indicating that the pathology in SHP-1 deficient mice is initiated by extrinsic rather than intrinsic factors. Additionally, a recent paper using a conditional (floxed) SHP-1 model in different mouse cells showed that neutrophils are responsible for the cutaneous inflammation whereas SHP-1 deficient DCs are responsible for the severe autoimmunity (Abram et al. 2013). Overall these studies illustrated the importance of SHP-1 as a negative regulator in immune cells.

To generate enhanced numbers of SHP-1 deficient T cells for adoptive T cell transfer studies, our laboratory has genetically crossed interleukin 1 receptor 1 knockout animals (B6.126S7-IL1r1^{tm1Imx}/J) with heterozygote C57BL/6J me+/- mice to generate IL-1r1$^{-/-}$ *me/me* mice (unpublished data). These mice survive up to 12 weeks due to a reduction in pathological inflammation caused by cells of the innate immune system.

Although no obvious differences in thymic development were seen in *motheaten* mice (Lorenz et al. 1996), studies using *motheaten* mice expressing a transgenic TCR showed an increased in mature double negative T cells (Johnson et al. 1999) as well as a role for SHP-1 in setting the threshold for positive selection (Carter et al. 1999). This suggested that SHP-1 signalling plays a role in thymic T cell development. It was shown that *me* thymocytes showed prolonged activity of the PTKs, LCK and Fyn when compared to wt cells (Lorenz et al. 1996). Another group showed increased levels of phosphotyrosine in SHP-1 deficient T cells post TCR activation (Pani et al. 1996). However, this is in disagreement with studies from our own group using *motheaten* thymocytes and peripheral T cells whereby no differences in the phosphorylation of the CD3 ζ chain, ZAP70, SLP-76 and LAT were observed when compared to wt cells (Johnson et al. 1999; Sathish et al. 2001b).

While data on the action of SHP-1 in determining phosphotyrosine levels in T cells is confusing, there is no doubt that loss of SHP-1 causes significant functional changes in T cells. The exact model of how SHP-1 is implicated in the inhibition of T cell activation and in the regulation of

the T cell activation threshold is still unclear and several different models have been proposed (Lorenz 2009). The main finding from multiple studies is that loss of SHP-1 leads to a lowered threshold for T cell activation and thus T cells enter proliferation more readily at lower Ag concentrations. It has been shown that *me/me* thymocytes proliferate more than their wt counterparts in response to anti-CD3 Ab and PHA and that the increased proliferation is not due to a decrease of cell death (Lorenz et al. 1996). Activated *me/me* T cells also produced more IL-2 than wt control cells. In another study, OVA specific SHP-1 deficient T cells gave an increased and prolonged maximal proliferation response to anti-CD3 and IL-2 or cognate peptide (Pani et al. 1996).

When thymocytes were activated with anti-CD3 and anti-CD28 Ab, no difference in proliferation was observed between SHP-1 deficient and wt cells, whereas anti-CD3 alone did show significant differences (Sathish et al. 2001b). This indicates that loss of SHP-1 might abrogate the need for co-stimulatory signalling, needed in wt cells for optimal priming, due to these cells being more easily activated. This would fit earlier findings where TCR transgenic SHP-1 deficient T cells from peripheral LNs had elevated levels of activation markers (CD44 and CD25) and cells were larger in size *ex vivo* (Johnson et al. 1999). These T cells had not been exposed to cognate peptide *in vivo* and activation may therefore have been due to interaction with MHC-self-peptide complexes, usually not causing activation in T cells from SHP-1 sufficient mice. One reason for the enhanced entrance into proliferation by *motheaten* T cells could be due to the observed increase in stable APC T cell conjugates formed by SHP-1 deficient T cells (Sathish et al. 2007). The formation of stable conjugates requires the interaction of integrins and their ligands and a reorganisation of the cytoskeleton and it is possible that SHP-1 is acting at this level. In this same study, enhanced proliferation was also observed *in vivo* where equal numbers of wt or *me* T cells were injected and 6 days later, more T cells were recovered. Additionally, more target cell killing was observed *in vivo* in this model, most likely due to increased T cell numbers.

To ensure that the phenotype in *me* T cells is due to the intrinsic loss of SHP-1 and not due to altered extrinsic signalling by other SHP-1 deficient cell types, a conditional (floxed) SHP-1 knockout was generated in T cells (Fowler et al. 2010). Results with these $CD8^+$ T cells confirmed previous findings from *motheaten* mice (Sathish et al. 2007) that the loss of SHP-1 leads to an enhanced number of cells entering proliferation *in vitro* without altering the cytolytic phenotype of the cells. When mice were challenged with virus, the SHP-1 deficient $CD8^+$ T cells showed enhanced proliferation *in vivo* and increased numbers of effector but not memory $CD8^+$ T cells were recovered from both primary and secondary viral challenges (Fowler et al. 2010). Another study using the conditional SHP-1 knockout mice showed that there was no difference in IL-2 production, whereas they did confirm the enhanced proliferative potential of SHP-1 deficient T cells (Johnson et al. 2013).

SHP-1 has been implicated in controlling T cell anergy, as heterozygote me^v T cells caused encephalomyelitis when exposed to a peptide that usually induces anergy in wt T cells (Wasserman et al. 2008). This could be linked to the enhanced formation of conjugates with APCs in SHP-1 deficient cells (Sathish et al. 2007).

SHP-1 has also been shown to alter signalling downstream of chemokine and cytokine receptors. One study showed that SHP-1 can dephosphorylate the IL-2βR and the downstream PTKs, Janus kinase 1 (Jak1) and Jak3, as catalytically inactive SHP-1 cells showed increased phosphorylation of these molecules (Migone et al. 1998). Migone *et al.* hypothesised that loss of SHP-1 could thus make T cells IL-2 independent as signalling via its receptor was not negatively regulated. Additionally, SHP-1 has been linked to controlling signalling via STAT1 and STAT6 (Christophi et al. 2008; Johnson et al. 2013) and STAT3 (Mauldin et al. 2012). T cells from me^v mice showed enhanced chemotaxis to stromal-cell derived factor 1 (SDF-1) and SHP-1 deficient T cells show heightened basal actin polymerisation (Kim et al. 1999).

Importantly, lowering of the threshold of T cell activation could potentially increase the responsiveness of T cells to poorly immunogenic tumour-associated Ag. Hence, loss of SHP-1 could be a target for ACT. To study this possibility, $CD8^+$ T cells from conditional SHP-1 knockout mice were used in an adoptive T cell therapy model of disseminated leukaemia and shown to be superior at protecting against leukaemia (Stromnes et al. 2012). Additionally, SHP-1 deficient T cells showed enhanced proliferation during the expansion phase with elevated effector T cell numbers, followed by a contraction phase and equal numbers of memory cells when compared to wt T cells (Fowler et al. 2010). A recent study showed that SHP-1 expression and activatory phosphorylation increased proportionally with the affinity of the TCR to the tumour Ag, NY-ESO-1 (Hebeisen et al. 2013), and further demonstrated that a pharmacological inhibitor of SHP-1 (SSG) could enhance the cytolytic function of T cells expressing a wide range of TCR affinities. The above mentioned sodium stibogluconate (SSG), in combination with IFN-α, showed promising reductions of tumour growth in mice (Yi et al. 2002). However, clinical benefits have not been observed in phase I clinical trials of patients with solid tumours (Naing et al. 2011; Yi et al. 2011). Meanwhile, in these patients, a change in the immune cell balance was observed with fewer T_{regs} and more NK cells. More specific SHP-1 inhibitors, such as tyrosine phosphatase inhibitor-1 (TPI-1) and analogues, have been identified and their administration has given decreased tumour growth in mice (Kundu et al. 2010). The absence of clinical benefit in humans could be due these inhibitors targeting both SHP-1 and SHP-2 and it was shown that SHP-1 and SHP-2 are functionally antagonistic in haematopoiesis in SHP-2 knockout/*motheaten* mice (Qu et al. 2001).

In summary, SHP-1 is thought to act on many levels of T cell signalling such as downstream of the TCR, cytokine receptors and chemokine receptors. These findings in mouse T cells indicate that loss of SHP-1 might be a valid target to try and generate greater numbers of tumour-specific $CD8^+$ T cells for ACT.

1.4 L-selectin and $CD8^+$ T cell homing

L-selectin or CD62L is a crucial molecule for leucocyte migration during homeostatic recirculation, immune surveillance and inflammation. Its former name of leucocyte adhesion molecule-1 (LAM-1) stresses the role L-selectin plays within the leucocyte adhesion cascade where leucocytes are recruited by high endothelial venules (HEVs) in to lymph nodes (LNs) (figure 1.7). L-selectin is expressed on most leucocytes and on T cells and L-selectin orchestrates the initial capturing (tethering) of the T cells by HEVs. The latter are specialised in recruiting lymphocytes, such as L-selectin expressing naïve and memory T cells, in order to ensure constant immune surveillance (Girard et al. 2012). Homeostatic trafficking of L-selectin positive T cells via HEVs is due to the expression of peripheral node addressin (PNAd) and CCL21, interacting with L-selectin and CCR7 respectively on naïve and central memory $CD8^+$ T cells. The importance of L-selectin is demonstrated in L-selectin deficient mice, where lymphocyte recruitment to peripheral LNs is dramatically decreased (Arbones et al. 1994). After cells tether on activated endothelial cells, signalling via L-selectin and chemokine receptors leads to the activation of integrins, resulting in a decrease in the rolling velocity of lymphocytes and their arrest on endothelial cells (Ley et al. 2007). Finally, cells will start the process of transendothelial migration (TEM), allowing lymphocytes to enter the LN.

After TCR engagement, L-selectin is lost from the cell surface and T cells recovered from inflamed sites are L-selectin negative, thus indicating that homing to inflamed tissues is L-selectin independent. Activation of $CD8^+$ T cells will upregulate the expression a range of homing and adhesion molecules such as selectins, chemokine receptors and integrins (Brinkman et al. 2013). For the $CD8^+$ T cell to access the right tissue, the vasculature needs to express the corresponding ligands.

Not all T cell recruitment to secondary lymphoid tissues is L-selectin dependant. T cell recruitment to mucosal LNs (mesenteric LNs and Peyer's patches) has been shown to be L-

selectin independent and mediated via the interaction of α4β7 on T cells and mucosal addressin cell adhesion molecule 1 (MAdCAM-1) on endothelial cells and recruitment to the spleen is L-selectin independent as the latter does not express HEVs (Guarda et al. 2007; Ivetic 2013). Additionally, L-selectin negative T cells have been shown to be able to migrate to LNs draining inflamed sites (Unsoeld and Pircher 2005).

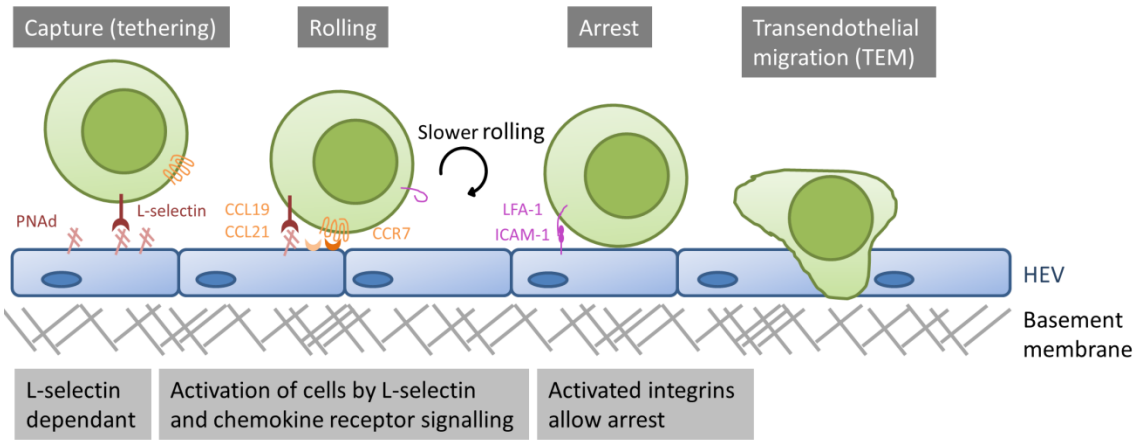

Figure 1.7: T cell recruitment to lymph nodes (LN) via high endothelial venules (HEVs). Under shear flow in LN HEVs, T cells (green) expressing L-selectin (red) will bind to their ligand (e.g.: PNAd) and this interaction initiates the capture of T cells from the blood stream. Engagement of L-selectin leads to outside-in signals which together with signals from chemokine receptors following engagement by chemokines presented on the luminal side of the endothelial cells (CCL21 on endothelial cells and CCR7 on lymphocytes in orange) will induce changes in the lymphocyte function-associated antigen 1 (LFA-1, purple) integrin conformation (Giblin et al. 1997; Steeber et al. 1997; Hafezi-Moghadam et al. 2001). The engagement of L-selectin and chemokine receptors leads to a decrease in the T cell rolling velocity, followed by the arrest of the lymphocyte on the endothelium due to ICAM-1 and LFA-1 interactions. Once arrested, cells start transcellular or paracellular transendothelial migration. Adapted from: (Ley et al. 2007).

1.4.1 L-selectin protein structure, regulation and function

L-selectin is a type I transmembrane cell adhesion molecule encoded by the *SELL* gene and found in the microvilli of T cells. It is composed of highly glycosylated extracellular domains which results in molecular masses ranging from 70 to 100 kDa depending on the leucocyte type (figure 1.8 A). The N-terminal C-type lectin domain was shown to interact with multiple ligands via different parts of the domain. Most ligands are glycoproteins, although glycolipids ligands have also been identified. The L-selectin ligands in HEVs are glycosylated mucins collectively known as PNAds which contain 6-sulphated sialyl Lewis X (sLe^x). Three known PNAds are CD34, GlyCAM-1 and podocalyxin. The best-defined interaction is with sialyl Lewis X (sLe^x) but it was shown that this interaction was not sufficient to support optimal rolling and sulphated esters and tyrosines are also needed. P-selectin glycoprotein ligand-1 (PSGL-1) is an L-selectin ligand which provides both binding motifs (McEver 2005). PSGL-1 is expressed on leucocytes and enables secondary tethering and rolling, where leucocytes tether on leucocytes already attached to the endothelium. This is thought to allow additional leucocyte recruitment when the endothelium is already covered in cells.

During T cell recruitment by endothelial cells, bonds between L-selectin and its ligands will need to form and dissociate quickly. The formation of ideal interactions between L-selectin and its ligands is dependent on shear stress provided by the blood flow. This type of interaction is called a catch bond and supports L-selectin dependant tethering and rolling (Yago et al. 2004). It is thought that the requirement for shear stress is to prevent unwanted cell adhesion in low shear environments such as sinusoids, large veins and the ascending aorta. Additionally it will prevent leucocytes binding to each other (Finger et al. 1996).

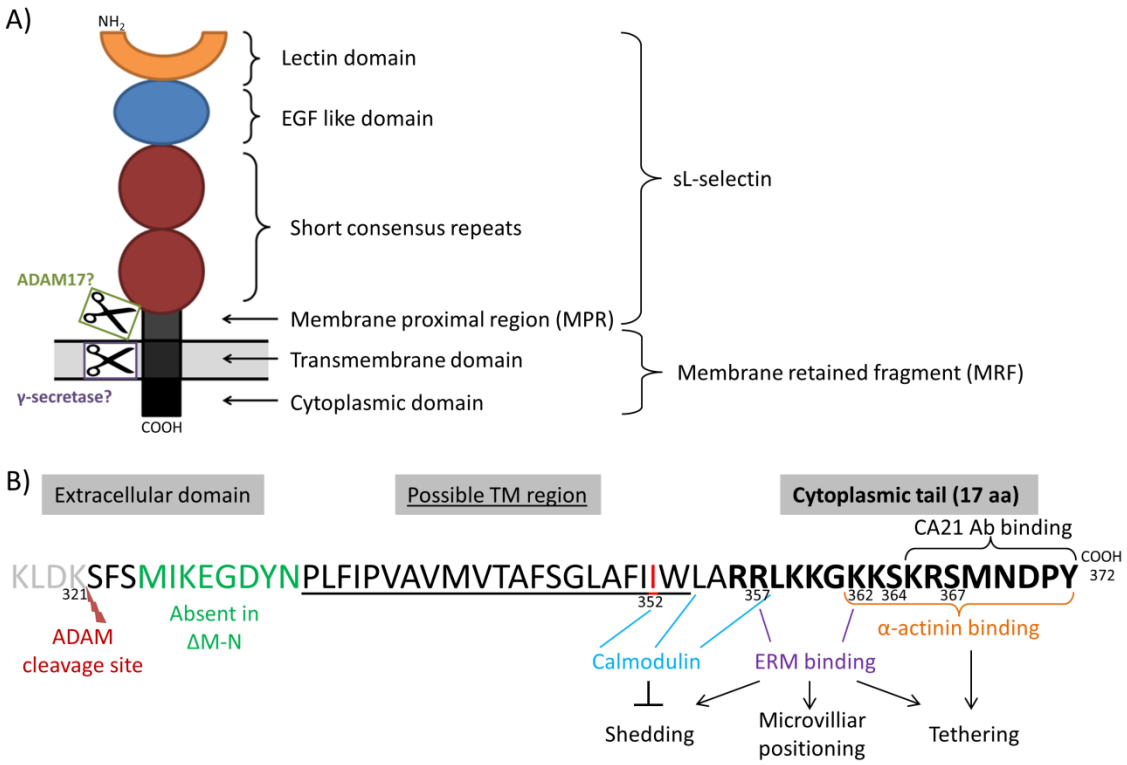

Figure 1.8: L-selectin protein and proteolytic cleavage. A) L-selectin is a heavily glycosylated type I transmembrane protein composed of an N-terminus lectin domain, epidermal growth factor (EGF) domain, two short consensus repeat (SCR) units followed by a membrane proximal region (MPR), a transmembrane domain and a 17 aa short cytoplasmic domain. Proteases implicated in L-selectin proteolysis are ADAM17 for the shedding of the extracellular fragment (sL-selectin) and γ-secretase for the regulated intramembrane proteolysis (RIPing) of the membrane retained fragment (MRF). B) The human L-selectin C-terminus aa sequence is shown. Within the extracellular domain the ADAM17 proteolytic site was identified to be between K^{321} S^{322} (red arrow) and the shed sL-selectin is shown in grey (Kahn et al. 1994). Shedding-resistant ΔM-N L-selectin contains a truncation of 8 aa (shown in green) upstream of the transmembrane (TM) domain (underlined) (Chen et al. 1995). Within the cytoplasmic tail (shown in bold), ERM proteins (purple) interact with R^{357} and K^{362} (Ivetic et al. 2002), α-actinin (orange) interacts with the COOH tail (Pavalko et al. 1995) and calmodulin (blue) interacts with I^{352}, L^{354} and L^{358} (Gifford et al. 2012). The importance of binding of these three intracellular proteins is shown for L-selectin shedding, microvillar positioning and tethering. Two possible phosphorylation sites are S^{364} and S^{367} (Steeber et al. 1997). The C-terminal 8 aa epitope for the CA21 Ab (Kahn et al. 1994) used for immunoblotting is shown. An I^{352} to K^{352} mutant (red) was generated and tested in this thesis. Adapted from (Ivetic et al. 2004).

The lectin domain is connected to an epidermal growth factor domain by a hinge region (Lou et al. 2006) giving the molecule more flexibility when contacting ligands under shear stress. Next are two short consensus repeat (SCR) units, distinguishing L-selectin from its family members E- and P-selectin which have 6 and 9 SCRs respectively.

A membrane proximal region (MPR) that is highly conserved between mouse, rat and human follows the SCRs. In 1994, phorbol-12-mystrate-13-acetate (PMA) activated cells were shown to release an extracellular fragment (sL-selectin) following a proteolytic event within the MPR, more specifically between K^{321} and S^{322} (figure 1.8 A and B) (Kahn et al. 1994). This proteolytic event leaves the cells with a 6 kDa membrane retained fragment (MRF) composed of 11 extracellular aas, 21 membrane aas and 19 intracellular aas. Shed extracellular L-selectin (sL-selectin) can be found at high concentrations in healthy human serum (1.5-2.0 μg/ml) and was shown to be able to reduce lymphocyte binding to activated endothelial cells (Schleiffenbaum et al. 1992). sL-selectin can thus be thought of as an adhesion buffer and might prevent excessive inflammation and pathology.

Small point mutations within the extracellular MPR did not alter PMA induced shedding, indicating that the protease involved recognises a conformational shape or length of the MPR rather than a specific aa sequence (Stoddart et al. 1996). This was confirmed by the inhibition of L-selectin shedding by more dramatic mutations within the MPR such as truncation of 15 aas within the MPR. Another shedding-resistant L-selectin mutation is a 8 aa truncation shown to completely abrogate constitutive and PMA-induced L-selectin shedding (Chen et al. 1995). This mutant is called ΔM-N L-selectin, and was used in this thesis (figure 1.8 B).

The first demonstration of L-selectin shedding induced by exposure to PMA was shown for mouse lymphocytes in 1990 (Jung and Dailey 1990). Additionally, L-selectin is rapidly shed from the surface of T cells after activation via the TCR (Chao et al. 1997). In a study using *in vitro* generated human tumour-specific $CD8^+$ T cells it was shown L-selectin was shed as early

as 1 h into the coculture with Mel526 melanoma target cells (Yang et al. 2011). This seemed to correlate with the accumulation of the cytolytic degranulation marker CD107a on the cell surface. Furthermore, the introduction of shedding-resistant L-selectin into a CTL cell line showed that the lytic activity of the shedding-resistant $CD8^+$ T cells was significantly lower than that of wt L-selectin expressing cells and the same was true for PMA activated cells. It was hypothesised that this was due to an altered cytoskeletal distribution in cells unable to shed L-selectin. This data together with reduced viral clearance shown in mice expressing shedding-resistant L-selectin on T cells (Richards et al. 2008) indicates that there is a possible link between granule mediated killing and shedding of L-selectin.

The intracellular tail of L-selectin has been shown to bind to intracellular proteins (figure 1.8 B). In a resting state, the tail interacts with calmodulin (Kahn et al. 1998; Gifford et al. 2012). Activation of cells by PMA leads to the dissociation of calmodulin from the cytoplasmic tail and the shedding of L-selectin, possibly due to a change in the conformation of L-selectin which causes the unmasking of the extracellular proteolytic target site (Kahn et al. 1998). Additionally, α-actinin (Pavalko et al. 1995) and ezrin and moesin (Ivetic et al. 2002) were found to bind to the intracellular tail of L-selectin. α-actinin binds to the membrane distal end of the cytoplasmic tail and connects L-selectin to the actin cytoskeleton but it is not essential for the positioning of L-selectin within microvilli (Pavalko et al. 1995). The microvilli positioning was found to depend on the ability of ezrin-radixin-moesin (ERM) molecules to bind to the membrane proximal region of the tail (Ivetic et al. 2004). ERM constitutively binds to the tail of L-selectin and abrogation of ERM binding was found to reduce PMA induced L-selectin shedding and tethering of cells on PSGL-1 (Killock et al. 2009). Two cytoplasmic serine residues (S^{364} and S^{367}) can be phosphorylated when cells are activated, however phosphorylation was not found to be essential for cells to adhere to ligand coated surfaces (Steeber et al. 1997).

In accordance with the above mentioned interactions of the cytoplasmic tail, L-selectin has been shown to not only act as an adhesion molecule, but also as a signalling molecule. *In vitro* crosslinking of L-selectin showed that outside-in signalling can activate integrins (Giblin et al. 1997; Steeber et al. 1997). Additionally, an *in vivo* homing study in mice showed reduced HEV egress of splenocytes treated with a spleen tyrosine kinase inhibitor, indicating that L-selectin is involved in outside-in signalling (Subramanian et al. 2012).

As well as by shedding of the extracellular domain, L-selectin surface expression is controlled on a transcriptional and post-transcriptional level. Experiments using mouse $CD4^+$ and $CD8^+$ T cells showed that within the first 4 h after anti-CD3 Ab stimulation up to 90% of L-selectin is shed (Chao et al. 1997). This is followed by a superinduction of L-selectin within the next 48 h leading to a 3-4 fold increase above unstimulated cells in L-selectin levels. This was found to be due to an increase in L-selectin mRNA quantity and stability. This timing corresponds with *in vivo* activation of T cells in LNs and re-expression of L-selectin 2-3 days later, when cells have exited LNs (Klinger et al. 2009). Finally, over the next 3-5 days the majority of activated T cells will almost completely lose L-selectin expression due to transcriptional silencing (Chao et al. 1997). More recent studies showed that SELL gene expression is controlled by the transcription factor (TF) Krueppel-like factor 2 (KLF2), which in turn is controlled by the TF Forkhead box protein O1 (FOXO1) (Fabre et al. 2008; Kerdiles et al. 2009). Activation of human $CD8^+$ T cells via the TCR or exposure to γ-chain cytokines such as IL-2 lead to the dephosphorylation of FOXO1, which leads to its degradation. As FOXO1 controls KLF2 expression, a reduction in KLF2 and subsequently a loss in L-selectin gene expression is observed (Preston et al. 2013). This correlates with the observation that naïve and memory T cells have high levels of KLF2. Loss of KLF2 is reversible and levels increase once stimulatory signals stop.

1.4.2 Proteolytic processing of L-selectin

To further understand the role of L-selectin and its function, it is crucial to understand its processing and regulation. As mentioned above, L-selectin is controlled at the transcriptional, post-translational and protein processing level. Further layers of L-selectin regulation are the topographic distribution of L-selectin on microvilli and the interaction with the actin cytoskeleton (Hasslen et al. 1995). It was shown that this localisation is not crucial in bringing together the protease that induces shedding and L-selectin when cells are activated with PMA (Fors et al. 2001). However, L-selectin localisation to microvilli might be of importance for tethering and rolling on endothelial cells in the blood stream as shown by abnormal rolling behaviour by lymphocytes from patient with abnormal microvilli structures in *in vitro* flow assays (Burns et al. 2010).

L-selectin shedding can be observed either constitutively to a limited extent or in response to ligand binding or cell activation to a much larger degree. Constitutive shedding might contribute to the production of sL-selectin which has been shown to function as an adhesion buffer within the plasma. However, no adverse effects were observed in mice where the levels of sL-selectin were reduced by 70% due to the shedding-resistant (LΔP) L-selectin being expressed on T cells (Galkina et al. 2007).

Inducible L-selectin shedding is mediated by two main triggers *in vivo*. Firstly, L-selectin is shed when T cells tether and roll on endothelial cells in HEVs (Faveeuw et al. 2001). In homeostatic conditions, it was shown that L-selectin surface expression on T cells is reduced by approximately 70% when cells bind to and transmigrate HEVs (Klinger et al. 2009). Additionally, this study showed that T cells within LNs express 30% of L-selectin found on cells in the blood and it is only once the T cells leave the LNs that they re-express L-selectin, giving it a cyclical expression pattern. It was found that T cells expressing only 50% of wt L-selectin levels, due to genetic modifications or T cells activated with PMA or via the TCR, showed

reduced rolling and increased rolling velocities *in vitro* and more importantly fewer cells homed to LNs *in vivo* (Galkina et al. 2007). Supraphysiological L-selectin expression did not enhance recruitment to the LNs. It was hypothesised that L-selectin shedding releases T cells and enables them to migrate from the lumen towards the basal membrane into the LN. On the other hand, more recent studies indicated that there might be a role for L-selectin shedding during TEM as L-selectin shedding was shown to take place at this stage and ligands might be present within the basal membrane (Klinger et al. 2009). *In vivo* data from shedding-resistant (LΔP) L-selectin mouse lymphocytes suggested that the lack of shedding did not inhibit constitutive lymphocyte migration (Galkina et al. 2007). However, migration of activated T cells was altered. Additionally it was shown that absence of L-selectin shedding, by using inhibitors or expression of LΔP L-selectin on lymphocytes, showed slower transmigration of HEVs with cells being 'stuck' within the HEVs for longer (Faveeuw et al. 2001; Galkina et al. 2003; Subramanian et al. 2012). Data from our lab show that LΔP $CD8^+$ T cells in mice home better to vaccinia infected ovaries than their wt counterparts as well as giving better protection in an i.p. vaccinia infection model and an intranasal influenza model (unpublished data, R. Mohammed).

Secondly, L-selectin is shed in response to Ag activation in LNs. This might lead to signalling events altering the expression of molecules involved in the mobility of the T cells out of the LNs such as sphingosine-1-phosphate receptor-1 (S1P1) (Chao et al. 1997). Loss of L-selectin on activated T cells might redirect their migration pattern from LNs to inflamed or cancerous tissue. However, a study of influenza challenged mice expressing shedding-resistant or wt L-selectin showed no differences in the recruitment of effector $CD8^+$ T cells to the site of inflammation (Richards et al. 2008).

Shedding of L-selectin was first found to be mediated by a non-soluble metalloproteinase that can cleave L-selectin in cis but not in trans (Preece et al. 1996). Further on, Peschon et al. demonstrated that the membrane-anchored metalloproteinase responsible for PMA induced

L-selectin shedding in mice was the disintegrin and metalloproteinase 17 (ADAM17), initially called TACE (TNF-α converting enzyme) for its proteolytic activity on TNF-α (Peschon et al. 1998). ADAMs are expressed in the perinuclear membrane compartments and the cell membrane and subcellular compartmentalisation is an important part of their regulation (Ager 2012). ADAMs are thought to be activated by outside-in signals.

ADAM17 is implicated in the shedding of over thirty proteins that are structurally and functionally diverse, for example TNF-α, L-selectin and the amyloid-beta precursor protein (Smalley and Ley 2005). It is thought that ADAM17 is the main sheddase involved in PMA induced shedding, although ADAM10 has been shown to be able to induce shedding in response to ionomycin but not PMA (Le Gall et al. 2009). ADAM10 was shown to be able to induce suboptimal shedding in the absence of ADAM17. Additionally, it was shown that in the absence of functional ADAM17, basal shedding of L-selectin occurs in fibroblasts (Walcheck et al. 2003) indicating a further role for ADAM10, yet fibroblasts are inherently different to T cells. Matrix metalloproteinase 1 and 3 (MMP1 and MMP-3) have been shown to also be able to cleave L-selectin and this might be the case in inflamed tissues (Preece et al. 1996).

To study the dependence of L-selectin shedding on ADAM17, multiple inhibitors are available. Low specificity metalloproteinase inhibitors such as GW280264X and GI254023X were found to preferentially inhibit ADAM17 or ADAM10 respectively (Hundhausen et al. 2003). A much more specific ADAM17 inhibitor is the D1(A12) Ab generated recently (Tape et al. 2011). It has not been shown to date whether L-selectin shedding is mediated by direct or indirect ADAM17 activity.

Once the extracellular domain of L-selectin is proteolytically released, the MRF is vulnerable to regulated intramembrane proteolysis (RIPing). Other molecules such as IL-6 and Notch have been shown to undergo ADAM17 mediated proteolysis followed by RIPing by γ-secretase (Chalaris et al. 2010). The cytoplasmic tail of Notch but not IL-6 does, once released, act as a

TF. The γ-secretase is a complex composed of 4 main subunits, with presenilin 1 and presenilin 2 being the two catalytic domains. Cleavage of the MRP is thought to occur in a stepwise manner with the γ-secretase cleaving every few amino acids. A γ-secretase specific inhibitor called DAPT has been shown to inhibit RIPing *in vitro* and *in vivo* (Dovey et al. 2001; Geling et al. 2002) and was used in this thesis.

1.4.3 L-selectin expression and ACT

In a study by Gattinoni *et al.* it was shown that early effector T cells expressing high levels of L-selectin are superior to T cells expressing low levels of L-selectin at protecting against tumour growth in mice, despite the cells expressing similar levels of activation markers and not showing any functional differences *in vitro* (Gattinoni et al. 2005). Furthermore, this paper showed that L-selectin knockout T cells were significantly worse at protecting mice against tumour growth than their L-selectin expressing counterparts. This was confirmed by unpublished mouse data from our group, where L-selectin deficient T cells gave weaker T cell protection from viral infections. These data indicate that whilst L-selectin might not have a crucial role *in vitro,* L-selectin was shown to enhance homing to LNs *in vivo*, where T cells encounter peptide loaded DCs and receive homeostatic cytokine signals (Gattinoni et al. 2005).

L-selectin could also be involved in the recruitment of T cells to tumours as many tumours have been shown to express HEVs (Martinet et al. 2011). High HEV density has been correlated with infiltration of $CD8^+$ T cells and smaller tumour size (Martinet et al. 2012), overall indicating a functional role for HEVs in recruiting immune cells. This might be partly via the L-selectin dependant recruitment of L-selectin expressing naïve and memory T cells. Additionally, it is possible that tumour blood vessels express a ligand for L-selectin, however no such reports have been published.

1.5 Genetic modifications of $CD8^+$ T cells for immunotherapy

In 1988, the first registered human gene transfer trial was run by Rosenberg *et al.* where patients' TILs were transduced with a retrovirus encoding a neomycin resistance gene and infiltration of these T cells into the tumour was studied (Rosenberg et al. 1990). A few years later, the first gene therapy trial aiming to replace the defective adenosine deaminase gene was performed in ADA-SCID children (Blaese et al. 1995). Since then over 2000 gene therapy trials have been registered with 64% of trials being in cancer patients (http://www.abedia.com/wiley/indications.php 2015) and some of these trials will have been discussed earlier.

As well as delivering genes to cells, more recently it became possible to induce targeted mutations into genes and replace faulty genes. This is achieved using programmable nucleases such as zinc finger nucleases. The latter were used in this thesis and will be discussed in more detail below. Two other types of programmable nucleases are transcription activator like nucleases (TALENs) and RNA-guided DNA endonucleases (RGENs) such as CRISPR which will be discussed further in the final discussion.

1.5.1 Discovery and design of zinc finger nucleases

Zinc finger nucleases (ZFNs) are engineered proteins composed of two separate domains; a DNA binding domain and a DNA-cleavage domain (figure 1.9 A). ZFNs have been studied for nearly 20 years and are the first members of the set of tools we now utilise for genome editing. In 2011, the year of the commencement of this study, ZFNs were named the Method of the Year by Nature Methods (2012).

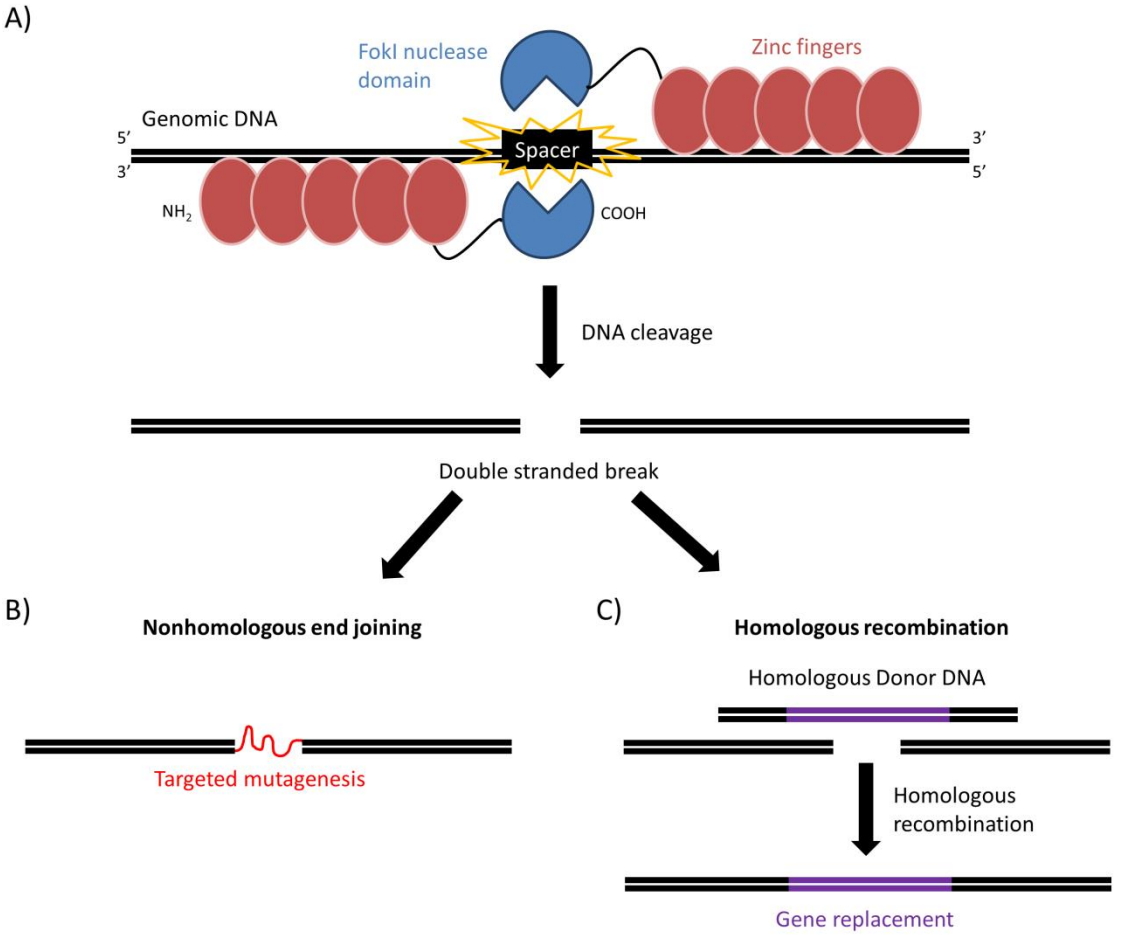

Figure 1.9: Zinc finger nucleases (ZFNs) as a tool for targeted genetic modifications. A) ZFNs are chimeric proteins composed of two main domains; the zinc finger (ZF) arrays, with each ZF (red) binding three nucleotides, and the FokI nuclease domain (blue). These two domains are connected by a short peptide linker. The catalytic FokI domain, once heterodimerised, induces double stranded breaks (DSBs). The spacer region, where the FokI nuclease domain can induce DSBs is between 5 and 7 bp long. The ZFNs shown here represent the SHP-1 specific ZFNs used in this thesis. They have a specificity of 30 bp (2 x 15 bp). B) and C) show the two different cellular responses to DSBs. B) Error prone non-homologous end joining (NHEJ) is executed by, amongst others, the DNA IV ligase. The repair of the DSB results in error-free repair or more commonly in the introduction of deletions, insertions or base substitutions (red), leading to loss-of-function mutations. C) Cells can fix DSBs by recombining homologous DNA (purple) within the region of the DSB. Delivering ZFNs and homologous donor DNA can thus be used to repair faulty genes or introduce new genes.

The nuclease domain was isolated from the type IIS *Flavobacterium okeanokoites* restriction endonuclease (FokI), which cleaves DNA outside of its recognition sequence. The FokI endonuclease is composed of a distinct DNA-cleaving domain and a separable DNA-binding

domain. It was shown that the FokI catalytic domain cleaves target DNA independently of the DNA-binding domain (Li et al. 1992). The same group showed that the DNA binding domain of FokI could be replaced with the DNA-binding domain of other molecules without altering the nuclease activity (Kim and Chandrasegaran 1994; Kim et al. 1996).

An example of such DNA-binding proteins are zinc finger proteins (ZFPs) which, due to their modular structure, are attractive for the design of DNA specific chimeric nucleases. ZFPs are made up of an array of Cys_2His_2 zinc fingers, each made up of approximately 30 aas with a ββα architecture and an ability to bind a single zinc atom. The crystal structure of a ZFP-DNA complex shows that each ZF interacts with three consecutive nucleotides (Pavletich and Pabo 1991) and these contacts are made by the alpha or recognition helix (Jantz et al. 2004). Slight variations in key aas give different fingers their specificity.

In 1996, ZFNs were for the first time shown to cleave DNA *in vitro* (Kim et al. 1996) and in 2001 it was shown that ZFNs can cleave DNA assembled into chromatin (Bibikova et al. 2001). The first ZFN was designed *de novo* to recognise a target gene in *Drosophila* (Bibikova et al. 2002). ZFNs are ideal for targeted gene editing as they introduce DSBs into usually inert DNA. DSBs are both mutagenic and recombinagenic. DSBs are dangerous to the cell as they can lead to cell cycle arrest, translocations, carcinogenesis and apoptosis. Therefore the cell is geared up to quickly repair the double helix by either non-homologous end joining (NHEJ) or homologous recombination (figure 1.9 B and C). (Wyman and Kanaar 2006)

NHEJ is an error prone mechanism wherein the cell fixes the DSB by inserting, deleting or substituting nucleotides (figure 1.9 B). Small insertions and deletions (indels) can lead to frameshifts in the coding region and transcript degradation by nonsense mediated decay. Thus ZFNs are used to generate 'loss of function' mutations by inducing NHEJ. ZFNs are able to bind and cut the target sequence until the possible mutations abrogate the binding site for either of

the two ZFNs. However, mutations can also abrogate the ZFN binding site while being in-frame.

Homologous recombination is a complex, high fidelity DNA repair mechanism requiring a >400-500 bp homologous sequence of DNA (figure 1.9 C). Briefly, DNA homologous to a DNA sequence close to the DSB recombines with the genomic DNA and is inserted (Isalan 2012).

To induce DSBs optimally, it was shown that the FokI nuclease domain needs to dimerise, either as a heterodimer or as a homodimer (Bitinaite et al. 1998; Smith et al. 2000). To reduce possible off-target effects, the FokI domain was modified to make it preferentially work as a heterodimer, thus doubling the degree of sequence specificity (Miller et al. 2007). In the study by Miller *et al.*, off-target effects were reduced from 18.9% to 1.7%. ZFNs encompassing 4-6 ZFs are thought to be ideal as anything shorter will be too unspecific whereas anything longer could start binding to non-specific sequences. Additionally, the sequence and length of the peptide linker, connecting the ZFP and the FokI nuclease, is crucial in determining the efficiency with which the ZFNs work and in determining the distance between the two FokI domains (Bibikova et al. 2001; Handel et al. 2009; Shimizu et al. 2009). Commercially available ZFNs have a short linker (approximately 6 aa), restricting the nuclease activity to a 5-7 bp spacer region (figure 1.9 A).

Multiple steps are taken during the ZFN design process. To avoid off-target effects, the genome is searched using algorithms for unique sequences. For example, Sigma-Aldrich in combination with Sangamo Biosciences, a company designing, testing and selling ZFNs will only accept ZFN binding sequences that differ from any other sequence by a minimum of 4 nucleotides. Regions of repeated sequence, single nucleotide polymorphisms and splice variants are generally avoided. Statistically, to generate ZFNs binding to a unique sequence in the genome, a recognition sequence of 16 bp or more is required. However not all DNA can be targeted successfully and compact chromatin structure and epigenetic DNA modifications such

as methylation add to the challenge of designing functional ZFNs (Carroll 2011). It was calculated that a functional ZFN pair can be designed for approximately every 100 bp of DNA (Kim et al. 2009).

Initially, it was thought that combining any ZFs will yield a functioning ZFP. However it has been found that ZFs can statically hinder each other and that each new combination of ZFs needs to be empirically tested. Sigma-Aldrich use a dual module assembly strategy where modules of two ZFs from a library are combined with other ZF modules and tested for functionality (Moore et al. 2001). Major efforts have been made to characterise combinations of ZFs that will work in combination but no formal rules for the combination of ZFs have been identified yet (Sander et al. 2011).

1.5.2 ZFN delivery

Multiple ZFN delivery methods have been trialled in cell culture, murine embryos and whole organisms (Ain et al. 2014). The safest methods for ZFN delivery are so called 'hit-and-run' methods, where ZFN proteins are expressed for a short time period and ideally no genetic material is inserted into the host genome. ZFNs can be delivered to cells in several forms; purified proteins, mRNA, plasmid DNA or encoded in viral vectors. Here the mechanisms for ZFN delivery to human T cells will be discussed but with emphasis on lentiviral transduction as lentiviral ZFN delivery was chosen in this thesis. This was based on lentiviral transduction being a commonly used method of gene delivery and expertise in lentiviral delivery of genes to primary T cells being available within Cardiff University.

The most recently developed and possibly safest delivery method is the direct delivery of purified ZFN proteins to cells (Gaj et al. 2012). This study showed that unmodified purified ZFN proteins have an intrinsic ability to cross cell membranes. In a range of human cells, including

primary $CD4^+$ T cells this induced mutation levels comparable to transient transfection with plasmid DNA. However, toxicity was observed in $CD4^+$ T cells when treated with high doses of ZFN protein. Additionally, it was shown that direct protein delivery reduced the off-target effect, probably by reducing ZFN half-life as ZFN degradation was observed within <4 h for protein delivery compared to 16-72 h for plasmid DNA delivery. A more recent report from the same group showed that including nuclear localisation signals within the ZFN increased the efficacy of delivery 13 fold and that there was little toxicity in primary T cells and haematopoietic stem cells (Liu et al. 2015). Additionally, two pairs of ZFNs could be delivered simultaneously and induce mutations simultaneously at two genetic loci.

Electroporation, nucleofection and liposome transfection methods are widely used to deliver plasmid DNA (Holt et al. 2010) and mRNA (Urnov et al. 2005). Due to safety considerations, mRNA delivery is preferable to DNA plasmid delivery as it avoids possible integration of the ZFNs genes into the genome.

Non-integrating viruses such as adenovirus and adeno-associated virus (AAVs) have been used to deliver ZFNs *in vitro* (Provasi et al. 2012) and *in vivo* (Li et al. 2011). Adenovirus transduction was shown to be transient with ZFNs being detected for no more than 3 days post-infection.

Integrase-deficient lentiviral vectors (IDLVs) have shown successful gene targeting in human primary T cells with mutation rates of up to 13% (Lombardo et al. 2007; Provasi et al. 2012). Additionally, IDLVs have been used to deliver ZFNs to human stem cells, but only a very low frequency (<0.1%) of cells showed homologous recombination. Hence, not many groups have used this method, possibly due to low success rates.

Integrase-proficient LV delivery is routinely used for the delivery of a variety of genes such as TCRs to T cells and can be used to deliver ZFNs (Provasi et al. 2012). However, LV delivery carries two major risks; increased off-target effects due to continuous ZFN expression and

potential tumourigenic integration. Integrase proficient LV delivery would thus not be a therapeutic option.

1.5.3 ZFNs and therapeutic use in humans

While TALENs and CRISPR are easier and quicker to use in many settings, ZFNs seem to be a safer option for now for therapeutic settings. Some key clinical applications in humans will be described below.

The basis for the first clinical trial using ZFN modified cells was the generation of CCR5 knockout $CD4^+$ T cells using a CCR5 specific ZFN pair delivered by adenovirus or nucleofection (Perez et al. 2008). Additionally, ZFN mediated knockout of CCR5 was achieved in haematopoietic stem cells, giving the possibility of this technique being used for bone marrow transplants in the future (Holt et al. 2010). The rationale behind the ZFN mediated CCR5 knockout is that loss of the HIV-1 co-receptor, CCR5, in a subpopulation (11-28%) of $CD4^+$ T cells renders these cells more resistant to HIV-1 infection. The first clinical trial giving HIV-1 patients *in vitro* ZFN modified autologous $CD4^+$ T cells has now finished and was deemed safe for all 12 patients studied (Tebas et al. 2014). Additionally, phase II clinical trials are underway and research is being undertaken into the use of CCR5 modified haematopoietic stem cells by Sangamo BioSciences.

As well as knocking out genes, ZFNs can be used to correct monogenetic diseases by employing the cell's homologous recombination repair mechanism. For this purpose, a ZFN pair and a donor DNA sequence, encoding for the corrected gene, are delivered to the host cell. Previous clinical trials in X-linked severe immunodeficiency (SCID) patients showed correction of the defective IL-2 receptor γ-chain gene in haematopoietic stem cells using retroviral delivery. However, two patients developed T cell leukaemia (Hacein-Bey-Abina et al. 2003). This was

due to the activation of an oncogene, LMO2, by the integration of the LTR-flanked IL-2 receptor γ-chain gene cassette. To avoid this potential eventuality, different groups have used ZFNs introducing targeted DSBs either into the faulty gene itself (Urnov et al. 2005; Yusa et al. 2011) or into a safe harbour locus (Merling et al. 2015). One such 'safe harbour' is the AAVS1 locus. AAVS1 has an open chromatin structure and most importantly it is flanked by insulator elements, thus avoiding the potential activation or disruption of neighbouring oncogenes or tumour-suppressor genes.

Of interest for human cancer therapy is a study that showed the feasibility of knocking out α and β chains of the endogenous TCR prior to lentiviral transfer of a tumour-Ag specific TCR (Provasi et al. 2012). The elimination of the endogenous TCR decreased the off-target effects of auto-reactive cells seen in cells expressing both endogenous and exogenous TCR. Additionally, enhanced target cell killing was observed. In this study, the most successful combination of gene delivery was done in two cycles of adenoviral delivery of the ZFN pairs specific for either the α or β chain, followed by cell sorting of $CD3^-$ cells and LV transduction of either the α or β TCR gene. This study proved the feasibility of multiple genetic manipulations, including transient ZFN expression in T cells.

1.5.4 Lentiviral vector gene delivery

Lentiviral vectors (LVs) are members of the *Retroviridae* family and are commonly used to deliver genes for research. Furthermore, lentiviral gene delivery has been used in over 101 clinical trials, representing 4.7% of all gene therapy trials (http://www.abedia.com/wiley/vectors.php 2015). There are several reasons why LVs are particularly good vectors for gene delivery. Firstly, LVs can carry up to approximately 8 kb of transgenic DNA (De Meyer et al. 2006). Secondly, LVs are able to transduce both dividing and

quiescent cells. Thirdly, LVs show low immunogenicity compared to AAVs for *in vivo* gene delivery. Additionally, LVs can stably integrate and provide prolonged gene expression. (Wanisch and Yanez-Munoz 2009)

In the early 1990s, groups started using replication-deficient vectors derived from human immunodeficiency virus type 1 (HIV-1) to transduce $CD4^+$ cells with antibiotic resistance to show their potential for gene delivery (Poznansky et al. 1991; Shimada et al. 1991). By including heterologous envelope proteins, LVs can be pseudotyped to change the vector tropism from $CD4^+$ cells to a more broad range of cells. One such protein with a broad tropism for phospholipids is the vesicular stomatitis virus G glycoprotein (VSV-G) and VSV-G pseudotyped LV was used in this thesis. It has recently been shown that VSV-G pseudotyped LV does not transduce quiescent T cells due to the lack of expression of the VSV-G receptor, low-density lipid receptor, in unstimulated T cells (Amirache et al. 2014). In cytokine stimulated T cells, receptor expression is upregulated thus allowing for efficient LV transduction. Once the LV enters the cell and membrane fusion occurs, single stranded RNA (ssRNA) is converted into double stranded DNA (dsDNA) by the reverse transcriptase delivered by the LV. The dsDNA is then imported to the nucleus and the transgene stably integrated into the host genome and this will enable persistent expression of the transgene. Depending on the promoter chosen for driving the expression of the transgene, cell type specific gene expression can be achieved. In this thesis, the spleen focus-forming virus (SFFV) or the human elongation factor (EF)-1α promoters were used to drive expression of transgenes from LV made using transfer vectors pSxW and pELN, respectively.

One major concern about using HIV-1 based gene therapy is the generation of pathogenic virus. To avoid this, replication-deficient HIV-1 based LV is generated by transfection of packaging cells (human embryonic kidney 293T cells) with three or four distinct plasmids (2^{nd} or 3^{rd} generation LV, respectively). These plasmids only encode genes essential for structural

proteins and enzymes involved in infection, namely *gag, pol* and *rev* (Zufferey et al. 1998). The *gag* genomic region encodes for capsid proteins, the *pol* region encodes for the reverse transcriptase and other essential enzymes. *Rev* encodes a phosphoprotein whose main function is to bind viral mRNA, export it from the nucleus to the cytoplasm and enable translation. By dividing the viral genes among two or three different plasmids, safety is enhanced due to the increased number of recombination events needed to produce wild-type virus. The only genetic material that will be packaged within the virion will be that from the transfer vector, expressing the transgene together with a ψ packaging sequences. To further enhance biosafety, a mutation in the 3' long terminal repeat (LTR) was generated to eliminate the endogenous enhancer activity associated with the LTR of the transfer vector (Zufferey et al. 1998). This mutation led to a tighter control of transgene expression, now mediated solely by the exogenous promoter. Additionally, it reduced the interference of the LTR with genes in the proximity of the integration site, thus lowering the risk of insertional mutagenesis.

As well as the transgene and the ψ sequence, the transfer vector may also encode the *Rev* responsive element (RRE), the Woodchuck post-transcriptional regulatory element (WPRE) and the central polypurine tract (cPPT). The RRE enables *Rev* to bind and thus promotes nuclear export and utilisation of the mRNA. The WPRE placed downstream of the transgene enhances transgene expression on a posttranscriptional level (Higashimoto et al. 2007). The cPPT has been proposed to enhance nuclear import of the transgene and thus enhance transduction (Van Maele et al. 2003).

LVs have been mapped to preferentially integrate within active genes located in the proximity of the nuclear membrane (Marini et al. 2015). Overall, LV integration site selection seems more favourable than that of other viruses as promoter regions are not usually targeted (Papayannakos and Daniel 2013). Nevertheless, integration of transgenes bears the risk of insertional mutagenesis. Considering this risk and the fact that not all gene therapy requires

prolonged expression of the transgene (e.g.: ZFNs), integrase-deficient LVs (IDLVs) have been developed. These IDLVs express deficient integrase protein due to mutations within the integrase gene such as the D64V mutation, used in this thesis (Yanez-Munoz et al. 2006). IDLV transduction has shown a reduction in integration of 3-4 logs compared to LV and is thus comparable to plasmid transfections (Leavitt et al. 1996). Transduction of cells with IDLV leads to the accumulation of double-stranded episomal DNA in the nucleus. Thus in dividing cells such as T cells, the transgene will be diluted out after a certain number of cell divisions, whereas in non-dividing cells such as hepatocytes, the transgene will persist for longer.

In order to detect and/or select cells transduced with LV, surface markers, antibiotic resistance genes or fluorescent proteins can be included into the transgene cassette. To generate these transgene cassettes encoding for more than one protein, different methods can be used. Internal ribosomal entry sites (IRES) can be used to direct ribosomes to initiate translation at internal sites of mRNAs. However, this leads to heterogeneous levels of gene expression of genes placed upstream or downstream of the IRES. Another downside of IRES sequences is that they are large at approximately 500 bp in lengths. An alternative method to express multiple proteins that avoids these issues is the use of 2A ribosomal skipping peptides. These are 18-22 aa sequences first discovered in foot-mouth disease virus (Ryan et al. 1991) that give stoichiometric expression of multiple proteins from a single mRNA. During translation, the ribosome skips the glycine-proline peptide bond and thus two separate proteins arise from a single mRNA. This leaves the upstream protein with a C-terminal tail of approximately 18 aas and the downstream protein with a short (approximately 2 aas) N-terminal aa addition. 2A ribosomal skipping elements were used in the generation of transfer vectors in this thesis.

1.6 Hypotheses and aims of the thesis

Work in this thesis was based on two main hypotheses.

1. Human SHP-1 deficient $CD8^+$ T cells are superior to SHP-1 sufficient $CD8^+$ T cells for ACT, due to the loss of SHP-1 leading to a decreased threshold for T cell activation and an increased proportion of tumour-specific cells entering proliferation. This is based on studies with SHP-1 deficient T cells from *motheaten* mice.

To test this hypothesis, the main aims were to:

- Generate SHP-1 deficient human T cells using ZFNs.
- Compare SHP-1 deficient and SHP-1 sufficient T cells for functional differences in *in vitro* experiments.
- Compare SHP-1 deficient and SHP-1 sufficient human $CD8^+$ T cells for differences in *in vivo* ACT experiments.

2. Continuous expression of L-selectin on activated human T cells can enhance their recirculation to LNs, where survival signals are provided, and possibly to tumours, thus enhancing their anti-tumour effect for ACT.

To test this hypothesis more needed to be known about the impact of continuous expression of L-selectin in human T cells. Thus in this thesis the aims were to:

- Generate human T cells expressing wt and shedding-resistant L-selectin under an exogenous promoter.
- Study the mechanism and signalling downstream of L-selectin shedding in response to TCR activation.

Chapter 2: Materials and Methods

2.1 Reagents and consumables

2.1.1 Antibiotics

Carbenicillin and Kanamycin were purchased from Sigma-Aldrich (St. Louis, USA) and reconstituted to 50 mg/ml in dH_2O, sterile filtered through a 0.45 μm syringe filter and stored at -20°C and freeze thawed no more than three times. Carbenicillin was used at a final concentration of 60 μg/ml and Kanamycin was used at a final concentration of 50 μg/ml.

Penicillin and Streptomycin were purchased from Gibco LifeTechnologies (Paisley, UK) and used at 100 IU/ml and 100 μg/ml, respectively and stored at -20°C.

Geneticin (G418 disulphate salt) (Sigma-Aldrich) was reconstituted to 250 mg/ml in PBS, stored at -80°C and used at 500 μg/ml.

2.1.2 Cell culture media and supplements

Roswell Park Memorial Institute medium 1640 (RPMI 1640), Dulbecco modified Eagle's minimal essential media (DMEM +4.5 g/L D-Glucose, +L-Glutamine) and all cell culture supplements were purchased from Gibco LifeTechnologies. Unless otherwise stated, all cell culture medium was supplemented with penicillin (100 IU/ml), streptomycin (100 μg/ml) and sodium pyruvate (1 mM). Additionally, RPMI 1640 was supplemented with L-glutamine (2 mM). 0.05% Trypsin-EDTA was used to dissociate adherent cells.

Cells were routinely grown in 10% fetal calf serum (FCS) from LifeTechnologies or Sigma-Aldrich. FCS was heat inactivated for 30 min at -56°C and aliquots were kept at -20°C. Hepes buffered solution was added at a final concentration of 10 mM to cell culture medium to prevent pH fluctuations. Phosphate buffered saline (PBS) was sterilised by autoclaving.

2.1.3 Chemical reagents

Chemicals were purchased from Fisher Scientific (Loughborough, UK), unless otherwise stated.

Dimethyl sulphoxide (DMSO) was bought from Sigma-Aldrich.Phorbol 12-myristate 13-acetate (PMA) (Sigma-Aldrich) was reconstituted to 10 mM in DMSO and stored at -20°C. The broad spectrum metalloproteinase inhibitors, GW280264X (GW) and GI254023X (GI), (Hundhausen et al. 2003), were a gift from GSK (Stevenage, UK). Stocks of GW and GI were reconstituted to 10 mM in DMSO and stored at -20°C. DAPT (N-[N-(3,5-difluoro-phenacetyl)-L-alanyl]-S-phenylglycine t-butyl ester, ALX-270-416) was purchased from Enzo, Life Sciences (Exeter, UK), reconstituted to 5 mM in DMSO and stored at -20°C.

Phytohaemagglutinin (PHA) (ThermoScientific, Oxoid, Waltham, USA) was reconstituted to 1 mg/ml in dH_2O and stored at -80°C.

2.1.4 Cytokines

Recombinant human IL-15 (rhIL-15) and IL-2 (rhIL-2) were purchased from Peprotech (Rocky Hill, USA) and the University Hospital Wales Pharmacy (Cardiff, UK), respectively. RhIL-2 was produced by Novartis (Basel, Switzerland). RhIL-15 stocks were made up to 25 µg/ml in dH_2O and 0.1% FCS and rhIL-2 was made up to 20,000 U/ml in dH_2O and aliquots stored at -80°C.

2.1.5 Distilled water (dH_2O) and ultrapure water (ddH_2O)

A Millipore (Billerica, USA) reverse osmosis system in combination with a Millipore Milli-Q filtration through two ion exchange columns was used to obtain dH_2O or ddH_2O, respectively. For cell culture, dH_20 was sterilised by autoclaving.

2.1.6 Peptides

The SLYNTVATL peptide used to activate T cells expressing the gag TCR was purchased from Eurofins (Luxembourg, Luxembourg), reconstituted to 5 mM in DMSO and stored at -80°C. The EAAGIGILTV peptide used to activate T cells expressing the Mel TCR was purchased from Severn Biotech (Kidderminster, UK), reconstituted to 5 mM in DMSO and stored at -80°C.

2.1.7 Plastics and tissue culture plastics

All tissue culture flasks (T25, T75 and T175), multiwell plates (6, 24, 48 and 96) and stripettes were purchased from Nunc ThermoScientific. Falcon tubes were purchased from Corning (Corning, USA). Syringes were purchased from BD (Franklin Lakes, USA). Millex-HP filters (0.45 μm and 0.22 μm) were purchased from Millipore.

2.2 Molecular biology

2.2.1 Restriction endonuclease digestion

To restrict up to 20 μg of DNA in a 50 μl reaction, 1 μl of each restriction endonuclease (NEB, Ipswich, USA) was used along with 5 μl of 10x buffer, selected according to the manufacturer's instructions. The restriction digestion was incubated for 1 h at 37°C before being analysed by gel electrophoresis or stored at -20°C.

2.2.2 Gel electrophoresis

Agarose gel was prepared by adding 0.5-2.5% of UltraPure Agarose (w/v) (Invitrogen) (table 2.2) and ethidium bromide solution (final concentration of 0.5 μg/ml) to 1x TBE buffer (table 2.1). The solution was heated in a microwave until all agarose was dissolved and the gel was poured into Peqlab gel electrophoresis tanks (VWR, Darmstadt, Germany). The DNA sample

was mixed 2:1 with either bromophenol or 6x Orange Gloading buffer (table 2.1) and up to 25 µl of DNA/loading buffer mix and 1-2 µl of the 1 kb Plus DNA (Invitrogen) or Hyperladder I (Bioline, London, UK) were added to the gel. A 120 V electric voltage was applied for 30-100 min (table 2.2). To visualise and record gel electrophoresis results, a UV transilluminator (UVP, Upland, USA) was used.

Buffer	Composition and preparation
1x TBE	0.45 M Tris, 0.45 M Boric acid, 10 mM EDTA pH 8.0
Bromophenol loading buffer	3.6 mM bromophenol blue and 1.2 M sucrose in dH_2O
6x Orange G loading buffer	0.25% Orange G (w/v) and 30% glycerol (v/v) in dH_2O

Table 2.1: Buffers used for gel electrophoresis.

DNA size	% agarose (w/v)	Time of 120 V electrophoresis
100-1000 bp	2.5%	30-60 min
>1 kbp	1%	60-100 min
Multiple fragments >2 kbp	0.7-0.5%	60-90 min

Table 2.2: Electrophoresis settings for differently sized DNA fragments.

2.2.3 Polymerase chain reaction (PCR)

Distinct DNA polymerases were used for different PCR reactions.

The proof-reading high-fidelity DNA polymerase, Phusion (NEB), was used in combination with the high-fidelity (HF) Phusion buffer and $MgCl_2$. Aliquots of 100 mM dATP, dCTP, dGTP and dTTP (NEB) were stored at -20°C and discarded after one use. All four nucleotides were mixed 1:1:1:1 before being added to the PCR reaction. The standard composition of the PCR reaction is indicated in table 2.3. Most PCR reactions had to be optimised by varying the concentrations

of primer, template DNA, $MgCl_2$ and DMSO. Primers (tables in the appendix A1-3) were designed using CLC DNA Workbench software, purchased from Eurofins and diluted to 100 pmol/µl in Tris-EDTA (TE) buffer. PCR cycling conditions are indicated in table 2.4 and a T Personal (Biometra, Goettingen, Germany) or a Peltier DNA Engine Dyad thermo cyclers was used. The annealing temperature for each primer pair was determined using the Tm temperature calculators on the NEB website.

The 'ready-to-use' PCR Supermix (LifeTechnologies) contained the non-proofreading *Taq* polymerase and was used for Cel-I assays (section 2.2.7).

Component	**Volume**	**Final Concentration**
dH_20	Up to final volume of 50 µl	/
5x Phusion HF buffer	10 µl	1x
dNTPs (100 mM each)	2 µl	100 µM
Forward primer (10 pmol/µl)	1.25 µl	0.25 µM
Reverse primer (10 pmol/µl)	1.25 µl	0.25 µM
Template DNA	X µl (corresponding to 5 ng to 30 ng)	0.1 ng/µl to 0.4 ng/µl
50 mM $MgCl_2$	1.5 µl	1.5 mM
DMSO (only for hard to amplify template DNA)	1 µl to 3 µl	1% to 3%
Phusion DNA polymerase	0.5 µl	0.02 U /µl

Table 2.3: Composition of a standard PCR reaction using the Phusion polymerase.

Cycle step	Cycle name	Temperature	Time
1	Initial denaturation	98°C	30 s
2	Denaturation	98°C	10 s
3	Annealing	X°C	20 s
4	Extension	72°C	25-30 s
5	Final extension	72°C	6 min
6	Pause	4°C	hold

Table 2.4: Cycling conditions for a standard PCR using the Phusion polymerase. Cycle steps 2 to 4 were repeated 35 times.

2.2.4 Isolation of PCR products and DNA from agarose gels

PCR product was purified using a PureLink Quick PCR purification kit (Invitrogen) by following the manufacturer's protocol. A QIAquick gel purification kit (Qiagen, Venlo, Netherlands) was used to purify DNA from agarose gels and the manufacturer's instructions were followed.

2.2.5 DNA cloning using the In-Fusion enzyme

An In-Fusion cloning kit (Clontech, Mountain View, USA) was used to clone PCR amplified DNA into linearised plasmid vector. The In-Fusion enzyme induces homologous recombination between linearised vectors and PCR products expressing homologous 3' and 5' ends (figure 2.1). The manufacturer's protocol was followed when designing primers. Briefly, primers had a 5' 15 bp homology with the linearised vector and a 3' 18-25 bp homology with the gene of interest.

An In-Fusion reaction was set up as described in table 2.5. A negative control reaction was set up omitting the PCR product to check for spontaneous religation of the linearised vector. The mix was incubated at 50°C for 15 min before 1-2 µl were used to transform DH5α cells.

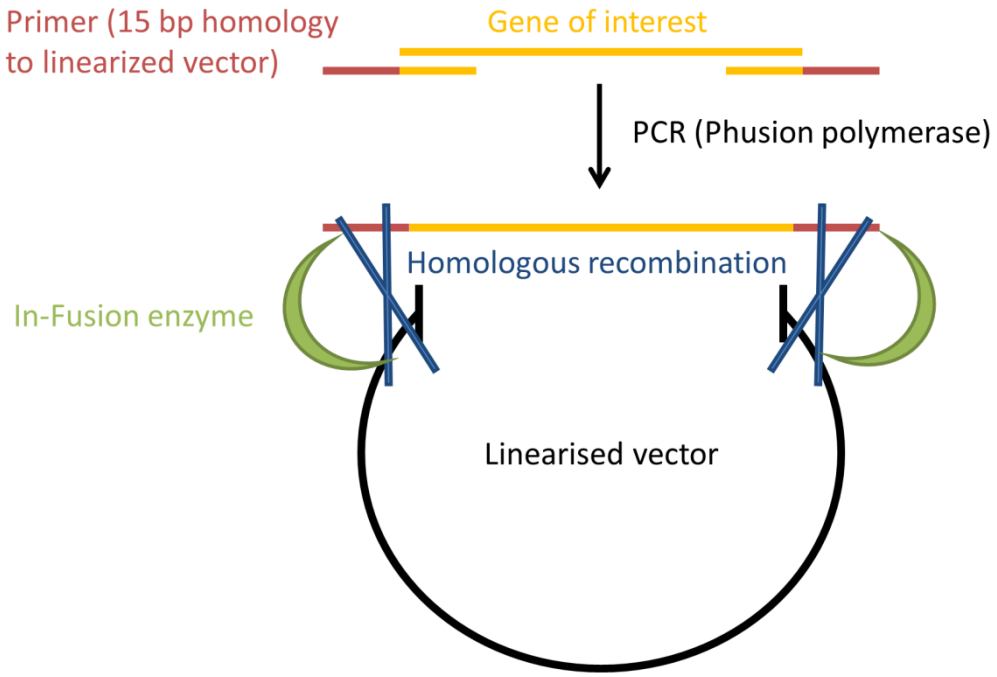

Figure 2.1: Recombination of DNA using the In-Fusion enzyme. Primers were designed, according to Clontech's instructions, to have a 5' 15 bp homology (red line) with the linearised vector (black open circle) and a 3' 18-25 bp homology (orange) with the gene of interest (orange). The Phusion DNA polymerase was used to amplify the gene of interest, the PCR product purified and an In-Fusion reaction set up. Incubation at 50°C for 15 min led to homologous recombination (blue crosses) of the PCR product and the linearised vector mediated by the In-Fusion enzyme (green).

Component	Sample	Negative control
5x In-Fusion HD enzyme premix	2 µl	2 µl
Linearised plasmid vector	180-200 ng	180-200 ng
Insert (PCR product)	80-100 ng	none
dH_2O	Up to final volume of 10 µl	Up to final volume of 10 µl

Table 2.5: Composition of an In-Fusion cloning reaction.

2.2.6 *In vitro* site-directed mutagenesis

Site-directed mutagenesis was used to eliminate the KpnI site in the pUC-ZFN1-T2A-GFP plasmid and to introduce the I-K mutations into the L-selectin gene. The PfuTurbo DNA polymerase (Stratagene, La Jolla, USA) was used to amplify the pUC-ZFN1-T2A-GFP plasmid using mutagenic primers number 17 and 18 (table A1) or the pLenti-L-selectin-P2A-CD2 plasmid using primers 64 and 65 (table A3). The PfuTurbo polymerase PCR reaction and the cycling conditions are shown in table 2.6 and 2.7. After confirmation of the success of the PCR reaction by gel electrophoresis and PCR product purification, parental methylated DNA was restricted by incubation with 1 µl DpnI restriction endonuclease at 37°C for 1 h. DH5α cells were transformed with 2 µl of the purified restriction digestion product and plasmids were sequenced to establish the successful introduction of the I-K mut.

Components	**Volume per reaction**
dH_20	Up to 50 µl
10x Pfu turbo DNA polymerase reaction buffer	5 µl
dNTPs (100 mM each)	1 µl of each dNTP
Primer 17 (10 pmol/µl)	1 µl
Primer 18 (10 pmol/µl)	1 µl
DNA template pUC-ZFN1-T2A-GFP	Volume corresponding to 12.5 ng
PfuTurbo DNA polymerase (2.5 U/µl)	1 µl

Table 2.6: Composition of a PCR using the PfuTurbo DNA polymerase.

Cycle step	Cycle name	Temperature	Time
1	Initial denaturation	95°C	30 s
2	Denaturation	95°C	30 s
3	Annealing	55°C	60 s
4	Extension	68°C	5 min
5	Final extension	68°C	5 min
6	Pause	4°C	hold

Table 2.7: Cycling conditions for a PCR using the PfuTurbo DNA polymerase. Steps 2-4 were repeated 12 times.

2.2.7 Cel-I mismatch assay

The Cel-I mismatch assay was used to detect mutations in the SHP-1 gene of cells expressing ZFNs. Genomic DNA (gDNA) was extracted from cells using the GenElute Mammalian genomic DNA Miniprep kit (Sigma-Aldrich) and the 398 bp SHP-1 region of interest was amplified by PCR using 300 ng of gDNA and 20 µl of Supermix polymerase and primers 55 and 56 (table 2.8, 2.9 and A1). To check for DNA contamination, a negative control PCR reaction was set up omitting gDNA. Gel electrophoresis (1% agarose gel) was used to confirm the presence of a 398 bp PCR product.

Component	Volume
Supermix	20 µl
Primer 55 (10 pmol/µl)	1.25 µl
Primer 56 (10 pmol/µl)	1.25 µl
gDNA	X µl (corresponding to 300 ng)

Table 2.8: Composition of a PCR reaction using Supermix for the Cel-I assay.

Cycle step	Cycle name	Temperature	Time
1	Initial denaturation	94°C	2 min
2	Denaturation	94°C	30 s
3	Annealing	55°C	22 s
4	Extension	72°C	1 min
5	Final extension	72°C	3 min
6	Pause	4°C	hold

Table 2.9: Cycling conditions for a PCR reaction using Supermix for the Cel-I assay. Cycle steps 2 to 4 were repeated 29 times.

Next, 15 µl of the PCR product were mixed with 5 µl of sterile, nuclease-free dH_2O and the mix of wt and possibly mutant PCR product was hybridised by heating and slow cooling using a thermocycler (table 2.10). The 20 µl of hybridised PCR product was mixed with components of the SURVEYOR Mutation detection kit (Transgenomic, Omaha, USA), more precisely 1 µl Cel-I nuclease, 1 µl enhancer S and 2 µl of $MgCl_2$. The reaction was incubated at 42°C for 60 min. The presence of Cel-I digested PCR product, thus mutant SHP-1, was detected by resolving 18 µl of the Cel-I assay product on a 2.5% agarose gel. As a negative control, 5-10 µl of non-digested PCR product was also resolved.

The approximate % of mutant SHP-1 product was determined by densiometry using ImageJ software. The intensities of the undigested band (398 bp) and the two Cel-I digestion bands (220 bp and 178 bp) were obtained as shown in figure 2.2. The following formula was used to determine the approximate % of cells expressing mutant SHP-1 alleles:

$$cut\ products \Big/ (cut + uncut\ product) \Big/ 2 * 100.$$

Cycle step	Temperature	Rate of temperature change	Time
1	95°C	-2°C/s	10 s
2	85°C	-0.3°C/s	1 min
3	75°C	-0.3°C/s	1 min
4	65°C	-0.3°C/s	1 min
5	55°C	-0.3°C/s	1 min
6	45°C	-0.3°C/s	1 min
7	35°C	-0.3°C/s	1 min
8	25°C	-0.3°C/s	1 min
9	4°C	none	Hold

Table 2.10: Cycling conditions for the hybridisation of the 398 bp SHP-1 PCR product for the Cel-I assay.

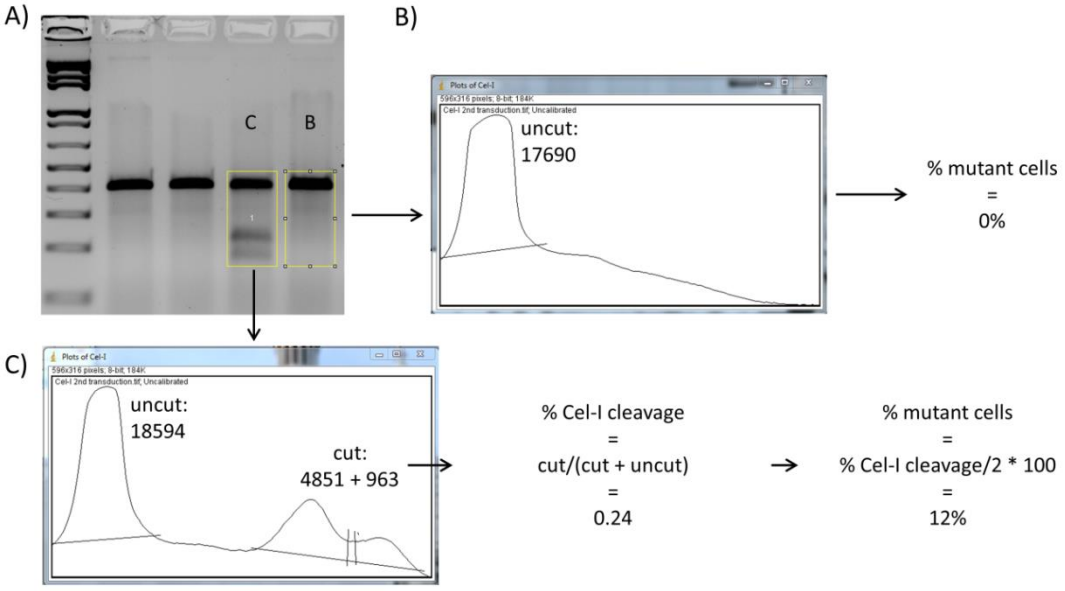

Figure 2.2: Analysis of the % of cells expressing mutant SHP-1 alleles using ImageJ software analysis of the Cel-I assay. A) Gel electrophoresis image showing a Cel-I digest of SHP-1 PCR product from untransduced (B) or ZFN LV transduced (C) cells. B) Densiometry plot of the area of interest encompassing both the undigested 398 bp and the Cel-I digested 220 bp and 178 bp DNA fragments. The intensity of the non-digested fragment is shown in terms of the area above the horizontal line (17,690). C) Densiometry plot of the same-sized area of interest as in B. The intensity of the undigested (18594) and the two Cel-I digested fragments (4851 and 963) is shown as well as the calculations used to get the final % of cells expressing mutant SHP-1 alleles.

2.2.8 *Escherichia coli* growth, transformation and clonal selection

Competent DH5α *Escherichia coli (E.coli)* cells (Invitrogen, Carlsbad, USA) were stored at -80°C in 50 µl aliquots. DH5α cells were transformed following the manufacturer's guidelines. Briefly, 1-10 ng of plasmid DNA was added to 50 µl of freshly thawed DH5α cells, cells incubated on ice for 10 min before cells were heat shocked for 20 s at 42°C. Cells were incubated in 1 ml of LB broth (table 2.11) for one h at 37°C and 90-110 rpm in an orbital shaker incubator (Gallenkamp), before being plated onto antibiotic selection agarose plates containing either Carbenicillin or Kanamycin (table 2.11). Plates were incubated overnight at 37°C. Colonies with antibiotic resistance were picked and grown in 5-400 ml of LB broth containing antibiotic. Plasmid DNA was extracted from bacteria using the PureLink Quick plasmid Miniprep kit (Invitrogen) for up to 10 ml cultures or the PureLink HiPure plasmid filter Maxiprep kit (Invitrogen) for up to 400 ml cultures by following the manufacturer's instructions. The Sorvall Evolution centrifuge and the SLA-3000 rotor (ThermoScientic) were used for centrifuging samples for the Maxiprep kit plasmid extraction. Bacterial colonies were screened by restriction digestion of the plasmid DNA and gel electrophoresis was used to visualise the DNA digestion pattern. Plasmid DNA purity (A260/280 ratio >1.8) and concentration was measured using the ND-1000 NanoDrop^{TM} spectrophotometer (ThermoScientific).

Buffer or broth	Composition and preparation
LB broth	1% bacto-tryptone (w/v), 0.5% bacto-yeast (w/v), 0.17 M NaCl, adjusted to pH7 and sterilized by autoclaving.
LB agar	LB broth with 1.5% of agar (w/v), autoclaved and cooled down to 50°C before addition of antibiotics. Approximately 30 ml were poured into Petri dishes and left to settle at room temperature before storing at 4°C.
Glycerol freezing buffer	65% glycerol (w/v), 0.1M MgSO4 and 0.23 M Tris pH 8.0

Table 2.11: Buffers and broths used for *E. coli.* growth and storage.

2.2.9 *E. coli* storage

To store bacteria, densely grown bacteria in LB broth were mixed 1:1 with glycerol freezing buffer (table 2.11) and stored at -80°C.

2.2.10 TA cloning

The pGEM-T Easy Vector system from Promega was used to perform TA cloning in order to establish the nature of the SHP-1 mutations within cloned cells. The manufacturer's protocol was followed. Briefly, the 398 bp SHP-1 sequence encompassing both ZFN binding sites was PCR amplified from gDNA extracted from clones. The PCR product was column purified and a ligation was set up with 20 ng of purified PCR product, 50 ng pGEM-T Easy vector and 3 Weiss units of T4 DNA ligase and incubated at 4°C overnight. Next, bacteria were transformed with 1-2 µl of ligation mix as described previously and bacteria plated on selection plates (LB agar plates with carbenicillin, 0.5 mM IPTG and 80 µg/ml X-Gal) and incubated at 37°C overnight. 8-16 white colonies were picked and for each clone, bacteria amplified and plasmid extracted using a Miniprep kit as described previously. Plasmids were restriction digested with EcoRI to check for the presence of a SHP-1 insert and positive plasmids were sent to be sequenced using the T7 and SP6 primers (table A2). 70% of the TA cloning was performed by an intercalating BSc student Adam Clark, Cardiff University.

2.2.11 DNA sequencing

To verify the DNA sequences of all cloned plasmids, sequencing was conducted by the Cardiff University Central Biotechnology Services (Cardiff, UK) or using the Smart Seq service from Eurofins. Sequencing primers were purchased from Eurofins and all sequencing primers used are shown in tables A2 and A3 in the appendix.

2.2.12 Origin of transgenes

The HIV gag TCR specific for the immunodominant HLA-A*02 restricted SLYNTVATL peptide was first described in 2008 (Varela-Rohena et al. 2008) and Jurkat and MOLT-3 cells expressing the gag TCR were provided by Dr John Bridgeman (Cardiff University, UK).

The LV packaging plasmid encoding the Mel TCR, also called MEL5, was provided by Dr John Bridgeman (Cole et al. 2009). The Mel TCR recognises the HLA-A*02 restricted $MART_{126-135}$ peptide (EAAGIGILTV).

The truncated rat CD2 (called rCD2 or CD2 throughout this thesis) (He et al. 1988) was provided in a plasmid from Dr John Bridgeman.

The SHP-1 specific ZFNs were designed and purchased from Sigma-Aldrich (CKOZFN1061-1kt).

Plasmid encoding the non-haematopoietic SHP-1 cDNA isoform (NCBI accession code BC002523) was purchased from ThermoScientific (MGC Human PTPN6 Sequence-Verified cDNA, clone 3140265).

2.3 Tissue culture and LV transduction

2.3.1 Cell lines

Cell culture of cell lines

All cells were grown in a humidified atmosphere at 37°C and 5% CO_2 in a HERA cell Hereaus incubator. The Jurkat, MOLT-3, C1R, Mel526, Mel624 and HEK293T cells lines were kindly provided by Dr John Bridgeman.

Leukaemic cells were routinely grown in R10 medium (table 2.12), split every 3 days and never grown above a density of 1.5 x 10^6 cells/ml. Jurkat 3 T3.5 cells, lacking TCR expression due to a

mutation in the TCR β chain, were lentivirally transduced with the GLuciferase NFAT reporter cassette and were cultured in R10 supplemented with 500 µg/ml of G418.

HEK293T, Mel526 and Mel624 cells were cultured in D10 medium (table 2.12). Cells were split once they reached 80% confluency. Cells were washed with PBS, 0.05% Trypsin-EDTA solution was added and cells incubated for up to 5 min at 37°C before D10 was added and cells pelleted using a Heraeus Megafuge 4R (ThermoScientific) at 1500 rpm (491 g) for 5 min.

Medium	**Composition**	**Use**
R10 (complete RPMI)	RPMI 1640 (4.5 g/L glucose), 10% FCS, 2 mM L-Glutamine, 100 IU penicillin, 100 µg/ml streptomycin and 1 mM sodium pyruvate	Culture of Jurkat, MOLT-3 and C1R cells
R20	RPMI 1640 (4.5 g/L glucose), 20% FCS, 2 mM L-Glutamine, 100 IU penicillin, 100 µg/ml streptomycin and 1 mM sodium pyruvate	$CD8^+$ T cells on day of isolation
R1	RPMI 1640, 1% FCS and 10 mM Hepes	L-selectin shedding experiments
R2	RPMI 1640 (4.5 g/L glucose), 2% FCS, 2 mM L-Glutamine, 100 IU penicillin, 100 µg/ml streptomycin and 1 mM sodium pyruvate	Peptide activation of T cells
Primary T cell stimulation medium	R10, 15 x 10^6 irradiated PBMCs from three different donors, PHA (1 µg/ml), rhIL-2 (20 IU/ml) and rhIL-15 (25 ng/ml)	Stimulation of $CD8^+$ T cell expansion
Complete DMEM (D10)	DMEM (4.5g/L glucose and 4.0 mM L-Glutamine), 10% FCS, 100 IU penicillin, 100 µg/ml streptomycin and 1 mM sodium pyruvate	Culture of HEK293T, Mel526 and Mel624 cells

Table 2.12: Composition of cell culture media.

Cell cloning of cell lines

To obtain leukaemic T cell clones, cells were resuspended in R10 at 1.25 cells/ml and 5 to 10 96 U-bottom well plates were plated with 200 µl of cells in R10 per well. Plates were incubated and inspected weekly for clonal colonies. Medium was changed once the culture medium had changed colour. Cells were expanded by transferring them into gradually increasing volumes of culture medium.

LV transduction of cell lines

Leukaemic T cells were transduced with LV by plating 1 x 10^6 PBS washed cells in a 24 well plate and adding up to 1 ml of R10, polybrene (4 µg/ml) and varying volumes of LV. Cells were incubated for 24 h before the medium was replaced with fresh R10 and cells grown as normal. Mel526 and Mel624 cells were transduced by growing cells to 80% confluency in D10 in a 24 well plate and by following the same protocol as described above using D10 instead of R10. Control cells were incubated with R10 or D10 and polybrene only. Cells were routinely analysed for transgene expression 72 h post transfection unless otherwise stated.

2.3.2 Culture of human umbilical vein endothelial cells (HUVEC)

HUVEC cells were grown in EGM-2 basal medium (Lonza, Basel, Switzerland) supplemented with fetal bovine serum and eight other supplements and growth factors provided in the EGM-2 SingleQuot supplement and growth factor kit (Lonza). Medium was incubated for 30 min at 37°C and 5% CO_2 before addition to cells. Cells were grown to 80%-90% confluency before splitting.

2.3.3 Peripheral blood monocyte cell (PBMC) isolation

PBMC isolation

PBMCs were isolated from fresh blood taken from healthy donors, with their consent, or from buffy coats obtained from the Welsh Blood Service (Pontyclun, UK). Fresh blood was diluted 1:1 with PBS 5 mM EDTA to prevent clotting. Fresh blood and buffy coats were diluted 1:1 in PBS and 30 ml were carefully layered on top of a 15 ml Ficoll gradient (Lymphoprep, Alere Limited, Cheshire, UK). The samples were centrifuged at 2000 rpm (872 g) for 20 min. The breaks on the centrifuge were deactivated to not disturb the gradient. The layer of PBMCs was removed using a plastic Pasteur pipette, cells washed in PBS and centrifuged at 1200 rpm (314 g) for 10 min. Red blood cells (RBC) were lysed by adding 5 ml of 1x RBC lysis (BioLegend, San Diego, USA) buffer for 5 min on ice. Cells were washed once more in PBS before being resuspended in R10 medium and counted.

Irradiation of feeder cells

For the generation of feeders for primary T cell cultures, PBMCs originating from three donors were exposed to 30 Gy (3000 rad) of radioactivity from a Caesium^{137} source in a Gammacell 1000 Elite Blood Irradiator (MDS Nordion, Ottawa, Canada), cells washed once and resuspended in T cell medium.

2.3.4 Primary CD8$^+$ T cell isolation, LV transduction and stimulation

CD8$^+$ T cell isolation from PBMCs by magnetic cell isolation and cell separation (MACS)

Primary CD8$^+$ T cells were isolated from PBMCs by following the human CD8 Microbeads MACS Miltenyi isolation protocol (Bergisch Gladbach, Germany). Briefly, 10 µl of CD8 Microbeads were added per 10^7 PBMCs in MACS buffer (PBS, pH 7.2, 0.5% BSA, 2 mM EDTA) and cells incubated for 15 min at 4°C. Cells were washed in 1-2 ml of MACS buffer per 10^7 cells and centrifuged at 1200 rpm (314 g) for 8 min. Cells were resuspended in MACS buffer and added

onto a MS MACS column inserted into a MACS magnet. Unlabelled cells were washed off the column by three MACS buffer washings before dissociation of the column from the magnet and collection of $CD8^+$ T cells. A small proportion of cells was used to check for the purity of the sort by flow cytometry. The remaining $CD8^+$ T cells were incubated overnight in R20 medium (table 2.12) at 1 x 10^6 cells/ml (figure 2.3).

$CD8^+$ T cell transduction with LV

The following day, cells were washed, counted and plated in 48 well plates at 1 x 10^6 cells in 1 ml/well of R10 medium supplemented with rhIL-2 (30 IU/ml) and 4 µg/ml of polybrene. Cells were activated with 25 µl of a human T-Activator CD3/28 Dynabeads (LifeTechnologies) and LV was added at volumes indicated in the corresponding experiments. Cells were incubated for two days, before starting the T cell stimulation cycle.

$CD8^+$ T cell stimulation and culture

LV transduced cells were collected, washed and resuspended in 12 ml of T cell stimulation medium (table 2.12) in a T25 flask and the flask incubated at a 45° angle. Medium was replaced 3-4 days later as indicated in figure 2.3, depending on the extent of cell growth. One week post stimulation, 11 ml of medium was removed and replaced with 12 ml R10 medium supplemented with high rhIL-2 (200 UI/ml) and rhIL-15 (25 ng/ml). Cells were grown for an additional one or two weeks and medium was exchanged if the colour of the medium had changed. At this point, cells were analysed by flow cytometry, used for experiments or a new stimulation cycle was started. For this, 1 x 10^6 cells were incubated at in 12 ml of stimulation medium in a T25 flask.

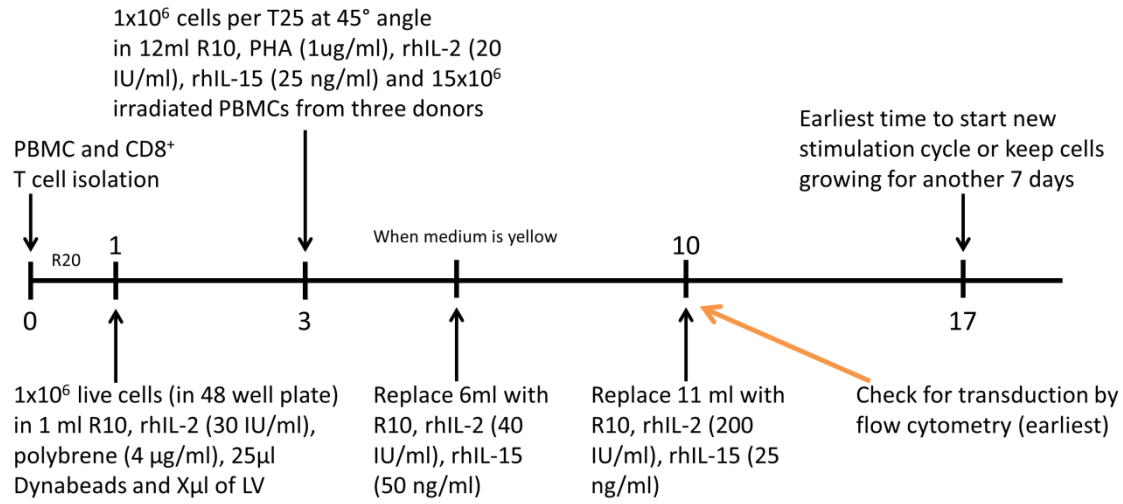

Figure 2.3: Primary CD8$^+$ T cell transduction and stimulation cycle.

2.3.5 Cryopreservation of cells

Cells were pelleted and resuspended in freezing buffer (60% FCS, 10% DMSO in RPMI 1640) at 1-6 x 10^6 cells/ml and added to cryo-vials. The latter were placed into Nalgene 5100 cryo freezing containers (Merc Laboratory Supplies, Dorset, UK) and stored at -80°C for up to 48 h before being transferred to liquid nitrogen storage tanks.

When cells were thawed from cryopreservation, vials were added to a 37°C water bath and once thawed, rapidly added into preheated R10 or D10 medium, pelleted by centrifugation at 1200 rpm (314 g) for 5 min and placed into culture.

2.4 Cell based techniques

2.4.1 Cell counting by trypan blue exclusion

Cells were mixed 1:1 with trypan blue (ThermoScientific) and live cells were counted using a haemocytometer (Hausser Scientific, Horsham, USA), based on the exclusion of trypan blue positive cells.

2.4.2 $CaCl_2$ transfection of HEK293T cells, LV production and LV quantification

LV was generated by $CaCl_2$ transfection of HEK293T packaging cells with either three or four distinct plasmids (2^{nd} or 3^{rd} generation of LV, respectively). The 2^{nd} generation transfer vector, pSxW, was used in combination with pMD29 and pCMVΔ8.91 or pCMVΔR8.74intD64V to generate integrase sufficient or integrase deficient LV, respectively (Demaison et al. 2002; Yanez-Munoz et al. 2006). The third generation transfer vector pELN was used in combination with pRSV.Rev, pVSV-G and pMDLg/pRRE (Richardson et al. 2008). All plasmids were resistant to ampicillin.

A $CaCl_2$ transfection protocol described below was used to produce LV and to transfect HEK293T cells with plasmids expressing ZFNs. Briefly, HEK293T cells were plated at 15-20 x 10^6 cells in 20 ml D10 medium in a T175 flask. After 24 h, medium was removed, 12 ml of pH 7.9 medium (table 2.13) added and 3 ml of transfection mix, made up with pH 7.1 medium, added carefully (table 2.13). The latter contains 30 µg of pSxW, 30 µg of pCMVΔ8.91/pCMVΔR8.74intD64V and 15 µg of pMD29 or 15 µg of pELN, 18 µg of pRSV.Rev, 7 µg of pVSV-G and 18 µg of pMDLg/pRRE for the generation of 2^{nd} or 3^{rd} generation LVs, respectively. After 24 h, medium was removed and replaced with 20 ml fresh D10. 48 and 72 h post transfection, medium was collected, replaced with 20 ml fresh D10 and both supernatant collections passed through a 0.45 µm filter and stored at 4°C. Pooled supernatant was added to 38.5 ml Beckmann Coulter (Brea, USA) thin walled centrifugation tubes placed into a Beckman Coulter SW28.1 rotor and centrifuged in a Beckman Coulter Optima L-100 XP Ultracentrifuge at 24,000 rpm for 2 h at 4°C. After centrifugation, supernatant was discarded, the pellet resuspended in 3.5 ml (10x LV concentration) or 0.35 ml (100x LV concentration) of R10 or D10 medium, aliquoted and snap frozen on dry-ice and stored at -80°C until use.

Medium	Composition	Use
pH 7.1 medium	DMEM, 25 mM Hepes, pH adjusted to pH 7.1. Filtered through a 0.22 µm filter.	Plasmid transfection of HEK293T
pH 7.9 medium	D10, 25 mM Hepes, pH adjusted to pH 7.9. Filtered through a 0.22 µm filter.	Plasmid transfection of HEK293T
Transfection mix	All plasmids in a final volume of 3 ml in pH 7.1 medium with a final $CaCl_2$ concentration of 50 mM.	Plasmid transfection of HEK293T

Table 2.13: Composition of media used for the $CaCl_2$ transfection of HEK293T cells.

2.4.3 LV quantification

To quantify the LV preparations, a Lenti-X p24 rapid titre ELISA kit (Clontech Laboratories) was used according to the manufacturer's instructions. All p24 ELISAs were kindly done by Dr Paul Michell (Cardiff University). LV preparations to be tested were lysed using Triton X-100 (Sigma-Aldrich).

2.4.4 Flow Cytometry

Ab staining for live and fixed cell analysis

2 x 10^5 cells/sample were resuspended in 100 µl PBS and stained with 1/1000 diluted AmCyan live/dead fixable stain (Invitrogen) for 30 min at 4°C. Cells were centrifuged, stained with Abs diluted to a final volume of 25 µl FACS buffer (PBS, 0.1% FCS) and incubated for 20 min at 4°C (table 2.14). Cells were washed in FACS buffer, centrifuged and fixed in 100 µl of 4% paraformaldehyde in PBS (ThermoScientific) for 15 min at room temperature. For analysis of live cells, cells were not fixed and the viability of cells was determined by adding Pacific Blue Cytox blue dead stain (Invitrogen) at a final dilution of 1/10000 to the cells prior to flow cytometric analysis. Finally, cells were resuspended in 200 µl FACS buffer and analysed on a BD FACS Canto II.

Tetramer staining of T cells

Tetramers were used to determine the frequency T cells expressing the Mel TCR. The high affinity FLTGIGIITV (FLT) tetramer (5.1 µM) and the lower affinity ELAGIGLTV (ELA) tetramer (18 µM) were used (Ekeruche-Makinde et al. 2012). To generate PE-conjugated tetramer, the final volume of Streptavidin-PE (LifeTechnologies) (15.8 µl Streptavidin per 10 µg of monomer) was divided into 5 doses and one dose added was added every 20 min to the monomer (provided by Dr Matt Clement and Andrea Schauenburg, Cardiff University), on ice. Cells were stained with live/dead stain, washed and incubated with 40 µl FACS buffer containing Dasatinib at a final concentration of 50 nM (Axon Medchem, Groningen, Netherlands) for 30 min at 37°C. 0.04-1 µg of tetramer was added to each well and cells were incubated for 15 min at 37°C. Next, 10 µl FACS buffer containing Abs was added (table 2.14) and cells incubated for 20 min at 4°C, before fixation. If cells were stained for FASC or MACS sorting, the tetramer incubation step was done at 4°C for 30 min to prevent T cell activation.

Compensation

Compensation was done using Abc anti-mouse compensation beads (LifeTechnologies) labelled with the individual Abs used in the experiment. To compensate the live/dead stain, ArC reactive beads were labelled with 2 µl of AmCyan live/dead stain stock solution. Beads were incubated for 20-30 min at 4°C, washed and centrifuged. Beads were resuspended in 200 µl FACS buffer and a drop of negative beads was added. Electronic compensation was done either using the BD Diva programme or FlowJo.

Cell counting using Cytocount beads by flow cytometry

Cytocount beads (Dako, Glostrup, Denmark) were used according to the manufacturer's protocol to count cell populations by flow cytometry. Briefly, 20 µl of cytocount beads were added by reverse pipetting to 200 µl of cells in FACS buffer prior to analysis using the BD Facs

Canto II. The formula used to enumerate cells from the flow cytometry plots was: $number\ of\ cells\ of\ interest / number\ of\ beads * bead\ concentration * dilution\ factor\ of\ sample.$

Specificity	Conjugate	Clone name (isotype)	Company name, product code (#)	Dilution
CD62L/ L-selectin (human)	PE	Dreg56 (IgG1, κ)	eBioscience, #12-0629-42	1/50
Isotype control	PE	P3.6.2.8.1 (IgG1, κ)	eBioscience, #12-4714-82	1/50
CD19 (human)	APC	HIB19 (IgG1, κ)	BD Pharmigen, #555415	1/25
Isotype control	APC	11711 (IgG1, κ)	R&D Systems, #IC002A	1/25
CD3 (human)	FITC	HIT3a (IgG2a, κ)	BD Pharmigen, #555339	3/25
Isotype control	FITC	20102 (IgG2a, κ)	R&D Systems, #IC003F	3/25
TCR V beta 5a	FITC	1C1 (IgG1, κ)	Thermo Scientific, #TCR2642	1/25
Isotype control	FITC	MOPC-31C (IgG1, κ)	BD Pharmigen, #550616	1/25
CD8α (human)	APC	RPA-T8 (IgG1, κ)	BioLegend, # 301014	1/50
CCR7 (human)	PE-Cy7	3D12 (IgG2a, κ)	BD Biosciences, # 557648	1/50
CD69 (human)	APC	FN50 (IgG1, κ)	BioLegend, # 310910	1/25
CD69 (human)	PE	FN50 (IgG1, κ)	BioLegend, # 310906	1/25
rCD2	PE	MCA154 (IgG2a, κ)	Serotec, #MCA154PE	1/10
rCD2	PE	OX-34 (IgG2a, κ)	BioLegend, #201305	1/100
Isotype control	PE	MOPC-173 (IgG2a κ)	BioLegend, #400212	1/100
rCD2	FITC	OX-34 (IgG2a, κ)	BioLegend, #201303	1/100
HLA-A2 (human)	FITC	BB7.2 (IgG2b)	AbD Serotech, #MCA2090F	1/50

Table 2.14: Antibodies used for flow cytometry. Dilution of Ab is shown for 0.2-1 x 10^6 cells. FACS buffer was used as a diluent.

2.4.5 Fluorescence activated cell sorting (FACS)

LV transduced T cells were stained with tetramer and Ab as described in section 2.4.4, not fixed, and filtered through a 70 µm cell strainer. Cells were run on a modified FACSAria II flow cytometer (BD Biosciences) by Dr Kristin Ladell or Kelly Miners (Cardiff University). After sorting, cells were added to prewarmed medium, centrifuged and cultured.

2.4.6 Magnetic cell isolation and cell separation (MACS)

LV transduced T cells were stained with PE conjugated tetramer or Ab as described in section 2.4.4 and cells incubated with anti-PE Microbeads (Miltenyi) as described in the manufacturer's protocol and in section 2.3.4. After sorting, cells were added to prewarmed medium, centrifuged and cultured.

2.5 Protein analysis

2.5.1 Immunoblot

Lysis of cells for L-selectin, ZFN and SHP-1 immunoblotting

For lysis, cells were collected, washed in PBS, counted and pelleted at 1-2 x 10^6 cells/well. To the pelleted cells, 35 µl of the complete lysis buffer was added and cells incubated for 30 min on ice. One Roche complete ULTRA Tablet (Basel, Switzerland) as well as a final concentration of 1 mM Sodium orthovanadate and 1.8 mg/ml 1,10 Phenanthroline was added to 10 ml of lysis buffer (25 mM Hepes pH 7.4, 150 mM NaCl, 10 mM $MgCl_2$, 1 mM EDTA, 2% glycerol, 1% Triton X-100) for the detection of L-selectin and V5 tagged and 3xFlag tagged ZFN proteins. For the detection of SHP-1 protein, the same lysis buffer was used but other protease inhibitors were added (10 µg/ml Aprotinin, 10 µg/ml Leupeptin, 10 µg/ml Pepstatin A, 1 mM EDTA and 1 mM Phenylmethylsulfonyl fluoride). Cells were centrifuged at 1500 rpm for 5 min and 15 µl of

supernatant added to 15 µl of 2x reducing buffer (660 mM Tris-HCl pH 6.8, 26% glycerol (v/v), 2.1% SDS (w/v), 0.01% bromophenol blue (w/v), 5% β2-mercaptoethanol (v/v)). This was stored at -20°C or used immediately.

SDS-polyacrylamide gel electrophoresis

Proteins were resolved using NuPAGE Novex 4-12% Bis-Tris gels (Invitrogen) and a XCell SureLock Mini Cell system (Invitrogen) filled with 1x MES SDS running buffer (Invitrogen) according to the manufacturer's protocol. Cell lysates were boiled for 5 min at 95°C and centrifuged at 1500 rpm for 5 min and the supernatant was added to the Bis-Tris gel. 10 µl of SeeBlue Plus 2 prestained protein standard (LifeTechnologies) was added as a protein ladder. The gels were resolved at 200 V for approximately 35 min or 60 min for SHP-1 protein resolution. For the 60 min running time, cooling elements were placed around the gel tank.

Immunoblotting

0.2 µm Immobilon-PSQ PVDF membrane (Millipore) and filter papers were soaked in dH_2O, followed by pure methanol and finally 1x transfer buffer (1x NuPAGE transfer buffer (Invitrogen), 10% or 20% methanol (v/v)) for 1, 1 and 10 min respectively. Electrophoresis gels were removed from their casing and added to transfer sandwiches according to Invitrogen's instructions. The protein transfer was done at 30 V for 60 min.

Immuno-detection of proteins

The PVDF membrane was removed from the blotting sandwich and incubated with blocking buffer (PBS, 5% non-skimmed milk) for 1 h at room temperature. All incubations were done on a rocker. To probe for L-selectin, ZFN or SHP-1 proteins, the membrane was incubated with blocking buffer containing primary Ab (table 2.15) overnight at 4°C. The following day, the membrane was washed 3x 10 min in washing buffer (PBS, 0.05% Tween 20) and the membrane incubated for 1 h in blocking buffer. Secondary Ab (table 2.15) was added to the blocking

buffer and incubated for 1 h before the membrane was washed 3x 10 min with wash buffer. In a dark room, the membrane was covered in SuperSignal West Pico Chemiluminescence developing solution (1:1 mix of Peroxide and Luminol/enhancer, ThermoScientific) and incubated for 1 min, before the liquid was drained and the membrane sealed in a cling film sleeve. Photographic film (GE Healthcare, Little Chalfont, UK) was exposed to the membrane for the indicated amount of time (10 s to 30 min) and the films developed using a Compact X2 Processor (X-Ograph Ltd, Wiltshire, UK).

Specificity	**Origin**	**Concentration**
V5 tag	Sigma-Aldrich, monoclonal mouse	1/2500
HRP-conjugated 3xFlag tag	Sigma-Aldrich, monoclonal mouse	1/2500
SHP-1, SH2 domain	Polyclonal rabbit antiserum made by Dr James Matthews	1/1000
L-selectin (CA21), cytoplasmic domain	Monoclonal mouse IgG, (Kahn et al. 1994)	1/400
Actin	Sigma-Aldrich, monoclonal rabbit	1/3000
GAPDH	Sigma-Aldrich , monoclonal mouse	1/3000
Secondary HRP-conjugated anti rabbit IgG (H +L)	BioRad, monoclonal goat	1/2500
Secondary HRP-conjugated goat anti-mouse IgG (H+L)	BioRad, monoclonal goat	1/2500

Table 2.15: Abs used for the detection of proteins by immunoblotting.

2.5.2 Luciferase assay

Luciferase protein in the supernatant was measured using the BioLux GLuciferase assay (NEB) by following the manufacturer's instructions. Briefly, the BioLux assay buffer was mixed with the substrate at a 100:1 ratio and 25 µl added to each well of a white walled half-area 96 well plate (Corning). 5 µl of culture supernatant was added quickly to each well and a FLUOstar Optima spectrometer (BMG Labtech, Offenburg, Germany), set to read luminescence, used to read the GLuciferase activity.

2.6 *In vitro* functional assays

2.6.1 Leukaemic T cell activation

For L-selectin shedding experiments, cells were incubated in R1 medium (table 2.12) and for other experiments R2 medium was used.

PMA activation of leukaemic T cells

1 x 10^6 gag^+ MOLT-3 or Jurkat cells were resuspended in 100 µl/well of medium supplemented with PMA (SIGMA, USA) or equivalent volumes of DMSO in 96 well U-bottom plates and incubated at 37°C, 5% CO_2 for 30 min, unless otherwise stated. The final concentration of PMA was 300 nM and 500 nM for MOLT-3 and Jurkat cells, respectively, unless otherwise indicated. To study the effect of shedding inhibitors, cells were incubated at 37°C, 5% CO_2 in R1 medium containing the indicated concentrations of GW or GI for 30 min or D1(A12) Ab for 60 min, before PMA was added to the medium. DMSO and IgG Ab were used as negative controls respectively. Cells were washed in cold PBS and stained with live/dead marker, anti-L-selectin Ab and if indicated, anti-CD69 or anti-TCRV5β Ab for flow cytometry (table 2.14). Stocks of ADAM-17 specific inhibitory Ab D1(A12) (Tape et al. 2011) were kept at 10 µM at -80 °C. The %

of L-selectin expression was calculated relative to DMSO treated cells, after subtracting the isotype or FMO MFI from all samples:

$$\%L-selectin = 100 * \frac{MFI\ sample - MFI\ isotype\ or\ FMO}{MFI\ untreated\ cells - MFI\ isotype\ or\ FMO}$$

Cognate peptide and CD3/28 Dynabead activation of leukaemic T cells

CD3/28 Dynabeads were used to induce L-selectin shedding for immunoblot analysis. Briefly, 25 µl of washed Dynabeads were incubated with 1 x 10^6 T cells in 100 µl/well of medium in a 96 well U-bottom plate for 1 h, before cells were centrifuged and lysed as described in section 2.5.1.

L-selectin shedding and TCR downregulation in response to cognate peptide stimulation were studied using SLYNTVATL peptide to activate gag TCR expressing cells and EAAGIGILTV to activate MEL TCR expressing cells. T cells and HLA-$A2^+$ C1R APCs were rested overnight in R2 medium (table 2.12) at 0.9 x 10^6 cells/ml. The following day, C1R cells were resuspended to 5 x 10^5 cells/ml in R2 medium, in the presence or absence of SLY or EAA peptide (10^{-4} M to $10^{-}8$ M) and 100 µl of the cells added into wells of a 96 well U-bottom plate. All peptide concentrations were set up in triplicates and cells were incubated for 1 h at 37°C before being washed once in R2 medium. MOLT-3 or Jurkat cells were added in 100 µl of 1.5 x 10^6 cells/ml in R2 medium, giving a final 3:1 ratio of effector:target cells. The cells were incubated for 1 h at 37°C, washed and stained with Abs for flow cytometry. To study the effect of shedding inhibitors, T cells were preincubated with GW, GI or D1(A12) for 30 min or 60 min, respectively and T cells in the R2 medium containing the inhibitors added to washed C1R cells in no medium.

NFAT Jurkat cell activation

Jurkat cells were rested overnight in R2 medium. The next day, 1 x 10^5 cells were incubated in 100 µl/well D10 medium with PMA/Ionomycin (81 nM / 669 nM), PHA (1 µg/ml) or equivalent volumes of DMSO in a 96 well U-bottom plate. 1 x 10^5 Jurkat cells were incubated with the equivalent of 1:1, 3:1 and 5:1 E:T ratios of Mel526 and Mel624 cells in a final volume of 100 µl D10. All conditions were set up in duplicates and cells incubated for 18 h at 37°C. Cells were centrifuged, the supernatant collected for the luciferase assay (section 2.5.2) and cells stained for flow cytometry.

2.6.2 CFSE dilution assay

CFSE was kept at a stock concentration of 5 mM at -20°C. Single cell suspensions was of unstimulated and stimulated MOLT-3 and Jurkat cells were prepared and resuspended at up to 4 x 10^6 cells/ml in PBS 0.1% FCS. A 2x working solution of CFSE (1 µM) in PBS 0.1% FCS was added to cells at a 1:1 ratio and cells mixed by pipetting. Cells were incubated for 10 min at 37°C in the dark. To quench the reaction, 1ml of ice cold R10 medium was added and cells left on ice for 5 min before centrifugation. Cells were washed twice in R10, counted and incubated at 0.7 x 10^6 cells per well in 1 ml R10 medium in a 48 well plate. To determine the level of staining at day 0, 2 x 10^5 of the labelled cells were fixed and analysed by flow cytometry. Cells from one well per condition were thereafter collected every 24 h, fixed and analysed by flow cytometry. Due to the frequent division of the leukaemic cells, cells were split every 2-3 days at a 1:3 ratio.

2.6.3 Killing assay using primary $CD8^+$ T cells and Mel526 cells

On day 0, 200 µl/well of 4 x 10^6 cells/ml RFP-$GLuciferase^+$ Mel526 cells were plated in D10 medium in a 96 flat-bottom well plate and primary $CD8^+$ T cells rested in R10 medium without cytokines. The following day, $CD8^+$ T cells were counted and resuspended in R10, rhIL-2 (20

IU/ml) and 10 mM Hepes. The D10 medium was removed from the Mel526 cells and T cells added to the adherent Mel526 cells in a final volume of 200 µl, to give final E:T ratios of 0.3:1 to 10:1. T cells at the start of the experiment were analysed by flow cytometry for CD2 and TCR expression and counted using cytocount beads. All conditions were set up in triplicate and wells without T cells and without Mel526 were set up as controls. Supernatant was collected at the indicated times and assayed for luciferase (section 2.5.2). To generate the 100% lysis control, Mel526 cells from three wells of 'Mel526 cells only' were detached and lysed by freeze/thawing three times using dry ice and a 37°C waterbath. The % of killing was obtained using the following formula:

$$\%\ lysis = 100 * \frac{luciferase\ of\ sample - background}{mean\ luciferase\ of\ (3\ lysis\ control\ wells - background)}.$$

At the end of the experiment, all non-adherent cells were collected and analysed by flow cytometry. At each time point, a representative well for each condition was photographed at 4x and 10x magnification using the Evos XL Core cell imaging system (LifeTechnologies).

2.6.4 *In vitro* flow assay

The *in vitro* flow assay was done at King's College in collaboration with Dr Aleksandar Ivetic. 35 mm coverslips were coated with 10 µg/ml of fibronectin for 1 h at 37°C, 5% CO_2. HUVEC cells were collected and plated onto the coverslips and grown for approximately three days until confluent. HUVECs were stimulated with 10 ng/ml TNF-α for 4 h at 37°, 5% CO_2. MOLT-3 cells were resuspended at 0.5 x 10^6 cells/ml in R10 medium, 10 mM Hepes. The GlycoTec flow chamber (Glycotech, Gaithersburg, USA) with a 200 µm gasket was attached to two tubes, one connected to a Harvard pump and the other tube immersed in the MOLT-3 cell suspension (figure 2.4). The flow chamber was carefully mounted onto the HUVEC coated coverslip and the vacuum started to create an isolated flow chamber. The latter was mounted onto the microscope slide holder, the Harvard pump set to generate a shear stress of 1.2 dyn/cm^2 and the flow started. The inverted microscope was surrounded by a heated chamber keeping cells

at 37°C. A 10x magnification objective was used and an automated camera was set to acquire one picture every 15 s from 4 areas per coverslide for a total of 15-20 min. The programme used to control the camera and acquire images was Volocity (PerkinElmer, Waltham, USA) and images were saved as TIFF files.

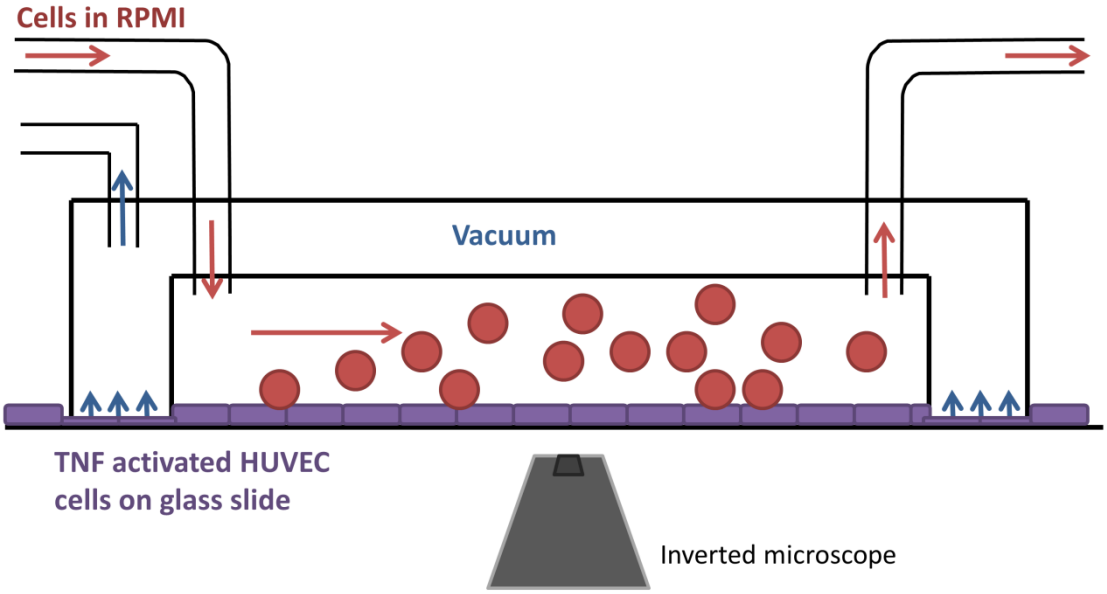

Figure 2.4: *In vitro* flow assay. The flow chamber was mounted onto a coverslip coated with TNF-α activated HUVEC cells (purple) and the vacuum (blue arrows) was activated to create the isolated flow chamber. MOLT-3 cells (red) flow over the HUVEC cells due to suction (red arrow) generated by the Harvard pump attached to the right tube.

2.7 *In vivo* experiments

2.7.1 Animal husbandry

NOD-SCID mice were kindly provided by Dr Susan Wong (Cardiff University, UK) who has maintained a colony for the last 15 years. The colony originated from the Jackson Laboratory (Maine, USA) and the full genotype is NOD.CB17-Prkdc^{scid}/J. All NOD-SCID mice used were male and age-matched within experiments. NOD-SCID mice were aged between 7 and 13 weeks at the start of the experiments. NSG (NOD.Cg-Prkdc^{scid} IL-2rg^{tm1Wjl}/SzJ) mice were purchased from

Charles River (Kent, UK) and received at 8 weeks of age. Female NSG mice were used for experiments and all mice were age matched within experiments. Mice were used for experiments 2-9 weeks post arrival at the Cardiff University facility. Animals were treated according to the UK Home Office laws under the project licence of Dr Ann Ager (PPL 30/3188) and the personal licence holder PIL 30/9878. All mice were housed in pathogen free Scantainers at the Cardiff University Heath Park facilities. Sentinel health screens of mice were done every three months. At the end of experiments or when mice were ill, mice were culled using CO_2 asphyxiation and dissociation of the neck, according to schedule 1.

2.7.2 Experimental procedures with mice

The left flank of mice was injected subcutaneously with 200 µl sterile saline solution containing between 0.5-15 x 10^6 $DsRed^+$ Mel526 cells. The area of injection was shaved before injection, and regularly thereafter, to enable better DsRed signal detection. For adoptive cell therapy experiments, 200 µl sterile saline containing up to 5.7 x 10^6 human $CD8^+$ T cells were administered intravenously. For experiments requiring host leucocyte depletion, mice were exposed to 2 Gy radioactivity from a $Caesium^{137}$ source in a Gammacell 1000 Elite Blood Irradiator (MDS Nordion, Ottawa, Canada).

2.7.3 Tumour growth monitoring *in vivo*

For imaging of DsRed tumour growth, mice were anaesthetised with isoflurane and white light and fluorescence pictures taken using a Bruker In-Vivo FX-Pro imaging system (CBS, Cardiff University). Overlays of the white light and fluorescent pictures and analysis of the DsRed signal strength was done using the Carestream MI SE molecular imaging analysis programme (Bruker, Massachusetts, USA). The excitation and emission wavelengths for DsRed detection are 550 and 580 nm and the excitation and emission filters used were 550 and 600 nm, respectively. The DsRed signal intensity was calculated by setting a fixed size region of interest

(ROI) around the tumour and one around the thorax of each mouse (background) and subtracting the sum intensity for the background ROI from the tumour ROI. The background ROI was not shaved and thus in some cases gave a higher background to the shaved tumour ROI.

Calliper measurements of tumours were done on a regular basis by measuring the height, width and depth (if big enough) of the tumour. Mice were weighed regularly and weights recorded. Tumour area was calculated using a formula requiring only height and width ($1.33 * \pi * height * width$) or a second formula taking into account the depth of the tumour $\left({}^{\pi}/_{6} * height * \ width * depth\right)$ was used to calculate tumour volume.

2.7.4 Organ harvest and processing

At the end of an experiment, mice were culled and tumours collected. Tumours were weighed and whole tumours fixed in 4% paraformaldehyde for histology. If adoptive T cell transfers were done, blood was harvested by cardiac puncture and collected into 700 µl of 13 mM sodium citrate dihydrate to prevent clotting. Additionally, the spleen, lungs, tumour draining LN and the tumour were harvested. In one experiment, the mesenteric, axillary, brachial and inguinal LNs were also collected. A single cell suspension was obtained by physically dissociating the organs on a 70 µm Nylon mesh (Fisher Scientific, New Hampshire, USA). Large tumours were cut into half, one half was fixed for histology and the rest was dissociated, washed in PBS and added to a Ficoll gradient to isolate lymphocytes. Briefly, 7 ml of Ficoll was added to tubes and 2-3 ml of the tumour cells in PBS added carefully before a spinning of the cells at 2000 rpm for 20 min and collecting the lymphocyte layer. Spleens, blood and some tumour samples were incubated for 5 min on ice with RBC lysis buffer, before washing with PBS. Once all cells were washed, cells were stained for flow cytometry.

2.8 Statistical analysis

All statistical analysis was done using Prism 5. Two-way ANOVA tests were done using the Bonferroni post-test. Tumour growth rates (k) were obtained by calculating the exponential growth equation of the nonlinear regression and obtaining the rate constant, k. A one-way ANOVA test with a Tuckey post-hoc test was used to analyse differences between tumour growth rates. Correlations between tumour area and/or DsRed and/or tumour weight were obtained by doing a Spearman correlation test (for non-parametric data) or a Pearson test (for data of Gaussian distribution as determined by a D' Agostino and Pearson test). The correlation coefficient 'r' was obtained from these tests.

2.9 Software used for data collection and analysis

DNA sequence data was analysis using the CLC DNA Workbench 7 programme (CLC bio by Qiagen, Venlo Netherlands). GraphPad Prism 5 (GraphPad Software, La Jolla, USA) was used to plot graphs and for statistical analysis. Flow cytometry data was acquired using the BD FACSDiva Software (BD Biosciences, Franklin Lakes, USA) and analysed using FlowJo V10 (Ashland, USA). To quantify the Cel-I DNA restriction fragments and immunoblot signals, ImageJ software was used (NIH, USA). Fluorescent images of mice were analysed using the Carestream MI SE molecular imaging analysis programme (Bruker, Massachusetts, USA). Annealing temperatures were determined using online calculation tools, such as the Tm calculator from NEB (http://tmcalculator.neb.com/#!/).

Chapter 3: Generation of SHP-1 deficient human leukaemic T cells

3.1 Introduction

It has been shown that mouse $CD8^+$ T cells deficient in SH2 domain-containing phosphatase-1 (SHP-1) more readily form conjugates with antigen presenting cells (APCs) and more likely enter into proliferation in response to cognate peptide stimulation than control T cells (Sathish et al. 2007). In order to generate human SHP-1 deficient $CD8^+$ T cells, it was decided to ablate the SHP-1 gene expressed in human T cells via delivery of two SHP-1 specific zinc finger nucleases (ZFNs); ZFN1 and ZFN2. The SHP-1 gene specific ZFNs are each composed of 5 ZFs recognising a distinct 15 bp (figure 1.9 A). The latter were designed, verified and purchased from Sigma-Aldrich (CKOZFN1061-1kt) in order to potentially introduce double stranded breaks within the first intron exon junction of exon 8 of the SHP-1 gene (figure 3.1). At the commencement of this study, lentiviral delivery of the ZFNs was estimated to be the best option.

In this study, we initially chose two leukaemic T cell lines expressing a human immunodeficiency virus-1 (HIV-1) Gag p17 (77-85) (SLYNTVATL) specific TCR (gag^+) to establish a robust model for ZFN delivery and for the detection of mutations (Varela-Rohena et al. 2008). The initial plan to deliver the two SHP-1 specific ZFNs together with a detectable surface marker, rat CD2 (rCD2 or CD2), in one single lentivirus (LV) proved to be ineffective in generating SHP-1 deficient T cells. It was therefore required to generate two LVs, each expressing one of the required pair of SHP-1 ZFNs. Additionally, the efficiency of gene delivery using LV and integrase-deficient LV (IDLV) was compared.

All primers used in this chapter, for cloning or sequencing, are listed in the appendix (tables A1 and A2) as are the sequences of all lentiviral transfer plasmids (appendix A2).

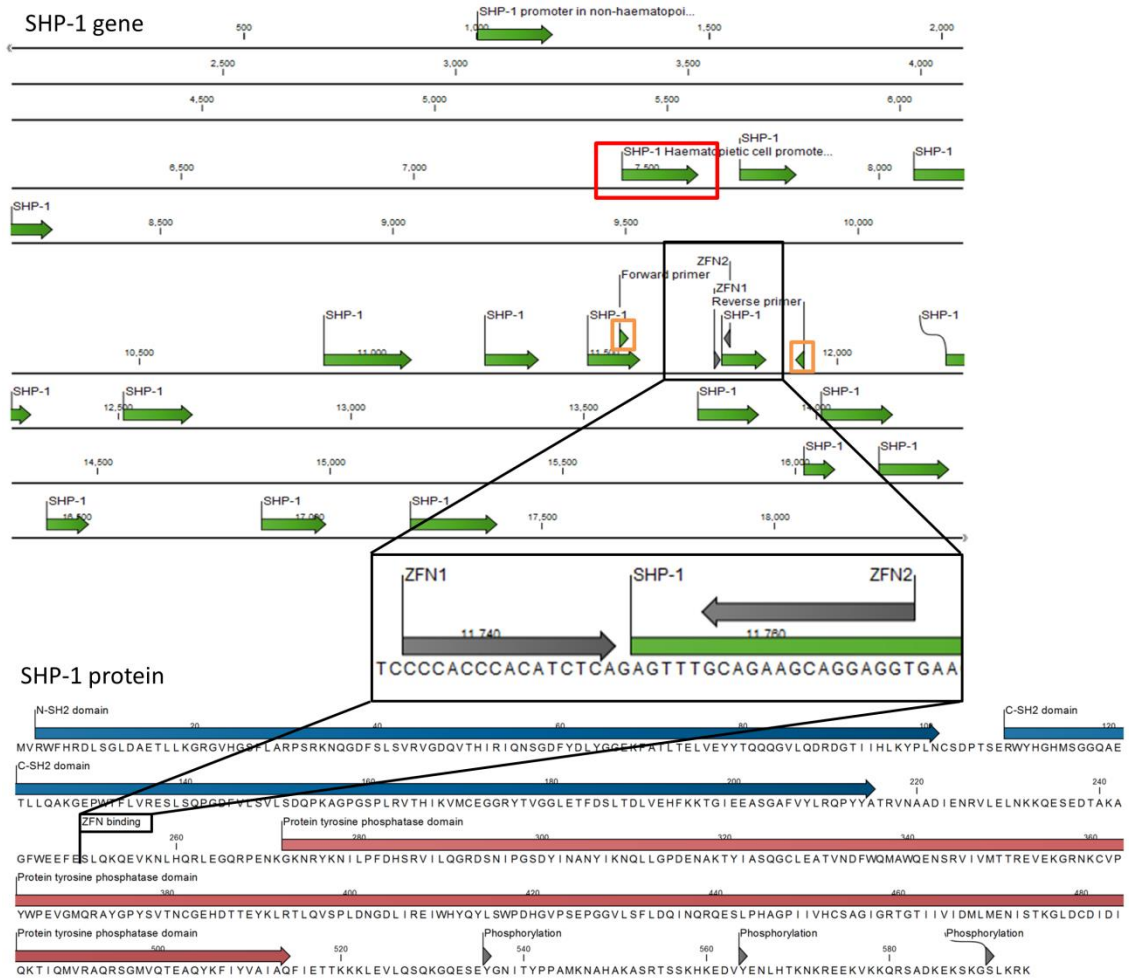

Figure 3.1: SHP-1 gene and protein sequence and ZFN binding sites. The hematopoietic PTPN-6 or SHP-1 isoform utilises promoter 2 of exon 2 (red box) leading to a SHP-1 protein 2 aa shorter than the non-hematopoietic isoform utilising promoter 1 of exon 1. The SHP-1 gene is composed of 17 exons and the binding sites for ZFN1 and ZFN2 (grey) are in the intron preceding exon 8 and within exon 8 respectively. The SHP-1 specific ZFNs were designed to introduce double stranded breaks within an exon intron junction that would lead to mutations in the SHP-1 gene upstream of the protein tyrosine phosphatase catalytic domain (dark red). The primer pair 55 and 56 (orange boxes) was used to PCR amplify a 398 bp SHP-1 DNA sequence encompassing the site of potential mutation. Mutations introduced in the ZFN cutting region can potentially lead to loss of SHP-1 protein expression due to splicing errors and frame shifts. The introduction of premature stop codons will lead to the loss of the catalytic protein tyrosine phosphatase domain (dark red) downstream of the two SH2 binding domains (blue). The NCBI accession numbers are: ID 5777 (gene), NM_002831.5 (mRNA) and NP_002822.2 (peptide).

3.2 Generation of a single lentiviral transfer plasmid encoding both SHP-1 specific ZFN1 and ZFN2

In order to generate SHP-1 mutant cells, LV encoding the SHP-1 specific ZFNS had to be made and cells transduced with the LV.

A DNA cassette encoding both SHP-1 gene-specific ZFN sequences and a rat CD2 (CD2) surface marker was generated where the three genes were separated by two 2A sequences (de Felipe et al. 2006), T2A and P2A (table 3.1), generating the ZFN1-T2A-ZFN2-P2A-CD2 gene cassette, from here onwards termed ZFN1/2-CD2. Stoichiometric gene expression was intended by using the T2A and P2A sequences. The ZFN1/2-CD2 gene cassette was introduced into the HIV based lentiviral transfer vector, pSxW, also referred to as pLenti (Demaison et al. 2002). Figure 3.2 outlines the five sub-cloning steps required to obtain the final pLenti-ZFN1/2-CD2 plasmid.

	Nucleotide sequence	**Amino acid sequence**
T2A	AGCGGCAGCGGGCGCAGCGGCAGCGGCGAAGGCCGCGGCAGC CTGCTGACCTGCGGCGATGTGGAAGAAAACCCTGGCCCGCGC	S**GSG**RS**GSG**EGRGSL LTCGDVEENPGPR
P2A	AGCGGCTCCGGTGCCACCAACTTCTCTCTGCTGAAGCAGGCCGG GGATGTCGAAGAGAATCCAGGCCCC	S**GSG**ATNFSLLKQAG DVEENPGP

Table 3.1: Nucleotide and amino acid sequence of the T2A and P2A ribosomal skipping elements used in the pLenti-ZFN1/2-CD2 plasmid. The P2A sequence originates from the porcine teschovirus-1 whereas T2A is isolated from the *Thosea asigna* virus (de Felipe et al. 2006). Underlined amino acid sequences indicate the original sequence of the 2A and bold GSG sequences were added to improve cleavage efficiency. The ribosomal skipping arises between the Glycine and Proline, highlighted in red.

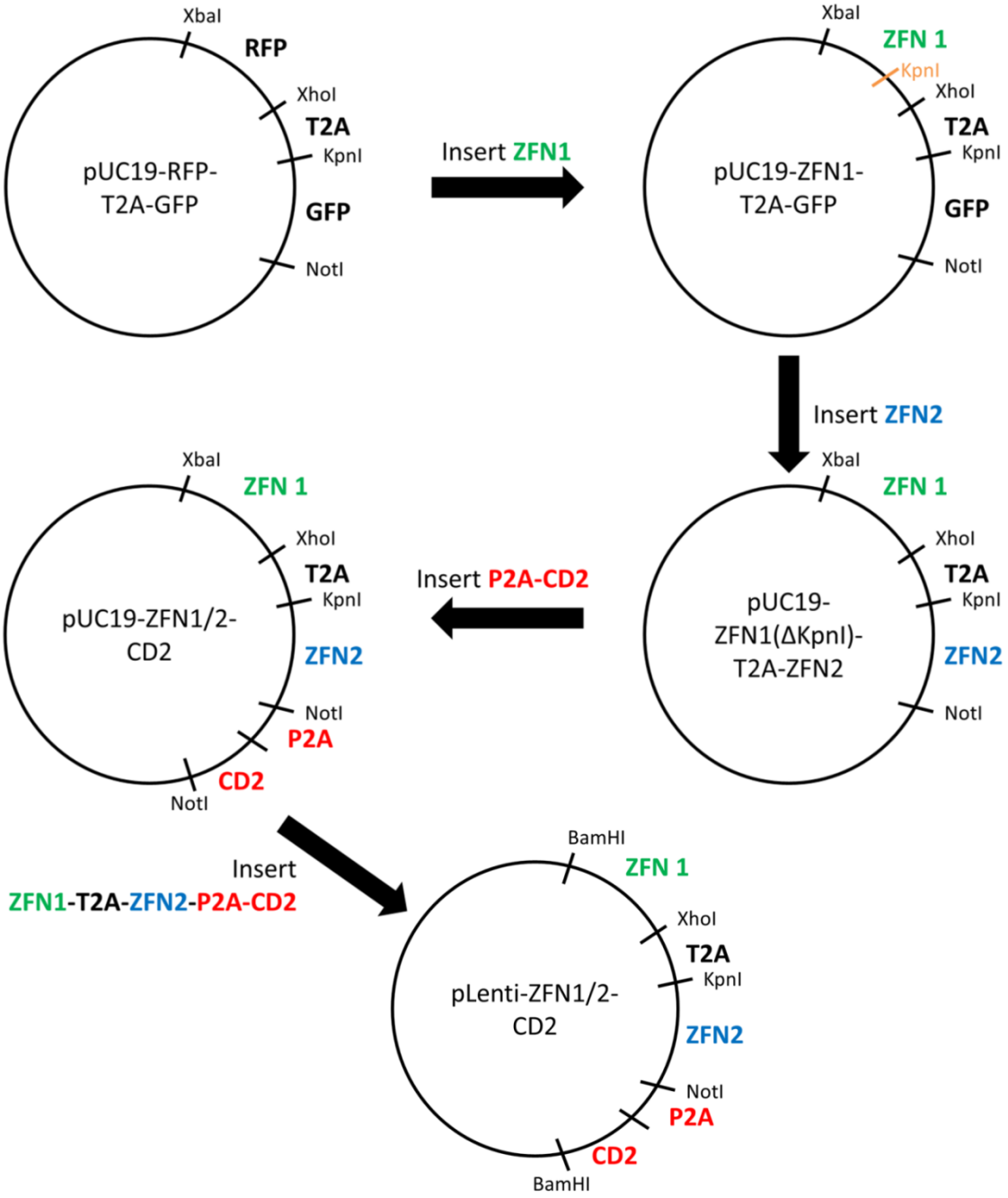

Figure 3.2: Cloning strategy to generate the lentiviral transfer vector pLenti-ZFN1/2-CD2. The pUC19-RFP-T2A-GFP plasmid was used to clone the ZFN1-T2A-ZFN2-P2A-CD2 cassette before it was introduced into the pLenti plasmid. First, an XbaI and XhoI double restriction digest allowed for the ZFN1 (green) to be introduced into the plasmid. The KpnI site within the ZFN1 sequence (orange) in the pUC19-ZFN1-T2A-GFP was removed by site-directed mutagenesis to enable a KpnI and NotI double restriction digest and allow for the ZFN2 (blue) to be inserted into the vector. A single restriction digest of pUC19-ZFN1-T2A-ZFN2 with NotI allowed for the P2A-CD2 sequence to be inserted. Finally, the ZFN1/2-CD2 gene cassette was inserted into the lentiviral transfer vector, pLenti.

The ZFN1 gene was PCR amplified from the plasmids provided by SIGMA using primers 9 and 10 (table A1) and introduced into the pUC19-RFP-T2A-GFP vector (made by Dr Pratigya Gautam) using the In-Fusion cloning technique (figure 3.3). Primer 9 introduced a Kozak consensus sequence (GCCGCCACC) upstream of the ZFN1 start codon. The T2A sequence of the pUC19-RFP-T2A-GFP vector has an additional amino acid sequence of SGSGRS upstream of the T2A and an additional R downstream, which do not influence the ribosomal skipping. The nucleotide sequence of the pUC19-ZFN1-T2A-GFP plasmid was confirmed by DNA sequencing using primers 11-16 (table A2).

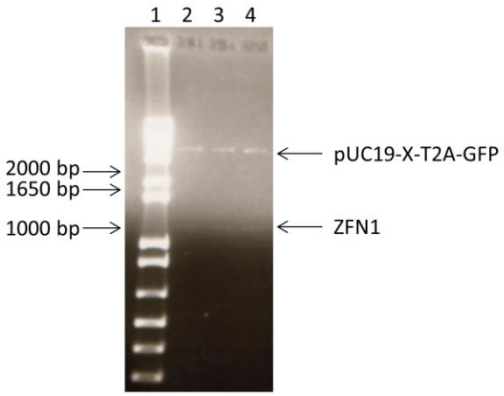

Figure 3.3: Cloning of the ZFN1 gene into a pUC19-X-T2A-GFP plasmid using the In-Fusion protocol. Lane 1 shows the 1kb plus DNA ladder. Lanes 2-4 show an XbaI and XhoI double digest of plasmids isolated from different DH5α colonies previously transformed with 2 µl of In-Fusion reaction comprising the ZFN1 PCR product (primers 9 and 10) and the XbaI and XhoI linearised pUC19-X-T2A-GFP plasmid. The lower sized DNA band corresponds to the 1164 bp ZFN1 DNA and the upper band to the 3474 bp pUC19-X-T2A-GFP, where X indicates the missing DNA due to the XbaI/XhoI restriction digestion. Plasmid electrophoresed in lane 3 was chosen to be sequenced and used for further steps.

In order to restriction digest the pUC19-ZFN1-T2A-GFP plasmid with KpnI and NotI, site-directed mutagenesis was done to first remove a KpnI site within the ZFN1 sequence (figure 3.4). The proofreading DNA polymerase, PfuTurbo, was used to amplify the pUC19-ZFN1-T2A-GFP plasmid with the mutagenic primers 17 and 18. The primers were designed to replace an

Adenosine by a Thymidine at the KpnI restriction site (GGT**A**CC→GGT**T**CC) whilst conserving the codon for Valine (GTA→GTT).

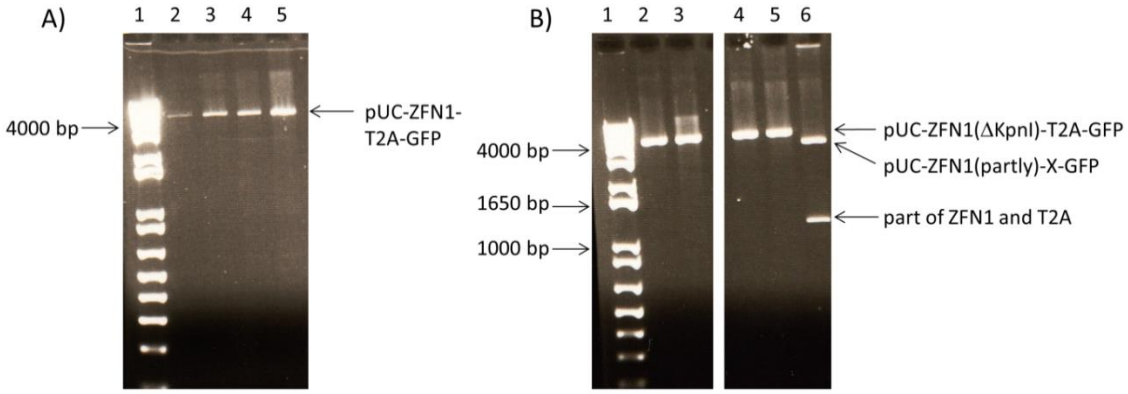

Figure 3.4: Site-directed mutagenesis of the KpnI site within the ZFN1 sequence of the pUC19-ZFN1-T2A-GFP plasmid. A) Lanes 2-5 show the result of different reaction conditions for the PCR amplification using the pUC19-ZFN1-T2A-GFP (4638 bp) as template with the mutagenic primers 17 and 18 and the proofreading DNA polymerase, PfuTurbo. The PCR product from lane 4 was restricted with the DpnI restriction enzyme that targets only parental methylated plasmid DNA for digestion. DH5α bacteria were transformed with the DpnI digest product and grown on Carbenicillin containing agar plates. B) Lanes 2-5 show a KpnI single restriction digest of plasmid DNA that was isolated from four different DH5α colonies transformed as described above. Lane 6 shows a KpnI restriction digest of non-mutated pUC19-ZFN1-T2A-GFP with the smaller sized DNA band corresponding to a 1132 bp ZFN1-T2A DNA fragment produced by the restriction with KpnI within the ZFN1 and downstream of the T2A sequence. The pUC19-ZFN1(ΔKpnI)-T2A-GFP plasmid from lane number 4 was DNA sequenced and used for further steps.

After confirmation of the modifications in the pUC19-ZFN1(ΔKpnI)-T2A-GFP plasmid by DNA sequencing using primers 11-16, it was possible to introduce the ZFN2 sequence into the NotI and KpnI restricted pUC19-ZFN1(ΔKpnI)-T2A-GFP (figure 3.5). The ZFN2 gene was amplified from the SIGMA plasmid using primers 19 and 20. For simplicity from here onwards, the ZFN1(ΔKpnI) will be called ZFN1. To sequence the pUC19-ZFN1-T2A-ZFN2 plasmid, two restriction digests had to be used because primers for sequencing ZFN1 also bind to ZFN2 due to a high sequence homology. First, the pUC19-ZFN1-T2A-ZFN2 plasmid was digested with XbaI and XhoI and the pUC19-X-T2A-ZFN2 linearised plasmid was sequenced using primers 22-26. In

a second restriction digest using BamHI, the ZFN1(partly)-T2A-ZFN2 fragment was sequenced using primer 21 and the pUC19-ZFN1-T2A-ZFN2 DNA sequence was confirmed.

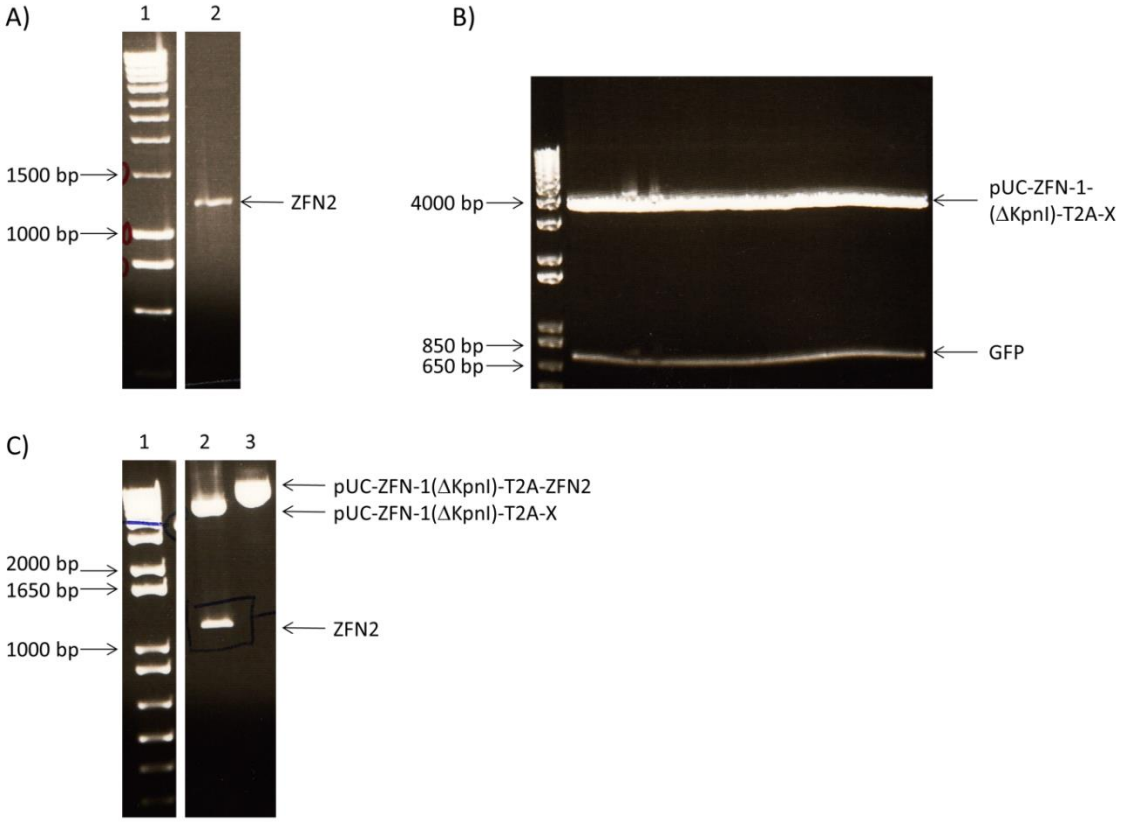

Figure 3.5: Cloning of the ZFN2 gene into the pUC19-ZFN1(ΔKpnI)-T2A-GFP plasmid using the In-Fusion protocol. A) Lane 2 shows the amplified 1186 bp ZFN2 gene from the PCR reaction using primers 19 and 20 and the SIGMA ZFN2 template. B) The preparative agarose gel was loaded with the KpnI and NotI restricted pUC19-ZFN1(ΔKpnI)-T2A-GFP. The lower band corresponds to the 717 bp GFP DNA fragment and the upper band to the linearised pUC19-ZFN1(ΔKpnI)-T2A-X. The latter was extracted from the gel and purified. An In-Fusion reaction was done using the PCR product in A) and the linearised vector in B) and DH5α cells were transformed with 2 µl of In-Fusion mix. C) Plasmid DNA extracted from DH5α colonies transformed as described above and selected for Ampicillin resistance was restriction digested with KpnI and NotI and was loaded in lane 2. The lower size band in lane 2 corresponds to the 1148 bp ZFN2 and the upper to the pUC19-ZFN1(ΔKpnI)-T2A-X. Lane 3 is non-restricted plasmid from the same clone. This plasmid was DNA sequenced and confirmed to be the pUC19-ZFN1(ΔKpnI)-T2A-ZFN2 nucleotide sequence.

As mentioned above, the DNA sequences of both ZFNs have a high homology resulting in primers binding to both ZFN sequences; hence the initial plan to introduce the ZFN1-T2A-ZFN2 cassette into a pUC19-X-P2A-CD2 vector had to be revised. The new strategy was to introduce the P2A-CD2 fragment into the NotI linearised pUC19-ZFN1-T2A-ZFN2-X plasmid (figure 3.6). To restore the reading frame altered by the introduction of an additional NotI site (8 bp) upstream of the P2A sequence, an additional adenosine was added to primer 57 to restore the reading frame. The plasmid was sequenced using primers 4-8.

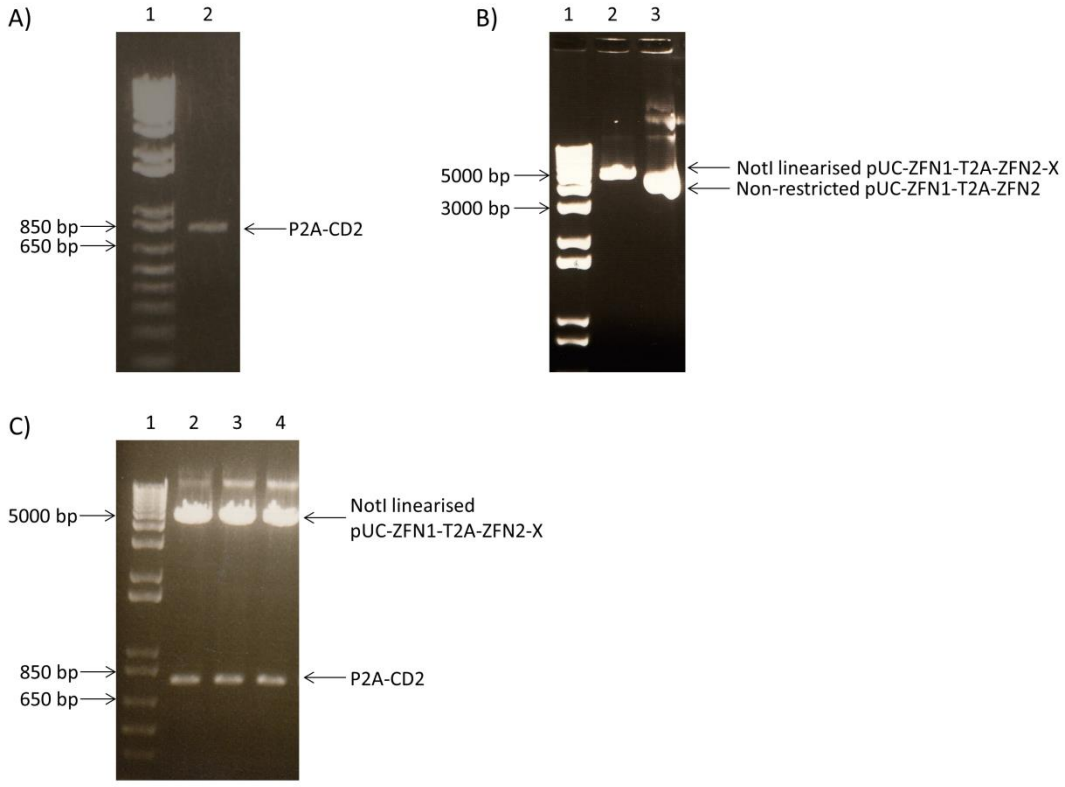

Figure 3.6: Cloning of the P2A-CD2 sequence into the pUC19-ZFN1-T2A-ZFN2 using the In-Fusion protocol. A) Lane 2 shows the 811 bp P2A-CD2 DNA sequence amplified by PCR using primers 57 and 30. B) Lane 2 shows the NotI single restriction digest of the pUC19-ZFN1-T2A-ZFN2-X plasmid whereas lane 3 shows the non-restricted pUC19-ZFN1-T2A-ZFN2 plasmid. The product in lane 2 was purified and used together with the PCR product in A) to set up an In-Fusion reaction. DH5α cells were transformed with 2 µl of In-Fusion mix. C) Plasmid DNA extracted from three different DH5α colonies transformed as described above and selected for Ampicillin resistance was restriction digested with NotI and resolved in lanes 2 to 4. The lower size band corresponds to the 786 bp P2A-CD2 DNA sequence. All three colonies had the pUC19-ZFN1/2-CD2 plasmid. The plasmid in lane 3 was DNA sequenced and confirmed to be the pUC19-ZFN1/2-CD2 sequence.

The ZFN1/2-CD2 cassette was introduced into the lentiviral transfer plasmid pLenti to give the final product of pLenti-ZFN1/2-CD2. Amplification of the cassette with primers 52 and 32 gave a shorter ZFN2-P2A-CD2 and the longer ZFN1/2-CD2 fragment due to the sequence homology between ZFN1 and ZFN2 leading to the forward primer 52 binding to both genes (figure 3.7). Only the full cassette was introduced into the pLenti vector and sequencing with primers 4, 6, 7, 22, 23, 33, 34, 53 and 54 confirmed the plasmid as pLenti-ZFN1/2-CD2.

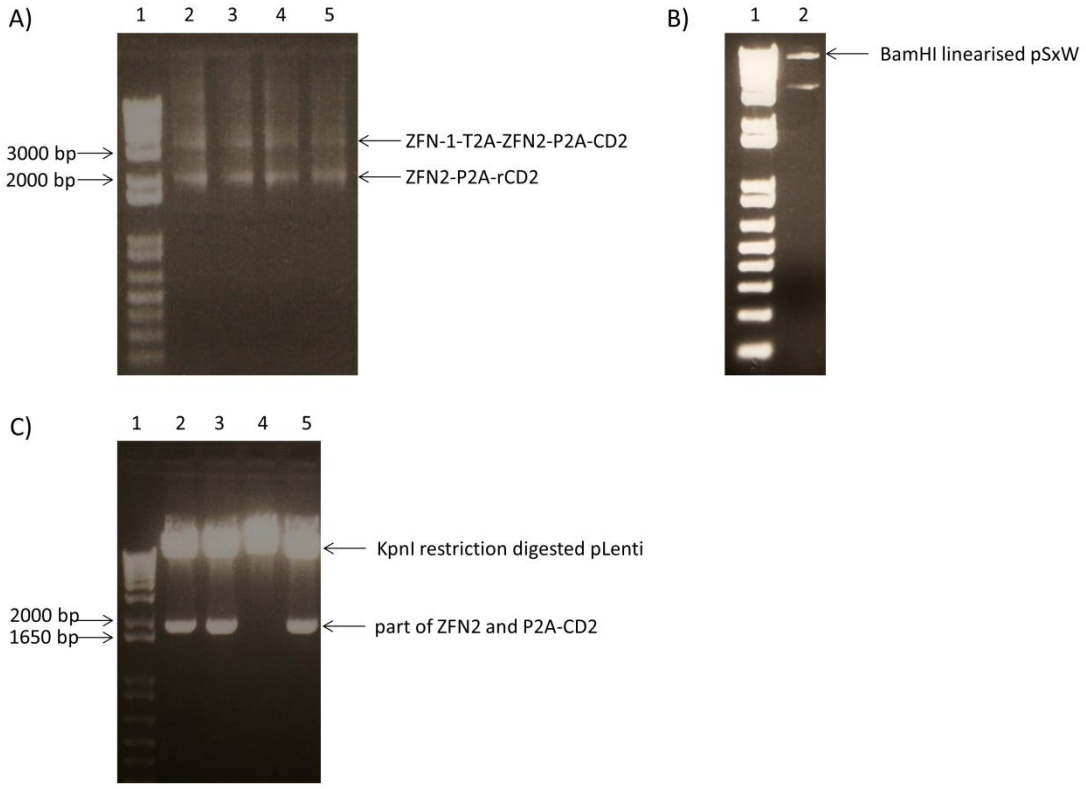

Figure 3.7: Cloning of ZFN1/2-CD2 into the BamHI linearised pSxW lentiviral transfer vector using the In-Fusion protocol. A) Lanes 2-5 show the PCR products from the amplification of ZFN1/2-CD2 from the pUC19-ZFN1/2-CD2 using primers 52 and 32. The ZFN homology led to the amplification of two products; the unwanted ZFN2-P2A-CD2 (1969 bp) and the ZFN1/2-CD2 (3223 bp) fragment. All four PCR products were pooled and the 3223 bp DNA band purified. B) Lane 2 shows the BamHI restriction digest of the pSxW plasmid. The linearised 8942 bp pSxW vector was purified and used together with the purified PCR product in A) to set up an In-Fusion reaction. DH5α cells were transformed with 2 µl of In-Fusion mix. C) Lanes 2-4 show plasmid DNA extracted from different Ampicillin selected DH5α colonies transformed as described above and digested with KpnI. This gave three diagnostic fragments for the pLenti-ZFN1/2-CD2 plasmid; one at 10174 bp, one at 119 bp (not visible) and a distinct 1843 bp band. The latter represents a part of the ZFN2 and the whole of P2A-CD2. Lane 4 did not show this pattern. The plasmid corresponding to lane 3 was DNA sequenced, confirmed to be the pLenti-ZFN1/2-CD2 and used for lentiviral production.

3.3 Analysis of gag$^+$ MOLT-3 cells transduced with CD2 or ZFN1/2-CD2 LV

As a control for LV production and transduction efficiency, LV encoding CD2 was made, as described in the Materials and Methods, using a pLenti-CD2 transfer vector kindly provided by Dr Liam Morgan. The LV used in the majority of experiments was not quantified and transductions were done with volumes of LV previously showing high transduction efficiency. Quantification of the gag protein for a limited number of LV productions was done by ELISA and readings of 1-30 ng/µl were measured. However, due to the expense and variability of results obtained with the ELISA, it was decided to revert back to using defined volumes of 10x or 100x concentrated LV.

MOLT-3 cells expressing the gag TCR (referred to as gag$^+$ MOLT-3), previously shown to express SHP-1 (Yi et al. 1992), were transduced with increasing volumes of 10x concentrated CD2 LV (figure 3.8 B). The highest LV dose (500 µl) gave the highest CD2 MFI while even the lowest dose of 40 µl LV yielded a majority of CD2$^+$ cells, although with a considerably lower MFI, indicating the potency of the LV at transducing MOLT-3 cells.

Recombinant ZFN1/2-CD2 LV was used at two different volumes of 10x concentrated LV to transduce gag$^+$ MOLT-3. After 72h, high levels of CD2 surface expression were observed by flow cytometry in cells transduced with 150 µl and 350 µl of LV (figure 3.8 C). Hence, the third gene of the ZFN1/2-CD2 cassette was properly folded and expressed on the cell surface, pointing towards the 2A ribosomal skipping elements yielding separate proteins as expected.

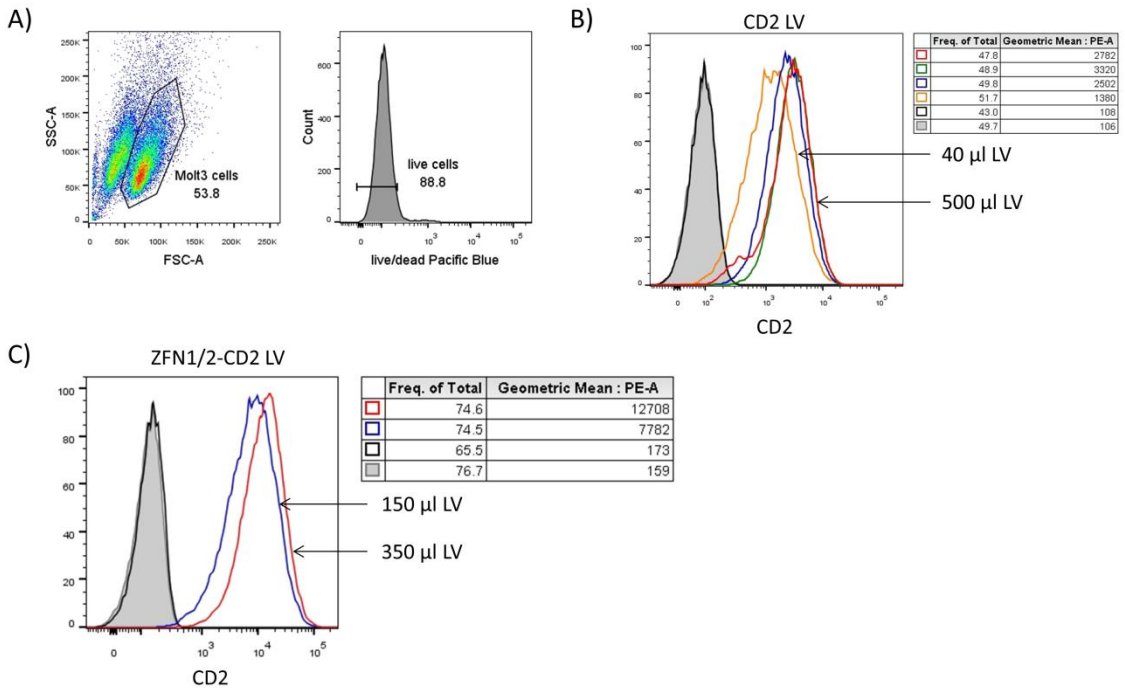

Figure 3.8: CD2 expression on gag$^+$ MOLT-3 cells transduced with varying volumes of CD2 or ZFN1/2-CD2 LV. A) Gating strategy for LV transduced gag$^+$ MOLT-3 cells in B) and C). B) Gag$^+$ MOLT-3 cells, incubated for 72 h with RPMI only (grey filled), 40 µl (orange), 125 µl (blue), 250 µl (green) or 500 µl (red) of 10x concentrated CD2 LV, were stained using a PE-conjugated anti-CD2 Ab or unstained (black). C) 2 x 10^5 gag$^+$ MOLT-3 cells were incubated for 72 h with RPMI only, 150 µl or 350 µl of 10x concentrated ZFN1/2-CD2 LV. Cells were either not stained for CD2 (black) or the PE-conjugated mouse anti-CD2 Ab was added to cells incubated with RPMI only (grey filled), 150 µl (blue) or 350 µl (red) of LV.

Both ZFN genes in the ZFN1/2-CD2 cassette encode a 3xFlag tag (Flag) upstream of the ZFN start codon (table 3.2). To determine whether the ZFN proteins were being expressed, the transduced gag$^+$ MOLT-3 cells depicted in figure 3.8 C cells were lysed and the Flag tag detected by immunoblotting. As shown in figure 3.9, both doses of LV gave a strong band at the expected size of the ZFN proteins (49 kDa), which was absent in non-transduced cells. However, as both ZFNs are Flag-tagged, it was not possible to distinguish between the expression of the ZFN1 and ZFN2 proteins.

	Nucleotide sequence	Amino acid sequence
ZFN1	ATGGACTACAAAGACCATGACGGTGATTATAAAGATCATGAC ATCGATTACAAGGATGACGATGACAAG	MDYKDHDGDTKDHDID YKDDDDK
ZFN2	ATGAGATCTGACTACAAAGACCATGACGGTGATTATAAAGAT CATGACATCGATTACAAGGATGACGATGACAAG	MRSDYKDHDGDYKDHD IDYKDDDDK

Table 3.2: 3xFlag sequences encoded in the pLenti-ZFN1/2-CD2 plasmid. Nucleotide and amino acid sequences of 3xFlag tags positioned upstream of the start codon of the ZFN1 and ZFN2. The underlined amino acids indicate the differences between the two ZFNs.

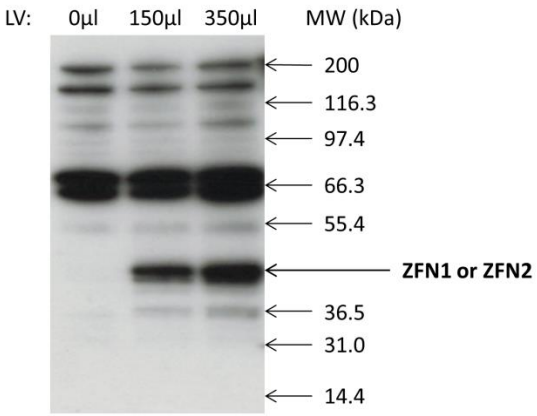

Figure 3.9: Immunoblotting for the Flag-tagged ZFNs in gag$^+$ MOLT-3 cells transduced with ZFN1/2-CD2 LV. Gag$^+$ MOLT-3 cells were either untransduced (0µl) or transduced with 150µl or 350µl of ZFN1/2-CD2 LV. Per condition, 0.5 x 10^6 cells were lysed and used for immunoblotting. An anti-Flag-HRP Ab was used to probe for the expression of the ZFNs. Bands at the expected size of the ZFNs are indicated. The expected sizes of the 3xFlag-ZFN1 and 3xFlag-ZFN2 with the T2A or P2A C-terminal tails would be 49.56 kDa and 49.43k Da, respectively.

3.4 Mutation analysis of the human SHP-1 gene in gag$^+$ MOLT-3 cells transduced with ZFN1/-2-CD2 LV

The ZFN1/2-CD2 LV transduced gag$^+$ MOLT-3 cells from figure 3.8 C (350 µl), were analysed for the presence of mutations in the SHP-1 gene using the Cel-I mismatch assay and sequencing of the ZFN target region.

Firstly, genomic DNA (gDNA) was isolated from the non-transduced or 350 µl LV transduced gag$^+$ MOLT-3 cells and a 398 bp region of the SHP-1 gene, encompassing the potential ZFN cutting site, was amplified by PCR using primers 55 and 56 (figure 3.1). Initially, to reduce the introduction of random mutations by the polymerase, a proofreading polymerase (Phusion) was used to amplify the SHP-1 region. However, no Cel-I signal was obtained and it was presumed that the PCR buffer mix was not compatible with the Cel-I enzyme, inhibiting further processing of the DNA by the Cel-I nuclease. Consequently a non-proofreading *Taq* polymerase mix (Supermix) was used for the PCR amplification. No false positive Cel-I signal was ever observed in non-transduced cells and thus this system was robust.

After amplification, the 398 bp SHP-1 PCR product (figure 3.10 A) was hybridised by heating and gradual cooling and finally it was incubated with the Cel-I nuclease. The Cel-I nuclease recognises mismatched DNA and introduces a double stranded break at the site. For the SHP-1 product, this would be expected to yield two shorter 178 bp and 220 bp DNA fragments. As shown in figure 3.10 B, a single band was observed, indicating a lack of SHP-1 mutations in the cells analysed.

To verify the lack of mutations in the SHP-1 gene, a longer sequence of the SHP-1 gene was amplified, encompassing the ZFN binding sites. Primers 58 and 59 were used and the PCR reaction yielded a 1733 bp SHP-1 fragment (figure 3.11 A) which was purified and sequenced using primers 55 and 56 (figure 3.11 B). The latter showed that the DNA perfectly matched

that of wild type SHP-1, confirming the absence of mutations in the gag$^+$ MOLT-3 cells. The absence of SHP-1 mutations was surprising due to the complete transduction of these cells shown by the CD2 surface staining (figure 3.8 C) and the presence of 3xFlag tag protein (figure 3.9) within the ZFN1/2-CD2 LV transduced gag$^+$ MOLT-3 cell pool.

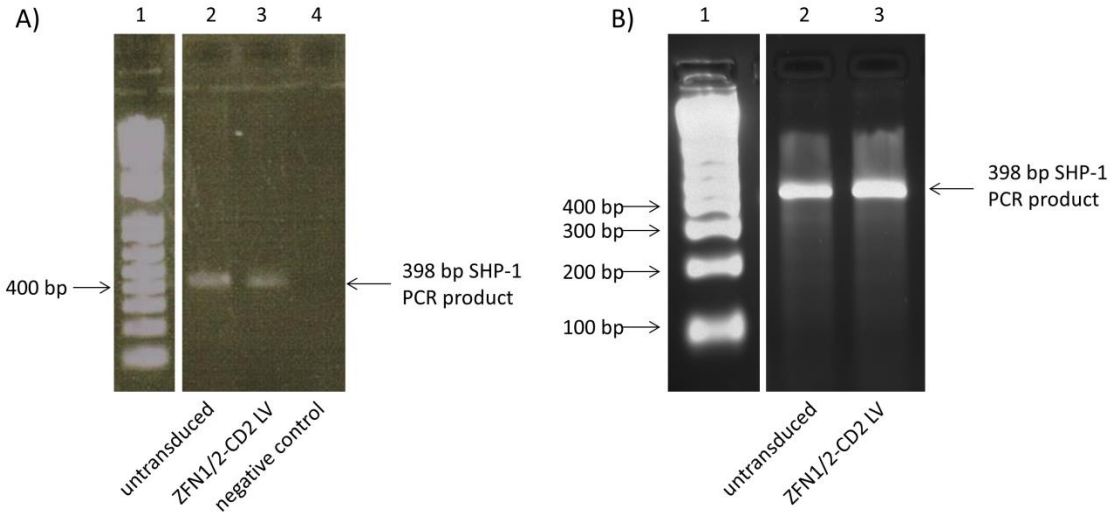

Figure 3.10: Cel-I mismatch assay of gag$^+$ MOLT-3 transduced with ZFN1/2-CD2 LV. Gag$^+$ MOLT-3 cells were either untransduced or transduced with 350 µl of ZFN1/2-CD2 LV. A) gDNA was extracted from the cells and a 398 bp SHP-1 gene sequence encompassing the potential ZFN cutting site was amplified using primer 55 and 56. Lane 4 shows the product from a PCR without gDNA and acts as a control for gDNA contamination. B) The PCR products from A) were hybridised and incubated with the Cel-I nuclease. A positive control provided by the manufacturer was incubated alongside to ensure the activity of the Cel-I enzyme (not shown).

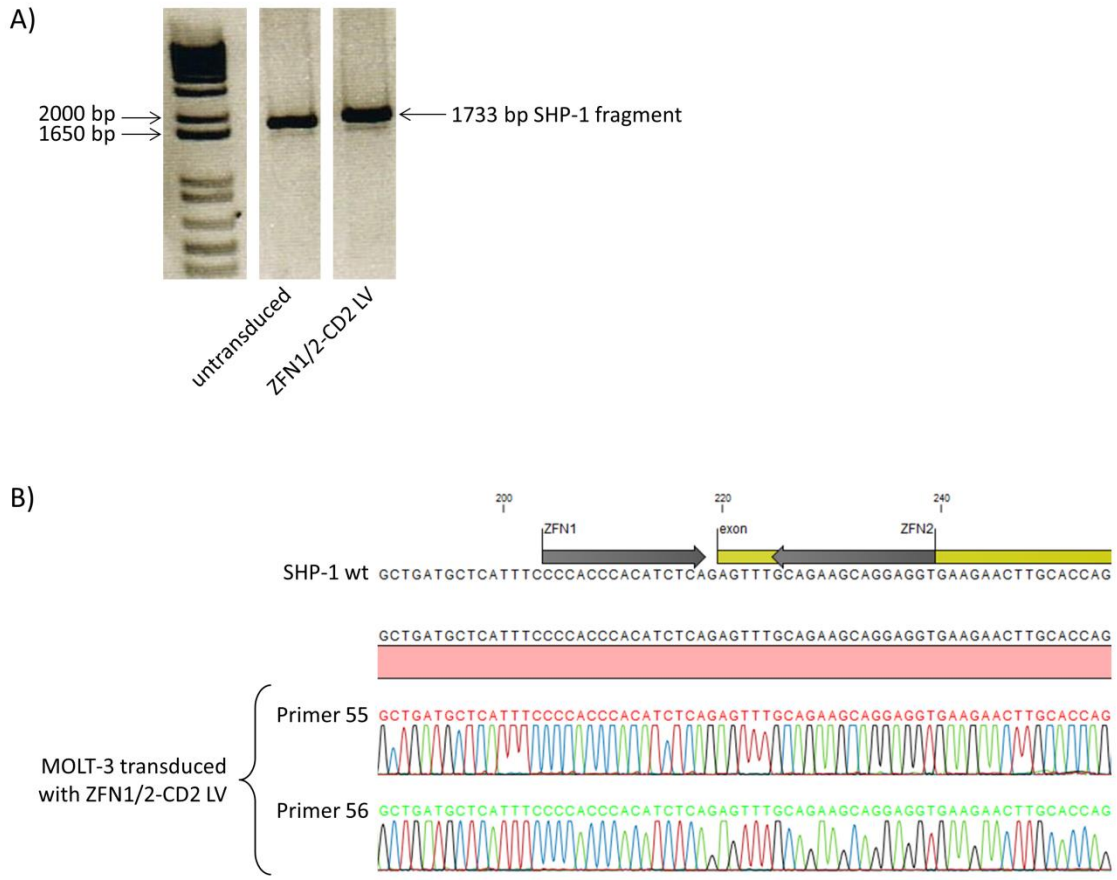

Figure 3.11: Sequencing of the SHP-1 gene sequence encompassing the ZFN cutting site from gag+ MOLT-3 transduced with ZFN1/2-CD2 LV. A) gDNA was extracted from 350 µl ZFN1/2-CD2 LV transduced gag^{+} MOLT-3 cells and a 1733 bp fragment encompassing the ZFN cutting site was amplified using primers 58 and 59. B) The PCR products from A) were purified and the 1733 bp DNA fragment was sequenced with primers 55 and 56. The results for both primer readings are shown.

3.5 SHP-1 specific ZFNs induce mutations in the SHP-1 gene in HEK293T cells

One hypothesis as to why the ZFNs did not induce any mutations in the leukaemic cells was that the 2A tails at the C termini of the ZFN proteins might inhibit nuclear translocation or proper protein folding and thus stop the ZFNs accessing the SHP-1 gene. In order to test this hypothesis, HEK293T cells were transiently transfected with the pLenti-ZFN1/2-CD2 plasmid

using $CaCl_2$. In parallel, cells were transfected simultaneously with two plasmids expressing either ZFN1 or ZFN2. The plasmids, called pZFN1 and pZFN2, were the plasmid constructs provided by SIGMA figure 3.12. The plasmids were amplified and used to transiently transfect HEK293T cells using $CaCl_2$.

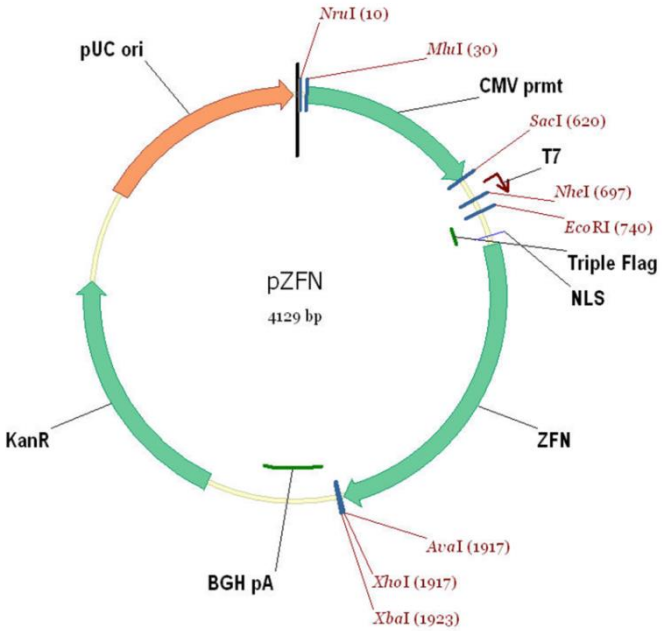

Figure 3.12: Vector map of the pZFN plasmid. The pZFN plasmids provided by SIGMA encode either the ZFN1 or ZFN2 sequence. ZFN gene expression is driven by the SFFV promoter. A 3xFlag tag is located upstream of the start codon of the ZFN gene.

HEK293T cells were transfected with 10 µg or 30 µg of pLenti-ZFN1/2-CD2 plasmid or with 2x5 µg or 2x15 µg of pZFN1 and pZFN2. Cells transfected with the pLenti-ZFN1/2-CD2 plasmid were analysed for CD2 surface expression at 41 h and 65 h post-transfection and shown to be successfully transfected shown by the high levels of CD2 (figure 3.13 B). The double peaked CD2 expression might indicate the transfection of two plasmids per cell. The shift of the CD2 peak, from the higher to the lower expression levels from 41 h to 65 h, confirms the transient gene expression as opposed to stable integration of the genes by LV transduction. Cells transfected with 10 µg or 30 µg of pLenti-ZFN1/2-CD2 or pZFN1 and pZFN2 were lysed at 41 h

and 65 h. The lysate was immunoblotted for the Flag tagged ZFNs and all transfected cells were shown to express ZFN protein (figure 3.13 C).

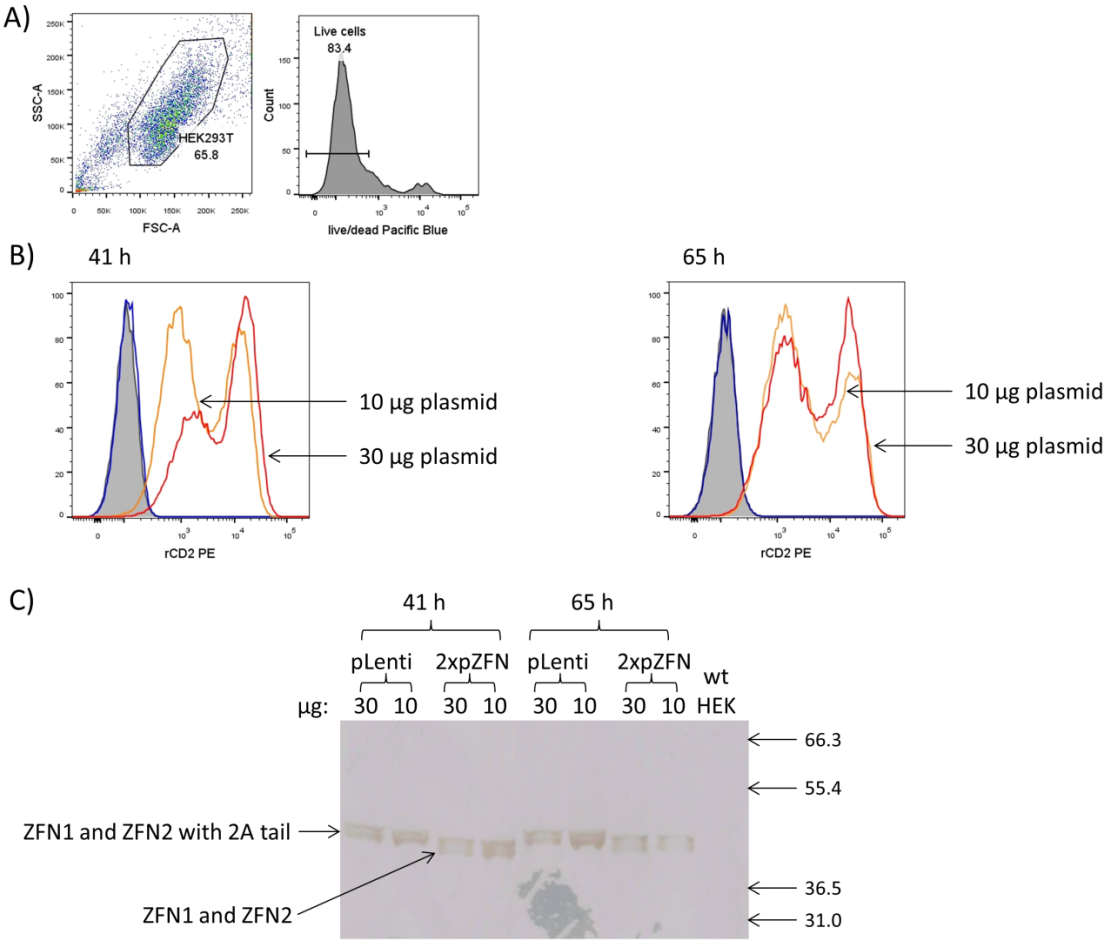

Figure 3.13: CD2 surface expression and ZFN protein expression in HEK293T cells transfected with pLenti-ZFN1/2-CD2 or pZFN1 and pZFN2. HEK293T cells were $CaCl_2$ transfected with 10 µg or 20 µg of the pLenti-ZFN1/2-CD2 (pLenti) or 2 x 5 µg or 2 x 10 µg of the pZFN1 and pZFN2 plasmids (2 x pZFN). A) HEK293T cells were dissociated from the culture flasks, at 41 and 65 h, using a non-enzymatic dissociation buffer and the gating strategy is shown. B) CD2 expression on HEK293T cells that were untransfected (grey filled) or transfected with 10 µg (orange) or 30 µg (red) of pLenti-ZFN1/2-CD2 plasmid and stained with an anti-CD2 Ab or unstained (blue). C) Lysate from untransfected (wt) or transfected cells, 41 or 65 h post transfection, was immunoblotted for the 3xFlag tag. The predicted sizes of the ZFN1 and ZFN2 are 44.33 kDa and 44.65 kDa, respectively. The predicted sizes for the C terminal tail of T2A and P2A and ZFN1 and ZFN2 in the pLenti-ZFN1/2-CD2 plasmid are 49.56 and 49.43 kDa, respectively. The immunoblot was not exposed as the signal was visible by eye.

After having established the expression of the plasmids in the HEK293T cells, gDNA was extracted and it was used for the Cel-I mismatch assay. As shown in figure 3.14, cells transfected either with the pLenti-ZFN1/2-CD2 plasmid or both the pZFN1 and pZFN2 plasmids, showed clear Cel-I nuclease digestion bands at 220 bp and 178 bp. Both transfections resulted in approximately 19% of cells expressing mutant SHP-1. Thus the pLenti-ZFN1/2-CD2 construct, when delivered by $CaCl_2$ transfection, is providing functional ZFN1 and ZFN2 proteins that can target the SHP-1 gene site and introduce double stranded breaks leading to mutations.

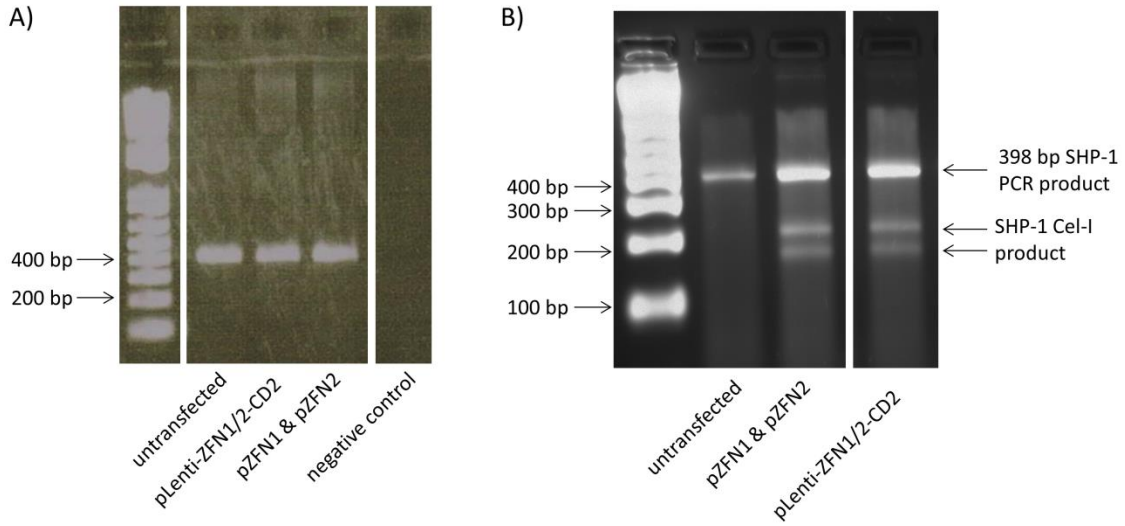

Figure 3.14: HEK293T cells, transfected with the pZFN1 and pZFN2 plasmids or the pLenti-ZFN1/2-CD2 plasmid, show mutations in the SHP-1 gene when analysed by the Cel-I mismatch assay. HEK293T cells were $CaCl_2$ transfected with 30 µg pLenti-ZFN1/2-CD2 plasmid or 2 x 15 µg pZFN1 and pZFN2 plasmid and the gDNA collected at 65 h post-transfection. A) gDNA from HEK293T cells was used to amplify a 398 bp SHP-1 gene sequence encompassing the potential ZFN cutting site with primers 55 and 56. B) The PCR products were hybridised and mismatched DNA was restricted by the Cel-I nuclease resulting in two smaller DNA bands (220 bp and 178 bp). The % of cells harbouring SHP-1 mutations was obtained by ImageJ analysis.

In summary, the ZFN proteins designed by SIGMA bind to the SHP-1 gene and introduce double stranded breaks when delivered by transient transfection, as shown in the HEK293T cells. Although lentiviral delivery showed expression of the CD2 protein and also expression of the 3xFlag of at least one of the ZFNs, no mutations were detected. This is likely due to

recombination events between the homologous ZFN sequences when the pLenti plasmid is packaged into the LV particle in the HEK293T packaging cells, resulting in the deletions of parts of the sequences. This has been observed in studies using TALENs and HIV-based lentiviral vectors (Holkers et al. 2013).

3.6 Generation of lentiviral transfer plasmids encoding each SHP-1 ZFN1 and ZFN2 separately

To avoid the recombination of the ZFN sequences, two single plasmids were generated encoding either the ZFN1 or ZFN2 genes.

The pLenti-3xFlag-ZFN1 (pLenti-ZFN1) plasmid construct was generated by amplifying the 3xFlag-ZFN1 gene from the SIGMA pZFN1 plasmid, using primers 60 and 61, and cloning it into the pLenti transfer vector (figure 3.15). The cloning was confirmed by sequencing the plasmid using primers 12-15 and 33-34.

To allow the detection of both ZFNs in transduced cells, the 3xFlag tag of the pZFN2 plasmid from SIGMA was exchanged for a V5 tag (figure 3.16). The V5 tag amino acid sequence (MGKPIPNPLLGLDST) is encoded by the DNA sequence ATGGGTAAGCCTATCCCTAACCCTCTCCTCGGTCTCGATTCTACG, which was introduced upstream of the ZFN2 start codon by adding it to primer 62. The pLenti-V5-ZFN2 (pLenti-ZFN2) plasmid was confirmed by sequencing using primers 22-25 and 33-34.

To be able to select viable transduced cells, the CD2 surface marker was introduced into the transfer vector alongside the ZFN2 gene. Primer number 66 and 32 were used to amplify the ZFN2 gene. Primer 66 was designed to introduce a Kozak sequence upstream of the start

codon of the ZFN2 thus eliminating the previously present 3xFlag tag. The pLenti-ZFN2-P2A-CD2 plasmid (pLenti-ZFN2-CD2) was constructed as described in figure 3.17 and sequenced using primers 4, 6-7, 22, 24-25 and 33-34.

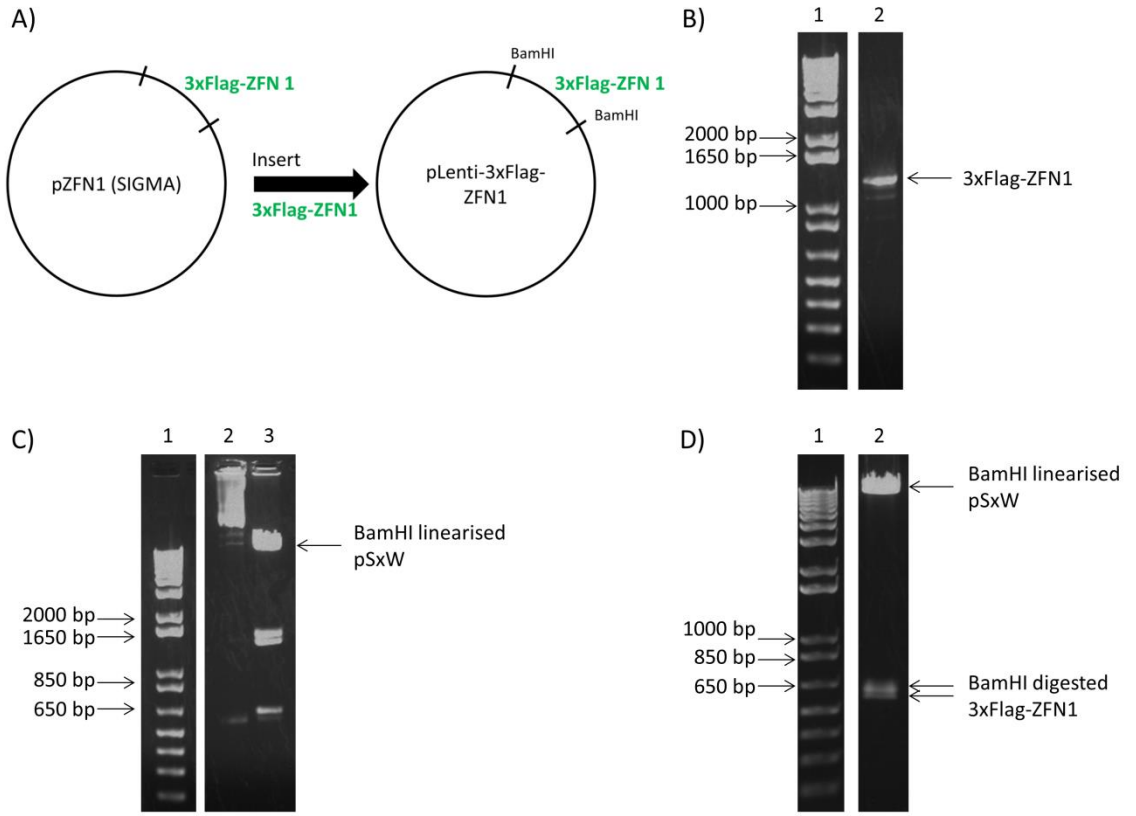

Figure 3.15: Generation of the pLenti-3xFlag-ZFN1 transfer vector. A) Cloning strategy to generate the lentiviral transfer vector pLenti-ZFN1. B) Lane 2 shows the 1193 bp 3xFlag-ZFN1 DNA amplified using primers 60 and 61 from the SIGMA pZFN1 plasmid. C) Lane 3 shows the BamHI restriction digest of the pSxW plasmid and lane 2 shows the non-restriction digested plasmid. The linearised 8942 bp pSxW vector was purified and used together with the purified PCR product in B) to set up an In-Fusion reaction. DH5α cells were transformed with 2 µl of In-Fusion mix. D) Plasmid DNA extracted from DH5α colonies transformed as described above and selected for Ampicillin resistance was restriction digested with BamHI is shown in lane 2. The upper band shows the BamHI linearised 8942 bp pSxW and the two lower bands correspond to the two BamHI restriction fragments of 3xFlag-ZFN1 (564 bp and 603 bp).

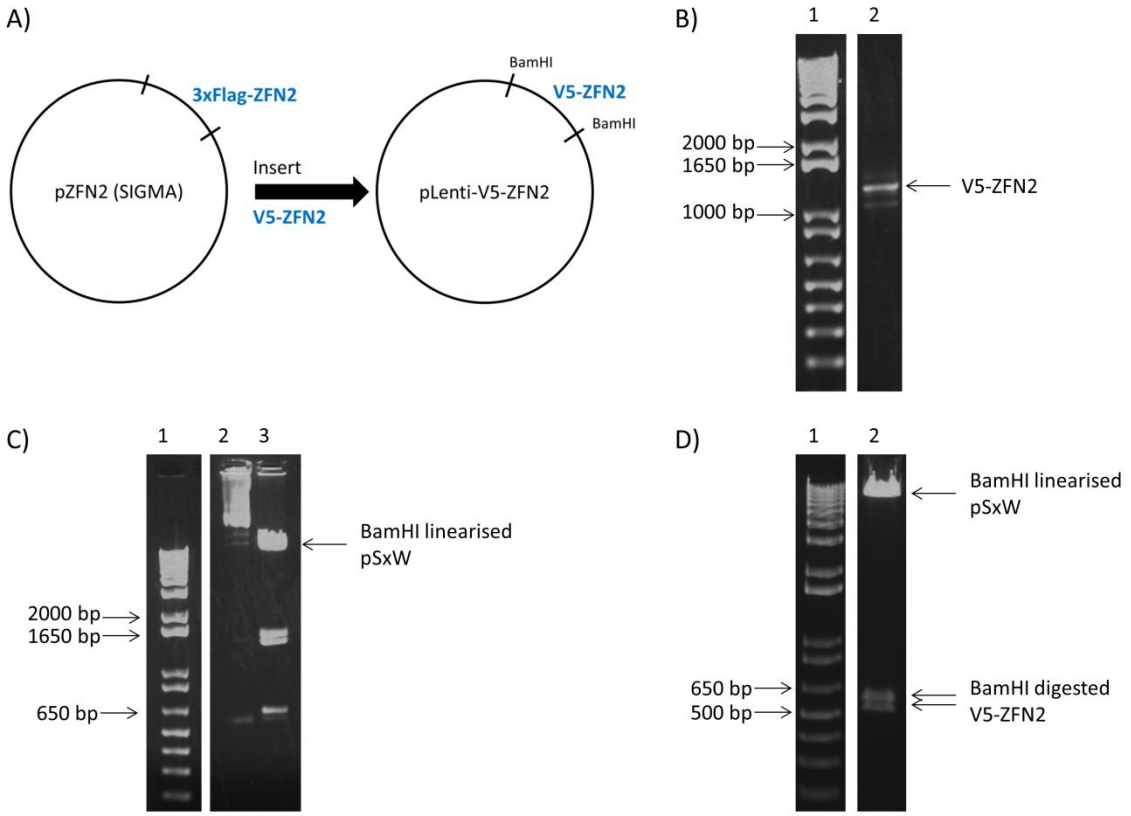

Figure 3.16: Generation of the pLenti-V5-ZFN2 transfer vector. A) Cloning strategy to generate the lentiviral transfer vector pLenti-ZFN2. B) Lane 2 shows the 1163 bp V5-ZFN2 DNA amplified using primers 62 and 63 from the pZFN2 SIGMA template expressing 3xFlag-ZFN2. Only the upper band was selected by gel excision for further steps. C) Lane 3 shows the BamHI restriction digest of the pSxW plasmid and lane 2 shows the non-restricted plasmid. The linearised 8942 bp pSxW vector was purified and used together with the purified PCR product in B) to set up an In-Fusion reaction. DH5α cells were transformed with 2 µl of In-Fusion mix. D) Plasmid DNA extracted from DH5α colonies transformed as described above and selected for Ampicillin resistance was restriction digested with BamHI is shown in lane 2. The upper band shows the BamHI linearised 8942 bp pSxW and the two lower bands correspond to the two BamHI restriction fragments of V5-ZFN2 (540 bp and 597 bp).

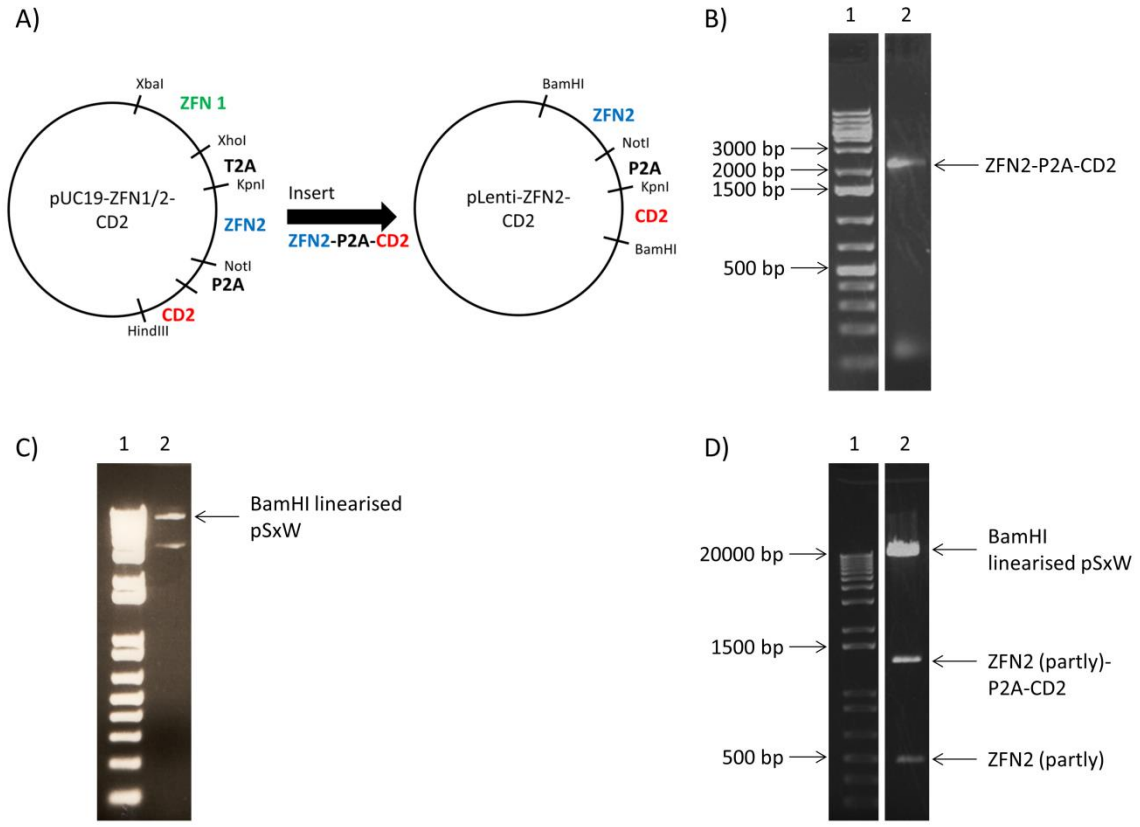

Figure 3.17: Generation of the pLenti-ZFN2-P2A-CD2 transfer vector. A) Cloning strategy to generate the lentiviral transfer vector pLenti-ZFN2-CD2. B) Lane 2 shows the PCR reaction for primers 66 and 32 and the DNA template of XhoI and HindIII restriction digested pUC19-ZFN1/2-CD2. The 1901 bp PCR product was purified and used for further steps. C) Lane 2 shows the BamHI restriction digest of the pSxW plasmid. The linearised 8942 bp pSxW vector was purified and used together with the purified PCR product in B) to set up an In-Fusion reaction. DH5α cells were transformed with 2 µl of In-Fusion mix. D) Plasmid DNA extracted from DH5α colonies transformed as described above and selected for Ampicillin resistance was restriction digested with BamHI is shown in lane 2. The upper band shows the BamHI linearised 8942 bp pSxW and the two lower bands correspond to the two BamHI restriction fragments of a part of 495 bp ZFN2 and the remaining of 1380 bp ZFN2-CD2.

3.7 Analysis of gag$^+$ leukaemic T cells transduced with ZFN1 and ZFN2 or ZFN2-CD2 LV

Gag$^+$ Jurkat cells were transduced with either 250 µl of 10x concentrated ZFN1 or ZFN2 LV. Cells were lysed 5 days post transduction and the lysate immunoblotted for V5 and 3xFlag tag (figure 3.18). Transduced gag$^+$ Jurkat cells gave strong signals for the tags, indicating successful transduction and protein expression of the ZFNs.

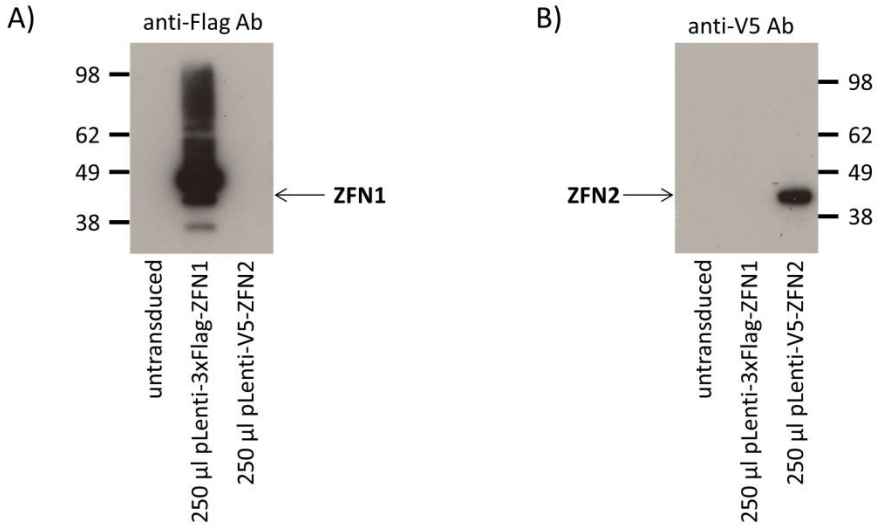

Figure 3.18: Gag$^+$ Jurkat cells, transduced with pLenti-3xFlag-ZFN1 or pLenti-V5-ZFN2 LV, express 3xFlag or V5 tag respectively. Gag$^+$ Jurkat cells were untransduced or transduced with 250 µl of 10x concentrated LV as indicated. Cells were collected and lysed 5 days post-transduction. A) Cell lysate was probed for the presence of the 3xFlag tag. The predicted size of the 3xFlag-ZFN1 protein is 44.33 kDa. B) Cell lysate was probed for the presence of V5 tag. The predicted size of the V5-ZFN2 protein is 45.09 kDa.

In order to detect and sort LV transduced cells, the CD2 surface marker was introduced into the ZFN2-CD2 LV and transduction of gag$^+$ Jurkat cells with 150 ng of each the ZFN1 and ZFN2-CD2 LVs was evaluated by flow cytometry for the cell surface expression of CD2 2 days post transduction (figure 3.19). All gag$^+$ Jurkat cells were transduced with the ZFN2-CD2 LV; however the efficiency of ZFN1 LV transduction could not be assessed.

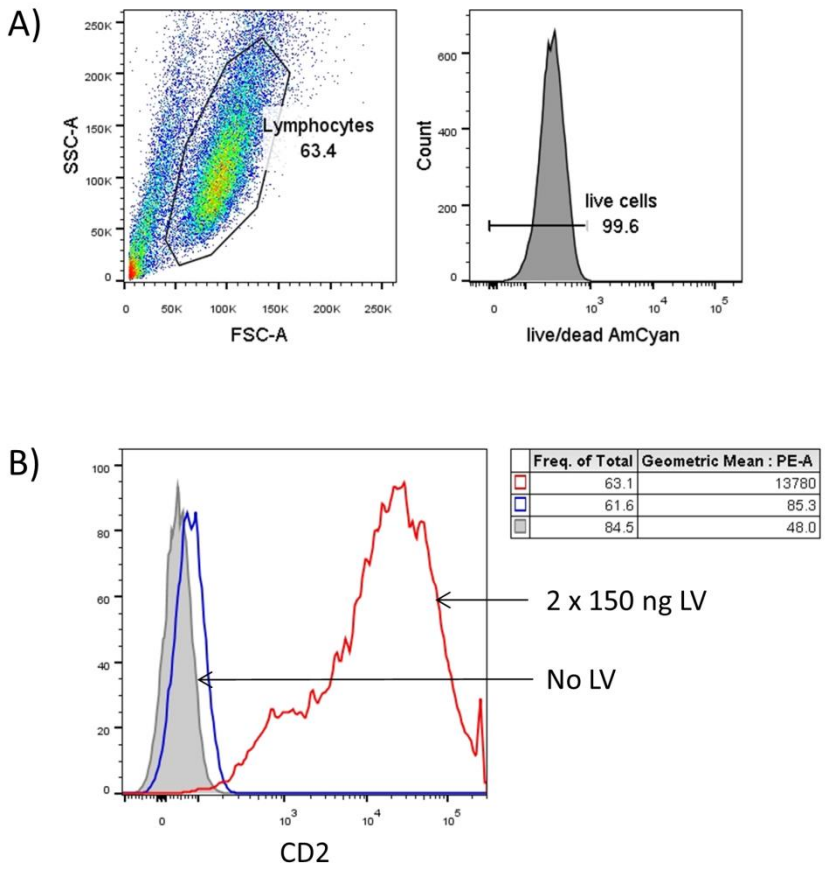

Figure 3.19: CD2 surface expression of gag$^+$ Jurkat cells transduced with ZFN1 and ZFN2-CD2 LV. Gag$^+$ Jurkat cells were transduced with 150ng of ZFN1 and ZFN2-CD2 LV and cells collected and stained for flow cytometry 48 h post-transduction. A) Gating strategy for transduced gag$^+$ Jurkat cells. B) Untransduced (grey filled) and transduced (red) cells were stained with anti-CD2 Ab and transduced cells were stained with isotype control (blue).

3.8 Mutation analysis in the human SHP-1 gene in gag$^+$ leukaemic T cells transduced with ZFN1 and ZFN2 or ZFN2-CD2 LV

Cells as highlighted in figure 3.18 were transduced with the ZFN1 and ZFN2 LV and analysed for mutations by performing a Cel-I assay (figure 3.20). Cel-I treated gDNA from gag$^+$ Jurkat cells transduced with both ZFN LVs, but not with a control CD2 LV or no LV, showed strong bands at 220 bp and 178 bp corresponding to approximately 30% of cells expressing mutant SHP-1. For the first time in human T cells, SHP-1 specific mutations induced by the SHP-1 specific ZFNs were detectable.

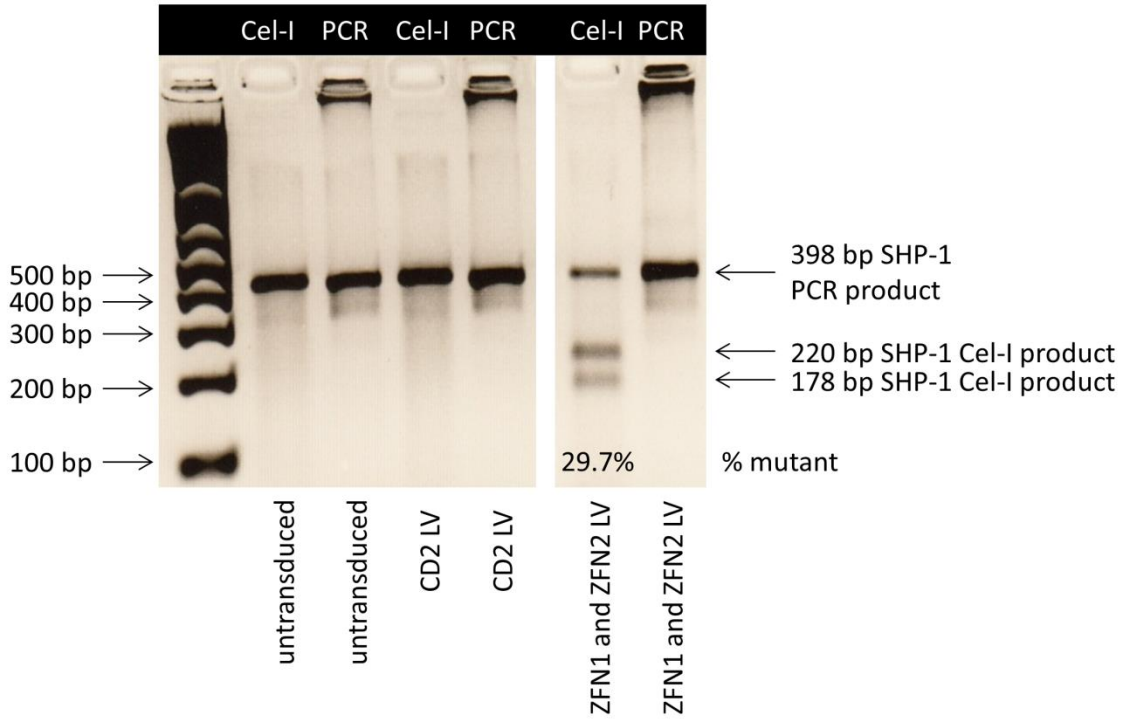

Figure 3.20: SHP-1 mutation analysis of gag$^+$ Jurkat cells, transduced with ZFN1 and ZFN2 LV. gDNA from gag$^+$ Jurkat cells, shown in figure 3.18, was used to amplify a 398 bp SHP-1 gene sequence encompassing the potential ZFN cutting site with primers 55 and 56. The PCR products were hybridised and mismatched DNA was restricted by the Cel-I nuclease resulting in two smaller DNA bands (220 bp and 178 bp). Untransduced and rCD2 LV transduced cells were used as negative controls.

To be able to sort on ZFN2 transduced cells, the ZFN2-CD2 and ZFN1 LVs were used for the transduction of gag$^+$ Jurkat (figure 3.19) and gDNA was extracted and restricted with the Cel-I nuclease (figure 3.21). Cells showed a strong signal when transduced with both ZFN expressing LVs, indicating that this combination of LVs can also give a high proportion of mutations in the SHP-1 gene. The transduced cells from this experiment were cloned and clone analysis is shown in chapter 4.

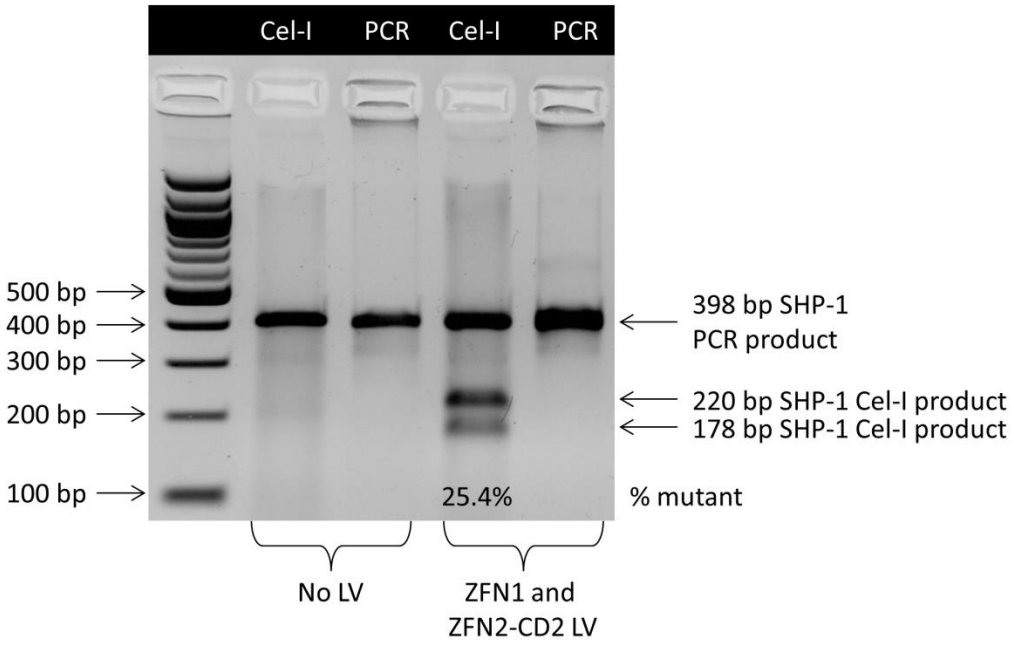

Figure 3.21: SHP-1 mutation analysis of gag$^+$ Jurkat cells, transduced with ZFN1 and ZFN2-CD2 LV. gDNA from gag$^+$ Jurkat cells, shown in figure 3.19, was used to amplify a 398 bp SHP-1 gene sequence encompassing the potential ZFN cutting site with primers 55 and 56. The PCR products were hybridised and mismatched DNA was restricted by the Cel-I nuclease resulting in two smaller DNA bands (220 bp and 178 bp). Untransduced and cells were used as a negative control.

3.9 Integrase deficient LV delivery of SHP-1 ZFNs to leukaemic T cells

In order to reduce the likelihood of potential off-target mutations by the SHP-1 specific ZFNs, a non-integrating ZFN gene delivery method would be preferential. An integrase-deficient LV (IDLV) was therefore produced in the same way as the LV with the exception of using a mutant D64V integrase encoding plasmid (Yanez-Munoz et al. 2006) when doing the LV packing reaction as described in Materials and Methods. Firstly, the time course of protein expression from an IDLV delivery was studied by using the CD2 IDLV. Secondly, both ZFN1 and ZFN2-CD2 IDLVs were used with the aim to introduce SHP-1 specific mutations in leukaemic T cells.

Gag^+ Jurkat and MOLT-3 cells were transduced with 250 µl of 10x concentrated IDLV or LV and cell surface expression was measured 3, 5 and 9 days post-transduction (figure 3.22). At day 3, LV and IDLV gave complete transduction of the cells with the LV delivery yielding more strongly CD2 expressing cells. Whereas the integrated CD2 gave a stable high expression level of CD2, the IDLV infection resulted in a quick dilution of the CD2 signal to a complete disappearance by day 9. This was not surprising considering the high division rate demonstrated by both leukaemic T cells (shown in Chapter 4). This result showed that the window for sorting cells on the basis of CD2 expression would have to be within the first three days.

Gag^+ MOLT-3 cells were transduced with ZFN1 and ZFN2-CD2 IDLV and LV. Despite a complete transduction of MOLT-3 cells using both the 2x200 ng and 2x400 ng IDLV doses (figure 3.23 A), no SHP-1 mutations were observed in these cells in comparison with 25% of cells carrying mutant SHP-1 when transduced with LV (figure 3.23 B).

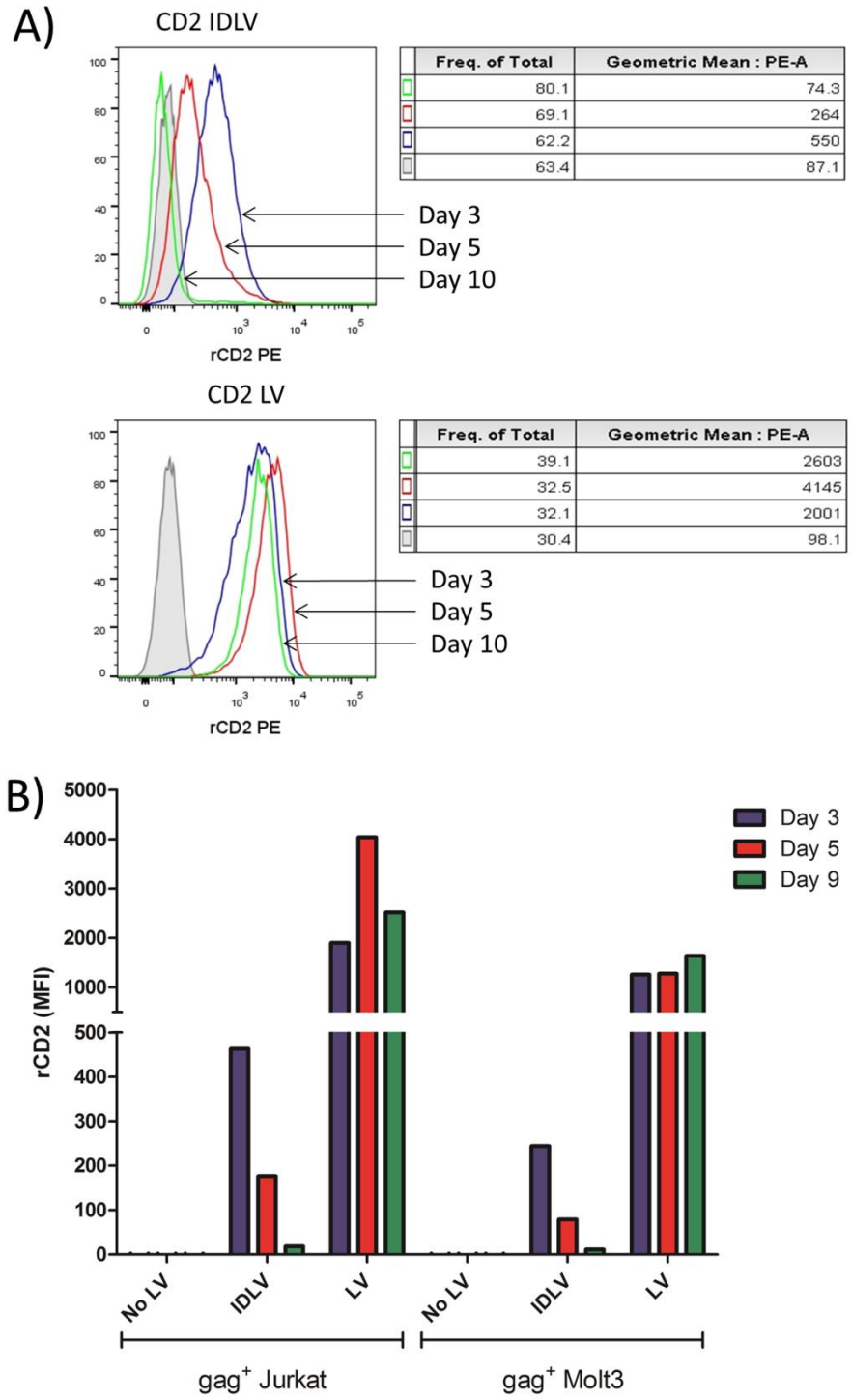

Figure 3.22: Time course of CD2 expression of CD2 IDLV or LV transduced leukaemic T cells. Gag$^+$ Jurkat and gag$^+$ MOLT-3 cells were transduced with 250 µl of 10x concentrated CD2 IDLV or LV and CD2 protein expression was measured by flow cytometry using an anti-CD2 Ab. Cells were gated on FSC/SSC, live/dead stain and single cell profiles. A) Histogram overlay of CD2 surface expression on gag$^+$ Jurkat cells at day 3 (blue), 5 (red) and 9 (green) days post-transduction. Unstained IDLV or LV transduced cells at day 3 are shown in grey filled and untransduced cells are shown as a black line. B) Levels of CD2 expression on Jurkat and MOLT-3 cells, transduced with CD2 IDLV or LV, shown using the CD2 MFI minus the MFI of the corresponding unstained cells.

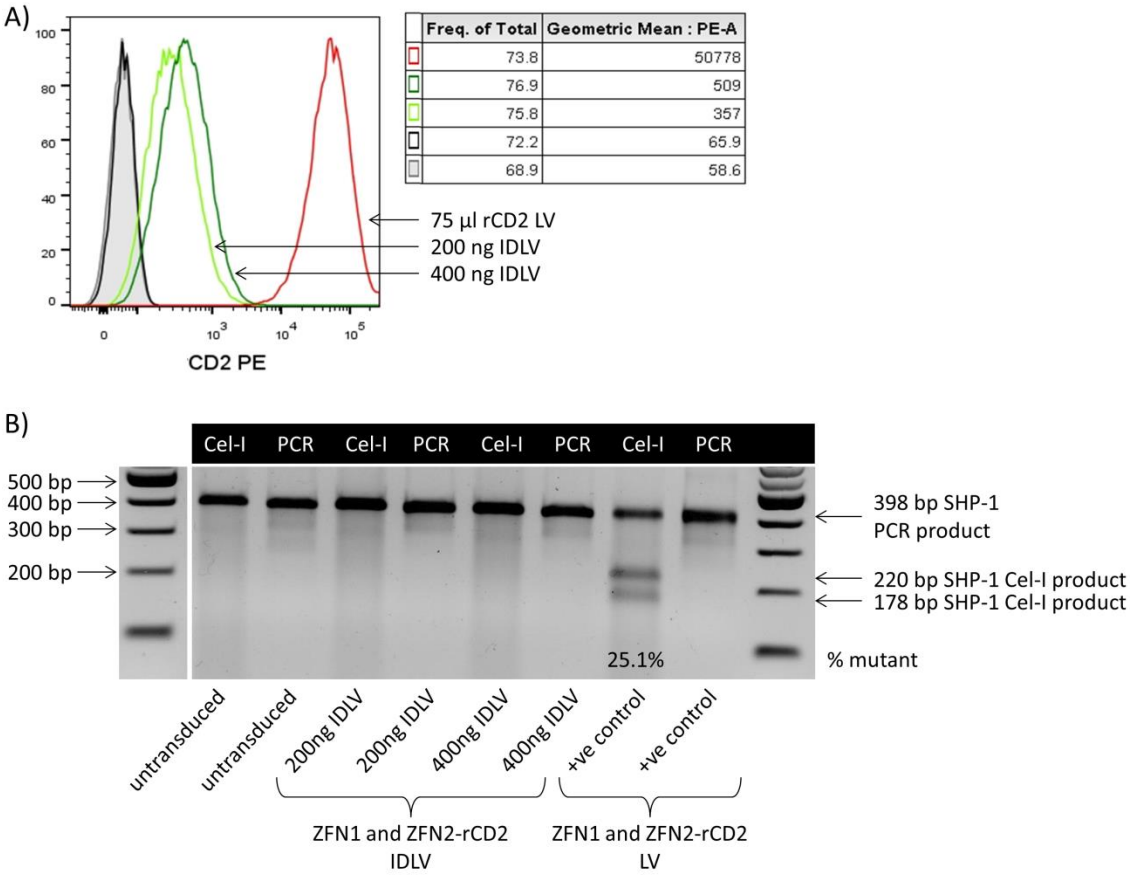

Figure 3.23: Gag$^+$ MOLT-3 cells, transduced with ZFN1 and ZFN2-CD2 IDLV or LV, were analysed for CD2 surface expression and SHP-1 mutations. A) Gag$^+$ MOLT-3 cells were transduced with 200 ng (bright green) or 400 ng (dark green) of ZFN1 and ZFN2-CD2 IDLV, alongside a control transduction of 75 µl of 100x concentrated CD2 LV (red) and non-transduced cells (grey filled). Cells were then stained using an anti-CD2 Ab and or left unstained (black). B) Gag$^+$ MOLT-3 from A) as well as cells transduced with ZFN1 and ZFN2-CD2 LV (+ve control) had their gDNA extracted and a 398 bp SHP-1 gene part amplified by PCR. This was then hybridised and used in the Cel-I mismatch assay.

3.10 Discussion

In this chapter it was shown that the SHP-1 specific ZFNs can induce mutations within the target SHP-1 DNA sequence in approximately 25-30% of ZFN expressing leukaemic T cells. However mutations were only observed when the two ZFNs were delivered in two separate integrase proficient LVs or when cells were transfected with the plasmid expressing both ZFNs. The initial attempt at delivering both ZFNs within a single LV was unsuccessful, most probably due to the deletion of parts of the ZFN sequences by homologous recombination. The two ZFNs have a high sequence homology, as illustrated by the difficulty faced when designing specific primers for sequencing of the pLenti-ZFN1-ZFN2-CD2 plasmid. It has previously been shown that the reverse transcription process, active when generating LV in HEK293T packaging cells, is very prone to recombination if repeat DNA sequences are present (Holkers et al. 2013). Additionally, the frequency of recombination depends on the distance between the repeat DNA sequences. At distances similar to that observed between ZFN1 and ZFN2 in the pLenti-ZFN1-ZFN2-CD2 plasmid (1200 bp), approximately 60-80% of the DNA will recombine (Delviks and Pathak 1999). This high level of deletion of ZFN sequence during LV production in HEK293T cells could thus explain the observed absence of mutated SHP-1 in MOLT-3 cells transduced with ZFN1/2-CD2 LV (figure 3.10-11).

Additionally, no SHP-1 mutations were observed when delivering the ZFNs with IDLVs and there are at least two possible reasons for this. The first possibility is the high proliferation rate of leukaemic cells and the resulting rapid dilution of ZFN transgenes and ZFN protein (no CD2 signal at day 9). However, this short expression should nevertheless be enough to induce mutations as the short duration of expression when ZFNs are delivered as mRNA has shown the induction of mutations. The second possibility is the lower transduction efficiency of IDLV (approximately 0.25x that of LV in figure 3.22). Both factors will lead to lower levels and shorter expression times of ZFN proteins in the cells, resulting in a lack of targeted SHP-1

mutations. Additionally, only two studies have reported the use of IDLV delivery of ZFNs (Lombardo et al. 2007; Provasi et al. 2012) indicating that this technique is not simple to get to work and the experiments by Lombardo *et al.* were done using commercially produced and purified high titre IDLV. Due to the unavailability of this service and the unsuccessful IDLV delivery, LV delivery of the ZFNs was chosen for the rest of this study.

Chapter 4: SHP-1 deficient leukaemic T cells and functional consequences

4.1 Introduction

In the previous chapter, lentiviral delivery of the two SHP-1 specific ZFNs successfully induced mutations in the SHP-1 gene. Here, leukaemic cells transduced with ZFN LVs will be examined, on a clonal level, for potentially altered SHP-1 protein expression and changes in T cell function.

Initially, gag^+ leukaemic cells were transduced with SHP-1 specific ZFN LVs, cells were cloned and the clones analysed for SHP-1 protein expression. Established SHP-1 deficient clones were activated with peptide pulsed antigen presenting cells (APCs). The APCs used were HLA-A2 expressing C1R cells, a leukaemic B cell line. T cell activation readouts such as TCR downregulation and CD69 upregulation were examined (figure 4.1 A) as CD69 is one of the earliest molecules to be expressed *de novo* during T cell activation (Cebrián et al. 1988).

A T cell activation reporter system was also used to measure activation in Jurkat cells expressing a tumour-specific TCR recognising the MART-1_{26-35} peptide (EAAGIGILTV) when presented by HLA-A2 (Cole et al. 2009). This TCR will subsequently be referred to as the Mel TCR. In this model, a Gaussia Luciferase (GLuciferase) gene is under the control of nuclear factor of activated T cells (NFAT) response elements (RE) and a minimal IL-2 promoter (Govers et al. 2011). Once cells are activated, dephosphorylation of the NFAT protein by the calmodulin and calcineurin complex leads to the nuclear translocation of NFAT, NFAT binding to the NFAT REs, initiation of the GLuciferase gene transcription and secretion of GLuciferase protein (figure 4.1 B).

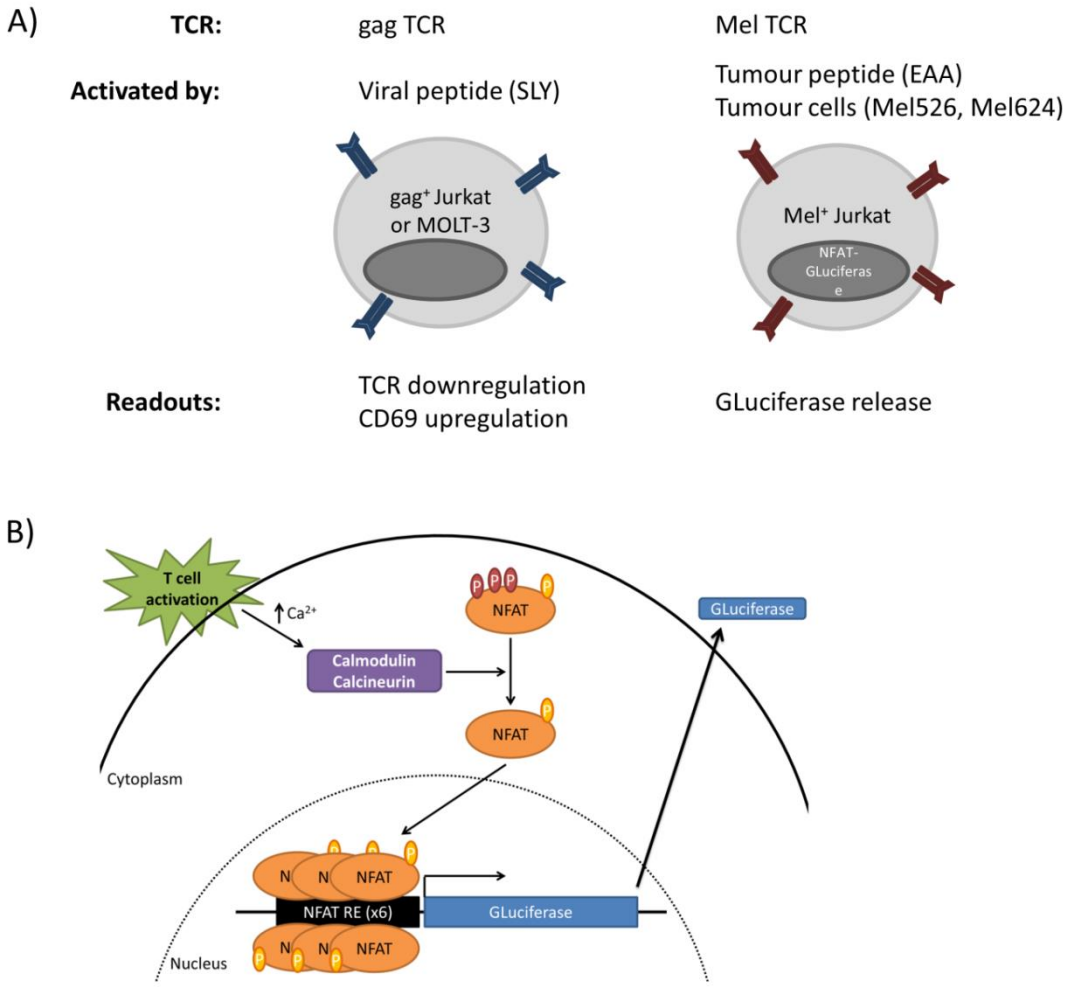

Figure 4.1: Leukaemic T cell models used to study the effect of SHP-1 deficiency on T cell activation. A) The two different TCRs used in this chapter are shown. The high affinity gag TCR, recognising viral peptide, was expressed in MOLT-3 and Jurkat cells and T cell activation readouts were TCR downregulation and CD69 upregulation. The melanoma specific Mel TCR was expressed in Jurkat cells alongside the NFAT reporter cassette. B) The lentivirally delivered GLuciferase gene cassette has a six times NFAT response element to which nuclear NFAT binds and initiates GLuciferase gene expression. Following activation of Jurkat cells, either via the TCR or by chemical stimulation, Ca^{2+} levels in the cytoplasm increase and the Ca^{2+} binds to calmodulin. The latter activates calcineurin which subsequently dephosphorylates NFAT allowing NFAT to translocate to the nucleus leading to GLuciferase protein secretion. GLuciferase activity in the supernatant of activated cells can be measured by adding luciferin substrate.

4.2 Cloning of ZFN LVs transduced gag$^+$ MOLT-3 cells and characterisation of SHP-1 deficient clones

To establish the clones shown in figure 4.2 A, gag$^+$ MOLT-3 cells were transduced with the ZFN1 and ZFN2 LVs and the cells analysed for SHP-1 mutations using the Cel-I assay (figure 4.2 B). Analysis of the signal intensity of the restricted DNA fragments (220 and 178 bp) in relation to the non-restricted fragment (398 bp), using ImageJ software, indicated a mutation frequency of 24%. This analysis was used as an estimate of the frequency as it is only semi-quantitative. Nevertheless, it is instructive to perform when considering cell cloning, as mutation frequencies lower than 1% are a counter-indication for cloning as stated by Sigma-Aldrich representatives.

To fully establish mutation frequencies, ZFN LV transduced cells were cloned and analysed for mutations in the SHP-1 gene by Cel-I (figure 4.3 B). After PCR amplification of the 398 bp SHP-1 DNA sequence, clones P3 3G and P2 3E showed a 398 bp wt DNA band as well as a smaller fragment (figure 4.3 A). This indicated deletions introduced by the SHP-1 specific ZFNs of roughly ten and one hundred nucleotides for the P3 3G and P2 3E clones, respectively. Interestingly, every clone showed Cel-I restriction fragments, thus each clone has at least one mutated SHP-1 allele (figure 4.3 B). These mutations are probably less than 10 nucleotides, as PCR products do not show two distinct bands. However, large deletions abrogating a PCR primer binding site are also possible and would not be picked up by these assays.

To further characterise the clones, cell lysates from wt cells and the clones were immunoblotted for the SHP-1 protein and an actin loading control. Thirteen gag$^+$ MOLT-3 cells were analysed for SHP-1 protein expression and 31% (4/13) were SHP-1 protein deficient, 46% (6/13) showed reduced SHP-1 protein expression and 23% (3/13) showed levels comparable to

wt (figure 4.4). Overall, a majority of analysed cells have mutations in the SHP-1 gene that affect protein expression.

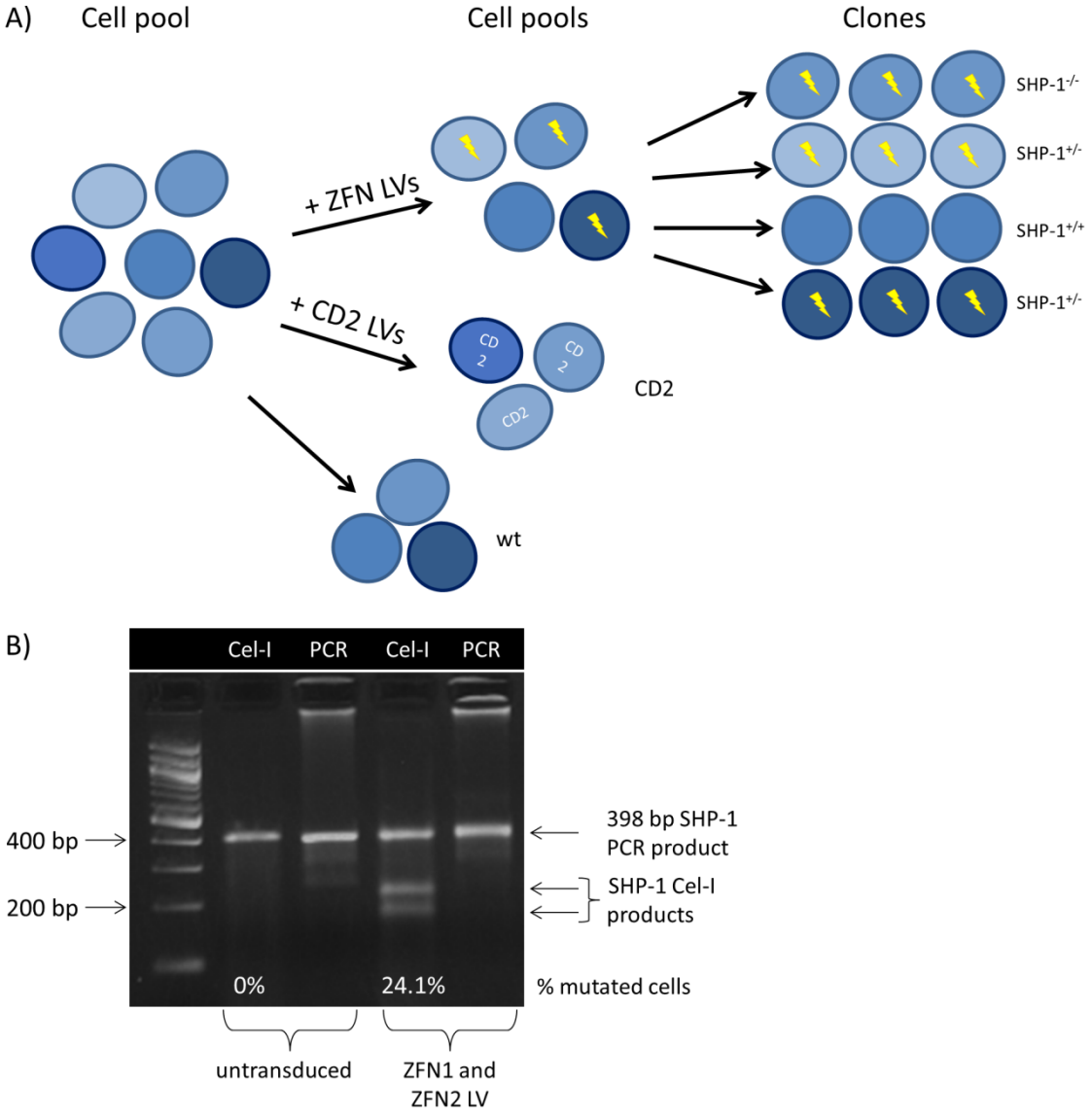

Figure 4.2: Overview of the cloning of ZFN LVs transduced gag^{+} MOLT-3 and analysis of SHP-1 mutations. A) Overview of the cloning strategy for gag^{+} MOLT-3 cells. Wt and CD2 cells were not cloned whereas the ZFN LVs transduced cells were cloned and analysed for SHP-1 mutations. Yellow arrows indicate mutations in the SHP-1 due to ZFN activity and SHP-1$^{+/-}$ and SHP-1$^{-/-}$ indicated cells with reduced or absent SHP-1 protein respectively. B) Gag^{+} MOLT-3 cells were either untransduced or transduced with 250 µl of 10x concentrated ZFN1 and ZFN2 LVs. Genomic DNA was isolated, the 398 bp SHP-1 DNA sequence was amplified by PCR and subsequently restriction digested with the Cel-I enzyme. The % of cells harbouring SHP-1 mutations was obtained by ImageJ analysis.

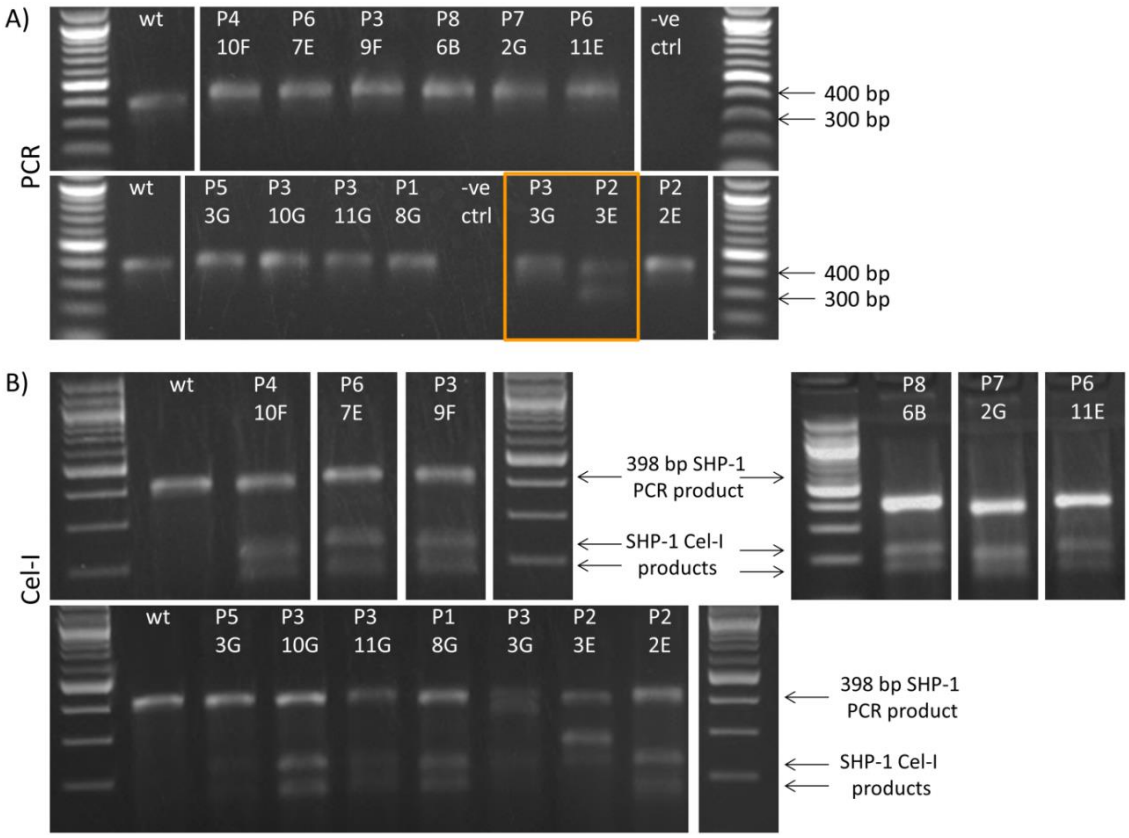

Figure 4.3: SHP-1 mutation analysis in gag$^+$ MOLT-3 cell clones transduced with ZFN1 and ZFN2 LV. Gag$^+$ MOLT-3 cells, previously transduced with ZFN1 and ZFN2 LV, were cloned and clone names are indicated at the top of the electrophoresis gels. A) Genomic DNA was isolated from clones and the 398 bp ZFN target site was amplified by PCR using primers 55 and 56. The wt wells show the PCR results for gDNA from untransduced cells and the negative control (-ve ctrl) shows the PCR result when no gDNA was added. Two clones showed visible deletions in the SHP-1 PCR product (orange box). B) The PCR products of each clone and wt cells were hybridised and restriction digested by the Cel-I nuclease, giving rise to the 200 bp and 178 bp restriction fragments.

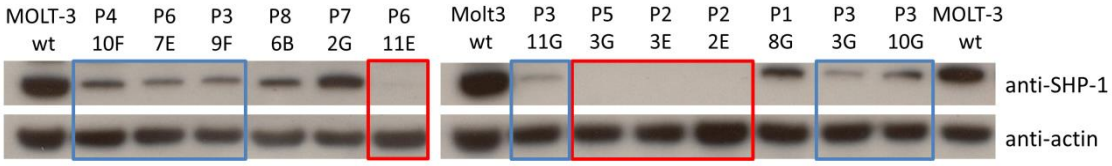

Figure 4.4: Immunoblotting for SHP-1 protein expression of gag$^+$ MOLT-3 clones. Gag$^+$ MOLT-3 wt cells and clones were lysed and the cell lysate immunoblotted with anti-SHP-1 and anti-actin Abs. Clones with complete SHP-1 protein loss and clones with intermediate levels of SHP-1 protein are encased by red and blue boxes, respectively. Non-transduced cells (wt) were used as a positive control. A repeat immunoblot with the clones gave similar results. The anti-SHP-1 blots were exposed for longer than the anti-actin blots.

Five clones, either deficient for SHP-1 protein (P6 11E and P5 3G) or with reduced SHP-1 protein levels (P4 10F, P6 7E and P3 10G), were selected for DNA sequence analysis of the 398 bp PCR product. Due to the ZFNs causing independent and most probably different mutations in each allele, the sequencing readings showed peaks for two nucleotides in regions where more than one sequence of PCR product was present. These regions of mutations are indicated by missing DNA sequence in figure 4.5 A. As expected, all five clones showed mutations within the region of the ZFN binding site and due to the mutations being close or within a splice acceptor site, these mutations are predicted to lead to a reduction of SHP-1 protein. The results for clone P5 3G were the only interpretable readings showing an insertion of a single nucleotide on one allele and a deletion of 9 nucleotides on the other allele (figure 4.5 A and B). The insertion introduces a premature stop codon in the following exon whereas the deletion gives a three amino acid truncation in the SHP-1 protein upstream of the protein tyrosine phosphatase domain (figure 3.1). As shown by immunoblotting, overall this led to the P5 3G clone being SHP-1 deficient. No additional genetic analysis was done for these clones.

Due to complete SHP-1 deficiency, clones P2 2E and P5 3G were selected to study the effect of SHP-1 loss on T cell activation and proliferation. T cell activation induced TCR downregulation was measured for two SHP-1 mutant clones, CD2 LV transduced cells and wt cells in response to cognate peptide (SLY) pulsed APCs (figure 4.6 C). The gag^{+} TCR has a TCRV5β chain and therefore an anti-TCRV5β Ab was used to detect TCR levels. At similar T cell to APC ratios, TCR levels decreased in a peptide dose dependent manner with 10^{-4} M SLY peptide (figure 4.6 C and D). The SHP-1 deficient clone P5 3G showed significantly greater decreases in TCR expression at 10^{-4} M peptide than the three other cell types, reflecting enhanced TCR activation. However, the P5 3G clone had much higher basal TCR levels than the other groups. Furthermore, the wt and CD2 transduced cells were not clonal and comparing clones to cell pools was not ideal (figure 4.6 B). The P2 2E SHP-1 deficient clone did not show any significant differences in activation when compared to wt or CD2 controls but it also had very low TCR

levels. Overall, these results indicate that cells with differing TCR levels are not useful for comparing activation potential.

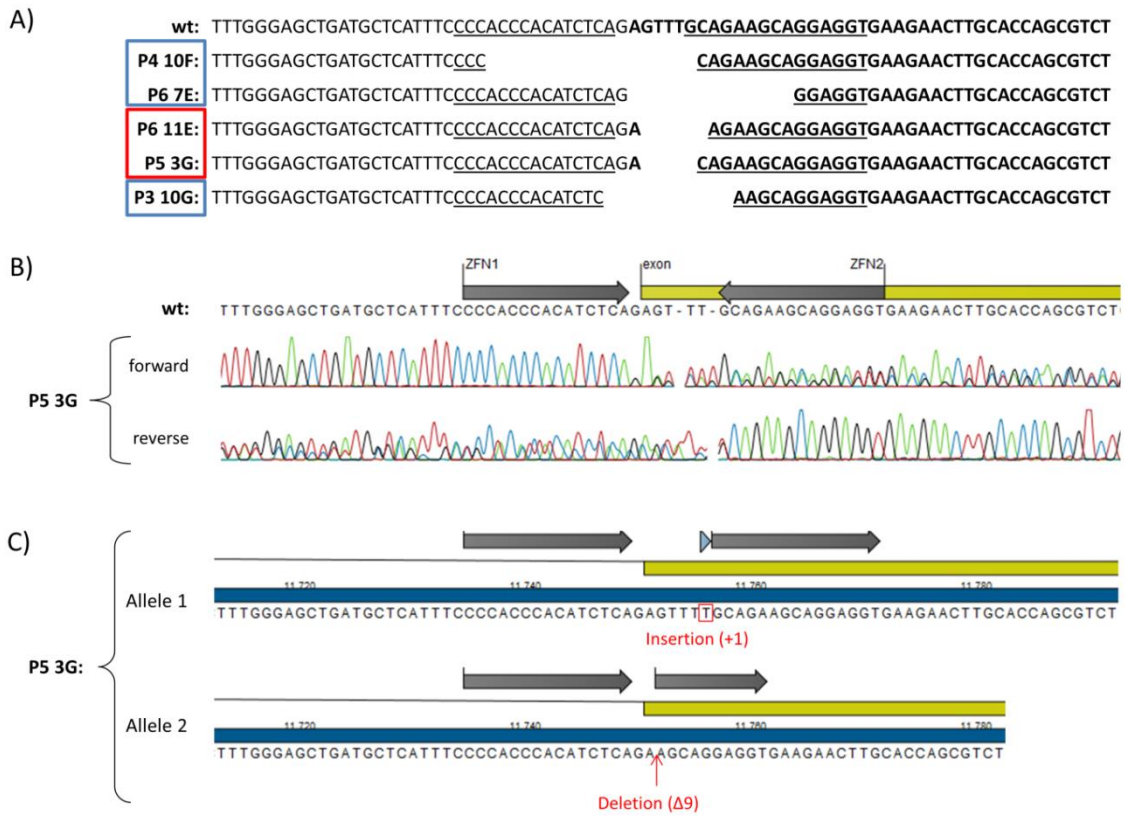

Figure 4.5: DNA sequencing of the 398 bp SHP-1 PCR products from gag$^+$ MOLT-3 clones transduced with ZFN1 and ZFN2 LV. Genomic DNA from five gag$^+$ MOLT-3 clones, previously transduced with the ZFN LVs, and wt cells was isolated, primers 55 and 56 used to PCR a 398 bp DNA sequence and the same primers were used for DNA sequencing of the PCR products. A) Results for the wt and five MOLT-3 clones are shown with red and blue boxes indicating loss or reduction in SHP-1 protein, respectively. The ZFN binding sites are underlined and sequence in bold indicates the SHP-1 exon 8. The regions of double peaked DNA sequence readings are indicated by missing nucleotides. B) The DNA sequencing results for the forward and reverse primer readings of the SHP-1 protein deficient P5 3G clone are shown. C) SHP-1 alleles of the P5 3G clone are shown after analysis of DNA sequencing results shown in B.

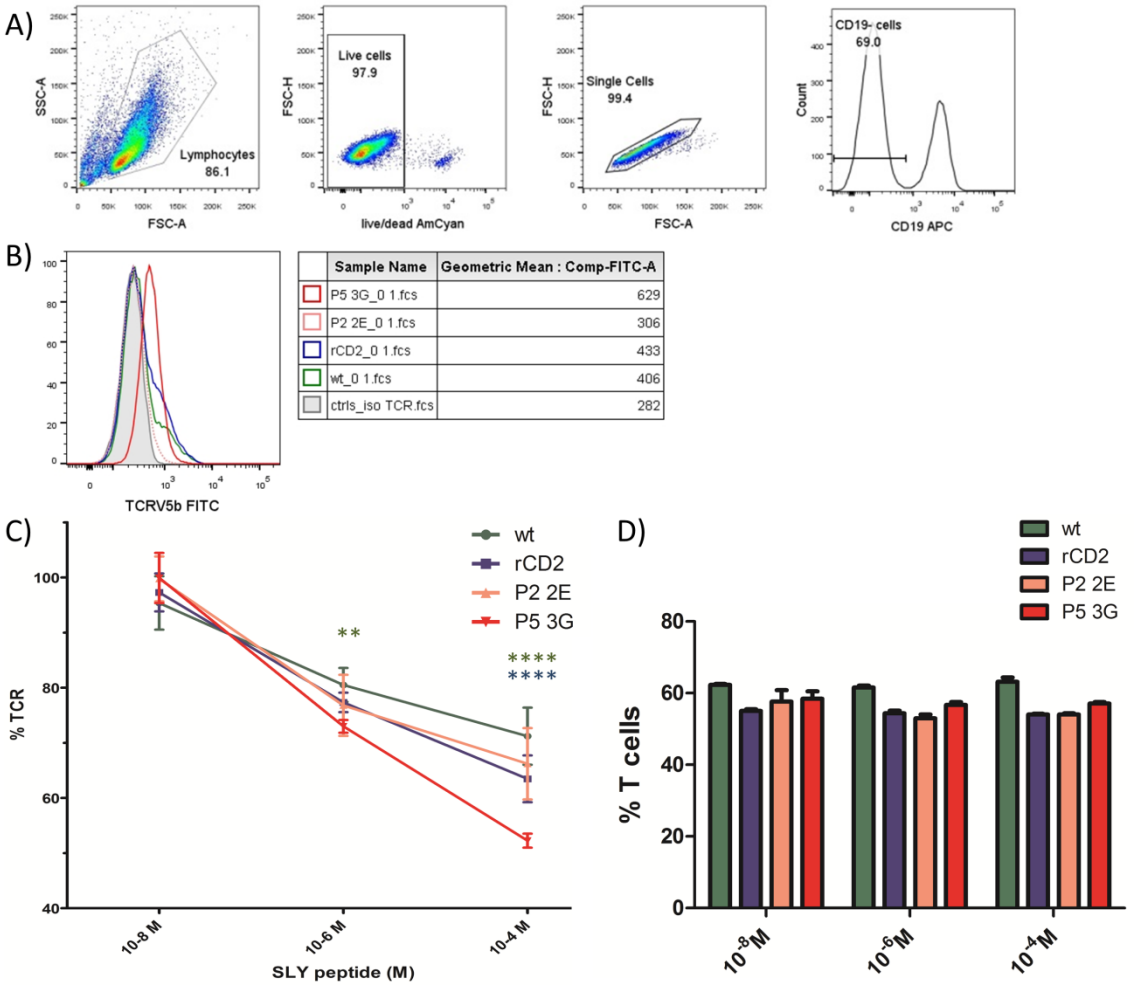

Figure 4.6: TCR downregulation in response to cognate peptide stimulation in SHP-1 deficient gag$^+$ MOLT-3 clones. Antigen presenting C1R cells were unpulsed or pulsed with increasing doses of cognate SLY peptide for 30 min. Control wt and CD2 transduced gag$^+$ MOLT-3 cells and two SHP-1 deficient gag$^+$ MOLT-3 clones, P2 2E and P5 3G, were stimulated with the APCs for 60 min, followed by staining for live/dead stain, anti-CD19 Ab and anti-TCRV5β Ab and flow cytometric analysis. A) Gating strategy for the analysis of cells in B-D. Cells analysed were live, single CD19 negative cells. B) TCRV5β cell surface levels for unstimulated wt (green), CD2 transduced (blue), P2 2E (pink dotted) and P5 3G (red) and unstained (grey filled) CD19 negative cells are shown. C) TCR downregulation is expressed as percentage of TCR expression in peptide pulsed cells relative to non-peptide pulsed cells for each cell type. The P5 3G clone showed significant differences with the wt (asterisk in green) and CD2 (asterisk in blue) cells. The P2 2E clone showed no significant differences when compared to wt and CD2 transduced cells. D) The percentage of T cells (CD19 negative) in the population of live single cells is shown. No significant differences were observed. C and D show pooled data from three independent experiments with triplicates for each condition and the error bars show the SEM. **p<0.01, ****p<0.0001. %TCR = MFI of sample / (mean of MFI of non-peptide pulsed cells)*100.

4.3 CFSE dilution in leukaemic T cells with or without peptide stimulation

Next, proliferation of unstimulated wt, CD2 transduced gag$^+$ MOLT-3 cells and SHP-1 deficient gag$^+$ MOLT-3 clones, P2 2E and P5 3G, was studied by doing a CFSE dilution experiment over 3 days (figure 4.7 B). Neither CD2 transduced cells nor the SHP-1 deficient P5 3G clone showed differences in basal proliferation compared to wt cells. The SHP-1 deficient P2 2E clone showed slightly slower division than wt MOLT-3 cells. The P2 2E clone was smaller in overall size in comparison to the three other cells types, which indicated that this clone is inherently different and thus the slower division might be related to this phenotypic change (figure 4.7 A). Overall, gag$^+$ MOLT-3 cells divide daily without the need of any external stimulation and in the absence of SHP-1, MOLT-3 cells did not show accelerated basal division.

In parallel to the above experiment using MOLT-3 cell clones, gag$^+$ Jurkat cell proliferation was analysed in response to cell activation. SHP-1 proficient gag$^+$ Jurkat cells were labelled with CFSE and division in response to cognate SLY peptide was analysed. No difference on CFSE dilution could be detected with the addition of up to 10^{-4} M SLY peptide (figure 4.8). In summary, neither leukaemic cell lines were suitable to studying the effect of SHP-1 deficiency on basal and TCR induced proliferation.

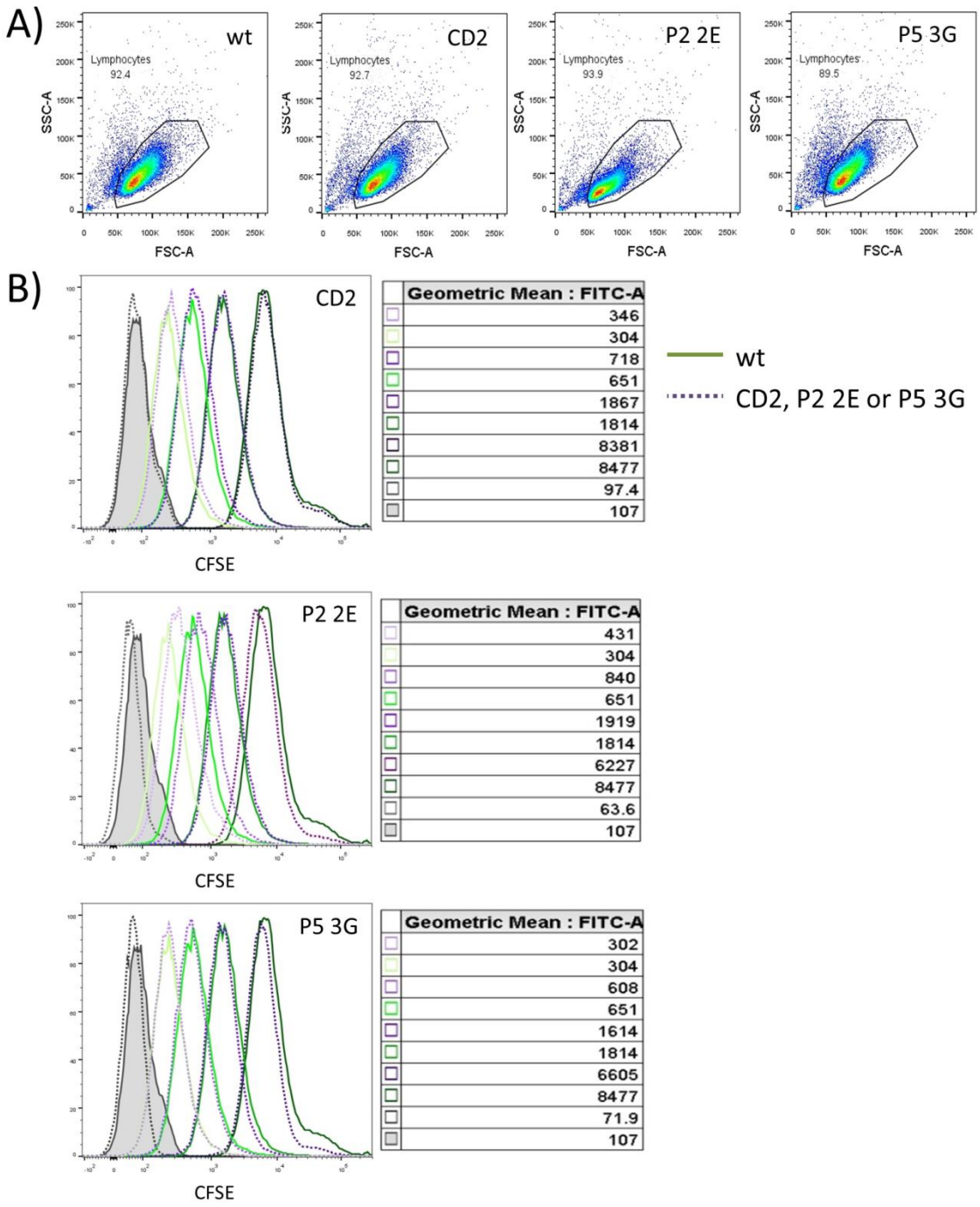

Figure 4.7: Proliferation of unstimulated SHP-1 deficient gag$^+$ MOLT-3 clones. Wt and CD2 transduced gag$^+$ MOLT-3 cells and SHP-1 deficient gag$^+$ MOLT-3 clones, P2 2E and P5 3G, were stained with 2 µM CFSE at day 0. A) Forward and side scatter plots of the wt, CD2, P2 2E and P5 3G cells. B) Cells were cultured and collected at 0 h, 24, 48 and 72 h (dark > bright line) and analysed by flow cytometry for the CFSE content of cells gated on FSC/SSC and single cells. The green line represents the wt cells and the dotted purple line represents either CD2 transduced cells, the P2 2E or the P5 3G clone. The grey filled and grey dotted lines show unstained cells at day 0 and the two peaks furthest to the right represent CFSE stained cells at day 0.

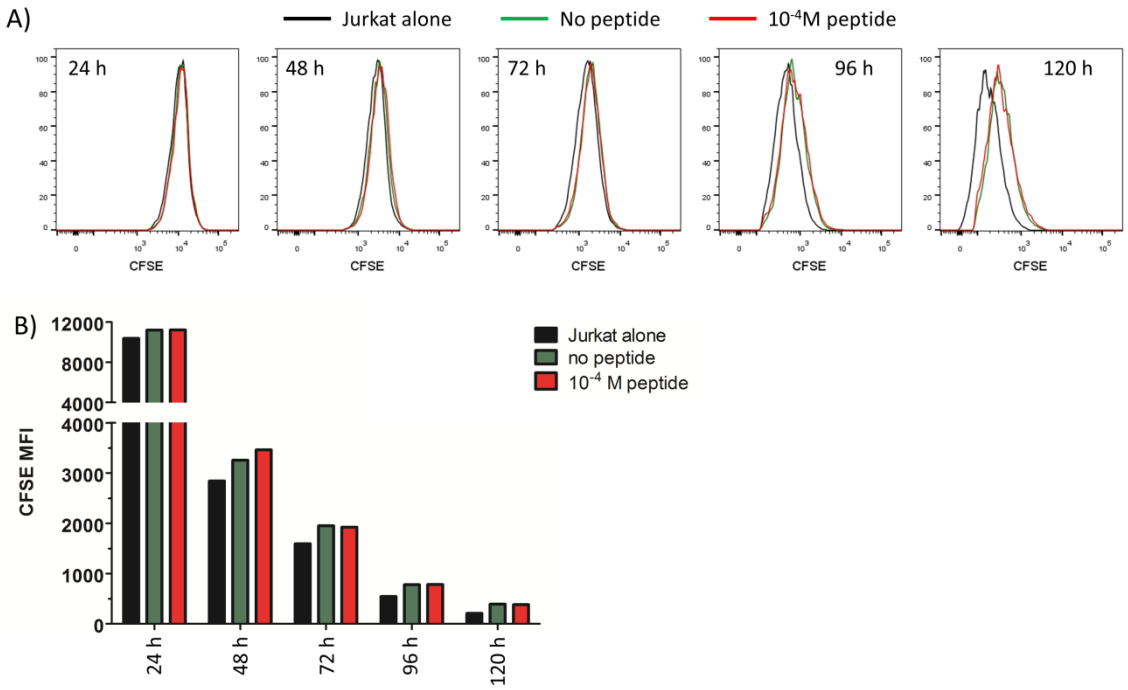

Figure 4.8: CFSE dilution of gag$^+$ Jurkat cells stimulated with SLY peptide pulsed APCs. Gag$^+$ Jurkat cells were labelled with 2 µM CFSE at day 0. CFSE labelled cells were cultured alone (black) or co-cultured with unpulsed (green) or 10^{-4} M SLY peptide pulsed (red) APCs. Cells were collected every 24 h as indicated and analysed by flow cytometry. Cells were gated on FSC/SSC and single cells. A) The overlays of the CFSE staining of the three CFSE labelled Jurkat culture conditions at five different time points (24 h – 120 h) is shown. B) CFSE MFI is shown for the three culture conditions at the five time points. Each condition represents a single observation.

4.4 Cloning of ZFN LVs transduced gag^{+} Jurkat cells and characterisation of SHP-1 deficient clones

For a better comparison of T cell activation, leukaemic clones proficient and deficient in SHP-1 protein with similar TCR levels were derived and studied in this section (figure 4.9). This goal required the cloning of gag^{+} Jurkat T cells generated in the previous chapter (figures 3.19 and 3.21). 35 individual clones were analysed for SHP-1 protein expression, out of which 26% (9/35) showed complete lack of SHP-1 protein, 20% (7/35) showed decreased SHP-1 protein levels and 54% (19/35) showed levels similar to wt (figure 4.10).

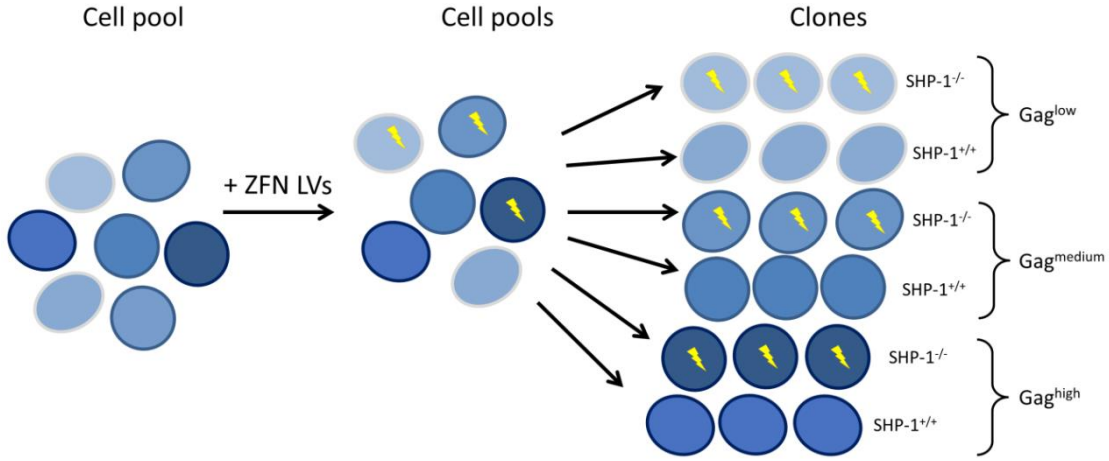

Figure 4.9: Overview of the cloning strategy for ZFN LVs transduced gag^{+} Jurkat cells. A gag^{+} Jurkat cell pool was transduced with ZFN LVs and cells were cloned. Yellow arrows indicate mutations in the SHP-1 gene due to ZFN activity and SHP-1$^{+/-}$ and SHP-1$^{-/-}$ indicated cells with reduced or absent SHP-1 protein respectively. The cell membrane colour indicates gag TCR levels.

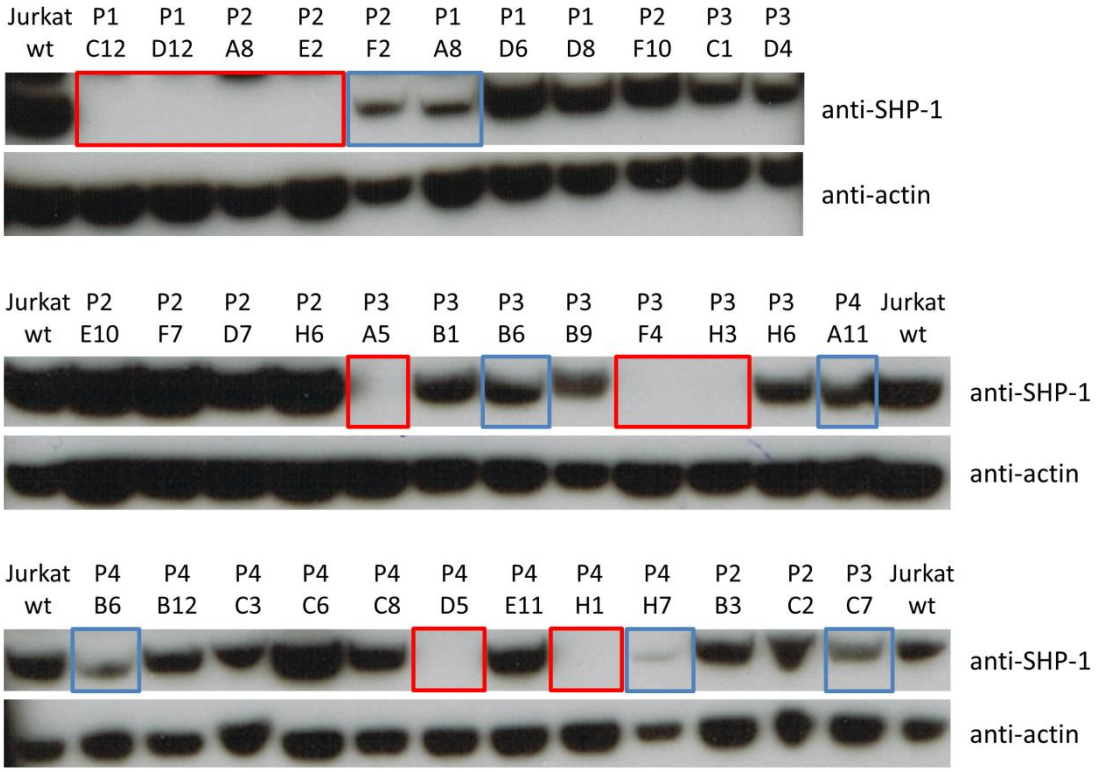

Figure 4.10: Immunoblotting for SHP-1 protein expression of gag$^+$ Jurkat cell clones. Gag$^+$ Jurkat clones, transduced with ZFN1 and ZFN2-CD2 LVs, and non-transduced wt cells were lysed and the cell lysate immunoblotted with anti-SHP-1 and anti-actin Abs. Clones with complete SHP-1 protein loss and clones with significant reductions in SHP-1 protein are encased by red and blue boxes, respectively. Non-transduced cells (Jurkat wt) were used as a positive control. The anti-SHP-1 blots were exposed for longer than the anti-actin blots.

In order to precisely map SHP-1 mutations on both alleles of a clone, TA cloning of the 398 bp SHP-1 PCR product was done as described in the 'Materials and Methods' and carried out mostly by Adam Clark, an intercalating BSc student. SHP-1 mutations in clones showing conclusive results are shown in table 4.1. All analysed mutations were concentrated within the expected ZFN spacer region. The minority of mutations (1/9) were substitutions, such as the C to T substitution in the intron region which matched the SHP-1$^{+/+}$ status of the clone obtained by immunoblotting (figure 4.10). The majority of mutations (7/9) were deletions of between 1-183 bp and 2/9 mutations were small insertions of 1-5 bp. For two clones, no second allele could be identified. Two possible reasons for this were the preferential PCR amplification of

shorter PCR products or the occurrence of a large deletion within the allele, deleting the primer binding site, 220 bp upstream or 178 bp downstream of the ZFN cutting site.

Clone	SHP-1 protein	Allele 1	Allele 2
P2 F10	SHP-$1^{+/+}$	Wt (3/6)	C →T in intron (3/6)
P2 C2	SHP-$1^{+/+}$	Δ9 in exon (7/14)	Δ1 in exon (5/14)
P3 F4	SHP-$1^{-/-}$	Δ29 in intron → deletion of 3' splicing site (6/6)	?
P3 A5	SHP-$1^{-/-}$	Δ9 in exon (14/14)	?
P4 H1	SHP-$1^{-/-}$	Δ1 and Δ6 → deletion of 3' splicing site (5/6)	+1 G in exon (1/6) → premature stop codon in exon 9 (1/6)
P2 A8	SHP-$1^{-/-}$	Δ183 of which 176 in intron and 7 in exon → deletion of 3' splicing and premature stop codon (14/15)	Δ1 and +5 Cs (1/15) → premature stop codon in exon 9

Table 4.1: Analysis of SHP-1 mutations on both alleles of Jurkat T cell clones. TA cloning was done for a number of Jurkat clones transduced with ZFN LVs and the types of mutations and consequences for the protein expression are shown. The number of TA cloning plasmids sequenced for each clone is shown in brackets. The size of deletions (Δ) and insertions (+) in nucleotides is shown. Immunoblotting was used to determine the SHP-1 protein expression.

As seen in gag^+ MOLT-3 clones (figure 4.6 B), gag TCR levels can vary between clones obtained from a pool of transduced cells. To enable comparison between gag^+ Jurkat clones, SHP-1 proficient and deficient clones with matched TCR levels were paired. Pairs were chosen to have high, medium and low TCR expression (figure 4.11 A, B and C respectively).

The three pairs of clones were activated with cognate SLY peptide pulsed APCs and downregulation of the gag TCR was analysed (figure 4.12). Two of the SHP-1 deficient clones, the ones with high and medium TCR levels, showed more TCR downregulation than their matched SHP-1 proficient clones at certain peptide doses (figure 4.12 B and C). However, despite trying to ensure equivalent T cell to APC ratios, it is important to highlight that the high

TCR pair showed a small but statistically significant difference in the T cell to APC ratio, with the SHP-1 proficient clone having been incubated with fewer APCs and thus observed differences in activation could be due to this factor. In addition, analysing overall levels of TCR downregulation between the three pairs showed that cells expressing high levels of TCR have a higher potential for TCR downregulation (50% downregulation versus 95%). Hence, the slightly higher TCR levels for the unstimulated SHP-1 deficient clones in pairs A and B might be contributing to the observed differences. This is however not true for the pair in C, as the SHP-1 proficient clone had a higher basal TCR level without showing enhanced TCR downregulation. Overall, these results show that the loss of SHP-1 protein enhanced gag^{+} Jurkat cell activation in this model system.

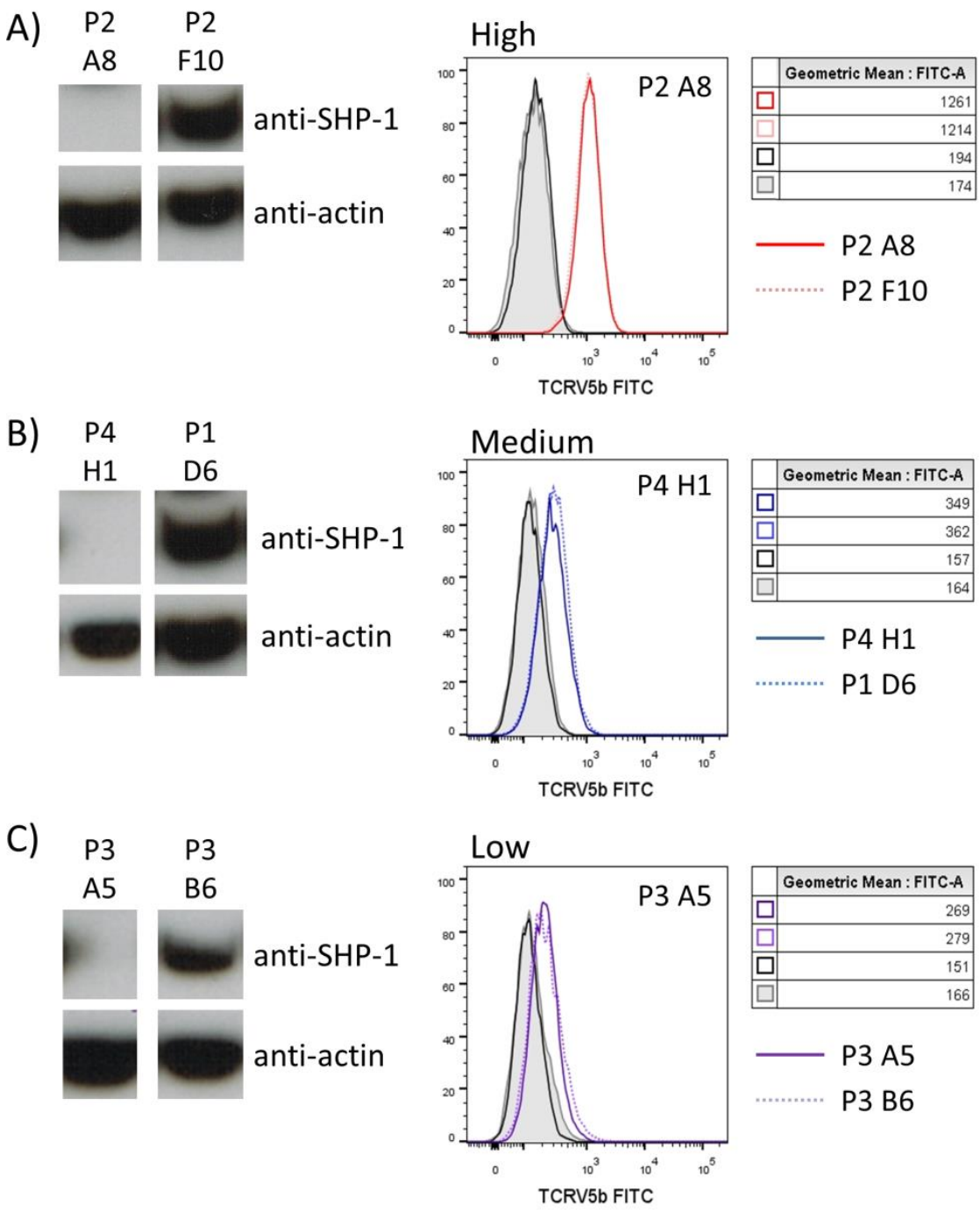

Figure 4.11: Analysis of SHP-1 protein and TCRV5β levels of gag$^+$ Jurkat clones. Gag$^+$ Jurkat clones were analysed for SHP-1 protein levels (immunoblot images from figure 4.9) and for TCRV5β levels by flow cytometry. SHP-1 deficient clones (left lane on immunoblot and solid lines on histogram) were matched for TCRV5β levels with SHP-1 proficient clones (right lane on immunoblot and dotted lines on histogram). Controls were unstained SHP-1 proficient (grey filled) and deficient (black line) cells. Gag$^+$ Jurkat clones were paired for high (A), intermediate (B) and low (C) TCRV5β levels.

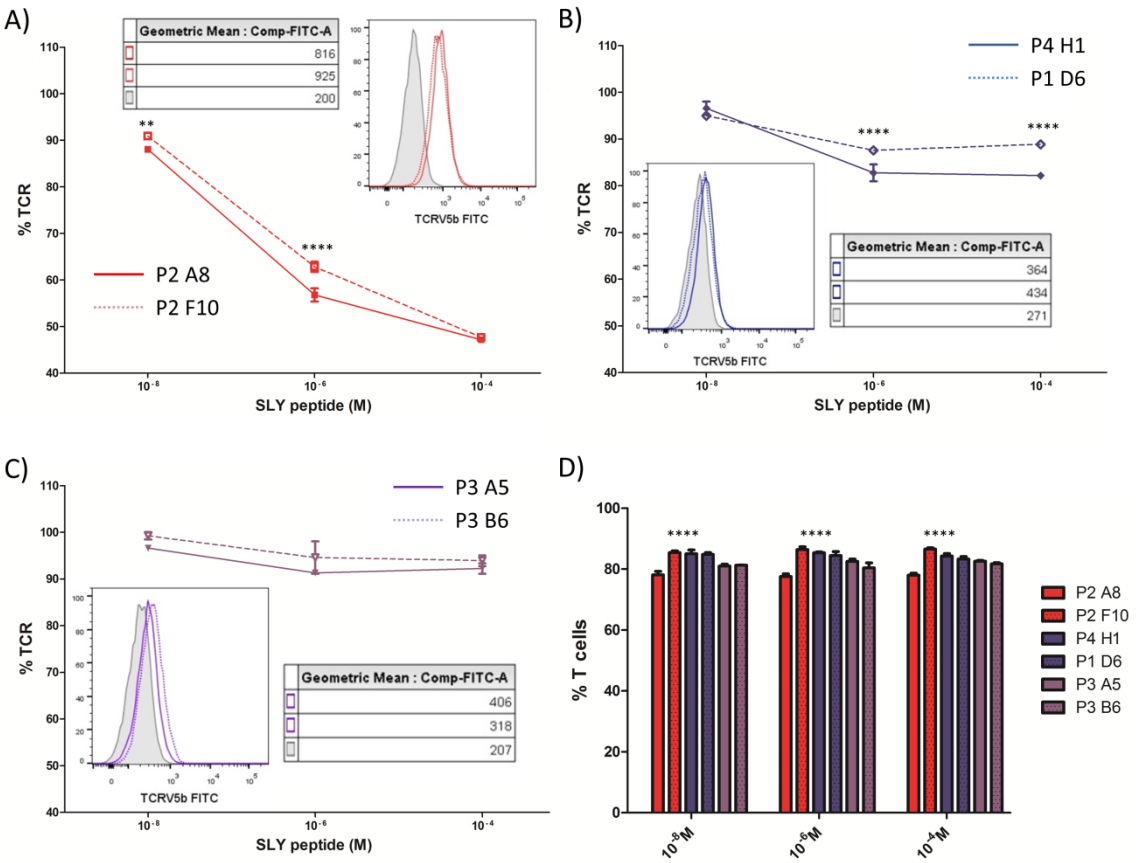

Figure 4.12: TCR downregulation in response to peptide stimulation of SHP-1 proficient and deficient Jurkat clones matched for gag TCR levels. APCs were pulsed with increasing doses of cognate SLY peptide or unpulsed for 30 min. SHP-1 proficient (dotted) and deficient (solid) Jurkat clones were incubated with peptide pulsed APCs for 60 min and stained for live/dead stain, anti-CD19 Ab and anti-TCRV5β Ab. The percentage of TCR downregulation for all three pairs of TCR matched clones in relation to unstimulated CD19 negative cells is shown in A), B) and C). D) Percentage of T cells (CD19 negative) for each peptide dose and clone is shown. Data shown is a single experiment with triplicate wells and the error bars show the SEM. **p<0.01 and ****p<0.0001. %TCR=sample MFI/(mean of MFI of non-peptide pulsed cells)*100.

4.5 Cloning of a gag^{high} Jurkat clone transduced with ZFN LVS and characterisation of SHP-1 deficient clones

To obtain SHP-1 deficient and proficient cells that are identical for gag TCR levels, a gag^{+} Jurkat clone expressing high levels of TCR (gag^{high}) was either left untransduced or transduced with CD2 or ZFN1 and ZFN2-CD2 LVs (figure 4.13). Cells were analysed for CD2 surface expression by flow cytometry, SHP-1 mutations by Cel-I and cloned as described before (data not shown). All clones (wt, CD2 and ZFN) were immunoblotted for SHP-1 and an absence of SHP-1 protein was established in 4/21 SHP-1 ZFN transduced clones (data not shown).

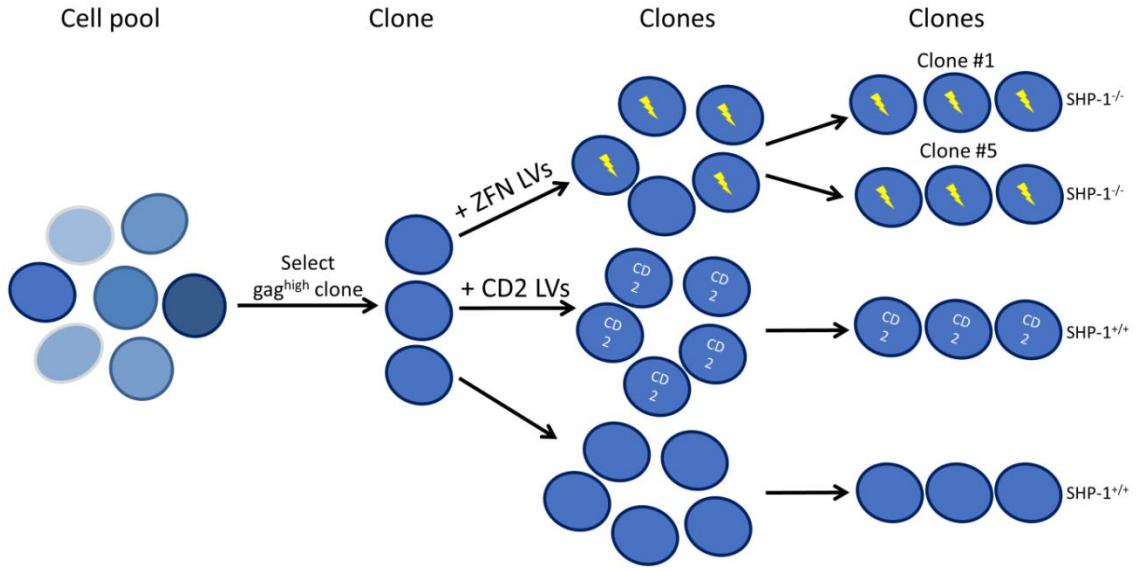

Figure 4.13: Overview of the cloning strategy to obtain gag^{high} clones deficient in SHP-1. Clones from a gag^{+} Jurkat cell pool were obtained and a gag^{high} clone was chosen to be transduced with either ZFN LVs, CD2 LV or left untransduced. Transduced and untransduced cells were cloned a second time and two SHP-1 deficient clones were chosen from the ZFN LVs transduced cells in addition to two clones representing control CD2 and wt cells. Yellow arrows indicate mutations in the SHP-1 gene due to ZFN activity and SHP-1$^{+/+}$ and SHP-1$^{-/-}$ labels represent cells with SHP-1 protein present or absent, respectively.

Based on SHP-1 protein levels and matching gag TCR levels, two SHP-1 deficient clones (#1 and #5), one wt clone and one CD2 transduced clone were selected (figure 4.14 A and B). Although all 21 ZFN transduced clones analysed originated from a single clone, varying levels of TCRV5β were observed after subcloning (data not shown). The two SHP-1 deficient and two control clones were activated with SLY peptide pulsed APCs (10^{-8} to 10^{-4} M) and levels of surface expression of CD69 were analysed (figure 4.14 C and D). The two SHP-1 deficient clones had significantly higher relative upregulation of CD69 than the CD2 transduced control for peptide doses above 10^{-8} M. Yet no significant differences were seen between the wt clone and the two SHP-1 deficient clones. All three transduced clones had less CD69 surface expression in the absence of peptide stimulation than the wt clone (figure 4.14 C). However, the potential to upregulate CD69 in response to high peptide stimulation was not dependant on initial CD69 levels as clone number 1 had lower basal levels than the CD2 clone but higher CD69 expression at 10^{-4} M (figure 4.14 C). No significant differences in T cell to APC ratios were observed (figure 4.14 E). Additionally, TCR levels did not seem the limiting factor for CD69 upregulation, as clone #5 with the lowest TCR levels showed the highest relative CD69 increase. In summary, when only examining transduced cells, the SHP-1 deficient clones were clearly more responsive to peptide stimulation than the CD2 control again suggesting that loss of SHP-1 might enhance T cell activation.

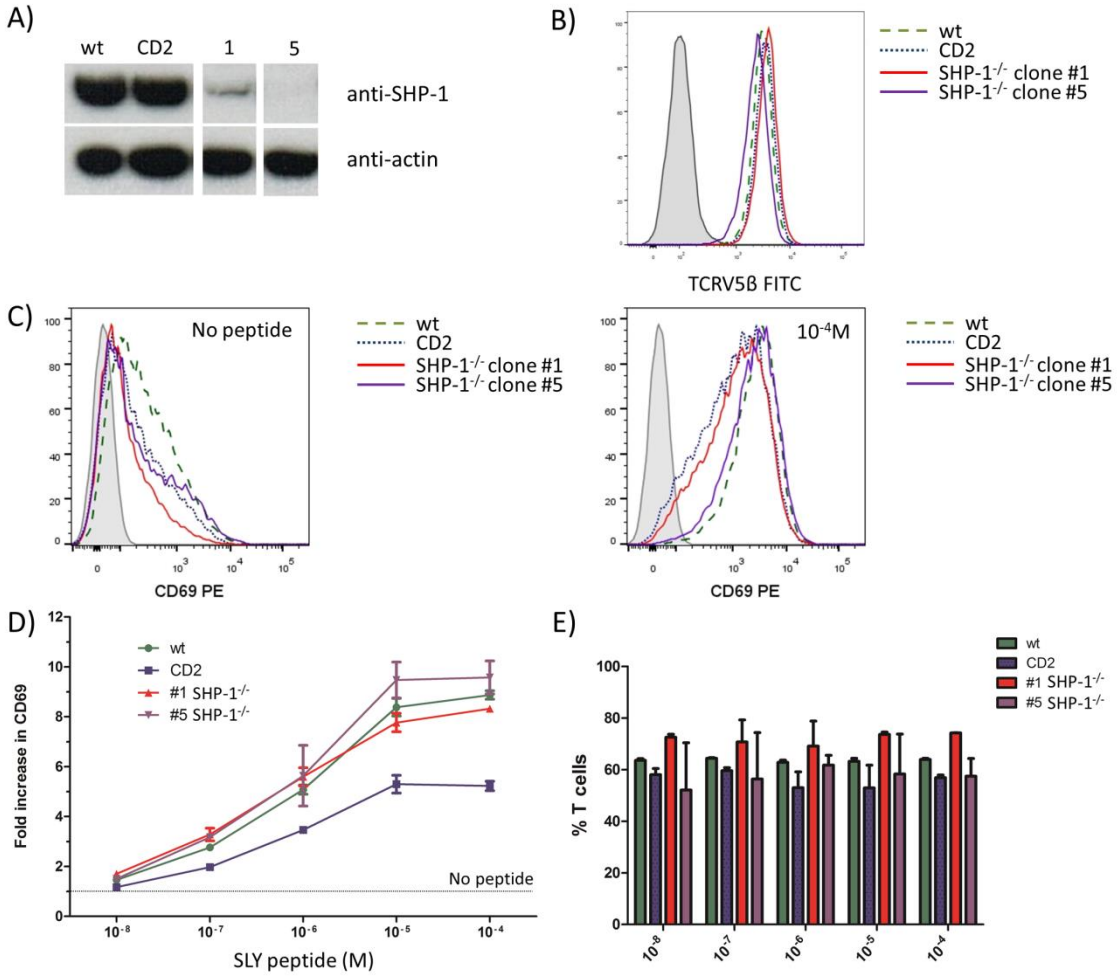

Figure 4.14: CD69 upregulation in response to peptide stimulation of two SPH-1 deficient and two control gag^{high} Jurkat clones. A) Immunoblot for SHP-1 and actin protein using cell lysate from two SHP-1 deficient gag^{high} Jurkat clones (#1 and #5), one CD2 transduced and one wt control gag^{high} Jurkat clones. B) The four clones in A were unstained (grey filled) or stained with anti-TCRV5β Ab and cells were gated on FSC/SSC, live dead and single cells. Gag TCR levels for wt (green dashed), CD2 transduced (blue dotted), SHP-1 deficient clones #1 (red) and #5 (purple) are shown. C) Histogram overlays for CD69 surface expression are shown for the four clones and the isotype control (grey filled) of CD19 negative Jurkat cells either incubated with unpulsed APCs (left) or 10^{-4} M peptide (right). Cells were gated on FSC/SSC, live dead, single cell and CD19 negative. D) The fold increase of CD69 surface expression above unstimulated cells is shown for cells gated as in C. The CD2 clone was significantly different for all peptide doses above 10^{-8} M (asterisks not shown). Clone #1 was significantly different at 10^{-5} M and 10^{-4} M peptide to clone #5 (*** and **** respectively). E) Percentages of CD19 negative cells (Jurkat cells) in total population are shown. No significant differences were observed. Data shown is a single experiment with triplicate wells and the error bars show the SEM. ***p<0.001 and ****p<0.0001. CD69 ratio=sample MFI/(mean of MFI of non-peptide pulsed cells).

4.6 Generation and characterisation of tumour specific, SHP-1 mutant NFAT reporter Jurkat cells

GLuciferase NFAT reporter Jurkat cells not expressing endogenous TCR were transduced with the ZFN LVs as well as a melanoma specific Mel TCR LV (figure 4.15 A and B). All doses of Mel TCR (5 µl, 15 µl or 30 µl) and/or ZFN1 and ZFN2-CD2 (5 µl or 15 µl) LV gave complete transduction of all cells as indicated by staining for CD2 and FLT tetramer. The Mel TCR encoding LV was a 3rd generation whereas the three other LVs were 2nd generation LVs and they use the pELN or pSxW (pLenti) transfer vectors respectively.

When analysed for SHP-1 mutations, all cells transduced with ZFN LVs alone or in combination with Mel TCR LV gave strong Cel-I digestion bands (figure 4.15 C). Cells transduced with 5 µl TCR and ZFN LVs showed the highest % of mutant SHP-1 cells at 21%, whereas transduction with 3x more LV showed only 14.7%. The LV transduced NFAT Jurkat cells were sorted for expression of CD2 and/or tetramer as shown in figures 4.15 D and E and the sorted cells used for functional experiments.

To look at differences in activation between tetramer sorted Mel TCR SHP-1 proficient (Mel^{+} SHP-1$^{+/+}$) or tetramer and CD2 sorted SHP-1 mutant (Mel^{+} SHP-1$^{+/-}$) NFAT Jurkat cells, cells were activated for 18 h and luciferase concentrations in the supernatant were measured. It is important to remember that the Mel^{+} SHP-1$^{+/-}$ NFAT Jurkat cells will be a mix of SHP-1 proficient and deficient cells. Duplicate wells of Jurkat cells were incubated with PMA/Ionomycin and PHA as positive controls and with two different melanoma target cell lines, Mel526 and Mel624 (figure 4.17). The latter two cell lines present melanoma Ag on HLA-A2 which can stimulate Mel TCR expressing Jurkat cells and were given to us by Dr John Bridgeman. Mel526 and Mel625 cells were checked for HLA-A2 expression and both were HLA-A2 positive as expected (figure 4.16).

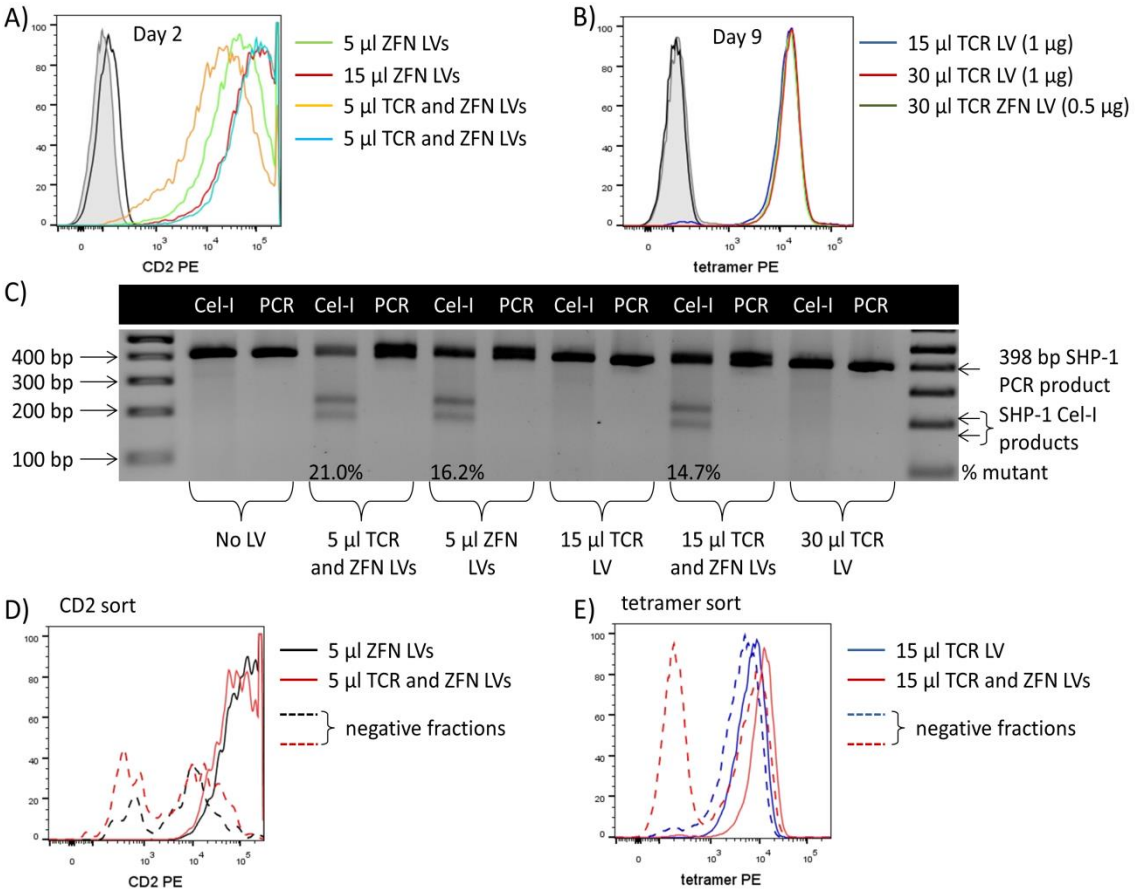

Figure 4.15: Analysis of NFAT reporter Jurkat cells for SHP-1 mutations and Mel TCR expression. NFAT reporter Jurkat cells were transduced with Mel TCR and/or ZFN1 and ZFN2-CD2 LV. A) Day 2 post-transduction, cells transfected with 5 µl (green) or 15 µl (red) ZFN1 and ZFN2-CD2 LV, 5 µl (orange) or 15 µl (blue) TCR plus ZFN1 and ZFN2-CD2 LV or untransduced (grey filled), were stained with live/dead stain, anti-CD2 Ab or isotype ctrl (black). Cells were gated on FSC/SSC, single cells and live/dead. B) Day 9 post-transduction, cells transduced with 15 µl (blue) or 30 µl (red) TCR LV were stained with 1 µg of FLT tetramer or 0.5 µg (green) of FLT tetramer for the 30 µl TCR LV cells or left unstained (black). Cells were gated on FSC/SSC and single cells only. C) At day 6 post-transduction, gDNA was extracted from cells transduced as indicated, the 398 bp SHP-1 fragment was amplified by PCR, the PCR product was hybridised and digested using Cel-I enzyme. Mutant SHP-1 DNA is indicated by Cel-I digestion DNA fragments of 220 bp and 178 bp. D) NFAT Jurkat cells, transduced with 5 µl ZFN1 and ZFN2-CD2 LV (black) or 5 µl Mel TCR plus ZFN1 and ZFN2-CD2 LV (red), were sorted for CD2 expression by MACS separation. Negative (dashed) and positive (solid) fractions of the CD2 sort were analysed by flow cytometry after gating on FSC/SSC and single cells. E) NFAT Jurkat cells, transduced with 15 µl TCR LV (blue) or 15 µl Mel TCR plus ZFN1 and ZFN2-CD2 LV (red), were sorted for tetramer expression by MACS separation. Negative (dashed) and positive (solid) fractions of the tetramer sort were analysed by flow cytometry after gating on FSC/SSC and single cells.

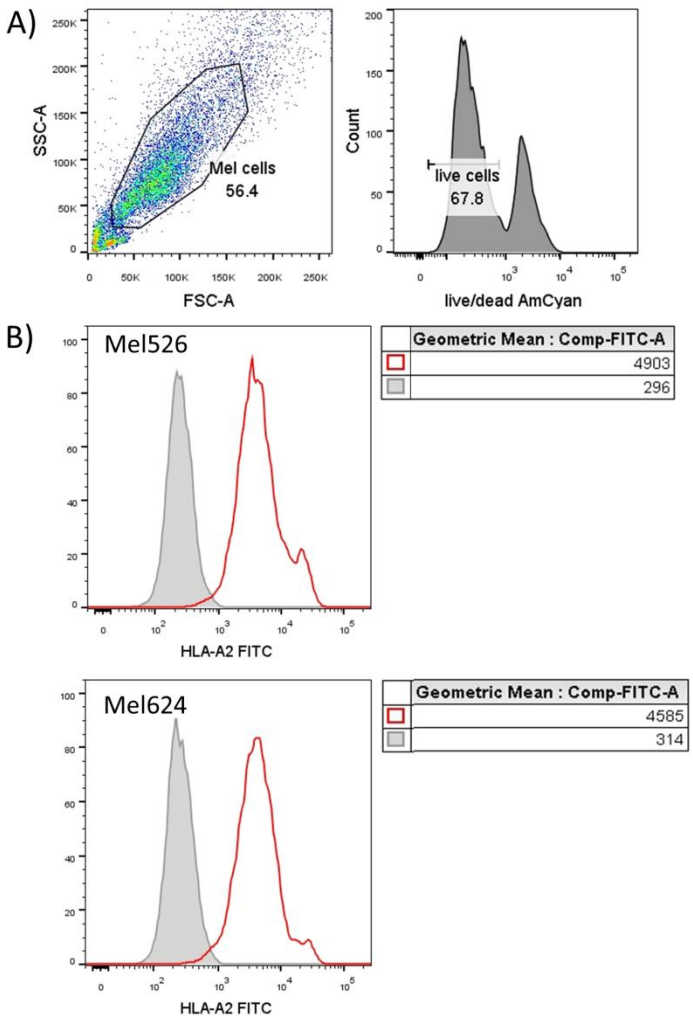

Figure 4.16: Mel526 and Mel624 express HLA-A2. Mel526 and Mel624 cells were collected using dissociation buffer and stained using live/dead stain and an α-HLA-A2 Ab. A) Gating strategy for Mel526 and Mel624 cells. B) Mel526 and Mel624 were stained with an α-HLA-A2 Ab (red) or unstained for HLA-A2 (grey filled).

As expected, cells expressing no Mel TCR (wt and SHP-$1^{+/-}$) did not secrete luciferase when activated with the melanoma cells whereas activation by PMA/Ionomycin and PHA gave strong signals (figure 4.17). Mel TCR expressing cells (Mel^{+} and Mel^{+} SHP-$1^{+/-}$) were activated by the Mel526 and Mel624 tumour target cells as shown by a 2-6 fold increase in luciferase release. Interestingly, the Mel^{+} SHP-$1^{+/-}$ Jurkat cells showed more activation than the Mel^{+} SHP-1 wt Jurkat cells when activated with target cells (2.6 versus 1.9 fold increase in luciferase at 3:1 T cells to Mel526 and 6.1 versus 3.4 fold increase at 3:1 T cells to Mel624 cells). However they

also showed an increase in activation by PMA/Ionomycin of 364 fold versus 282 fold for the Mel^{+} cells.

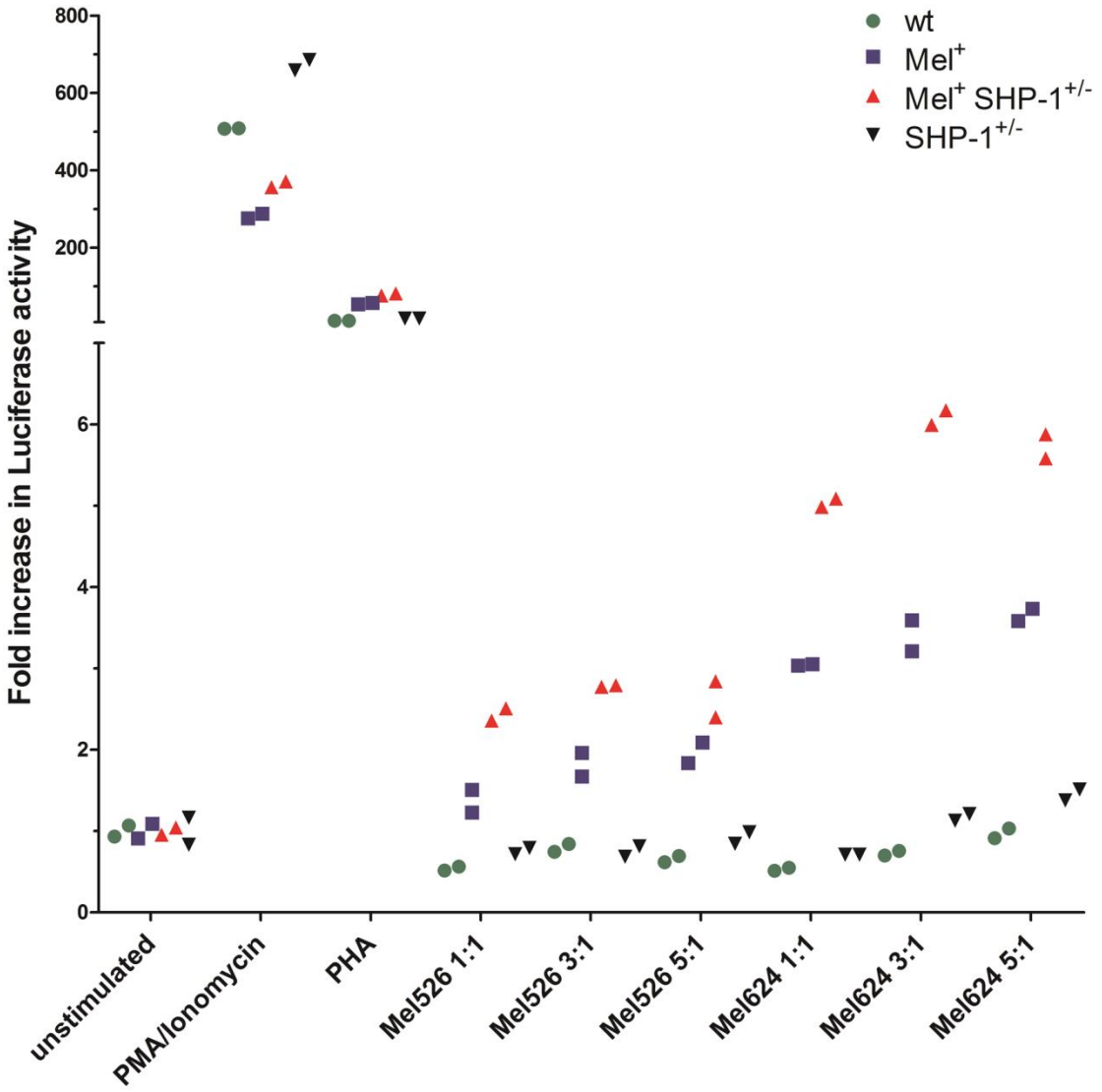

Figure 4.17: Activation of Mel TCR expressing NFAT Jurkat cells, wt or mutant for SHP-1, by Mel526 and Mel624 melanoma cells. Mel TCR LV (Mel^{+}), Mel TCR and ZFN LVs (Mel^{+} SHP-1$^{+/-}$), ZFN LVs (SHP-1$^{+/-}$) transduced and untransduced (wt) GLuciferase NFAT reporter Jurkat cells were activated for 18 h with melanoma target cell lines (Mel526 and Mel624) at different E:T ratios. PMA/Ionomycin and PHA were used as positive controls for Jurkat activation. GLuciferase activity in the supernatant was measured and the data expressed as fold increase of luciferase activity over unstimulated cells. The experiment was done in duplicates and each single well is shown.

In order to test whether reconstituting the Mel^{+} SHP-$1^{+/-}$ Jurkat cells would lead to a decrease in Jurkat cell responsiveness to TCR stimulation, SHP-1 rescue cells were generated by transducing cells with a LV encoding the haematopoietic SHP-1 cDNA. To generate the LV encoding the SHP-1 cDNA, plasmid encoding the non-haematopoietic SHP-1 cDNA isoform (NCBI accession code BC002523) was purchased from ThermoScientific (MGC Human PTPN6 Sequence-Verified cDNA, clone 3140265). The haematopoietic SHP-1 isoform is distinguished from the non-haematopoietic SHP-1 isoform by the use of alternative promoter exons, encoding the amino acid sequences MLSRG and MVR, respectively.

A pLenti-SHP-1 lentiviral transfer plasmid was designed to encode a Kozak sequence followed by the haematopoietic SHP-1 cDNA sequence and a stop codon. Primer 68 encoded the Kozak sequence (GCC GCC ACC) upstream of the start codon, the sequence for haematopoietic SHP-1 cDNA (ATG GTG AGG → MVR) as well as a short DNA sequence homologous to both SHP-1 isoforms (TGG TTT CAC CGA GAC CTC). Primer 68 and 69 were used to amplify the SHP-1 cDNA from the purchased plasmid (figure 4.15 A). The PCR product was purified further amplified using primers 70 and 71 to generate a SHP-1 cDNA with homology for the pLenti vector, thus allowing for an In-Fusion recombination reaction (figure 4.18 B and C).

NFAT Jurkat cells, previously transduced with the Mel TCR and ZFN LVs (Mel^{+} SHP-$1^{+/-}$) (figure 4.15), were transduced with the haematopoietic SHP-1 cDNA LV (Mel^{+} SHP-$1^{+/-}$ 'rescued') and it was shown by immunoblotting that the Mel^{+} SHP-$1^{+/-}$ 'rescued' Jurkat cells strongly express SHP-1 whereas mutations in the SHP-1 gene were still observed by the Cel-I assay (figure 4.19). In fact, all three cell types transduced with ZFNs contain approximately 25% of cells with SHP-1 mutations (figure 4.19 A). The SHP-1 protein expression in the LV transduced cells is driven by the SFFV promoter and consequently the SHP-1 levels are not physiological (figure 4.19 B). It is of note that the SHP-1 cDNA will not be liable to mutation by the ZFNs as the binding site of ZFN1 is located in an intron and thus absent in the cDNA. Additionally primers 55 and 56 will

not amplify the cDNA as primer 55 binds within the intron. This matches with the equal percentage of SHP-1 mutant cells observed.

To check the SHP-1 'rescued' Mel^+ Jurkat cells for altered activation, cells were activated with peptide pulsed APCs and the supernatant assayed for luciferase activity (figure 4.20 A). The APCs were pulsed with increasing doses of cognate EAAGIGILTV peptide (10^{-8} M to 10^{-4} M). At similar T cell to APC ratios, the Mel^+ and Mel^+ SHP-$1^{+/-}$ cells showed a significant difference at 10^{-5} M peptide but at no other peptide doses (figure 4.20 A and B). Meanwhile, the Mel^+ SHP-$1^{+/-}$ 'rescued' cells showed significantly lower activation at the two highest peptide doses. Thus this suggests that the SHP-1 mutations present in the Mel^+ SHP-$1^{+/-}$ cell population may lead to increased Jurkat activation whereas overexpression of the SHP-1 protein clearly inhibits activation.

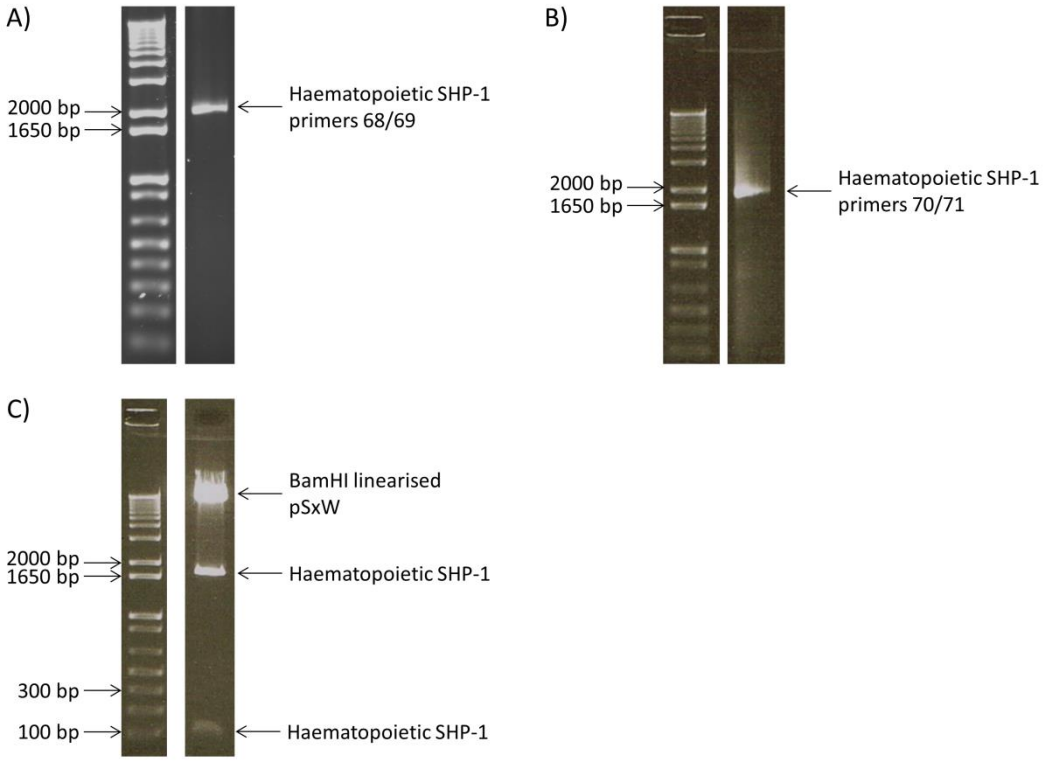

Figure 4.18: Cloning of the haematopoietic SHP-1 cDNA into the pLenti transfer plasmid. A) Lane 2 shows the 1797 bp Kozak and haematopoietic SHP-1 cDNA sequence amplified from the ThermoScientific plasmid template using primers 68 and 69. The PCR product was gel purified. B) Lane 2 shows the 1829 bp PCR reaction product of the purified PCR product from A) and primers 70 and 71. The linearised pSxW vector was purified and used with the purified PCR product to set up an In-Fusion reaction. DH5α cells were transformed with 2 µl of In-Fusion mix. C) Plasmid DNA extracted from DH5α colonies transformed as described above and selected for Ampicillin resistance was restriction digested with BamHI. The upper DNA fragment shows the BamHI linearised 8942 bp pSxW and the two lower bands correspond to the two BamHI restriction fragments of the haematopoietic SHP-1 (1631 bp and 172 bp respectively). Primers 33-34 and 72-77 were used to sequence the pLenti-SHP-1 plasmid and the correct sequence was confirmed.

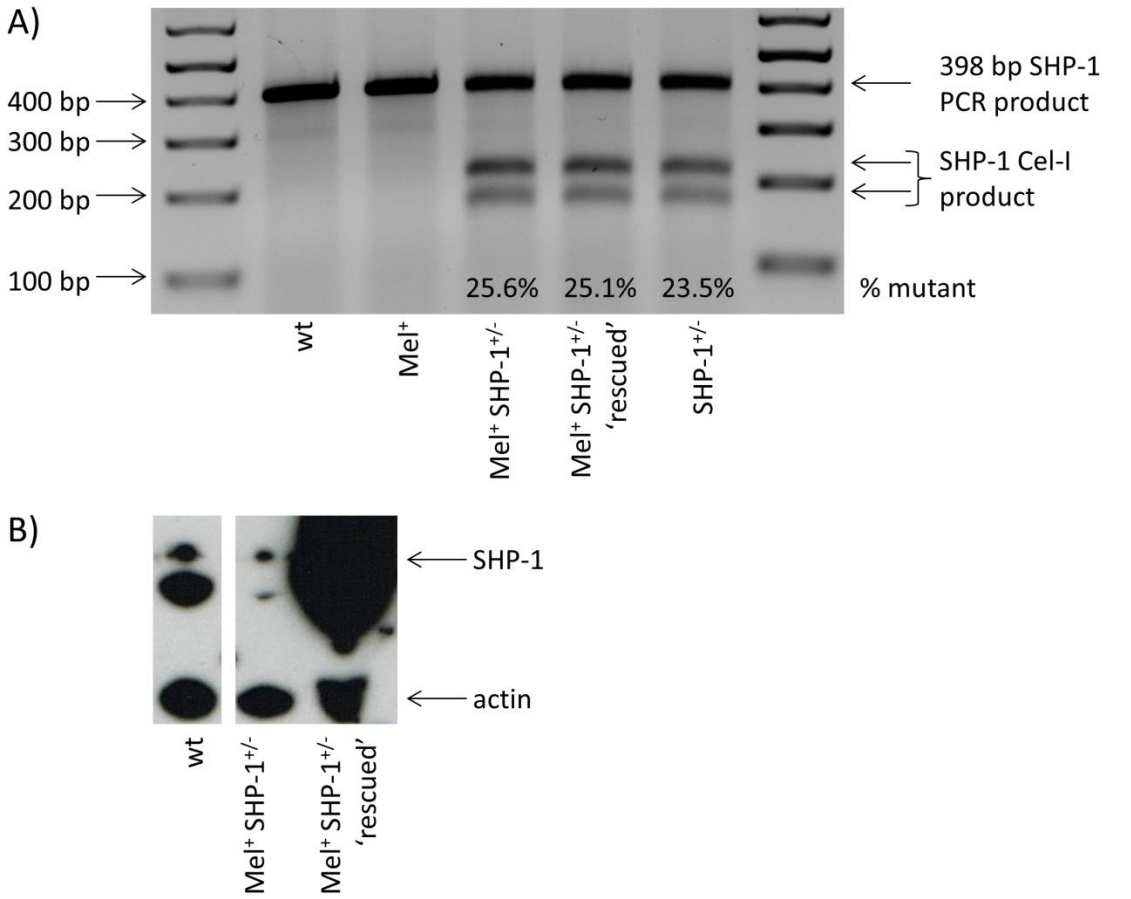

Figure 4.19: SHP-1 gene and protein analysis in Mel^{+} SHP-1$^{+/-}$ 'rescued' NFAT Jurkat cells. NFAT Jurkat cells were either left untransduced (wt), transduced with Mel TCR LV (Mel^{+}), ZFN LVs (SHP-1$^{+/-}$) or with Mel TCR and ZFN LVs (Mel^{+} SHP-1$^{+/-}$). The latter cells were additionally transduced with haematopoietic SHP-1 cDNA LV (Mel^{+} SHP-1$^{+/-}$ 'rescued'). A) Genomic DNA was extracted from cells and the Cel-I assay was done giving 398 bp wt and 220 bp and 178 bp Cel-I restriction bands. B) Cell lysate was extracted from cells as indicated and an immunoblot using anti-SHP-1 and anti-actin Abs was done.

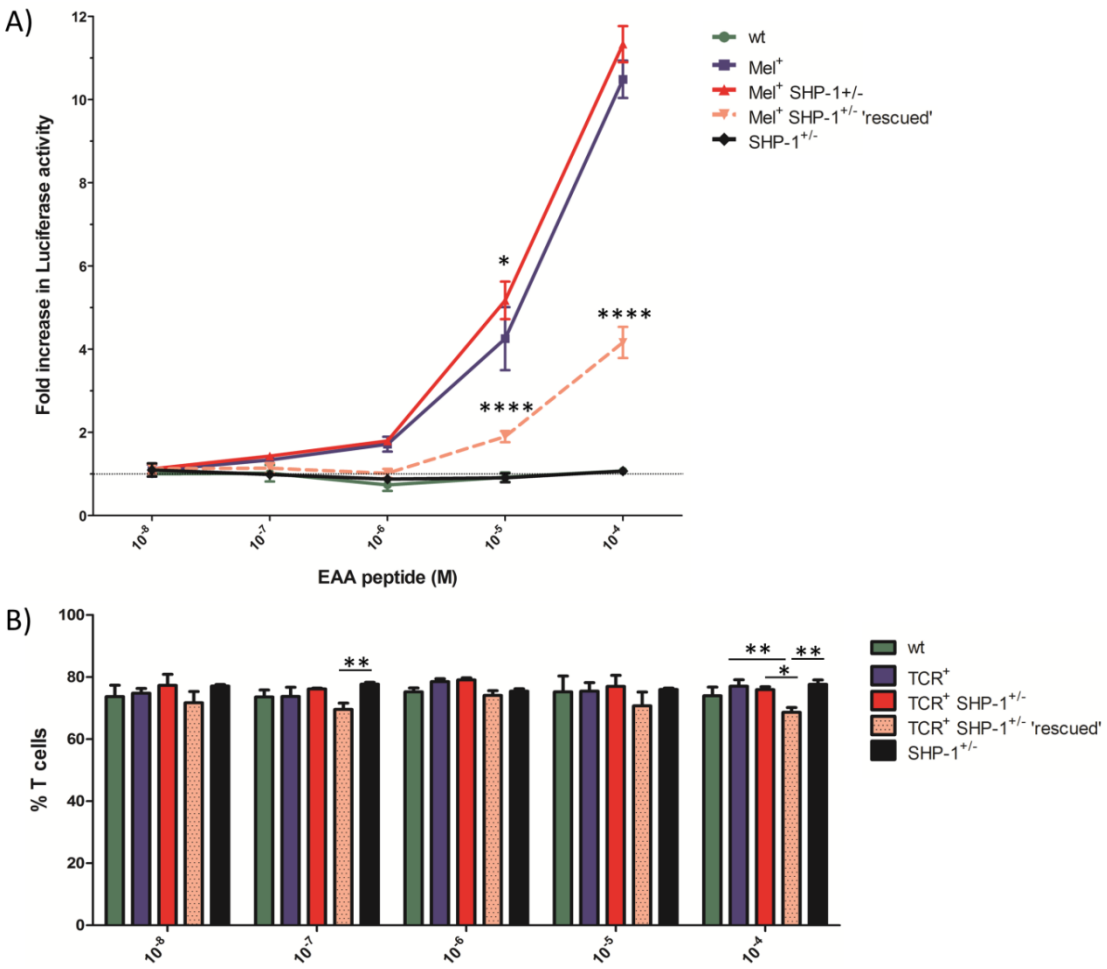

Figure 4.20: Activation of Mel TCR expressing NFAT Jurkat cells, wt, mutant or 'rescued' for SHP-1, by peptide pulsed APCs. Mel TCR LV (Mel^+), Mel TCR and ZFN LVs (Mel^+ $SHP\text{-}1^{+/-}$) and Mel^+ $SHP\text{-}1^{+/-}$ 'rescued' cells, ZFN LVs ($SHP\text{-}1^{+/-}$) transduced and untransduced (wt) GLuciferase NFAT reporter Jurkat cells were activated for 18 h with APCs pulsed with a titration of cognate EAA peptide. A) Luciferase activity in the supernatant was measured and the fold increase over unstimulated cells is shown for each cell type. Statistical analysis was done and significant differences between Mel^+ and Mel^+ $SHP\text{-}1^{+/-}$ or Mel^+ $SHP\text{-}1^{+/-}$ 'rescued' cells are indicated. B) The ratio of Jurkat cells to APCs was measured by flow cytometry. Cells were gated on FSC/SSC, live/dead, single cells and CD19 negative. Each condition was done in triplicates and the SEM is shown. *p<0.05, **p<0.01 and ****p<0.0001.

4.7 Discussion

In this chapter, nearly 100 leukaemic T cell clones, lentivirally transduced with SHP-1 specific ZFNs, were analysed for SHP-1 protein expression by immunoblotting (table 4.2) and overall, approximately a quarter of cells showed a complete lack of detectable SHP-1 protein.

	SHP-$1^{+/+}$	**SHP-$1^{+/-}$**	**SHP-$1^{-/-}$**	**unclear**	**Number of clones studied**	**Chapter heading**
gag^+ Jurkat clones	19 (54%)	7 (20%)	9 (26%)		35	4.4
gag^+ high Jurkat clones	9 (43%)	4 (19%)	4 (19%)	4 (19%)	21	4.5
Total gag^+ Jurkat cells	28 (50%)	11 (19.6%)	13 (23.2%)	4 (7.1%)	56	
gag^+ MOLT-3 clones	3 (23%)	6 (46%)	4 (31%)		13	4.2
gag^+ high MOLT-3 clones	3 (20%)	5 (33%)	6 (40%)	1 (7%)	15	not shown
gag^+ high MOLT-3 clones	4 (29%)	7 (50%)	1 (7%)	2 (14%)	14	not shown
Total gag^+ MOLT-3 clones	10 (23.8%)	18 (42.9%)	11 (26.2%)	3 (7.1%)	42	
Total	38 (38.8%)	29 (29.6%)	24 (24.5%)	7 (7.1%)	98	

Table 4.2: Summary of SHP-1 protein expression of all ZFN1 and ZFN2 or ZFN2-CD2 LV transduced leukaemic cell clones. Percentages of SHP-1 proficient (SHP-$1^{+/+}$), SHP-1 intermediate (SHP-$1^{+/-}$) and SHP-1 deficient (SHP-$1^{-/-}$) gag^+ Jurkat and gag^+ MOLT-3 cells are shown from all the cells analysed after ZFN1 and ZFN2 or ZFN2-CD2 transduction.

As well as immunoblotting for the SHP-1 protein, cells were analysed using the Cel-I mismatch assay. Both assays were used as it is possible that the Cel-I assay gives an overestimation of the extent of SHP-1 protein loss, due to some mutations being silent or in-frame, whereas immunoblotting can give an underestimation of SHP-1 protein loss, due to the presence of functionally defective full length SHP-1. Conversely, the Cel-I assay showed a low signal for

clone P5 3G but no SHP-1 protein was detected by immunoblotting and it is thus of use to perform both assays.

To analyse the precise nature of SHP-1 mutations on both alleles of a clone, TA cloning was performed and it was shown that the predominant mutations were deletions which is in accordance with other studies such as the ZFN mediated knockout of CCR5 (Perez et al. 2008).

Once SHP-1 deficient T cell clones were identified, they were used for functional assays such as CD69 upregulation, TCR downregulation and proliferation. Although clones were grown under the same conditions during the cloning process, differences in TCR were observed indicating that levels of other molecules could also differ and that the final clones were inherently distinct. This was even observed, albeit to a lesser degree, when cloning was set up from a single clone.

The most likely explanation for the lack of a clear phenotype in SHP-1 deficient leukaemic T cell clones is that the most pronounced effect of SHP-1 loss is on increasing the likelihood of cell entry into proliferation (Sathish et al. 2007). However, the latter cannot be studied in leukaemic T cells, as shown in this chapter, due to the rapid and constitutive proliferation of these cells under basal conditions. Additionally, it is possible that cells expressing wt levels of SHP-1 as demonstrated by immunoblotting had acquired mutations by the time the functional assays were started, due to the nature of the integrase proficient ZFN delivery.

In addition, most of the functional assays were done with cells expressing the high affinity gag TCR which may also have contributed to the lack of consistent statistically significant differences observed between SHP-1 sufficient and deficient cells. As mentioned in the Introduction, the phenotypic differences seen in SHP-1 deficient T cells might only be applicable when T cells are stimulated suboptimally (Migone et al. 1998; Sathish et al. 2001b).

The inhibition of T cell activation observed in Jurkat cells overexpressing SHP-1 (figure 4.20) is in contrast to findings by Plas *et al.* that showed that overexpression of SHP-1 in a T cell hybridoma cell line did not change the activation of these cells (Plas et al. 1996). However, the SHP-1 overexpression in the Plas study was not as marked as the one seen here and might thus not have had such a strong effect. This observation was not studied further in this thesis.

Overall, it was shown that the mutations induced by the SHP-1 specific ZFNs can lead to the complete loss of SHP-1 protein expression in leukaemic T cell clones. Meanwhile, no clear phenotype could be identified in SHP-1 deficient leukaemic T cells therefore further experiments were performed in primary $CD8^+$ T cells.

Chapter 5: Generation of mutant SHP-1 tumour-specific primary CD8$^+$ T cells and functional analysis

5.1 Introduction

In this chapter, the growth and subsequent lentiviral transduction of primary CD8$^+$ T cells was optimised in order to obtain tumour-specific mutant SHP-1 CD8$^+$ T cells (figure 5.1 A and C). The T cells were transduced with the melanoma-specific Mel TCR recognising the HLA-A2 presented MART-1_{26-35} peptide. Additionally, the ZFN1 and ZFN2-CD2 LVs (also referred to as ZFN LVs) were delivered to the T cells to induce mutations in the SHP-1 gene. Different strategies of transduction were tried such as delivering the three lentiviruses simultaneously or consecutively, at different ratios and varying LV quantities (figure 5.1 C). The delay between the consecutive transductions was either very short (15 or 30 min) or a whole restimulation cycle (2-3 weeks). Mel TCR expressing (Mel$^+$) and mutant SHP-1 (ZFN2-CD2$^+$) cell populations were generated and sorted using two different techniques, MACS or FACS separations. All LV used in this chapter was 100x concentrated and the ZFN LVs were generated using a 2nd generation packaging system whereas the Mel LV and RFP-GLuciferase LVs were generated using the 3rd generation packaging system. Initially, LV was quantified using a p24 ELISA and the four different LV preparations tested gave readings of 1-28 ng/µl. However due to inaccuracy and high costs, this assay was not used throughout. An assumption had to be made that each LV preparation would contain approximately the same quantity of LV and hence the amount of LV was estimated by volume.

The Mel526 melanoma target cell line was genetically engineered to express non-secreted GLuciferase protein, which is only released upon lysis (figure 5.1 D). The GLuciferase Mel526 cells were used as targets for the SHP-1 sufficient and mutant SHP-1 Mel$^+$ CD8$^+$ T cells and

cytotoxicity assessed by measuring GLuciferase released into the supernatant. Additionally, cell survival and proliferation was estimated for both the SHP-1 sufficient and mutant SHP-1 Mel^{+} CD8^{+} T cells.

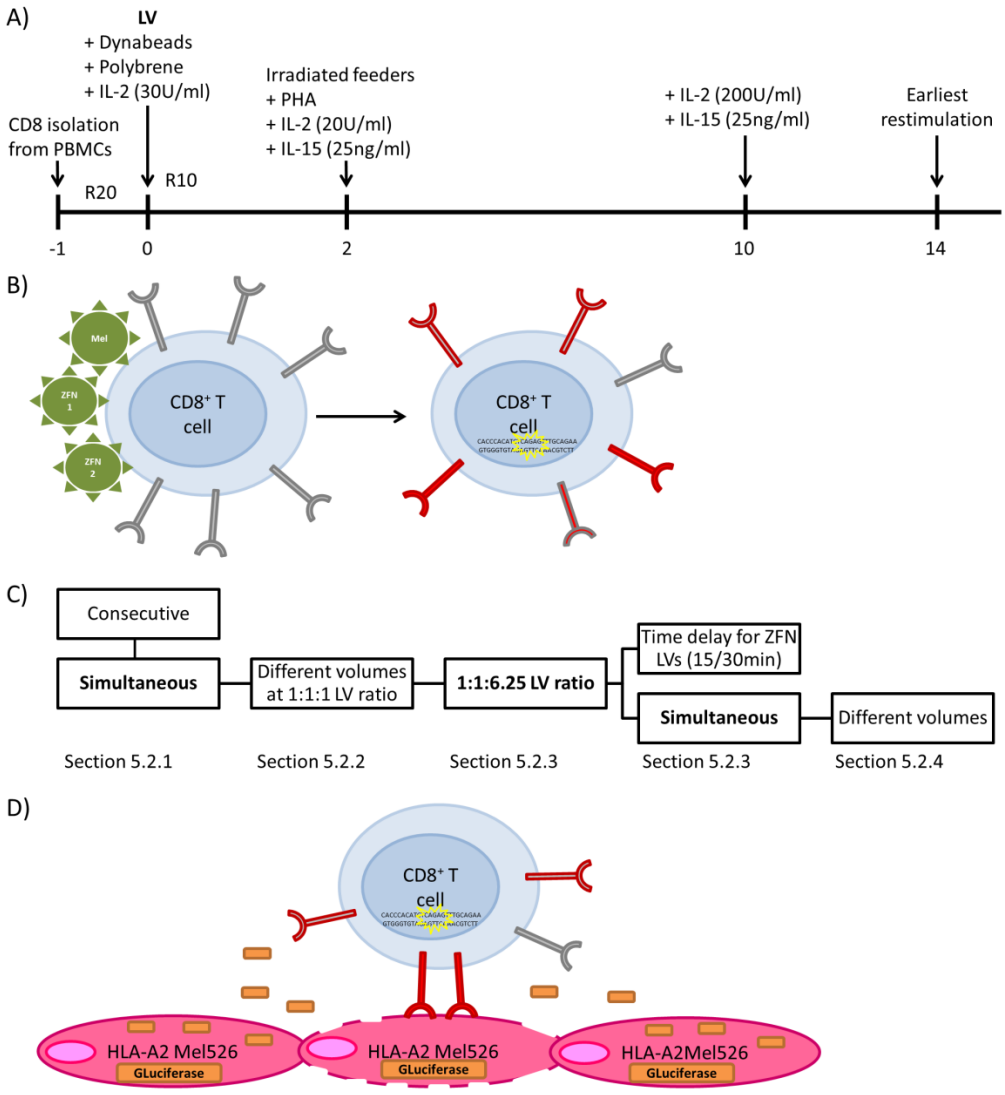

Figure 5.1: Summary of the growth and LV transduction of primary CD8^{+} T cells and the CD8^{+} T cell cytotoxicity assay used in this chapter. A) Protocol for the growth and LV transduction of primary CD8^{+} T cells isolated from PBMCs. A more detailed protocol can be found in the 'Material and Methods'. B) Primary CD8^{+} T cells were transduced with Mel TCR, ZFN1 and ZFN2-CD2 LVs to generate mutant SHP-1 (yellow encircled DNA) Mel TCR expressing (red receptors) CD8^{+} T cells. C) The optimisation steps for the LV transduction of CD8^{+} T cells with the ZFN and Mel LVs are shown along with the corresponding sections in this chapter. The ratio of LV shown indicates ZFN1:ZFN2:Mel LV. D) The HLA-A2^{+} Mel526 melanoma cell line was transduced with an RFP-GLuciferase LV to obtain RFP^{+} (pink) Mel526 cells expressing the non-secreted GLuciferase protein (orange box). The CD8^{+} T cells generated in B were used in Mel526 killing experiments, whereby the release of GLuciferase into the supernatant was used as a readout for cytotoxicity.

5.2 Optimisation of the generation of mutant SHP-1 melanoma-specific primary CD8$^+$ T cells

To generate melanoma-specific CD8$^+$ T cells deficient in SHP-1, three lentiviruses expressing the melanoma-specific Mel TCR plus the two SHP-1 specific ZFNs were delivered to cells. Multiple optimisation steps were needed to achieve this goal as described below.

5.2.1 Simultaneous and consecutive transduction of CD8$^+$ T cells with ZFN1 and ZFN2-CD2 LVs

PBMCs, from an HLA-A2 negative O$^-$ buffy coat obtained from the Welsh Blood Service, were isolated by Ficoll density gradient centrifugation and CD8$^+$ T cells selected by a positive CD8 MACS sort (figure 5.2 A and B). The transduction protocol described in 'Materials and Methods' was followed and cells that were initially rested in RPMI, 20% FCS overnight, were transduced with either 10 µl or 20 µl of 100x concentrated ZFN1, ZFN2-CD2 LV stock or both LVs together. Cells were expanded two days post-transduction with irradiated PBMCs and eight days post-transduction, were stained for CD2 surface expression after gating on live CD8$^+$ cells (figure 5.2 C-F). Cells transduced with 10 µl or 20 µl ZFN2-CD2 LV were 91% and 89% CD2$^+$ respectively, whereas only 60-61% of cells transduced with both the ZFN1 and ZFN2-CD2 LVs were CD2$^+$. This indicated the possibility of the LVs competing for access to the cells and/or integration into the genome.

To test whether cells could be consecutively transduced after one cycle of restimulation (day 12 post-transduction), ZFN1 LV was added to cells previously transduced with ZFN2-CD2 LV and vice versa. Consecutive transduction was less successful than simultaneous transduction as only 3.4-7.6% of cells were CD2$^+$ (figure 5.2 G and H). Moreover, the frequency of CD2$^+$ cells

in the population of cells initially transduced with ZFN2-CD2 LV decreased after the second transduction with ZFN1 LV from 71% to 35% (figure 5.2 I).

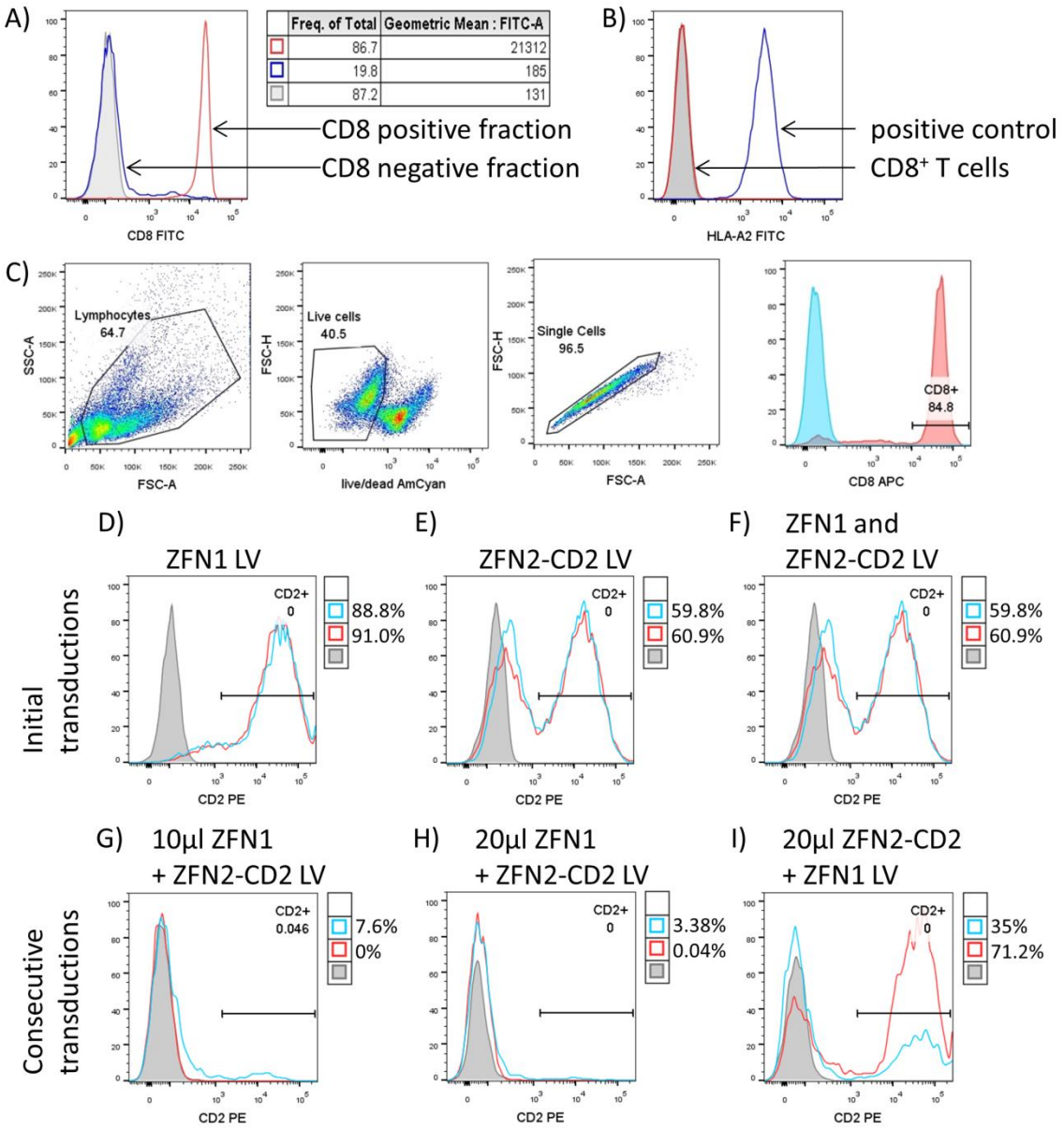

Figure 5.2: Simultaneous and consecutive transduction of HLA-A2$^-$ CD8$^+$ T cells with ZFN1 or/and ZFN2-CD2 LVs. A) PBMCs were isolated from buffy coats and CD8$^+$ T cells were sorted by positive MACS selection. The positively (red) and negatively (blue) sorted fractions of cells were stained using an anti-CD8 Ab and analysed by flow cytometry. B) The CD8$^+$ T cells were stained for surface expression of HLA-A2 (red). A HLA-A2 positive cell line, C1R, was used as a staining control (blue). C) Gating strategy for CD8$^+$ T cells stained with live/dead stain and anti-CD8 Ab. D-F) CD8$^+$ T cells were transduced with either 10 µl (red) or 20 µl (blue) of ZFN1 or/and ZFN2-CD2 LVs and stained with anti-CD2 Ab, 8 days post-transduction. G-I) Cells transduced with either 10 µl or 20 µl ZFN1 or 20 µl ZFN2-CD2 LV were transduced a second time with 10 µl ZFN2-CD2 or ZFN1 LV respectively (blue) or not transduced (red) and stained with anti-CD2 Ab.

Cells consecutively transduced with ZFN1 and ZFN2-CD2 LV, were positively sorted for CD2 and the Cel-I assay performed on gDNA extracted from CD2 negative and positive fractions as well as cells from single transductions (figure 5.3). Cells that were transduced simultaneously with both ZFN LVs (figure 5.2 F) showed a mismatch signal indicating 8.3% of mutated cells whereas the consecutively transduced $CD2^+$ cells did not show any signal. This indicates that the small number of cells that were transduced in the second round were the cells that had not been transduced with the first LV and thus did not express both ZFNs necessary to induce mutations. Overall, this indicated that SHP-1 mutations can be achieved in $CD8^+$ T cells transduced simultaneously with both ZFN LVs, rather than consecutively.

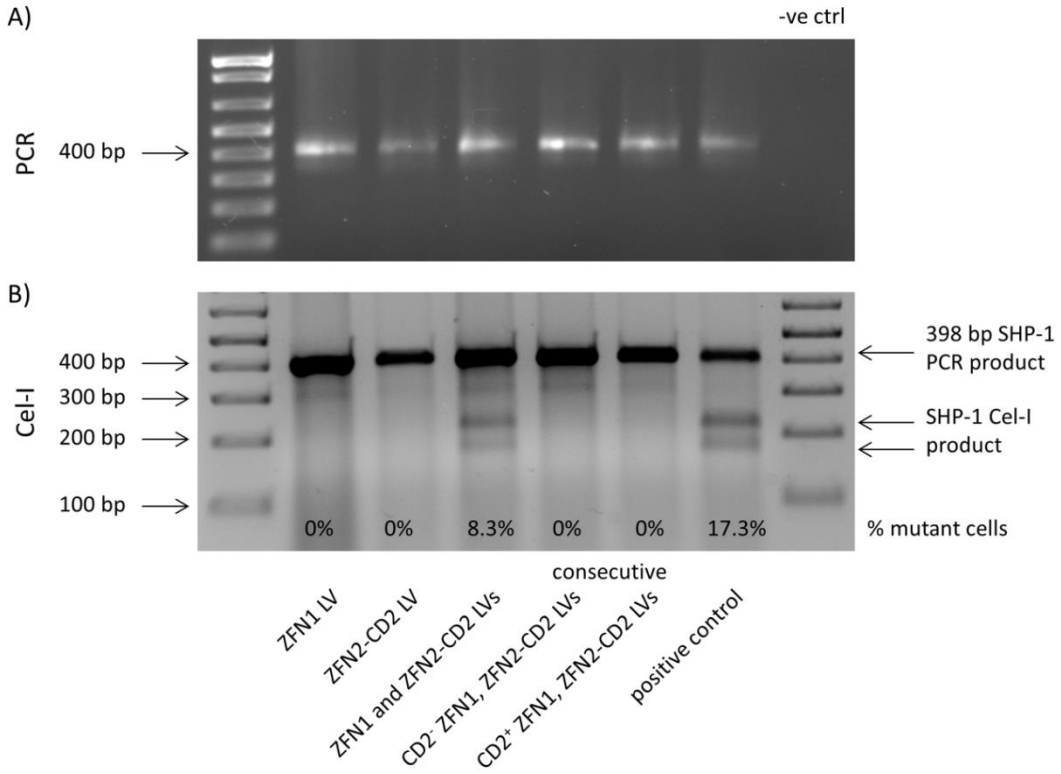

Figure 5.3: Cel-I assay of $CD8^+$ T cells transduced with ZFN1 or/and ZFN2-CD2 LVs. A) gDNA was extracted from cells transduced with different combinations of LVs, as indicated below each lane. The $CD2^+$ and $CD2^-$ fractions represent cells from a CD2 positive MACS sort of cells consecutively transduced with ZFN1 and ZFN2-CD2 LV. A 398 bp SHP-1 genomic segment was amplified by PCR. The negative control (-ve ctrl) was a PCR reaction without gDNA. B) After hybridisation of the PCR product and digestion of the DNA with the Cel-I enzyme, mutated SHP-1 DNA is indicated by 178 bp and 220 bp DNA cleavage fragments. Gag^+ MOLT-3 cells transduced with the ZFN1 and ZFN2 LVs were used as a positive control. The % of cells harbouring SHP-1 mutations was obtained by ImageJ analysis.

5.2.2 Transduction of HLA-A2$^+$ CD8$^+$ T cells with ZFN and Mel LVs

Cells from a HLA-A2$^+$ donor were transduced simultaneously with both ZFN and the Mel LVs, in order to generate SHP-1 deficient CD8$^+$ T cells that can recognise the HLA-A2$^+$ melanoma cell lines Mel526 and Mel624 (figure 5.4 A).

Cells were either transduced with control CD2 LV (100 µl), ZFN1 and ZFN2-CD2 LVs (50 µl / 80 µl), Mel LV (50 µl or 150 µl) or the latter three LVs together (3 x 50 µl or 3 x 100 µl) (figure 5.4 B). At day 12 post-transduction, 90% of the CD2 transduced cells were CD2$^+$ whereas only 34-44% of the ZFN1 and ZFN2-CD2 transduced cells were CD2$^+$. Doubling the volume of LV used, from 50 µl to 100 µl, did not increase the fraction of transduced cells thus the lower dose of the ZFN LVs was used in the subsequent experiments.

To determine the transduction efficiency of the Mel LV, cells were stained with FLT tetramer. Cells transduced with Mel LV alone showed 16-20% of FLT tetramer$^+$ staining. However, cells transduced with Mel LV and the two ZFN LVs showed a maximum of 0.5% tetramer$^+$ cells (figure 5.4 B and C). At equivalent volumes of Mel LV, the singly transduced cells gave a much larger tetramer$^+$ population than the triply transduced cells, with 16.4% and 0.5% respectively. Once more, this indicated that there is competition between the LVs when added to cells simultaneously and showed that the ZFN LVs outcompete the Mel LV.

Cells shown in figure 5.4 were stained using an FLT tetramer in the absence of the reversible protein kinase inhibitor Dasatinib, which has been shown to inhibit T cell activation by the tetramer and thus inhibit TCR downregulation and cell death (Lissina et al. 2009). Staining of the cells 3 days later in the absence or presence of Dasatinib showed an increase of tetramer staining from 16.7% to 25.4% (figure 5.4 B and figure 5.5) for the 150 µl Mel LV transduced cells. Thus tetramer staining in figure 5.4 gave an underestimation of successfully transduced tetramer$^+$ cells. However, in the presence of Dasatinib, the triply transduced cell did not show

any tetramer staining above background. Dasatinib was subsequently included in all tetramer staining.

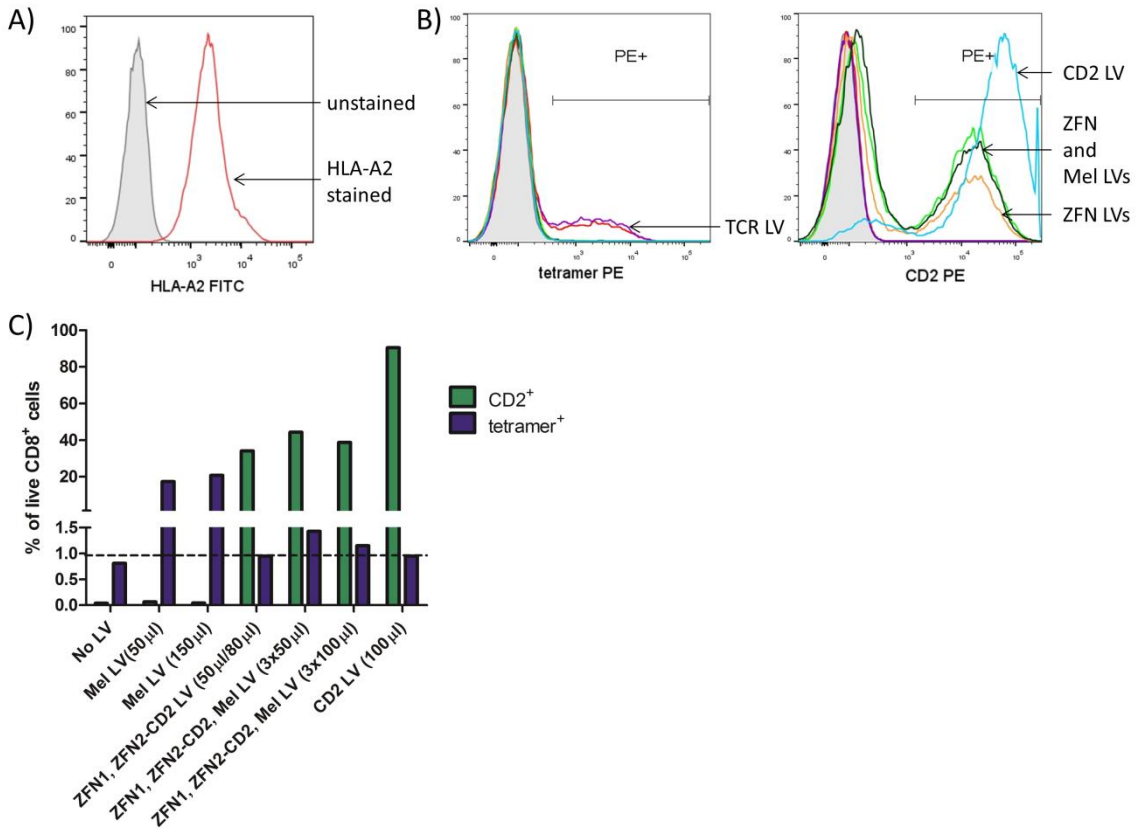

Figure 5.4: Transduction of HLA-A2$^+$ CD8$^+$ T cells with Mel and/or ZFN LVs. CD8$^+$ T cells isolated from an HLA-A2$^+$ donor were transduced with varying volumes of Mel and/or ZFN LVs and stained with anti-CD2 Ab or FLT tetramer 12 days post-transduction. Cells were gated on FSC/SSC, live/dead stain, single cells and CD8$^+$. A) Cells were stained with anti-HLA-A2 antibody (red) or left unstained (grey filled) and an overlay of both samples is shown for live CD8$^+$ T cells. B) Histograms showing overlays for tetramer (left) or CD2 (right) staining. Cells were transduced with 50 µl (red) or 150 µl (purple) of Mel LV, 50 µl of ZFN1 and 80 µl ZFN2-CD2 of LVs (orange), 50 µl (bright green) or 100 µl (dark green) of the ZFNs and Mel LVs and 100 µl of CD2 LV (blue). C) Frequencies in % of CD2$^+$ (green) and tetramer$^+$ (blue) cells in the PE gated, live CD8$^+$ cells populations shown in B). The dotted line indicates the background levels of tetramer staining.

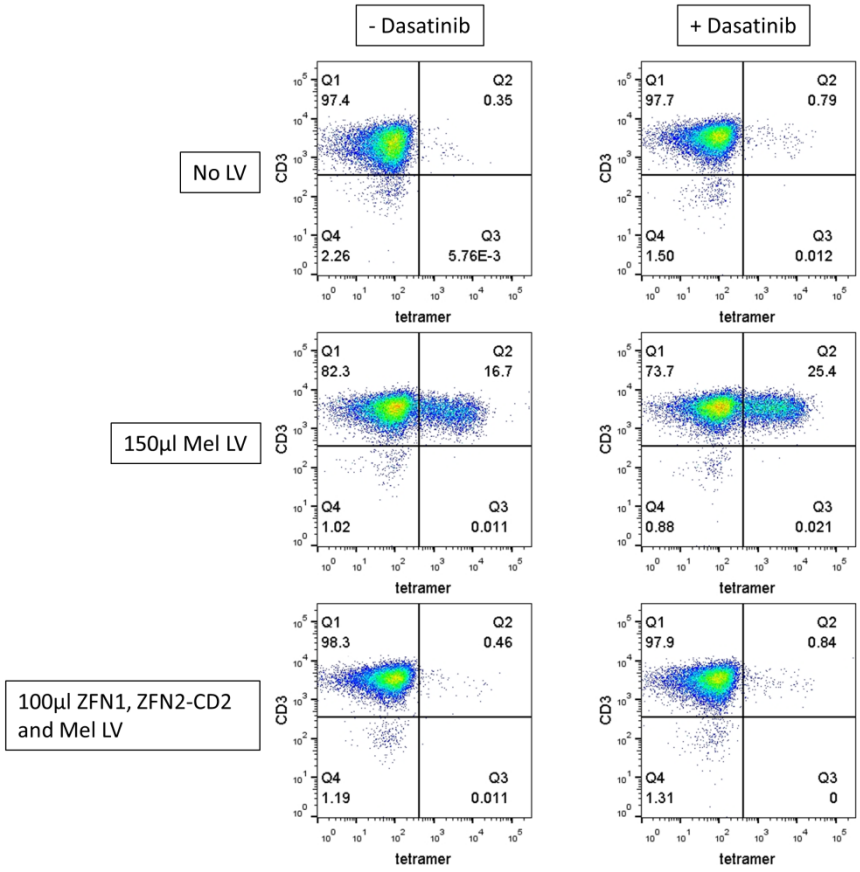

Figure 5.5: Effect of the protein kinase inhibitor Dasatinib on FLT tetramer staining of CD8$^+$ T cells transduced with Mel LV. CD8$^+$ T cells, transduced as described in figure 5.4, were stained with FLT tetramer and anti-CD3 Ab, in the presence or absence of Dasatinib, 15 days post-transduction. Cells were gated on FSC/SSC, live/dead stain, single cells and CD8$^+$.

T cells were stained with either PE conjugated anti-CD2 Ab or FLT tetramer and cells sorted using a PE positive MACS sort (figure 5.6). 96% and 91% of the positively sorted cells for CD2 and tetramer, respectively, showed strong CD2 expression. The negatively sorted fractions showed a mix of CD2 positive and negative cells with 27% of CD2$^+$ cells in the CD2 negative sorted fraction of the ZFNs and TCR transduced cells and 14% of tetramer$^+$ cells in the negative tetramer fraction. Thus this sorting method results in a loss of a substantial fraction of the CD2 and tetramer expressing population, reducing the number of potential mutant SHP-1 Mel$^+$ cells available for further studies.

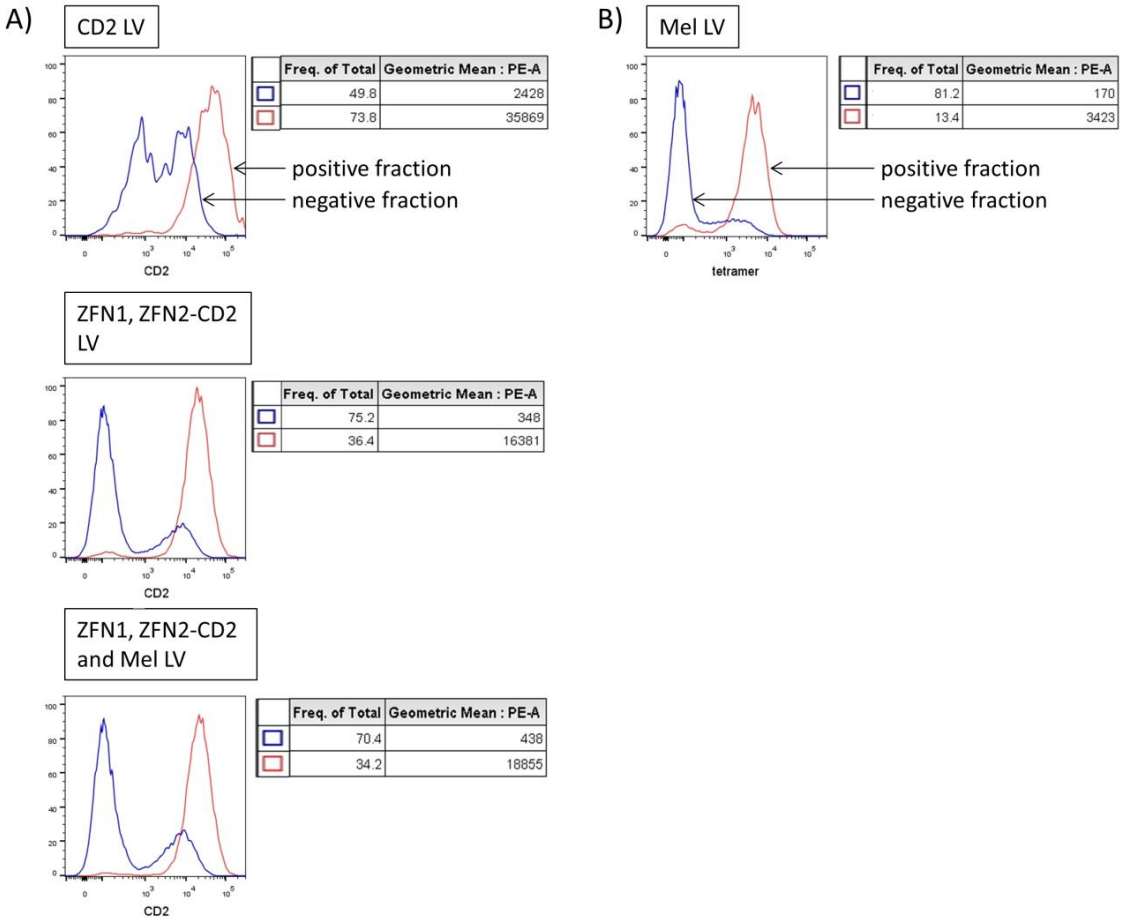

Figure 5.6: Lentivirally transduced CD8$^+$ T cells were sorted for CD2$^+$ or tetramer$^+$ by MACS separation. Cells shown were gated on FSC/SSC profile and single cells only. A) CD8$^+$ T cells transduced with control CD2 LV, both ZFN LVs or both ZFN and Mel LVs were stained with a PE conjugated anti-CD2 Ab and sorted into PE positive (red) and PE negative (blue) fractions using MACS columns. B) CD8$^+$ T cells transduced with Mel LV were stained with PE-conjugated FLT and sorted for PE positivity into a PE positive (red) and a PE negative (blue) fraction using MACS columns.

Unsorted and sorted cells were collected, gDNA extracted and used for the Cel-I mismatch assay shown in figure 5.7. Mutant SHP-1 cells were found in all cell populations transduced with both ZFN LVs (lanes 3 and 5-9). The strongest Cel-I signal of 12% mutant cells was seen in the CD2$^+$ sorted cells transduced with both ZFN LVs but not the Mel LV in lane 3. Comparing CD2$^+$ sorted cells to unsorted cells (lanes 3 and 5) showed that sorting cells for expression of ZFN2-CD2 clearly increased the Cel-I signal from 2% to 12% of mutant cells. The CD2$^-$ sorted cells in lane 6 encompass a population of 2.5% of mutated cells matching the observation that

the $CD2^-$ population includes cells expressing ZFN2-CD2 (figure 5.6 A). Interestingly, cells transduced with the three LVs and positively sorted for CD2 in lane 8, showed much lower mutation frequencies than sorted cells transduced with the ZFN LVs alone in lane 3 (3.5% versus 12%). Overall, transduction of multiple LVs seems to reduce the frequency of uptake of any of the three LVs, hence the possibility that fewer cells will express both non-tagged ZFN1 and ZFN2-CD2 when Mel LV was added causing the overall reduction of mutant SHP-1 alleles.

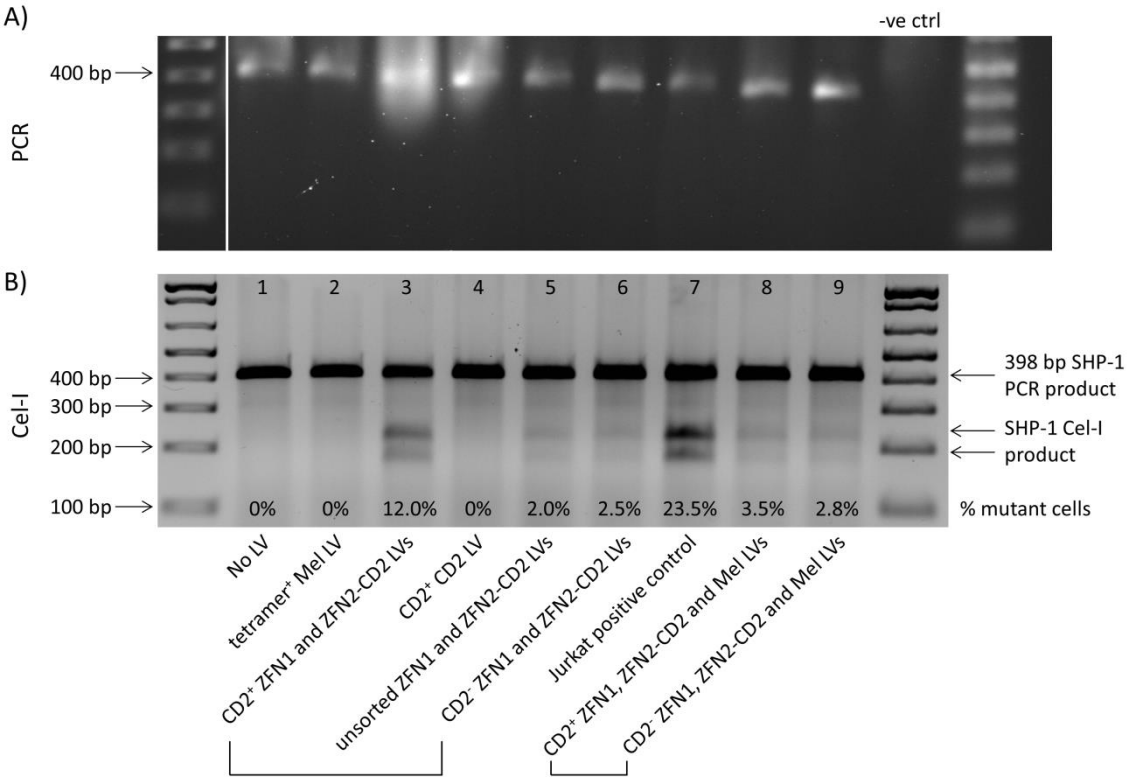

Figure 5.7: Cel-I assay of $CD8^+$ T cells transduced with the ZFN and/or Mel LVs. A) gDNA was extracted from cells transduced with LVs as indicated below each lane and a 398 bp SHP-1 genomic segment was amplified by PCR. The negative control (-ve ctrl) was a PCR reaction without gDNA. B) After hybridisation of the PCR product and digestion of the DNA with the Cel-I enzyme, the presence of mutated SHP-1 DNA is indicated by 178 bp and 220 bp DNA cleavage fragments. $Tetramer^+$ or $CD2^+$ indicates cells that were sorted for PE positivity by MACS (Mel TCR or ZFN2-CD2, respectively). Gag^+ Jurkat cells transduced with the ZFN LVs were used as a positive control.

To increase the number of mutant SHP-1 cells expressing Mel TCR, $CD2^+$ sorted cells were transduced a second time with Mel LV (figure 5.8 B). Cells stained 20 days later showed a very low frequency of $tetramer^+$ cells previously transduced with control CD2 LV (1.15%) and only background tetramer staining for cells previously transduced with the ZFN LVs (0.23%). This result together with results shown in figure 5.2 E confirm that consecutive lentiviral transductions is not efficient for primary $CD8^+$ T cells whereas it was for leukaemic T cell lines. The strategy used for future experiments was to co-transduce T cells with all three LVs simultaneously.

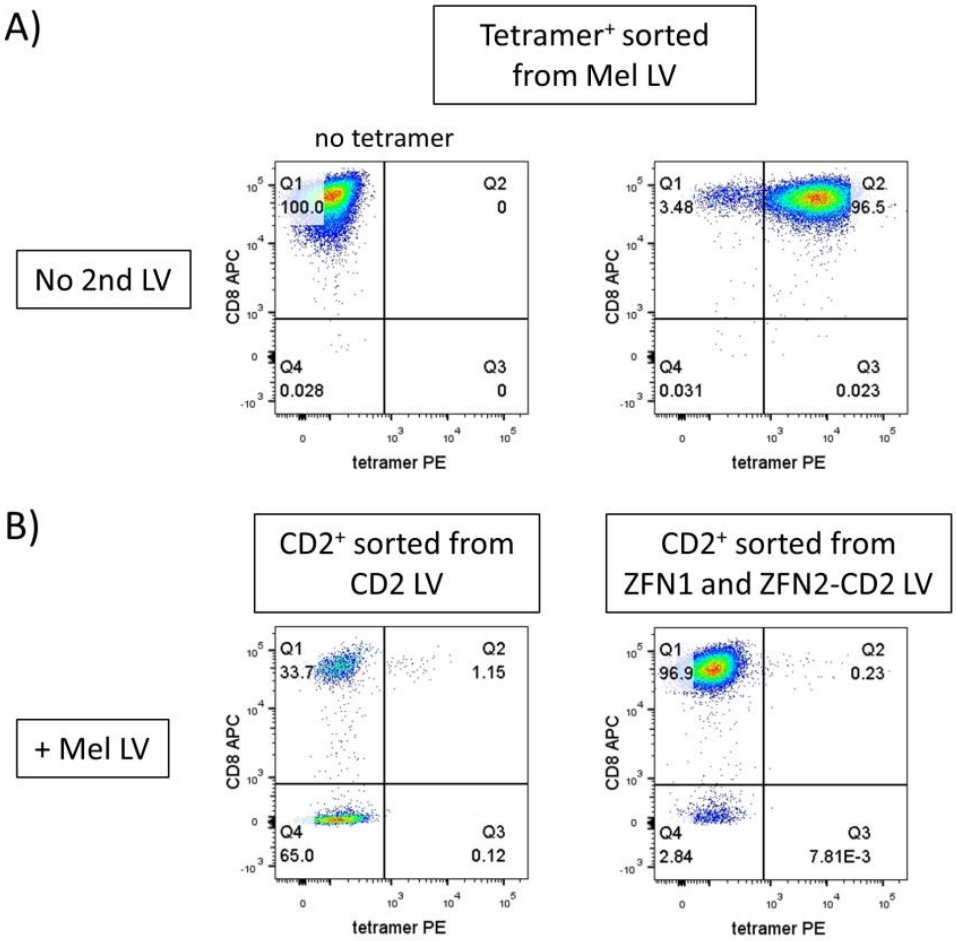

Figure 5.8: Transduction with Mel LV of $CD2^+$ sorted $CD8^+$ T cells previously transduced with ZFN LVs. A) $CD8^+$ T cells transduced with Mel LV and $tetramer^+$ sorted were stained with anti-CD8 Ab and FLT tetramer (right panel) or no tetramer (left panel). These cells were used as a positive and negative controls for B. B) $CD8^+$ T cells transduced with CD2 (left panel) or ZFN LVs (right panel) were $CD2^+$ sorted and subsequently transduced a second time with Mel LV. Cells were stained with anti-CD8 Ab and FLT tetramer 20 days post-transduction. All graphs were gated on FSC/SSC, live/dead and single cells.

5.2.3 Transduction of HLA-A2$^+$ CD8$^+$ T cells with delayed addition of ZFN and Mel LVs at a different ratio

Previous results seemed to indicate that the 2nd generation ZFN LVs outcompete the 3rd generation Mel LV, so to optimise transduction with all three LVs, the ratio between the ZFN LVs and the Mel LV was altered from a 1:1:1 to a 1:1:6.25 ratio. Additionally, the ZFN LVs were added with a delay of 15 or 30 min to test whether this could increase Mel LV transduction of T cells. Earlier results had shown that different volumes of ZFN2-CD2 LV (50, 80 or 100 µl) gave similar levels of transduction of approximately 38%, indicating that lower LV volumes might be sufficient. Here, 16 µl of each of the ZFN LVs were added to cells. As shown in figure 5.9, delayed addition of the ZFN LVs to the Mel LV gave a lower frequency of 'tetramer$^+$' or 'tetramer$^+$ CD2$^+$' cells. However the 1:1:6.25 ratio of Mel to ZFN LVs did increase the frequency of double positive cells to 1.4% above background, compared to 0.5% in figure 5.4 at a 1:1:1 ratio.

Cells transduced with the Mel LV only or with all three LVs were sorted for Mel TCR expression by MACS column separation. The latter were expanded for two weeks and then sorted for CD2 expression by MACS column separation. The tetramer$^+$ sorted cells were stained two weeks later with both the high affinity FLT tetramer (5.1 µM) and the lower affinity ELA tetramer (18 µM) (Ekeruche-Makinde et al. 2012) to compare staining as the ELA tetramer was more readily available (figure 5.10 A). Although the ELA tetramer gave a slightly lower frequency of tetramer positive cells (77.5% versus 80.7%), the ELA tetramer was used for all further Mel TCR staining due to its availability.

The tetramer and CD2 MACS separations yielded large populations of double negative (19-28%) or CD2$^+$ (26%) cells (figure 5.10 A). To enrich for single and double positive cells, flow cytometry sorting was done after cells had undergone a further, 3rd cycle of restimulation. The sort reports are shown in figure 5.10 B and C for 'tetramer$^+$' sorts of the Mel LV cells and

'tetramer$^+$ CD2$^+$' or 'tetramer$^-$ CD2$^-$' sorts of the Mel and ZFNs LVs cells respectively. The doubly negative 'tetramer$^-$ CD2' cells were isolated to use as a control in cytotoxicity assays.

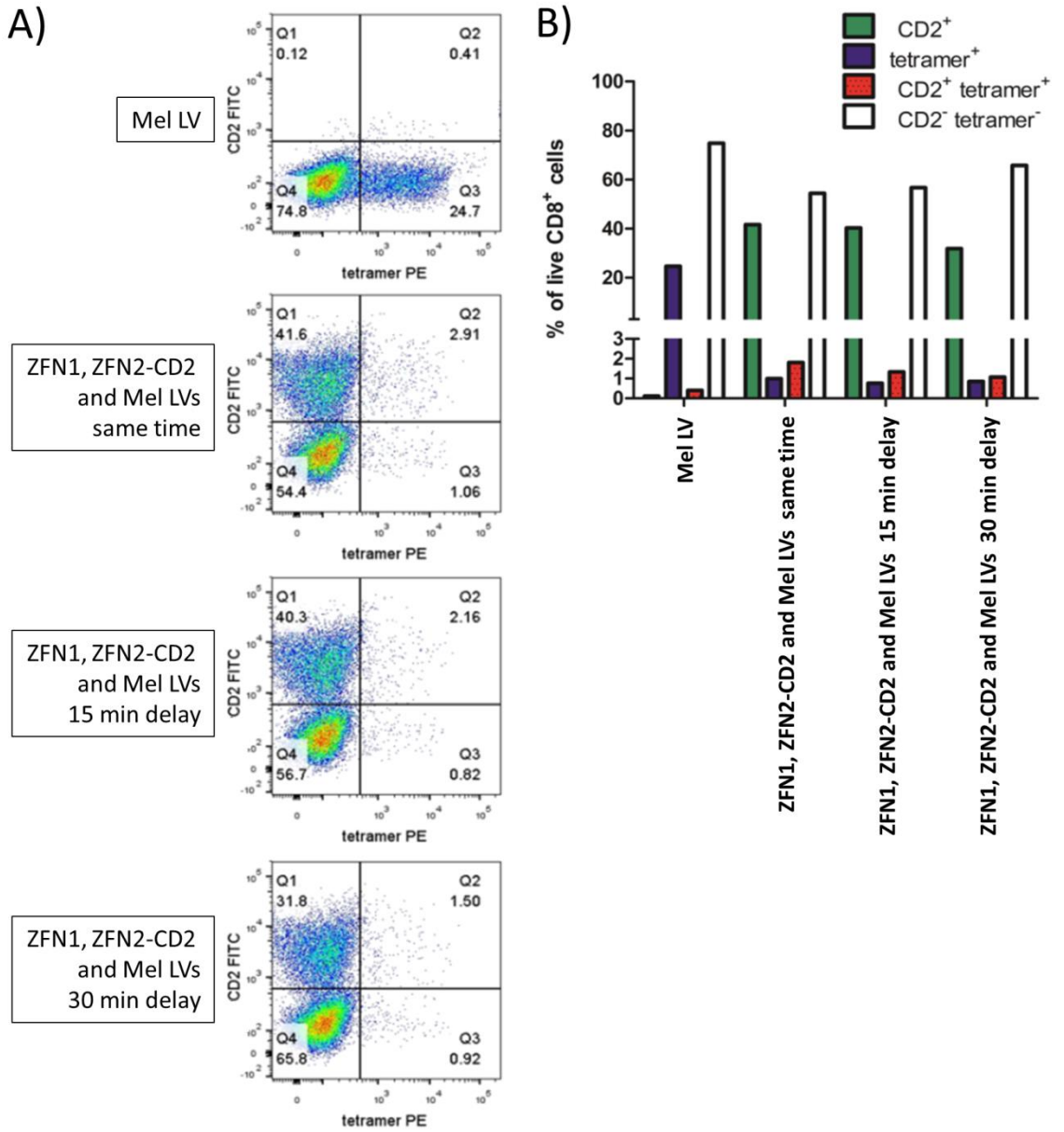

Figure 5.9: Delayed addition of ZFN LV to Mel LV treated HLA-A2$^+$ CD8$^+$ T cells. A) CD8$^+$ T cells from an HLA-A2$^+$ donor were transduced with 100 µl Mel LV and 16 µl each of the ZFN1 and ZFN2-CD2 LVs were added either simultaneously or with a 15 min or 30 min delay. Ten days post-transduction, cells were stained using an anti-CD2 Ab and FLT tetramer and gated on FSC/SSC, live/dead stain, single cells and CD8$^+$. B) Frequencies of CD2$^+$ (green), 'tetramer$^+$' (blue) or 'CD2$^+$ and tetramer$^+$' cells in the live CD8$^+$ T cell population shown in A.

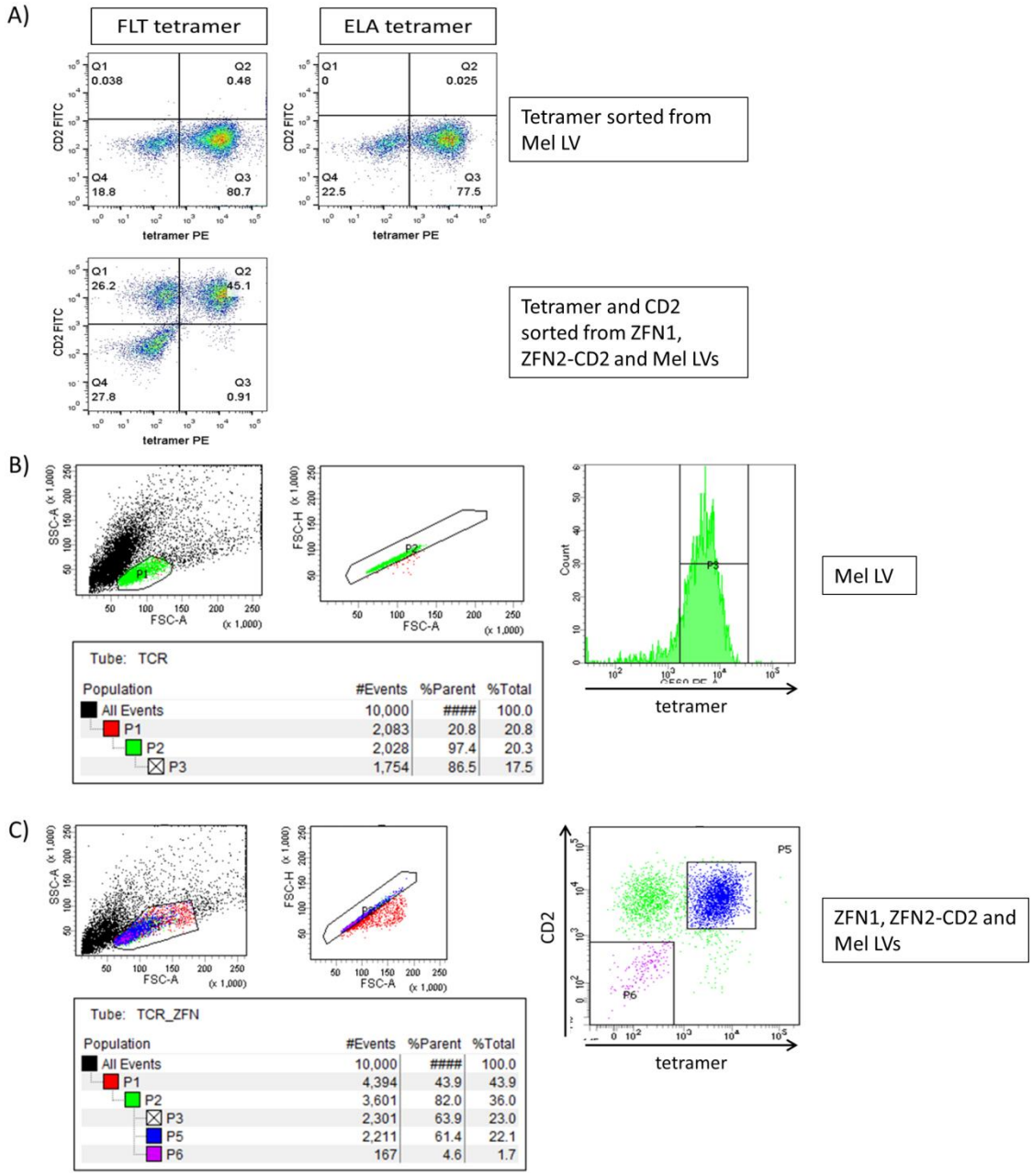

Figure 5.10: MACS and FACS sorting of Mel and/or ZFN LVs transduced CD8$^+$ T cells into 'tetramer$^+$' and 'tetramer$^+$ CD2$^+$' populations. A) CD8$^+$ T cells transduced with Mel LV (top panels) or Mel and ZFN LVs (bottom panel) were sort by anti-PE MACS separation columns for tetramer or tetramer and CD2, respectively. Cells were expanded for two weeks before undergoing the second MACS sort for CD2$^+$ cells. Cells were gated on FSC/SSC, live/dead stain and single cells. B) Tetramer$^+$ sorted cells from A, top panel, were stained with 1.42 µg FLT and 2.06 µg ELA tetramer and sorted by flow cytometry. Cells were gated on FSC/SSC (P1), single cells (P2) and 2.8 x 10^6 'tetramer$^+$' cells (P3) were collected and expanded. C) 'Tetramer$^+$ and CD2$^+$' sorted cells from A, bottom panel, were stained with 1.42 µg FLT and 2.06 µg ELA tetramer and sorted by flow cytometry. Cells were gated on FSC/SSC (P1), single cells (P2) and 5.4 x 10^6 'tetramer$^+$ CD2$^+$' cells (P5) and 0.8 x 10^6 double negative cells (P6) were collected and expanded.

The Cel-I mismatch assay was done on the 'tetramer^{+}', 'tetramer^{+} CD2^{+}' and 'tetramer^{-} CD2^{-}' FACS sorted cells (figure 5.11). A Cel-I signal indicating 3.7% mutant cells was observed with the 'tetramer^{+} CD2^{+}' cells. The low level of SHP-1 germline mutations may have resulted from cells not having been transduced with the ZFN1 LV and thus not expressing both ZFNs necessary to induce mutations. However, the lack of reporter gene in the ZFN1 LV meant that no further sorting was possible.

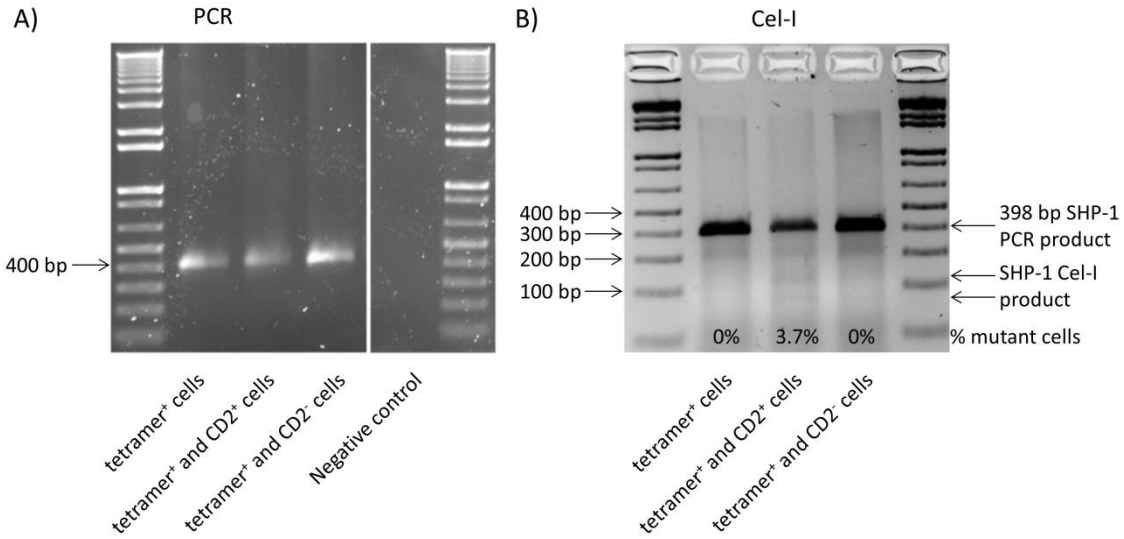

Figure 5.11: Cel-I assay of 'tetramer^{+}', 'CD2^{+} and tetramer^{+}' or 'tetramer^{-} CD2^{-}' CD8^{+} T cells. A) gDNA was extracted from tetramer^{+} populations of Mel LV only cells and CD2^{+} and tetramer^{+} or double negative populations of Mel and ZFN LVs cells. A 398 bp SHP-1 genomic segment was amplified by PCR. The negative control was a PCR reaction without gDNA. B) After hybridisation, the PCR product was digested with the Cel-I enzyme and mutated SHP-1 DNA is indicated by the presence of 178 bp and 220 bp DNA cleavage fragments.

5.2.4 Transduction of HLA-A2$^+$ CD8$^+$ T cells with varying volumes of ZFN and Mel LVs

As the previous transductions showed no improvement when delaying the addition of ZFN LVs, all three LVs were added simultaneously to cells and at the same ratio as before (1:1:6.25). To optimise transduction further, not only 100 µl but also 50 µl of the Mel LV was added, keeping the same ratio. Similarly to the previous experiment, transduction of HLA-A2$^+$ CD8$^+$ T cells with 60 µl Mel LV gave 18% 'tetramer$^+$' cells, whereas 22% of cells were CD2$^+$ when transduced with 16 µl of each of ZFN1 and ZFN2-CD2 (figure 5.12). Most importantly, transduction with Mel LV and ZFN LVs showed only 0.03-0.86% 'tetramer$^+$ CD2$^+$' cells above background of non-transduced cells.

Cells from the Mel LV transductions were pooled and FACS sorted for tetramer$^+$, ZFN LVs transduced cells were pooled and FACS sorted for CD2$^+$ and triply transduced cells were pooled and FACS sorted into 'tetramer$^+$ CD2$^+$' or 'tetramer$^-$ CD2$^-$' populations. Sort reports are shown in figure 5.13.

Sorted cells were analysed for SHP-1 mutations using the Cel-I mismatch assay. However, due to an inadvertent bacterial infection in the CD2$^+$ sorted ZFN LVs transduced population, only the 'tetramer$^+$', 'tetramer$^-$ CD2$^-$' and the 'tetramer$^+$ CD2$^+$' cell populations were analysed (figure 5.14). The samples from the Cel-I assay in figure 5.11 B were run on the same electrophoresis gel as the samples in figure 5.14 B, and when comparing the two, the latter transduction showed a higher transduction frequency indicated by 7.2% of mutant cells compared to 3.7% previously.

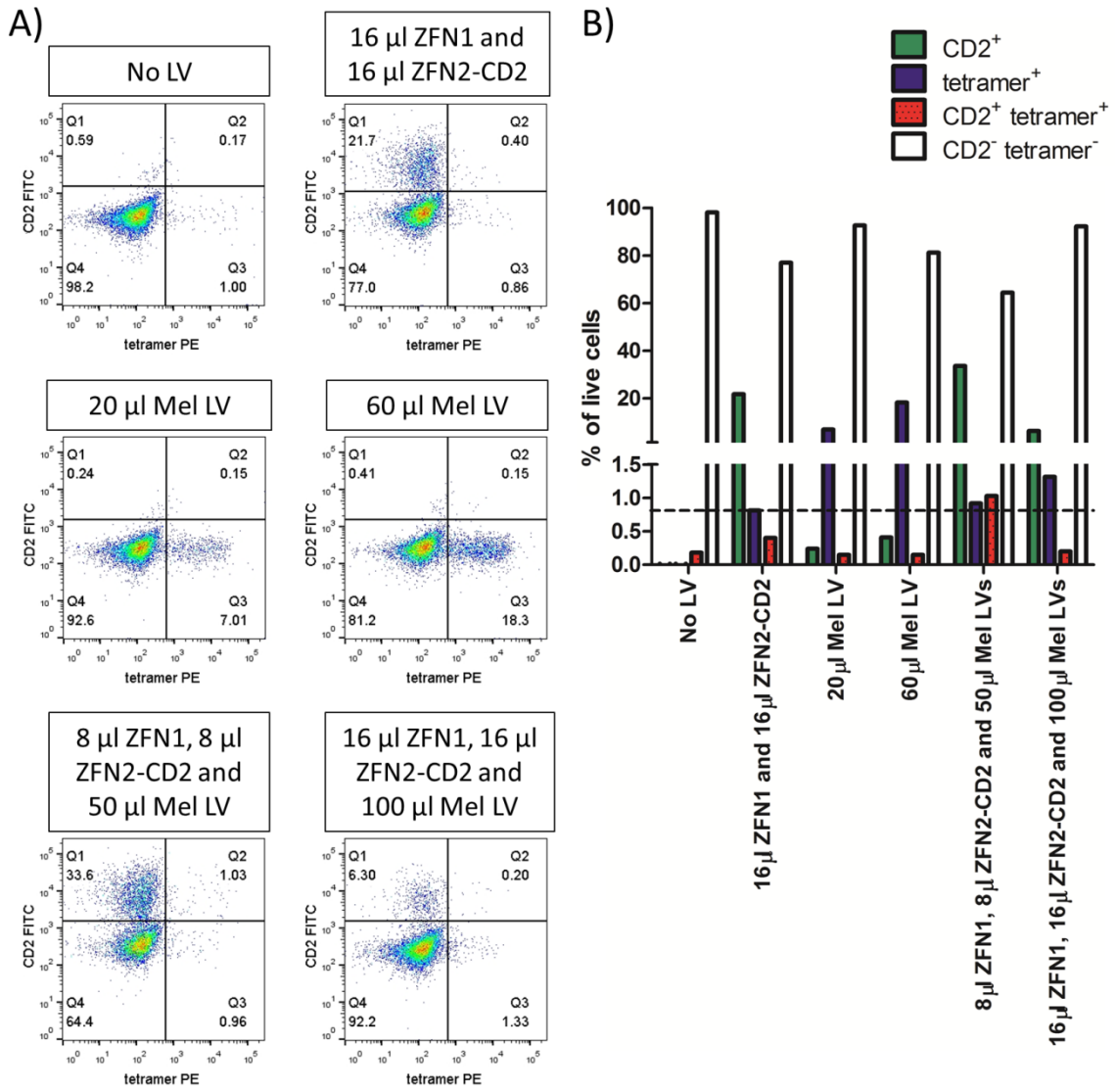

Figure 5.12: Transduction of HLA-A2$^+$ CD8$^+$ T cells with the Mel and/or ZFN LVs. A) CD8$^+$ T cells isolated from an HLA-A2$^+$ donor were transduced with 16 µl of ZFN1 and ZFN2-CD2 LVs (top right panel), 20 µl or 60 µl Mel LV (middle two panels), 50 µl or 100 µl Mel and 8 µl or 16 µl ZFN LVs (bottom two panels) and stained with anti-CD2 Ab and FLT tetramer 9 days later. Cells were gated on FSC/SSC, live/dead stain, single cells and CD8$^+$. B) Frequencies of CD2$^+$ (green), 'tetramer$^+$' (blue) or 'tetramer$^+$ CD2$^+$' (red) cells are shown for cells gated as in A, after subtracting the frequency of the matching population of the FMO controls.

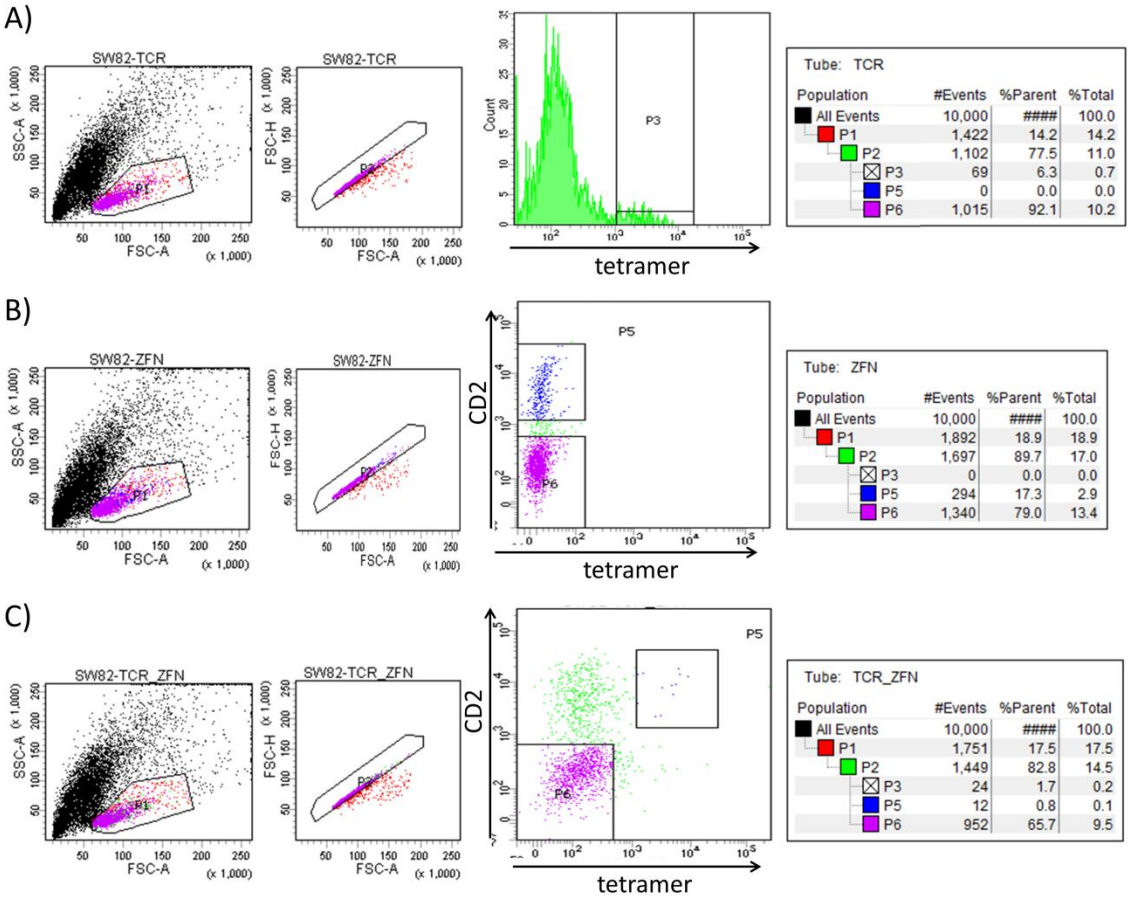

Figure 5.13: Mel and/or ZFN LVs transduced CD8$^+$ T cells were sorted into 'tetramer$^+$' or 'tetramer$^+$ CD2$^+$' populations by FACS. CD8$^+$ T cells transduced with Mel LV (A), ZFN1 and ZFN2-CD2 LVs (B) or Mel and ZFN LVs (C) were stained with anti-CD2 Ab, 1.42 µg FLT and 2.06 µg ELA tetramer and sorted by flow cytometry. All cells were gated on FSC/SSC (P1) and single cell gates (P2). A) 0.2 x 10^6 tetramer$^+$ cells (P3) were collected and expanded. B) 0.6 x 10^6 CD2$^+$ cells (P5) were collected and expanded. C) 0.02 x 10^6 'tetramer$^+$ CD2$^+$' cells (P5) and 2.1 x 10^6 double negative cells (P6) were collected and expanded.

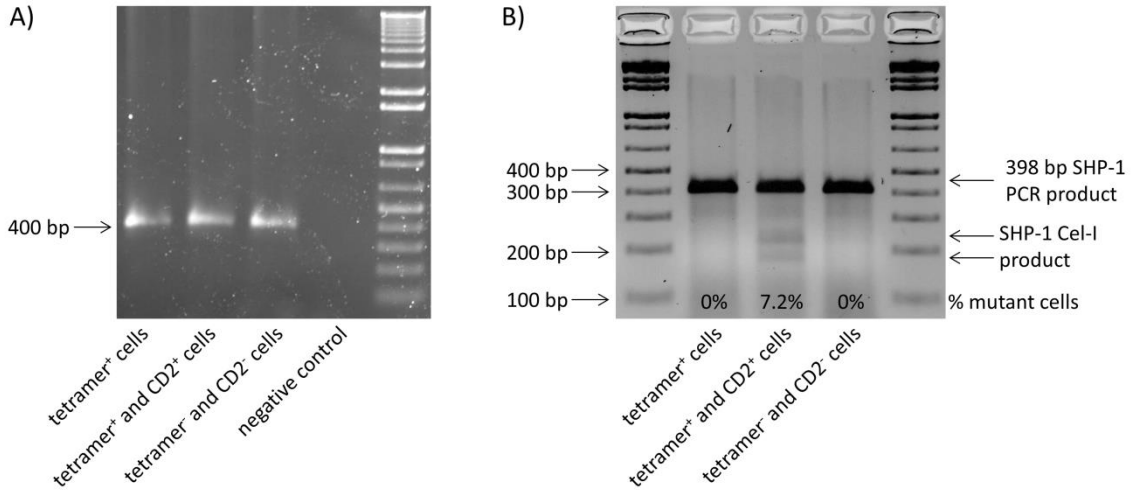

Figure 5.14: Cel-I assay of 'tetramer^{+}', 'tetramer^{+} CD2^{+}' or 'tetramer^{-} CD2^{-}' CD8^{+} T cells. A) gDNA was extracted from 'tetramer^{+}', 'tetramer^{+} CD2^{+}' or 'tetramer^{-} CD2^{-}' FACS sorted cells and a 398 bp SHP-1 genomic segment. The negative control was a PCR reaction without gDNA. B) After hybridisation of the PCR product and digestion of the DNA with the Cel-I enzyme, mutated SHP-1 DNA is indicated by 178 bp and 220 bp DNA cleavage fragments.

5.3 Killing and proliferation of mutant SHP-1 Mel$^+$ CD8$^+$ T cells in response to melanoma target cells

As shown in experiments in the previous chapter, the Mel TCR recognises the HLA-A2$^+$ Mel526 and Mel624 melanoma cell lines (figure 4.18). Here, killing of melanoma target cells by SHP-1 sufficient and mutant SHP-1 Mel$^+$ CD8$^+$ T cells was studied as well as cell survival and proliferation of these cells. Table 5.1 shows the different cells used in the following experiments. It is important to remember that the mutant SHP-1 population will only have a small percentage (<4-8% as shown by Cel-I assays) of cells with complete lack of functional SHP-1 protein and is hence not referred to as a SHP-1 deficient population.

	wt/CD2$^+$ CD8$^+$	Mel$^+$ CD8$^+$	Mel$^-$ CD2$^-$ CD8$^+$	Mel$^+$ CD2$^-$ CD8$^+$ (SHP-1 sufficient)	Mel$^+$ CD2$^+$ CD8$^+$ (mutant SHP-1)
Mel TCR	-	+	-	+	+
SHP-1	+/+	+/+	+/+	+/+	+/+, +/- and -/-
LV used	none/CD2	Mel	ZFN and Mel LVs	Mel LV	ZFN and Mel LVs
Reference	Figure 5.10 A	Figure 5.10 A	Figure 5.10 B / 5.13 C	Figure 5.10 B / 5.13 A	Figure 5.10 B / 5.13 C

Table 5.1: Characterisation of primary CD8$^+$ T cells used in killing experiments. Orange shaded boxes indicate cells expressing the Mel TCR and the green box indicates cells carrying mutated SHP-1.

5.3.1 Generation of GLuciferase expressing Mel526 and Mel624 cells

To quantify the extent of melanoma cell killing by $CD8^+$ T cells, Mel526 and Mel624 cells were transduced with lentivirus encoding a non-secreted GLuciferase gene. Upon melanoma cell death, the GLuciferase will be released into the supernatant and measured using a luciferase assay. Additionally, the lentiviral transfer vector encodes a RFP gene, followed by a T2A ribosomal skipping element as well as the above mentioned GLuciferase gene. The expression of the gene cassette is driven by an EF-1α promoter (figure 5.15 A). The construct was kindly provided by Dr John Bridgeman (manuscript in preparation). The RFP-GLuciferase transduced Mel526 and Mel624 cells were sorted by flow cytometry for high levels of RFP expression (figure 5.15 B and C). The sorted cells were expanded and used for *in vitro* (Chapter 5) and *in vivo* (Chapter 7) experiments.

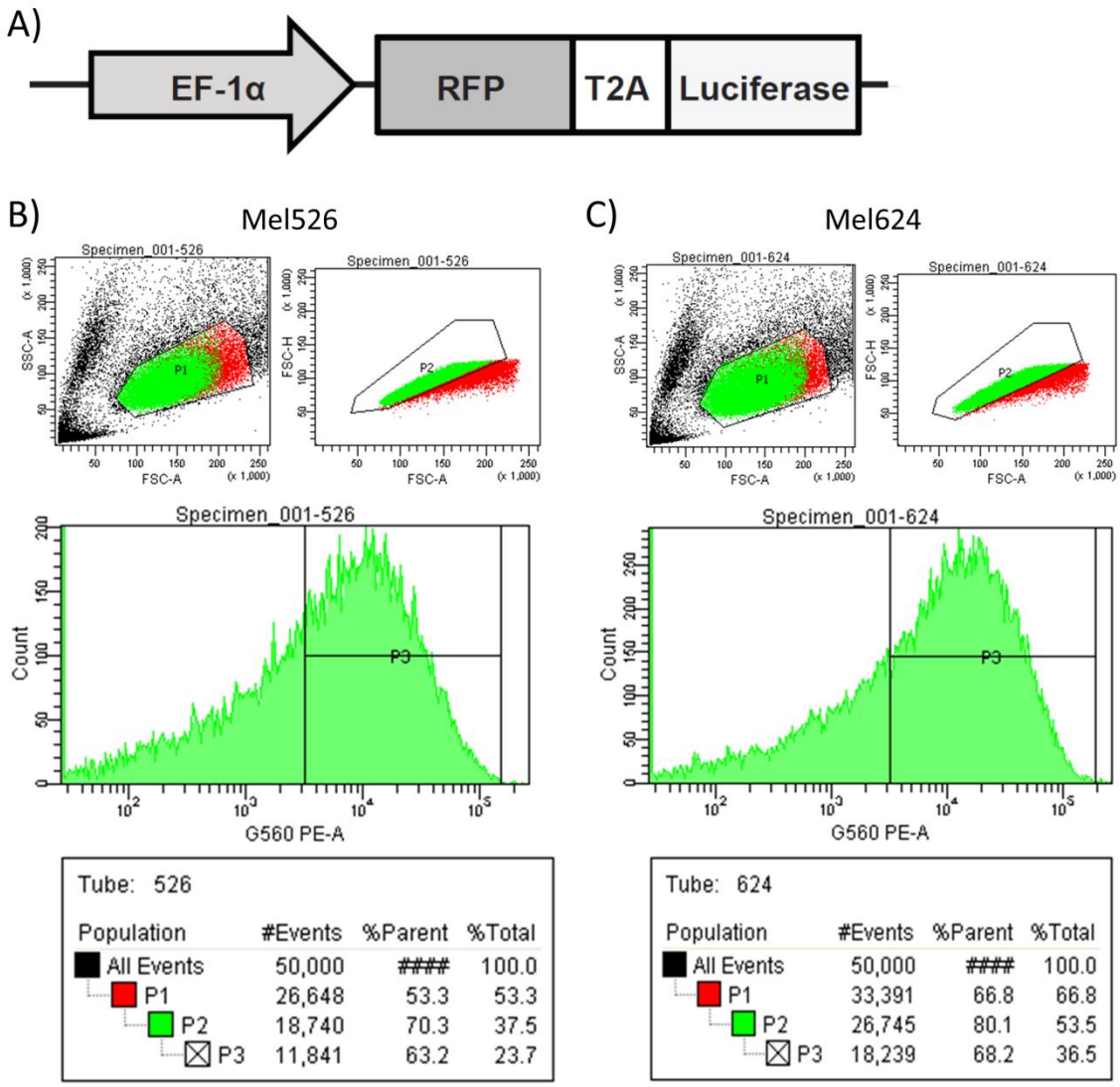

Figure 5.15: FACS sort of RFP-GLuciferase LV transduced Mel526 and Mel624. A) The pELN lentiviral transfer plasmid encoding the RFP-T2A-GLuciferase cassette, under the control of the EF-1α promoter, was used to produce LV to transduce Mel526 and Mel624 cells. B) and C) show the gating strategy used for the FACS sorting of RFP-GLuciferase LV transduced Mel526 and Mel624 cells respectively. Cells were sorted on FSC/SSC (P1), on single cells (P2) and for high levels of RFP expression in the PE channel (P3). The sort statistics are shown in the table.

5.3.2 Optimisation of a cytotoxicity assay using primary CD8$^+$ T cells expressing the Mel TCR

To optimise the Mel TCR dependent melanoma cell killing assay, MACS sorted Mel$^+$ CD8$^+$ T cells were incubated for the indicated amount of time onto 80% confluent RFP-GLuciferase FACS sorted Mel526 cells. Control Mel TCR negative T cells were pooled from untransduced and CD2 LV transduced T cells (wt/CD2$^+$) due to low CD2$^+$ cell numbers. All cells went through a total of 4 stimulation cycles before being used in this experiment. As shown in figure 5.16, wt/CD2$^+$ CD8$^+$ T cells do not kill the tumour target cells, whereas the Mel$^+$ CD8$^+$ T cells kill the Mel526 cells in a dose dependent manner (16 h). At a 3:1 ratio of T cells to Mel526, the majority of Mel526 cells are killed in less than 16 h. At the lowest T cell dose of 0.3:1, maximum killing is reached at 48 h. High T cell:Mel526 ratios showed decreased cytotoxicity beyond 24 h possibly due to technical aspects of the assay. Possibly the continuous proliferation of Mel526 cells and thus increase in GLuciferase protein in 'Mel526 cells only' control wells used to obtain the 100% lysis reading (by freeze thawing the cells) may have been a contributing factor in conjunction with the constant level of GLuciferase in the supernatant of wells with high T cell numbers due to the quick initial killing of all Mel526 cells (<16 h).

Figure 5.17 shows the above experiment as a representation of killing against time. It demonstrates that this assay is most efficient for short incubation periods (<48 h) with very potent cytotoxic cells at high ratios, whereas it can be used for long-term killing (>48 h) of less potent T cells or T cells at lower ratios.

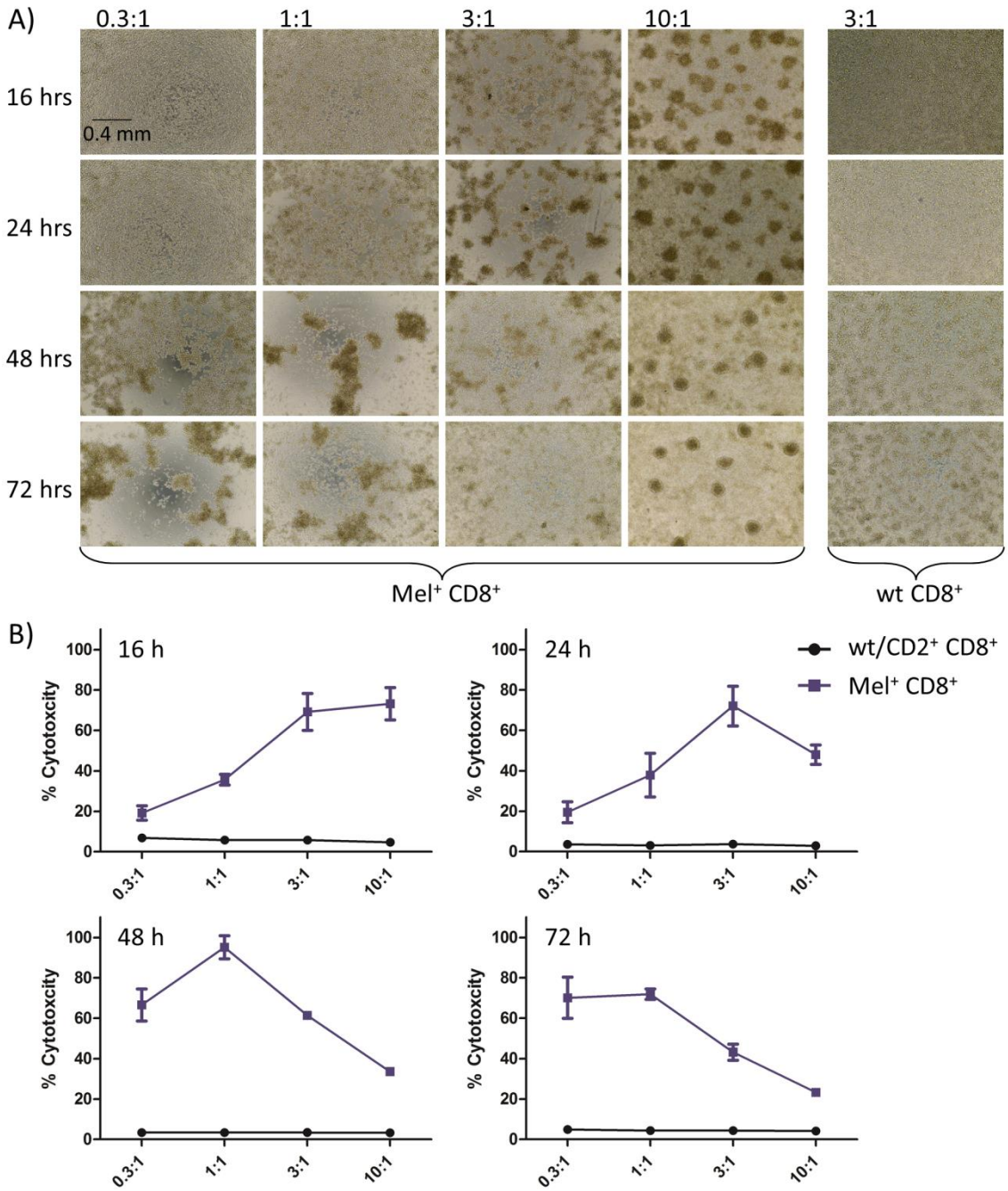

Figure 5.16: Mel526 tumour cell killing by wt/CD2$^+$ and Mel$^+$ CD8$^+$ T cells. RFP-GLuciferase sorted Mel526 cells were grown to confluency before either control wt/CD2$^+$ or Mel$^+$ CD8$^+$ T cells were added at different ratios and cells co-incubated for 72 h. A) Representative wells coated with RFP-GLuciferase Mel526 and incubated with varying numbers of either wt/CD2$^+$ or Mel$^+$ CD8$^+$ T cell (T to Mel526 ratios of 0.3:1 to 10:1) were photographed at four different times (10x magnification). B) GLuciferase, released by lysed RFP-GLuciferase Mel526, was measured for wells incubated with wt/CD2$^+$ (black) and Mel$^+$ (blue) CD8$^+$ T cell. GLuciferase released into the supernatant was expressed as a % of total GLuciferase in RFP-GLuciferase Mel526 cell only wells. Data shown is one experiment with triplicates for each condition and the error bars represent the SEM.

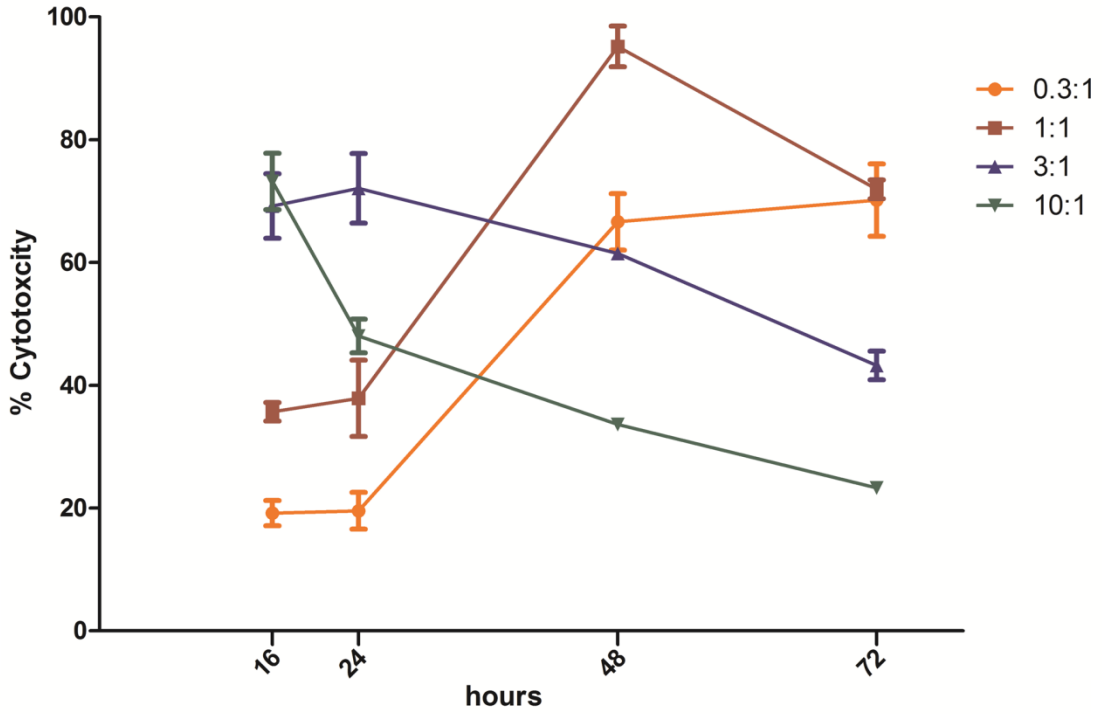

Figure 5.17: Mel526 tumour cell killing by Mel$^+$ CD8$^+$ T cells over a 72 h period. Data shown are represented as % cytotoxicity over time for the Mel$^+$ CD8$^+$ T cells only and is from the same experiment as figure 5.16. Different colours indicate different T cell to Mel526 cell ratios. Triplicates for each condition are shown and error bars indicate the SEM.

5.3.3 Mel526 tumour cell killing by SHP-1 sufficient and mutant SHP-1 Mel$^+$ CD8$^+$ T cells

The ability of FACS sorted SHP-1 sufficient (Mel$^+$ CD2$^-$) and mutant SHP-1 (Mel$^+$ CD2$^+$) Mel$^+$ CD8$^+$ T cells to kill Mel526 cells was compared using GLuciferase expressing targets. It is important to recall that only 3.7% of the 'mutant SHP-1 Mel$^+$ CD8$^+$ T' cells were found to contain mutated SHP-1 genes (figure 5.11 B). The 'Mel$^-$ CD2$^-$', 'Mel$^+$ CD2$^-$' and 'Mel$^+$ CD2$^+$' cell populations used in the experiment were stained with FLT tetramer and anti-CD2 antibody as shown in figure 5.18 B. It is also important to note that the control 'Mel$^-$ CD2$^-$ CD8$^+$' cell population, obtained from a double negative FACS sort of ZFN and Mel LV transduction, also contained a low number of 'Mel$^+$ CD2$^+$' cells (3.44%), presumably due to an impure FACS sort.

Additionally, a substantial frequency of Mel^- cells was observed in positively sorted cells with a frequency of 4.0% for the 'Mel^+ $CD2^-$' and 9.7% for the 'Mel^+ $CD2^+$' populations. To cross-check the cell counting done using a haemocytometer, input cell numbers at one ratio (3:1 T:Mel526) were measured by flow cytometry using cytocount beads (figure 5.18 C). Importantly, after gating on live and single cells similar numbers were observed for the two Mel^+ populations, however, about 2.5 times more for the control double negative cells.

No cytotoxicity was detected at 4 h, however, the Mel^+ T cells showed maximal killing at 24 h at high T:Mel526 ratios (figure 5.19). The control Mel^- $CD2^-$ T cells also showed very potent target cell killing at 72 h which is likely due to the contamination of the cells with 4% Mel^+ cells and fits with the slower killing of low T:Mel526 ratios observed in the previous experiment (figure 5.17). It is of note that the ordinate axis in B for 24 and 72 h exceeds 100% cytotoxicity. This might be due to incomplete cell lysis of the control Mel526 wells or possibly the addition of T cells promoted Mel526 proliferation before bringing about killing.

Supporting the luciferase data, the microscopic pictures in figure 5.19 A show that at 24 h most of the Mel526 cells were lysed for the 1:1-10:1 ratios of the Mel^+ $CD2^-$ cells, whereas the same was not true for the 1:1 ratio of the Mel^+ $CD2^+$. This experiment might indicate that the mutant SHP-1 Mel^+ $CD8^+$ T cells are slower and potentially less potent at killing target Mel526 cells. However, the difference in frequency of Mel^+ cells for the SHP-1 sufficient (96%) and mutant SHP-1 cells (90%) observed in figure 5.18 B may have been a contributing factor.

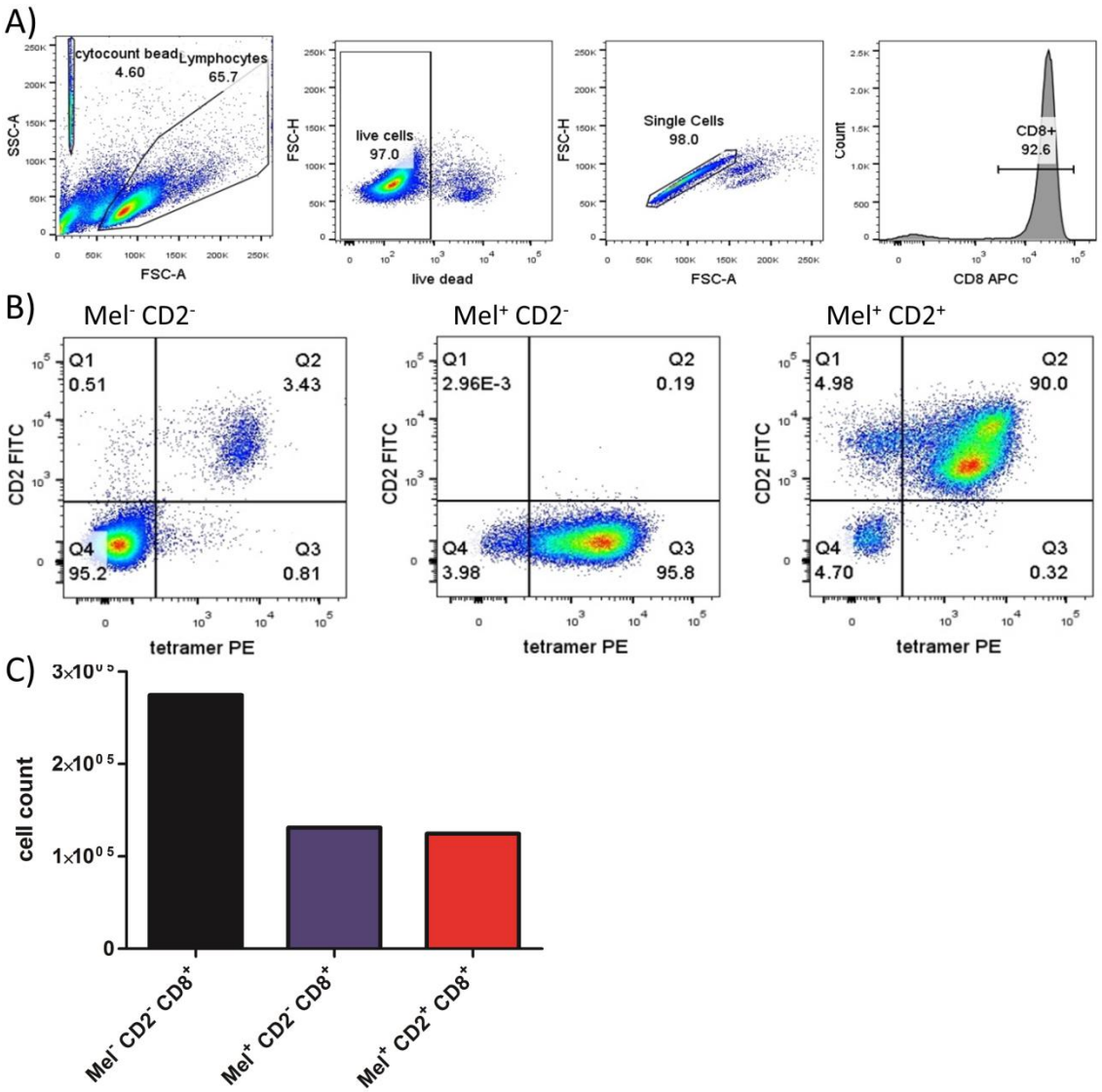

Figure 5.18: Characterisation of input SHP-1 sufficient and mutant SHP-1 Mel$^+$ CD8$^+$ T cells for a cytotoxicity assay. FACS sorted cells were stimulated for one cycle after the sort, cells analysed by flow cytometry and assessed for cytotoxicity. 'Mel$^-$ CD2$^-$', 'Mel$^+$ CD2$^-$' and 'Mel$^+$ CD2$^+$' CD8$^+$ T cells stained with AmCyan live/dead, anti-CD8 APC antibody, anti-CD2 FITC antibody and ELA tetramer PE. A) Cells were gated on FSC/SSC, live/dead stain, single cells and CD8$^+$. Cytocount beads were added to the T cells to enumerate the exact T cell numbers. B) T cells gated as shown in A were further analysed for CD2 and ELA tetramer staining. C) T cell numbers from the 3:1 T:Mel526 ratio for each group were enumerated using cytocount beads as reference.

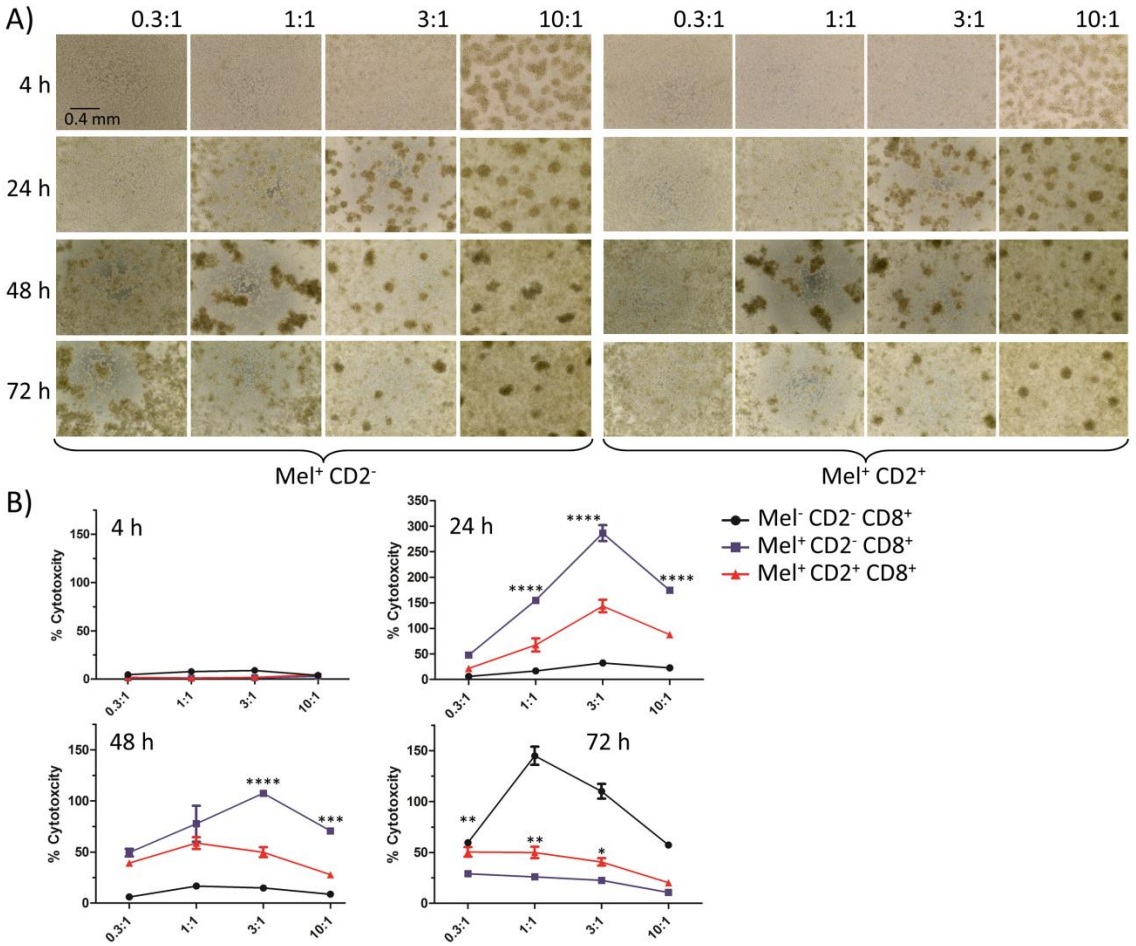

Figure 5.19: Mel526 tumour cell killing by SHP-1 sufficient and mutant SHP-1 Mel$^+$ CD8$^+$ T cells. RFP-GLuciferase sorted Mel526 cells were grown to confluency before either control 'Mel$^-$ CD2$^-$', 'Mel$^+$ CD2$^-$' or 'Mel$^+$ CD2$^+$' CD8$^+$ T cells were added at different ratios and cells co-incubated for 72 h. A) Representative wells coated with RFP-GLuciferase Mel526 and incubated with varying numbers of 'Mel$^+$ CD2$^-$' or 'Mel$^+$ CD2$^+$' CD8$^+$ T cell (T to Mel526 ratios of 0.3:1 to 10:1) were photographed at four different times (10x magnification). B) GLuciferase, released by lysed RFP-GLuciferase Mel526, was measured for 'Mel$^-$ CD2$^-$' (black), 'Mel$^+$ CD2$^-$' (blue) and 'Mel$^+$ CD2$^+$' (red) CD8$^+$ T cell. GLuciferase released into the supernatant was expressed as a % of total GLuciferase in RFP-GLuciferase Mel526 cell only wells. Data shown is one experiment with triplicates for each condition and error bars indicate the SEM. Asterisks show statistically significant differences between the SHP-1 sufficient and mutant SHP-1 Mel$^+$ T cells with *p<0.05, **p<0.01, ***p<0.001 and ****p<0.0001.

To compare survival and proliferation of SHP-1 sufficient and mutant SHP-1 cells, non-adherent cells from the above Mel526 killing experiment were collected after 72 h and live $CD8^+$ T cells counted for each condition (figure 5.20 A). No significant differences were observed between the SHP-1 sufficient and mutant SHP-1 Mel^+ cells. Higher 'Mel^- $CD2^-$' cell numbers were present at the 10:1 ratio, which considering the 2.3 fold higher input cell number (figure 5.18 C) actually indicates a decrease in cell survival of these 'Mel^- $CD2^-$' cells.

Experimental design allowed looking at T cell survival and/or proliferation of the three different T cell groups. T cell numbers at the start of the experiment were recorded for the 3:1 T cell:Mel526 ratio (figure 5.18 C) and control wells with T cells only at the equivalent of the 1:1 ratio were used as controls for the luciferase assay. All the T cell numbers extrapolated from this experiment were used to calculate the fold increase of the three groups of T cells. The fold increase of '0 versus 72' h was obtained from dividing stimulated T cell numbers at 72 h by the input T cell numbers (0 h) at the 3:1 ratio. The fold increase of 'stimulated versus non-stimulated' cells was obtained from dividing the T cell numbers of stimulated (+Mel526) wells by T cell numbers of non-stimulated (no Mel526) wells at 72 h at the 1:1 ratio. The 'Mel^- $CD2^-$' control cells did not expand when incubated with Mel526 cells, presumably as they were not stimulated by cognate antigen (figure 5.20 C). Compared to the SHP-1 sufficient Mel^+ T cells, the mutant SHP-1 Mel^+ T cells showed a slightly larger fold increase from 0 to 72 h and a significantly higher fold increase in cell expansion of stimulated versus non-stimulated cells.

All in all, these results hint towards an increased survival and/or proliferation profile of the mutant SHP-1 cells with a possibly slower and less potent cytotoxic potential, when compared to SHP-1 sufficient cells.

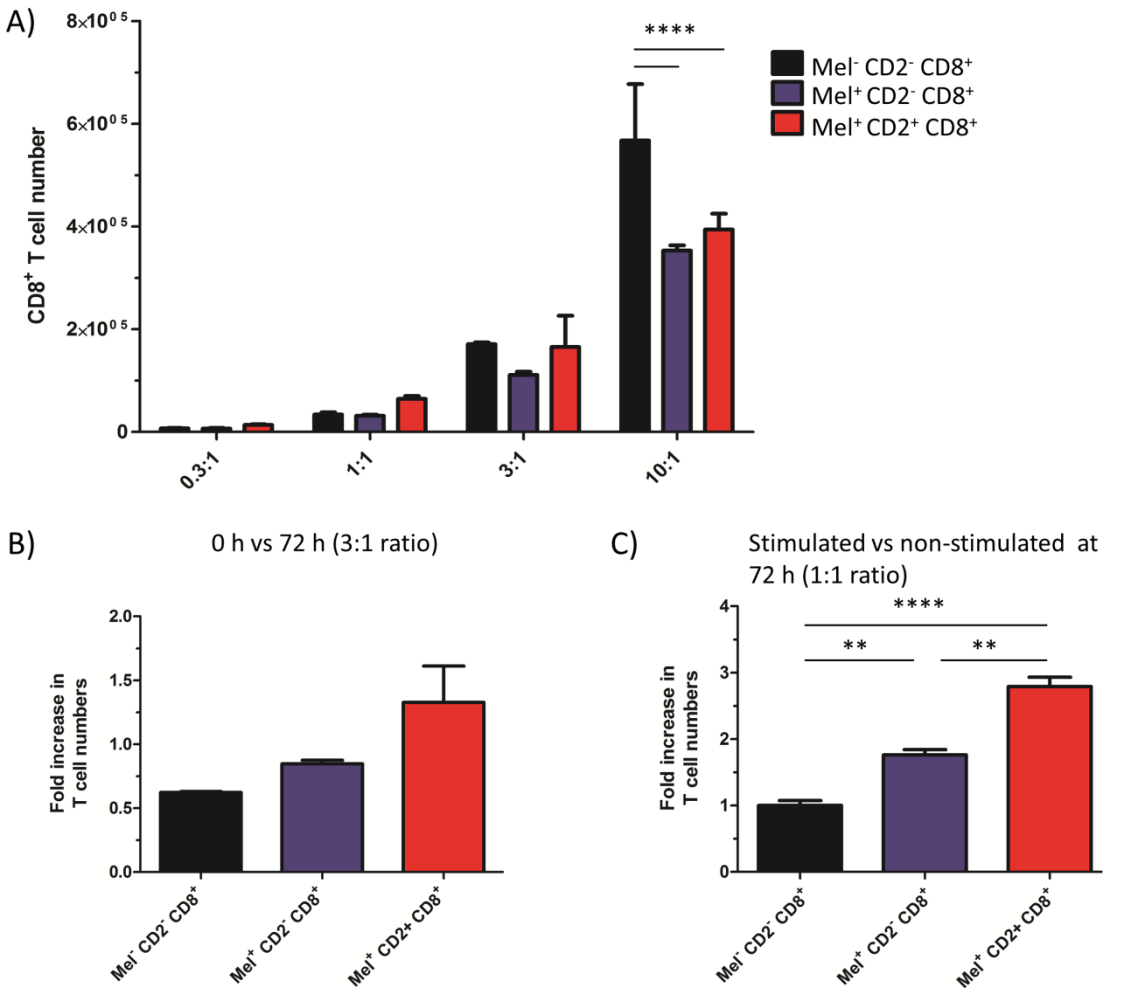

Figure 5.20: Survival and proliferation of SHP-1 sufficient and mutant SHP-1 Mel$^+$ T cells during a cytotoxicity assay. A) At the end of the 72 h cytotoxicity assay shown in figure 5.19, non-adherent cells were collected and the number of CD8$^+$ T cells determined using flow cytometry and cytocount beads as in figure 5.18 A. Error bars show the SEM for triplicates of each condition. B) The fold increase in live CD8$^+$ T cell numbers at 72 h over the input cell numbers at 0 h at the 3:1 ratio are shown. One cell count was obtained for the input cells and triplicate counts were at 72 h. Error bars show the SEM. C) The fold increase in live CD8$^+$ T cell numbers of Mel526 stimulated over non-stimulated (no Mel526) T cells is shown at the 1:1 ratio. Error bars show the SEM. Asterisks indicate statistically significant differences with **p<0.01 and ****p<0.0001.

5.3.4 Repeat of Mel526 cytotoxicity assay using SHP-1 sufficient and mutant SHP-1 Mel^+ $CD8^+$ T cells

To test the reproducibility of the above findings, the experiment was repeated by comparing the killing of Mel526 cells by SHP-1 sufficient and mutant SHP-1 Mel^+ $CD8^+$ T cells. The 'Mel^- $CD2^-$', 'Mel^+ $CD2^-$' and 'Mel^+ $CD2^+$' $CD8^+$ T cells used here were generated during an independent LV transduction, FACS sort and stimulation experiment. It was shown that 7.2% of the mutant SHP-1 Mel^+ $CD8^+$ T cells contained mutant SHP-1 genes (figure 5.14 B). Input cell numbers were checked by flow cytometry and the numbers of live $CD8^+$ Mel^+ SHP-1 sufficient and mutant SHP-1 cells added were similar, whereas approximately 9x fewer control cells were added (figure 5.22 A).

As shown with the previous Mel526 killing experiment, the SHP-1 sufficient and mutant SHP-1 Mel^+ cells demonstrated no differences in killing at the low 0.3:1 T cell ratio after 24 h (figure 5.21). However, at the 1:1 ratio, the mutant SHP-1 Mel^+ cells were less potent at killing target cells than their SHP-1 sufficient counterparts. The control Mel^- $CD2^-$ cells did not lyse Mel526 cells.

After 72 h, live $CD8^+$ T cell numbers from unstimulated T cell (T cells only) and Mel526 stimulated wells were obtained (figure 5.22 B). When looking at cell numbers in A and B, it is notable that the mutant SHP-1 Mel^+ cells survive better than the SHP-1 sufficient Mel^+ cells. Additionally, the fold increase in cell numbers of the 'stimulated over the unstimulated' cells showed that at the 0.3:1 ratio, the mutant SHP-1 Mel^+ cells proliferated about three times more compared to the other two groups (figure 5.22 C). However, at the 1:1 ratio, there is no significant difference between the Mel^+ SHP-1 sufficient and mutant SHP-1 cells. When data from the previous experiment and this experiment are combined, significant differences are seen (figure 5.22 D), supporting that the mutant SHP-1 Mel^+ T cells survive and/or proliferate better than their SHP-1 sufficient counterparts.

In summary, mutant SHP-1 Mel$^+$ cells show less target cell killing within 72 h than the SHP-1 sufficient Mel$^+$ cell although there are higher numbers of mutant SHP-1 cells surviving. There are at least two possible explanations for this. Firstly, the mutant SHP-1 cells are slower at killing but proliferate more or secondly the SHP-1 sufficient cells kill quickly and die after having lysed all the targets.

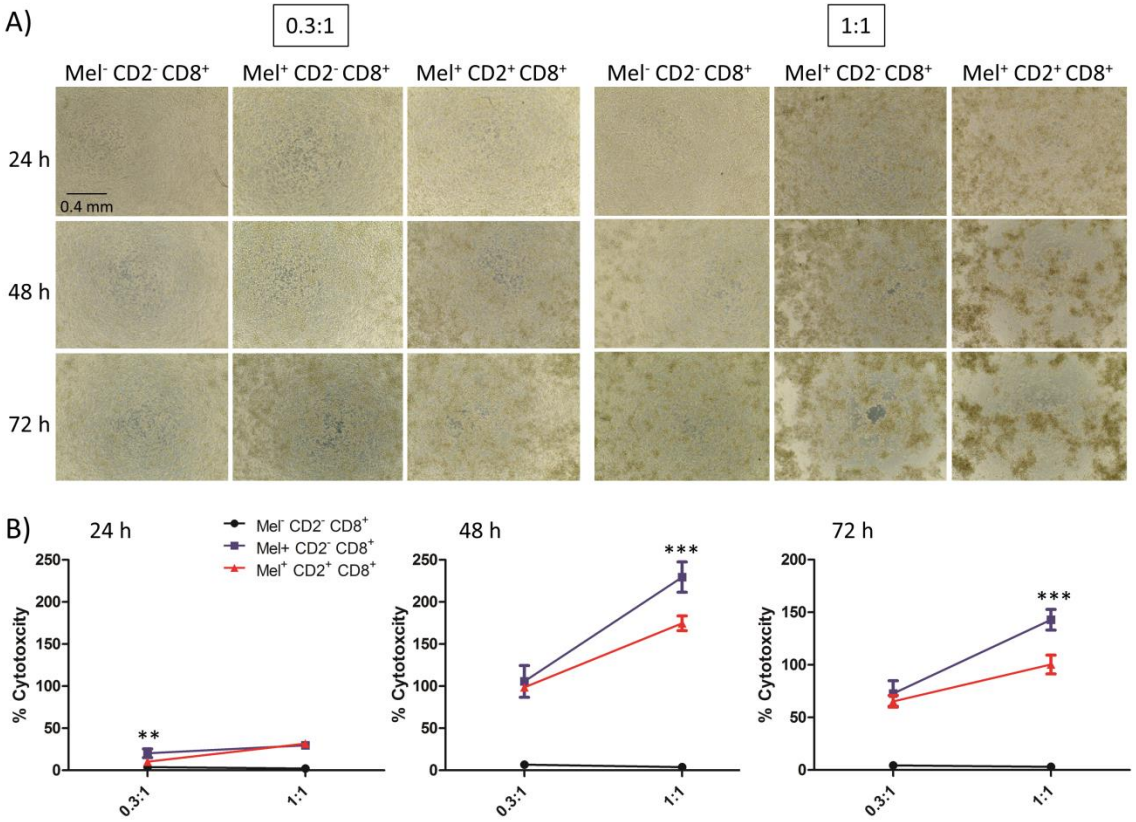

Figure 5.21: Mel526 tumour cell killing by SHP-1 sufficient and mutant SHP-1 Mel$^+$ CD8$^+$ T cells. RFP-GLuciferase sorted Mel526 cells were grown to confluency before either control Mel$^-$ CD2$^-$, Mel$^+$ CD2$^-$ or Mel$^+$ CD2$^+$ CD8$^+$ T cells were added at different ratios and cells co-incubated for 72 h. A) Representative wells coated with RFP-GLuciferase Mel526 and incubated with 'Mel$^-$ CD2$^-$', 'Mel$^+$ CD2$^-$' or 'Mel$^+$ CD2$^+$' CD8$^+$ T cell at either 0.3:1 or 1:1 T:Mel526 ratios were photographed at three different times (10x magnification). B) GLuciferase, released by lysed RFP-GLuciferase Mel526, was measured for 'Mel$^-$ CD2$^-$' (black), 'Mel$^+$ CD2$^-$' (blue) and 'Mel$^+$ CD2$^+$' (red) CD8$^+$ T cell. GLuciferase released into the supernatant was expressed as a % of total GLuciferase in RFP-GLuciferase Mel526 cell only wells. Data shown is one experiment with triplicates for each condition and error bars indicate the SEM. Asterisks show statistically significant differences between the SHP-1 sufficient and mutant SHP-1 Mel$^+$ T cells with **p<0.01 and ***p<0.001.

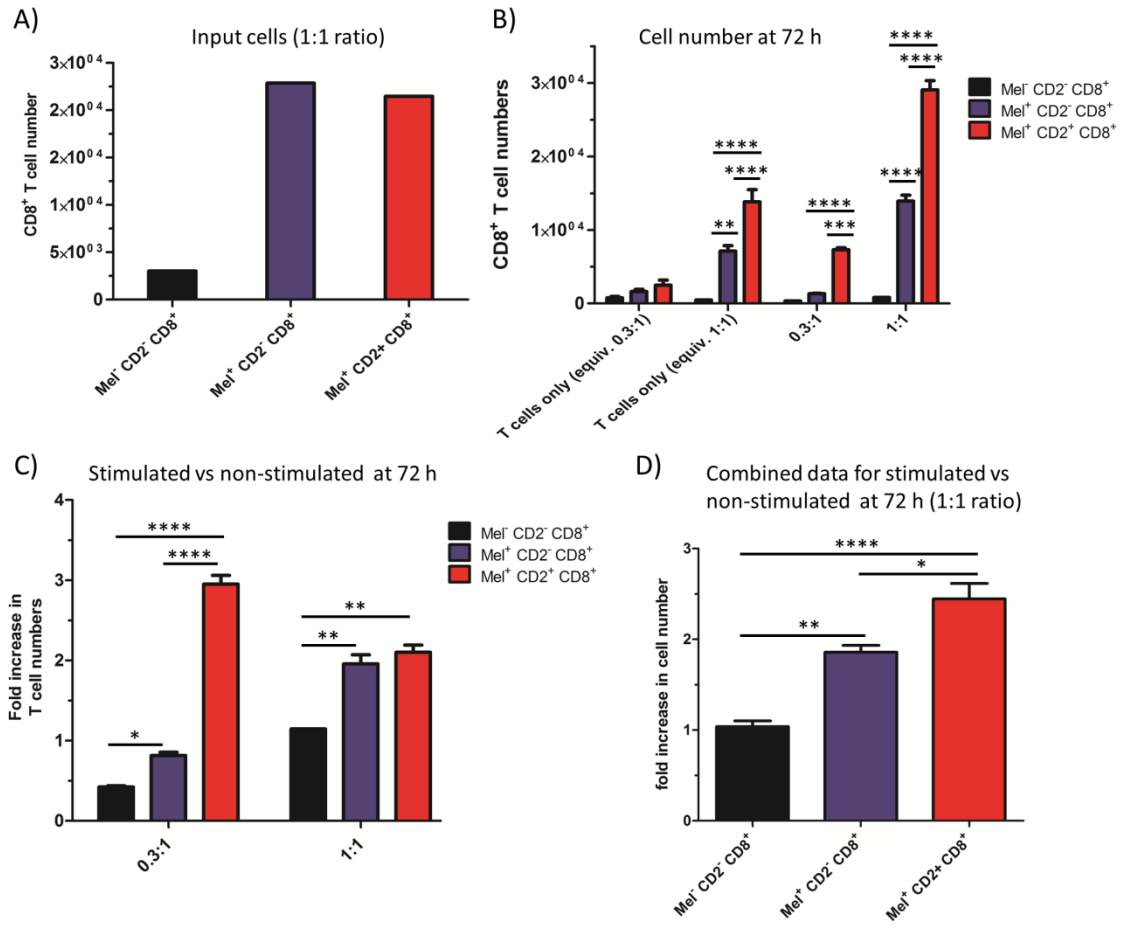

Figure 5.22: Survival and proliferation of SHP-1 sufficient and mutant SHP-1 Mel$^+$ T cells during a cytotoxicity assay. A) Flow cytometry analysis of the 1:1 T:Mel526 cell ratio was used to extract T cell numbers for each group using cytocount beads. Cells were gated on FSC/SSC, live/dead stain, single cells and CD8$^+$. B) At the end of the 72 h cytotoxicity assay, non-adherent cells were collected and the number of CD8$^+$ T cells determined using flow cytometry and cytocount beads. Triplicates are shown for all but the 1:1 'Mel$^-$ CD2$^-$' T cells only, where only one value was obtained. Error bars show the SEM. C) The fold increase in live CD8$^+$ T cell numbers of Mel526 stimulated over non-stimulated (no Mel526) T cells is shown at the 0.3:1 and the 1:1 ratio triplicates are shown for all but the 1:1 'Mel$^-$ CD2$^-$' T cells only, where only one value was obtained. D) Combined data of the fold increase of stimulated over unstimulated T cells at a 1:1 ratio of the two killing experiments in figure 5.20 C and 5.21 B. Error bars show the SEM. Asterisks indicate statistically significant differences with *p<0.05, **p<0.01 and ****p<0.0001.

5.4 Conclusion

It was shown that LV delivery of both the ZFNs and the Mel TCR can be achieved in primary $CD8^+$ T cells, albeit with significantly lower transduction efficiencies than those observed in leukaemic T cells. Ideally it would be possible to sort for cells lacking SHP-1 protein, but as SHP-1 is an intracellular protein this is not possible. Hence, multiple transduction optimisation steps, as well as MACS or FACS sorting of transduced cells was necessary to obtain a maximal Cel-I signal of 7.2%. This could probably be enhanced by including a selection marker into the ZFN1 expressing transgene cassette as it possible that the low frequency of mutations observed is due to the absence of ZFN1 in a majority of cells. Here it was shown that the SHP-1 specific ZFNs only induce targeted mutations when heterodimerised, as expression of ZFN1 or ZFN2 alone did not induce detectable mutations.

There are multiple reasons why the consecutive, and to a lesser degree the simultaneous, LV transductions were inefficient. For the consecutive transduction it is possible that the exposure of the cells to LV induces an antiviral response (IFN-α/β) and this leads to the upregulation of restriction factors (Evans et al. 2014). Another hypothesis is that LVs compete for the transduction of the cells due to the limited amount of available proteins involved in the integration and transcription of transgenes in a single cell.

Mel526 target cell killing by wt, Mel^+ or SHP-1 mutant Mel^+ T cells was evaluated using a luciferase release assay. This killing assay is advantageous to conventional chromium release assays as it is a non-radioactive, direct measure of luciferase release which is proportional to the number of lysed Mel526 cells. It was shown that the Mel^+ $CD8^+$ T cells containing up to 7.2% of SHP-1 mutants did not kill target cells better than the SHP-1 sufficient Mel^+ $CD8^+$ T cells. However, the SHP-1 mutant Mel^+ $CD8^+$ T cell population did show significantly higher cell numbers at the end of the experiment indicating possible enhanced survival or proliferation of these cells. These findings would be in line with previous reports showing no difference in *in*

vitro cytotoxic killing of SHP-1 deficient cells but an enhanced entrance into proliferation (Sathish et al. 2007). It is important to remember that in the mouse studies, pure populations of SHP-1 deficient T cells were used and the functional effect of SHP-1 loss in the cells in this chapter might be masked by the large number of SHP-1 sufficient T cells still present. Ideally, if time had allowed, a pool of SHP-1 deficient clones would have been generated and cytotoxicity, proliferation and survival would have been studied in comparison to a pool of SHP-1 sufficient $CD8^+$ T cells.

Chapter 6: L-selectin shedding in human T cells

6.1 Introduction

L-selectin is a critical protein in the first steps of the leucocyte adhesion cascade, namely those of tethering and rolling. In T cells, it plays a crucial role in the homing of T cells to LNs via HEVs and furthermore has been shown to be shed from T cells during the tethering and rolling on HEVs (Faveeuw et al. 2001). Here it is hypothesised that prolonging L-selectin expression on activated tumour-specific T cells could enhance their potential for cancer therapy by enabling their recirculation to LNs for further activation and survival and/or allowing their recruitment to tumours expressing HEVs or L-selectin ligands on tumour blood vessels. It has previously been shown that many tumours express HEV like structures and that these are associated with enhanced numbers of B and T cell infiltrates in tumours (Martinet et al. 2011).

L-selectin downregulation is controlled on multiple levels such as transcriptional silencing (Chao et al. 1997) or ectodomain proteolytic shedding from the cell surface both in humans and in mice (figure 6.1 A and C) (Chen et al. 1995; Zhao et al. 2001). By expressing L-selectin under a heterologous SFFV promoter in T cells, transcriptional silencing was overcome. The second level of regulation, namely shedding of the ectodomain, was overcome by expressing a shedding-resistant form of L-selectin in T cells. The ΔM-N mutant has a truncation of 8 aa in the membrane proximal region rendering it resistant to proteolytic attack by ADAMs (figure 6.1 B).

Additionally, an *in vitro* endothelial flow assay was used to determine the impact of L-selectin expression on the rolling and transmigration of MOLT-3 leukaemic cells expressing either wt or ΔM-N L-selectin. This assay was done to determine whether lentivirally delivered L-selectin was functional and to study the impact of shedding on the recruitment of T cells on cytokine activated endothelium.

All primers used in this chapter, for cloning or sequencing are listed in the appendix (tables A3) as are the sequences of all lentiviral transfer plasmids (A2).

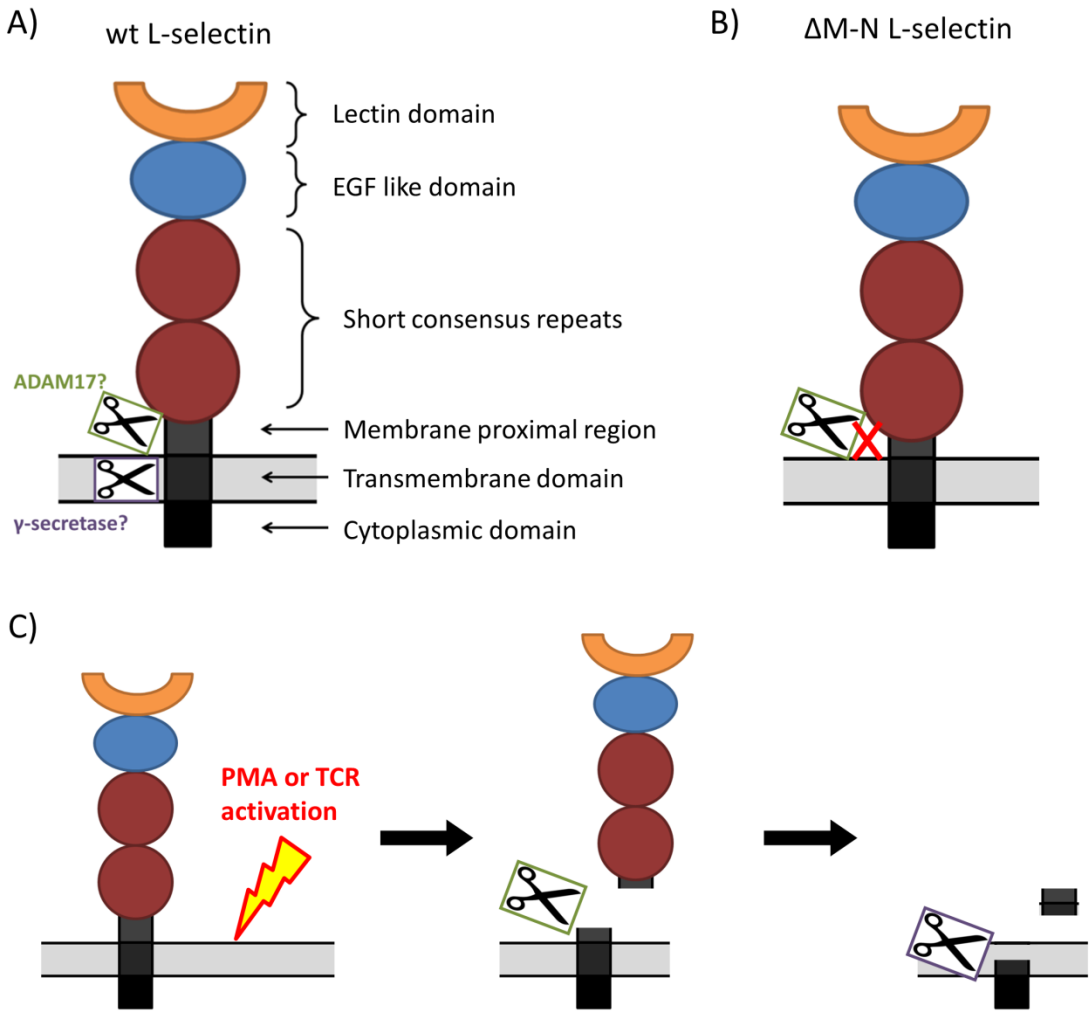

Figure 6.1: L-selectin and the possible enzymes involved in its proteolysis upon activation of T cells. A) L-selectin is a type I transmembrane protein encompassing multiple domains; the lectin domain at the N terminus, an epidermal growth factor domain (EGF), two short consensus repeats, a membrane proximal region (MPR), a transmembrane domain and a cytoplasmic tail. ADAM17 (green scissor) and γ-secretase (purple scissor) are two enzymes hypothesised to be involved in the shedding and further processing of L-selectin. B) The ΔM-N mutant form of L-selectin gene has a truncation of eight amino acids in the MPR, thereby inhibiting proteolysis (red X). C) In this chapter the proteolysis of L-selectin following stimulation with PMA or activation of the TCR (left) was studied to determine the enzymes involved in the initial shedding event. The ectodomain of L-selectin is shed first possibly by ADAM17 (middle), followed by a second proteolytic step targeting the membrane retained fragment possibly orchestrated by the γ-secretase complex (right).

6.2 Generation of lentiviral transfer plasmids expressing wt, ΔM-N or I-K L-selectin

6.2.1 Generation of pLenti-L-selectin wt or ΔM-N

To study the effect of shedding-resistant L-selectin expression on human T cells, gag^+ MOLT-3 L-selectin negative T cells were transduced with LV encoding wt or shedding-resistant ΔM-N L-selectin. The two LV transfer vectors were generated as shown in figure 6.2 and all primers used can be found in table A3.

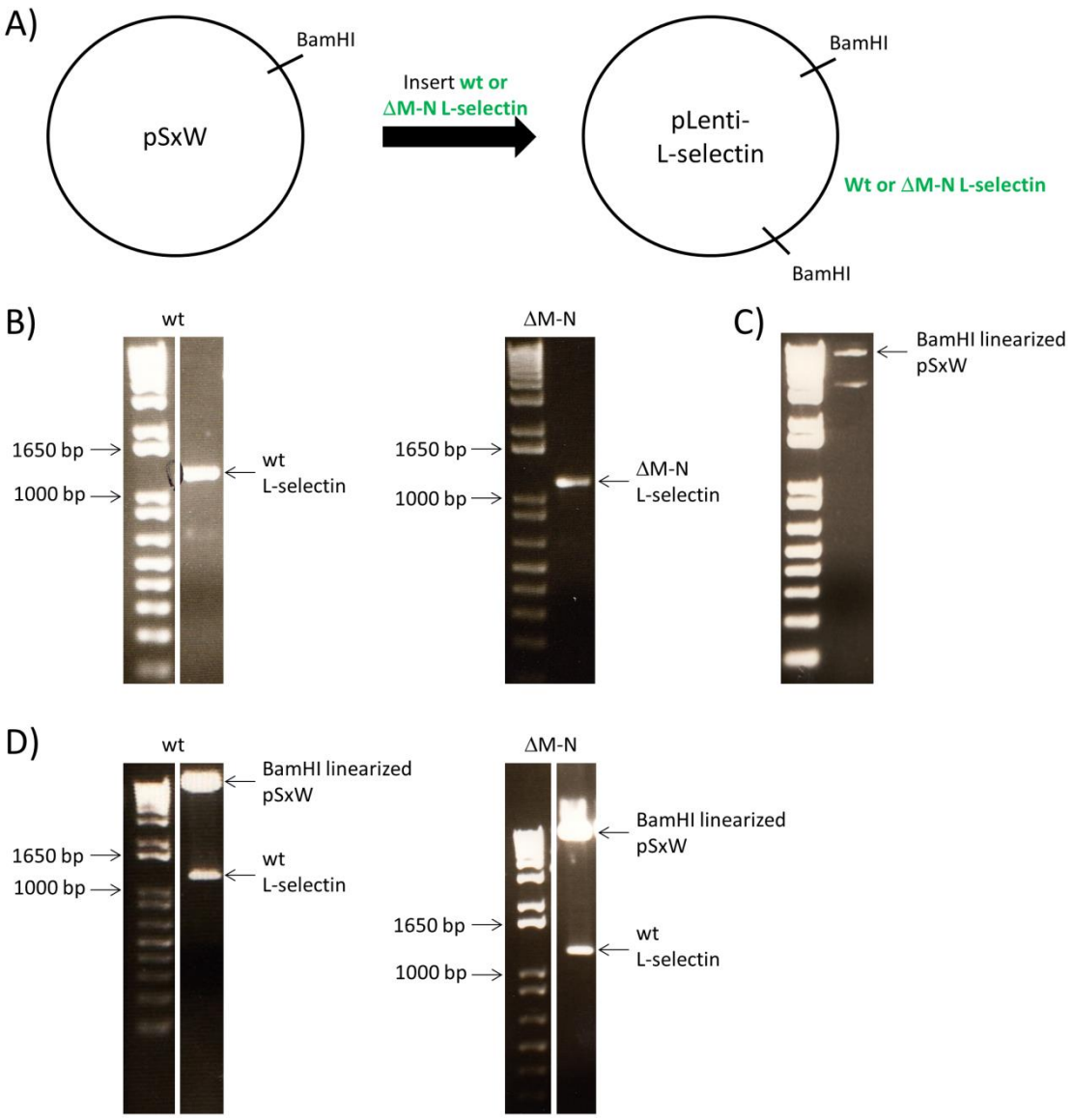

Figure 6.2: Cloning of the lentiviral transfer vector pLenti-L-selectin wt or ΔM-N. A) A single In-Fusion step was needed to clone either the wt or ΔM-N L-selectin (in green) into the BamHI linearised pSxW vector. B) Both gels show the 1kb plus DNA ladder in lanes 1. Lanes 2 show the PCR product of 1184 bp wt L-selectin (left) or 1160 bp ΔM-N L-selectin (right) using primers number 45 and 46. The wt plasmid was provided by Dr Aleksander Ivetic and the ΔM-N plasmid was provided by Prof. Tom Tedder. Primer number 45 introduces a Kozak consensus sequence (GCCGCCACC) upstream of the L-selectin start codon and primer 46 introduces a stop codon (TAA) downstream of the L-selectin sequence. C) Lanes 2 shows the BamHI restriction digest of the pSxW plasmid. The linearised 8942 bp pSxW vector was purified and used together with the purified PCR products in A) to set up In-Fusion reactions. DH5α cells were transformed with 2 µl of In-Fusion mix. D) Lanes 2 show plasmid DNA extracted from Ampicillin selected DH5α colonies transformed as described above and digested with BamHI. The lower size band corresponds to the 1173 bp wt L-selectin (left) or 1149 bp ΔM-N L-selectin (right) and the upper band to the 8942 bp pSxW. The plasmids were sequenced using primers 33-34 and 38-41 and confirmed to be the pLenti-L-selectin wt or ΔM-N sequence.

6.2.2 Generation of pLenti-CD2-L-selectin wt or ΔM-N

To enable the identification of L-selectin LV transduced T cells expressing endogenous L-selectin, a second set of lentiviral transfer vectors was generated to include the rat CD2 (CD2) surface marker, separated from the wt or ΔM-N L-selectin gene by the P2A ribosomal skipping element (figures 6.3). The CD2 gene was placed upstream of the L-selectin gene as the P2A ribosomal skipping element leaves a 24 amino acid tail attached to the upstream protein, potentially more than doubling the 17 amino acid long cytoplasmic tail of L-selectin. Figures 6.4-6.6 show the three In-Fusion cloning steps required to generate the pLenti-CD2-L-selectin wt and ΔM-N plasmids.

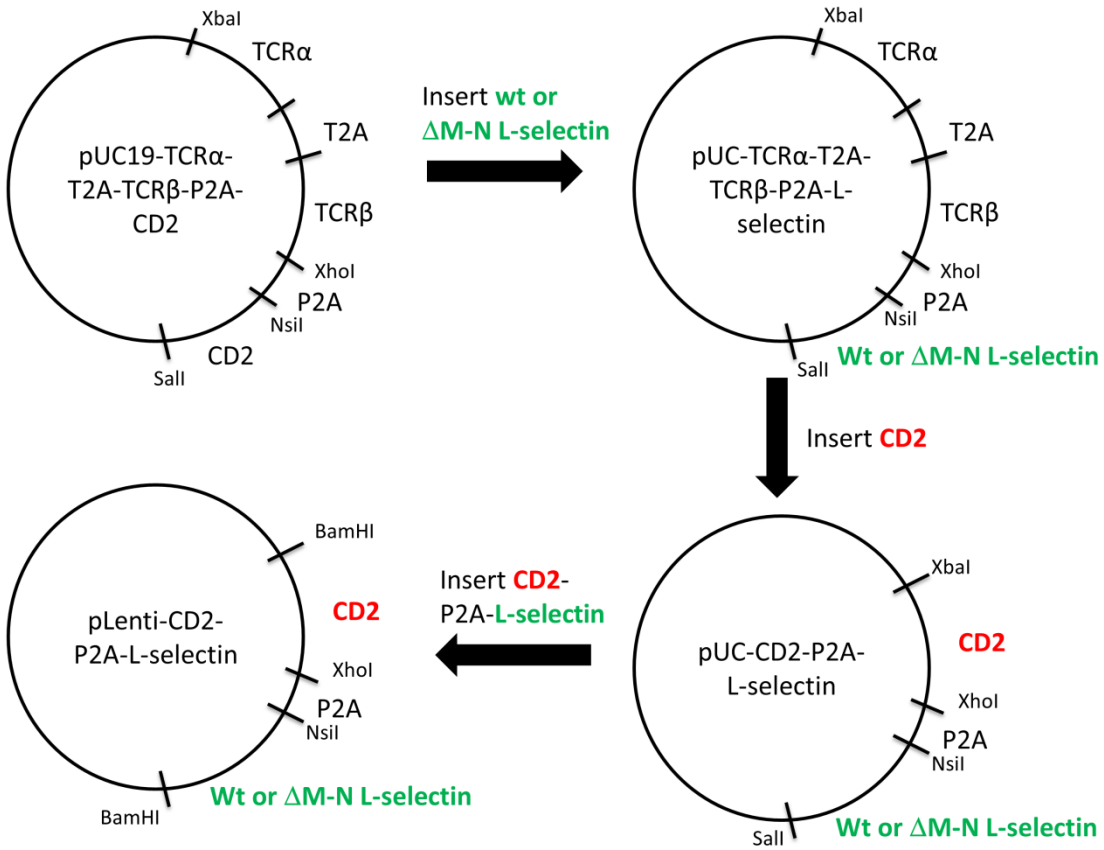

Figure 6.3: Cloning strategy to generate the lentiviral transfer vectors pLenti-CD2-L-selectin wt or ΔM-N. A NsiI and SalI restriction digest of the pUC19-TCRα-P2A-TCRβ-P2A-CD2 plasmid was used to replace the CD2 gene with the L-selectin wt or ΔM-N gene (green) downstream of the P2A sequence. In order to insert the CD2 gene (red) upstream of L-selectin, an XbaI and XhoI restriction digestion was done to replace the TCRα-T2A-TCRβ fragment with the CD2 gene. Finally the CD2-P2A-L-selectin wt or ΔM-N cassette was inserted into the lentiviral transfer vector pSxW giving the pLenti-CD2-L-selectin wt or ΔM-N plasmids.

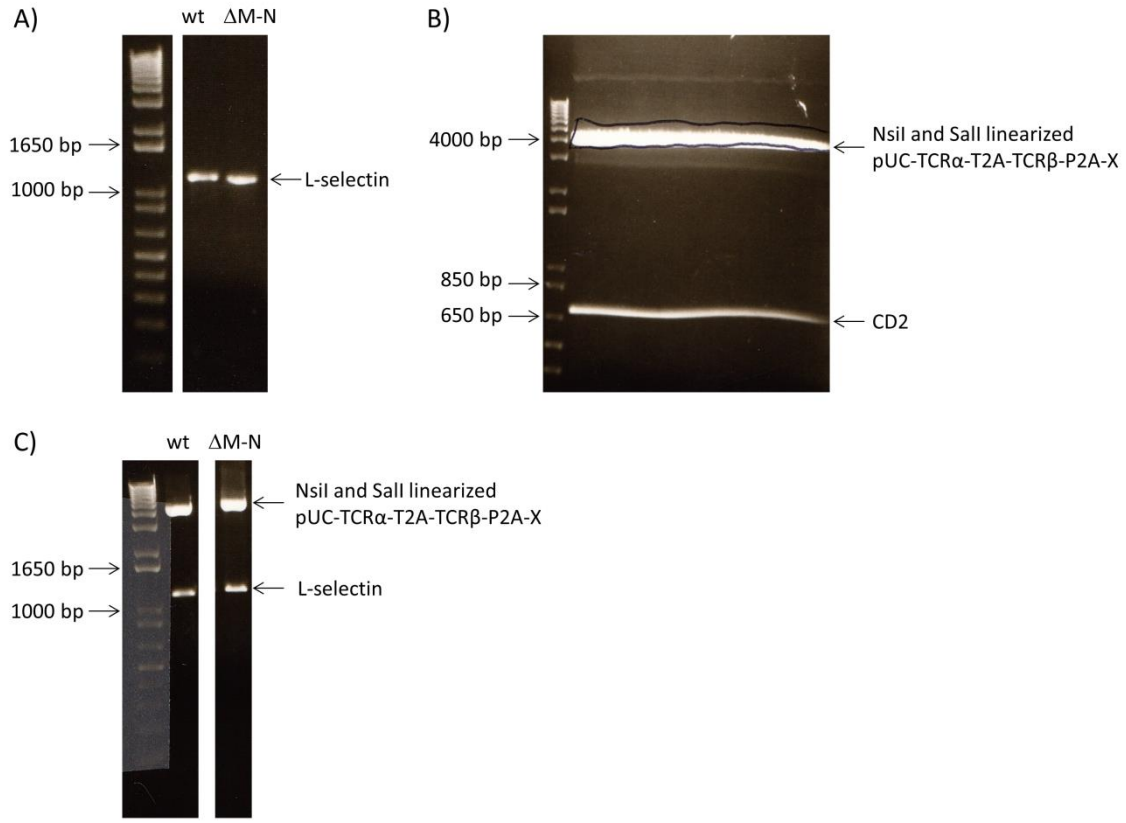

Figure 6.4: Cloning of wt or ΔM-N L-selectin into the pUC-TCRα-T2A-TCRβ-P2A-X vector. A) Lane 1 shows the 1kb plus DNA ladder. The 1184 bp wt and the 1160 bp ΔM-N L-selectin PCR products shown in lane 2 and 3 respectively were obtained using primers 47 and 48. Primer 48 introduced a TAA stop codon downstream of the L-selectin cDNA. B) Lane 2 shows the NsiI and SalI restriction digest of the pUC-TCRα-T2A-TCRβ-P2A-CD2 plasmid (plasmid provided by Dr. John Bridgeman). The linearised 4236 bp pUC-TCRα-T2A-TCRβ-P2A-X vector was purified and used together with the purified PCR products in A) to set up In-Fusion reactions. DH5α cells were transformed with 2 µl of In-Fusion mix. C) Lanes 2 and 3 show plasmid DNA extracted from Kanamycin selected DH5α colonies, transformed as described above and digested with NsiI and SalI. The lower size DNA bands in lanes 2 and 3 correspond to the 1160 bp wt and the 1136 bp ΔM-N L-selectin genes. The upper band corresponds to the linearised 4236 bp pUC-TCRα-T2A-TCRβ-P2A-X plasmid. The plasmids were sequenced using primers 37-42 and confirmed to be the pUC-TCRα-T2A-TCRβ-P2A-L-selectin wt or ΔM-N sequences.

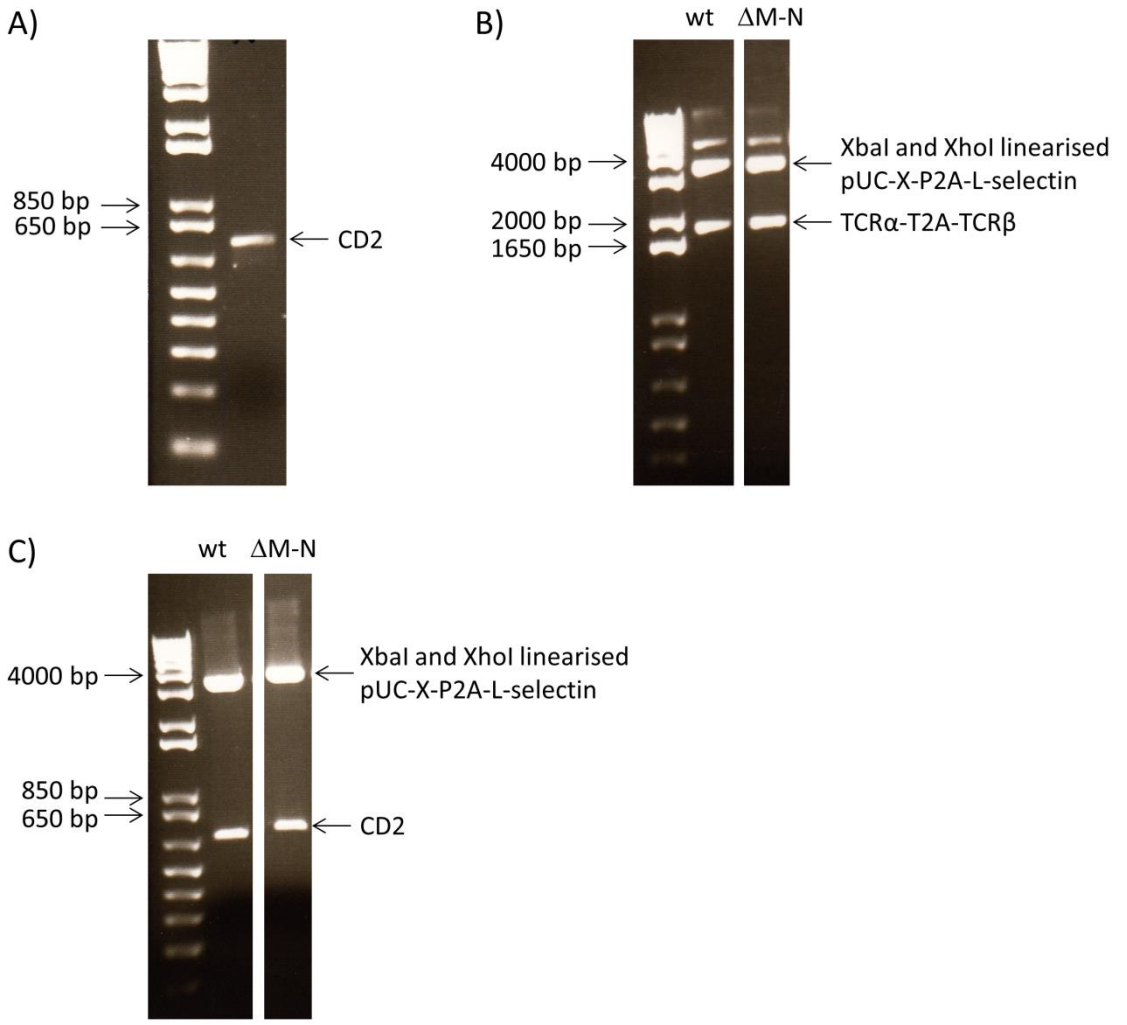

Figure 6.5: Cloning of CD2 into the pUC-X-P2A-L-selectin wt or ΔM-N vector. A) Lane 1 shows the 1kb plus DNA ladder. Lane 2 shows the 740 bp CD2 PCR reaction product using primers 49 and 50. Primer 49 introduces a Kozak (GCCGCCACC) consensus sequence upstream of the CD2 cDNA. B) Lane 2 and 3 show the XbaI and XhoI restriction digest of the pUC-TCRα-T2A-TCRβ-P2A-L-selectin wt orΔM-N plasmid. The linearised pUC-X-P2A-L-selectin wt (3552 bp) or ΔM-N (3528 bp) vector was purified and used together with the purified PCR products in A) to set up In-Fusion reactions. DH5α cells were transformed with 2 µl of In-Fusion mix. C) Lanes 2 and 3 show plasmid DNA extracted from Kanamycin selected DH5α colonies transformed as described above and digested with XbaI and XhoI. The lower size DNA bands in lanes 2 and 3 correspond to the 714 bp CD2. The upper band corresponds to the pUC-X-P2A-L-selectin wt or ΔM-N. The plasmids were sequenced using primers 4-8 and 37-42 and confirmed to be the pUC-CD2-P2A-L-selectin wt or ΔM-N sequences.

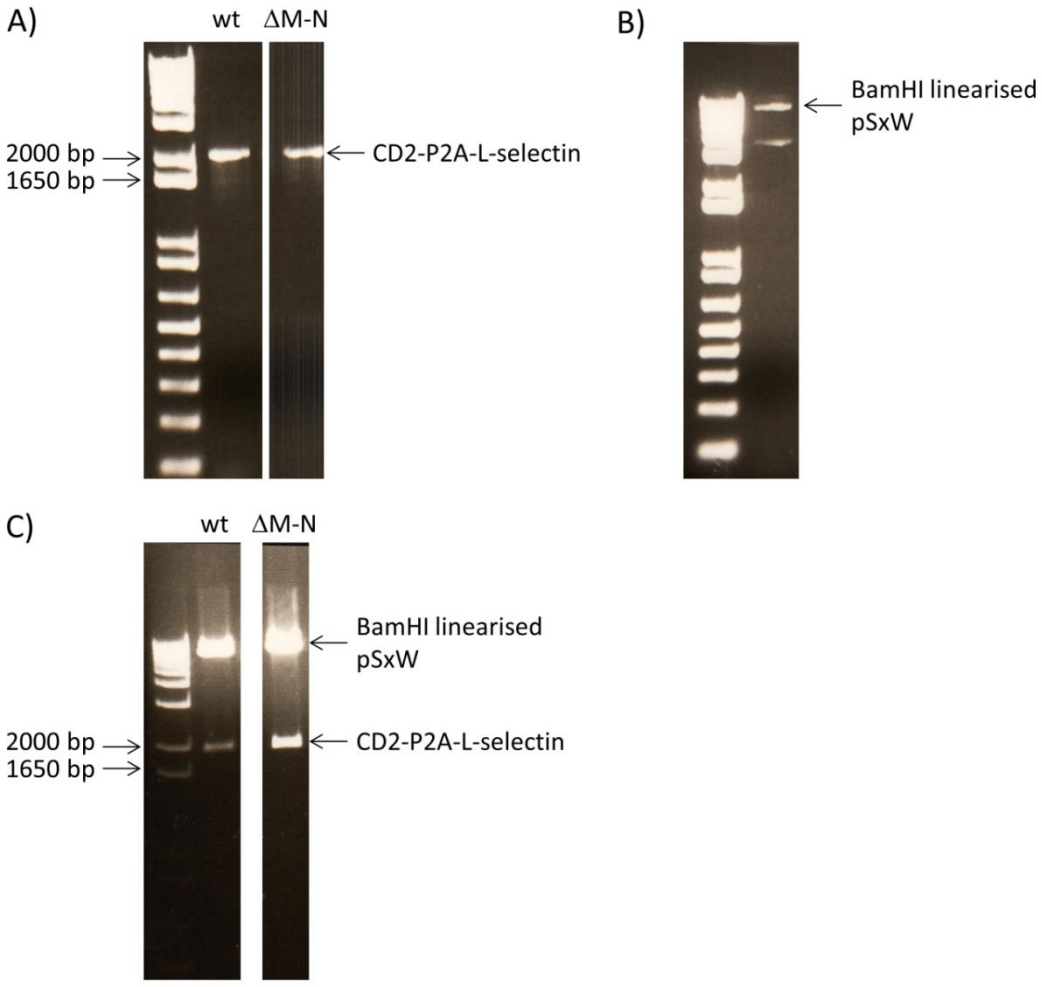

Figure 6.6: Cloning of CD2-P2A-L-selectin wt or ΔM-N into the pSxW lentiviral transfer vector. A) Lane 1 shows the 1kb plus DNA ladder. Lanes 2 and 3 show the 1979 bp and 1955 bp CD2-P2A-L-selectin wt and ΔM-N products of the PCR reaction using primers 51 and 46. B) Lane 2 shows the BamHI restriction digest of the pSxW plasmid. The linearised 8942 bp pSxW vector was purified and used together with the purified PCR products in A) to set up In-Fusion reactions. DH5α cells were transformed with 2 µl of In-Fusion mix. C) Lanes 2 and 3 show plasmid DNA extracted from Ampicillin selected DH5α colonies transformed as described above and digested with BamHI. The lower size DNA bands correspond to the 1953 bp or 1929 bp CD2-P2A-L-selectin wt or ΔM-N sequences respectively. The upper band corresponds to the 8942 bp pSxW. The plasmids were sequenced using primers 4-8, 33-34 and 38-41 and confirmed to be the pLenti-rCD2-P2A-L-selectin wt or ΔM-N sequences.

6.2.3 Generation of pLenti-I-K-L-selectin

Shedding of the L-selectin ectodomain is followed by a second cleavage within the membrane retained fragment. It was hypothesised that the γ-secretase complex orchestrates the second cleavage event. To study the effect of abrogating this cleavage, a point mutation was introduced into the transmembrane domain leading to an isoleucine to lysine change at position 352. The mutant was called I-K L-selectin. The I-K mutant was based on a publication where a similar mutation abrogated the γ-secretase cleavage of Trop2, a protein undergoing similar proteolysis to L-selectin by both ADAM17 and γ-secretase (Stoyanova et al. 2012). Site directed mutagenesis was done by a fellow PhD student, Andrew Newman, using primers 64 and 65 to change the ATT to an AAG codon (table A3). The I-K L-selectin gene was then introduced into the lentiviral transfer vector pLenti (figure 6.7).

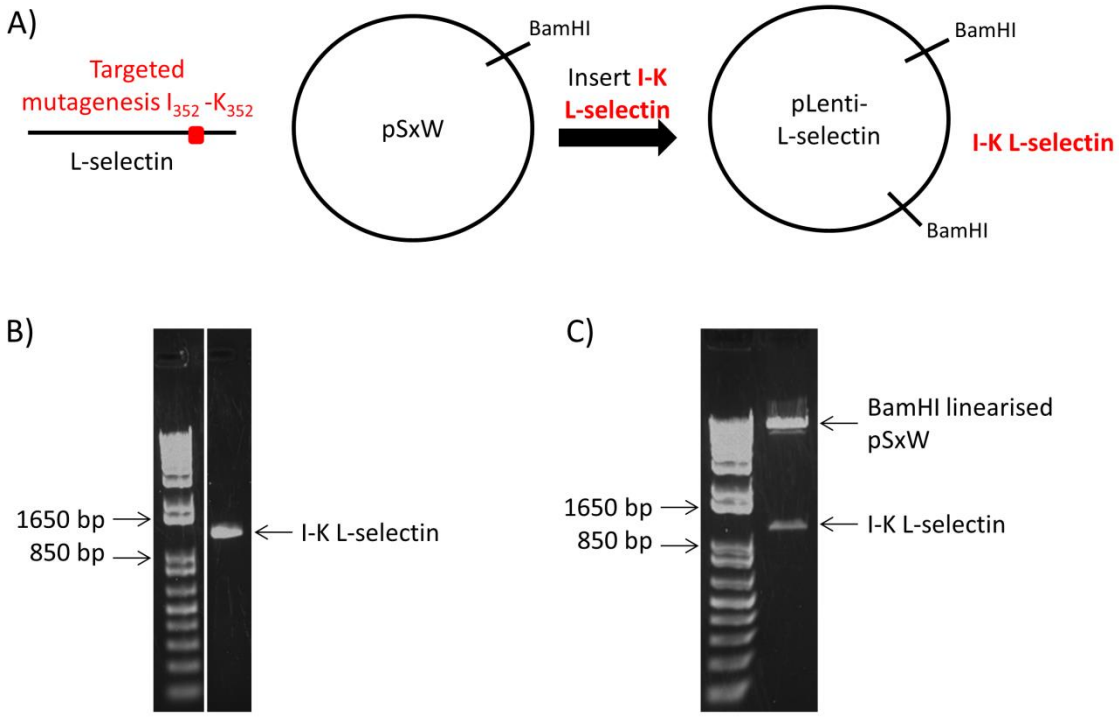

Figure 6.7: Cloning of the pLenti-L-selectin I-K. A) Targeted mutagenesis using primers 64 and 65 was performed to generate a new L-selectin mutant with a point mutation at position 352 of a lysine (K) instead of isoleucine (I). Subsequently, the L-selectin I-K gene was inserted into the BamHI linearised pSxW plasmid. B) Lane 1 shows the 1kb plus DNA ladder. Lane 2 shows the 1184 bp I-K L-selectin product of the PCR reaction using primers 45 and 46. BamHI linearised pSxW vector was purified and used together with the purified PCR product in B) to set up an In-Fusion reaction. DH5α cells were transformed with 2 µl of In-Fusion mix. C) Lane 2 show plasmid DNA extracted from Ampicillin selected DH5α colonies transformed as described above and digested with BamHI. The lower size band corresponds to the 1173 bp I-K L-selectin and the upper band to the 8942 bp pSxW. The plasmid was sequenced using primers 33-34 and 38-41 and confirmed to be the pLenti-I-K-L-selectin.

6.3 Generation of gag$^+$ MOLT-3 cells expressing wt or ΔM-N L-selectin

It was established that gag$^+$ MOLT-3 cells do not express any L-selectin protein on their cell surface, neither before nor after transduction with control CD2 LV (figure 6.8 A). This made MOLT-3 cells ideal to study the biology of L-selectin shedding, as the level of L-selectin protein present in the cells could be controlled using an exogenous promoter as well as the use of the shedding-resistant ΔM-N mutant. As a result, gag$^+$ MOLT-3 cells were transduced with a titration of 10x concentrated wt or ΔM-N L-selectin LV (figure 6.8 B-C). The highest volume of 500 μl LV gave the highest level of transduction, with the level of L-selectin expression in the ΔM-N cells higher than that in the wt L-selectin expressing cells. This might be due to constitutive L-selectin shedding in the wt but not the ΔM-N L-selectin cells.

Cells transduced with 500 μl of LV were expanded for several weeks, during which a marked decrease in expression of the transgenes was observed. To achieve equal levels of L-selectin and gag TCR surface expression, cells were sorted by flow cytometry as shown in figure 6.9 into wt and ΔM-N L-selectin high or low expressing cells with high levels of gag TCR.

Levels of L-selectin transgene expression in L-selectin^{high} gag$^+$ MOLT-3 cells was compared to cells expressing endogenous L-selectin, namely gag$^+$ Jurkat cells and primary CD8$^+$ T cells freshly isolated from blood (figure 6.10). The primary CD8$^+$ T cells showed two populations, L-selectin positive and L-selectin negative cells whereas Jurkat cells all express high levels of L-selectin. The FACS sorted L-selectin^{high} MOLT-3 cells express lower levels of L-selectin than both the Jurkat and the L-selectin expressing primary CD8$^+$ T cells.

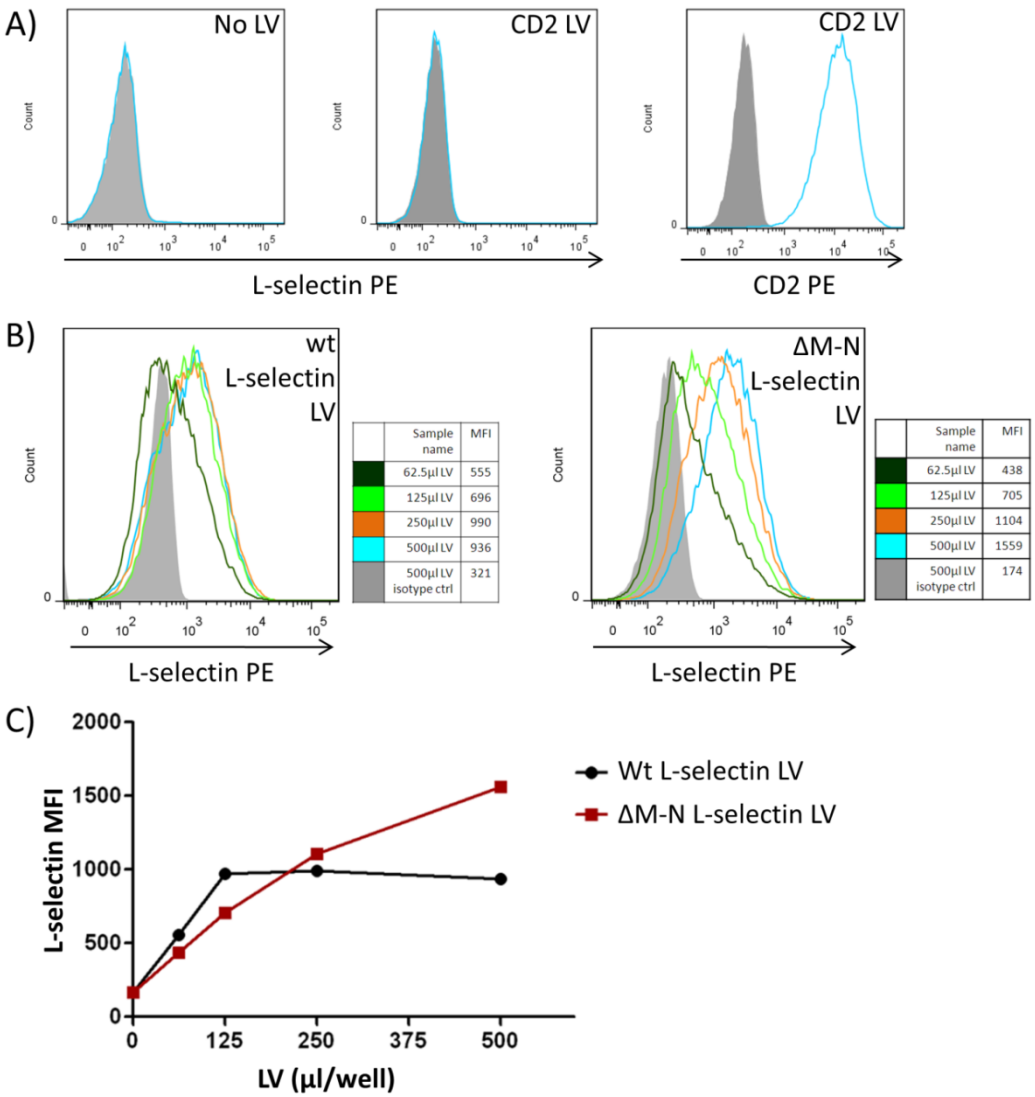

Figure 6.8: Transduction of L-selectin negative gag$^+$ MOLT-3 cells with wt or ΔM-N L-selectin LV. A) Gag$^+$ MOLT-3 cells were transduced with 250 µl CD2 LV (middle and left) and stained with anti-L-selectin Ab (blue in left and middle) or anti-CD2 Ab (blue in right). Cells were stained with PE-conjugated isotype control (grey in all). B) Gag$^+$ MOLT-3 cell were transduced with 500 µl (blue), 250 µl (orange), 125 µl (light green) and 62.5 µl (dark green) wt or ΔM-N L-selectin LV. Cells were stained with anti-L-selectin Ab or isotype control (grey filled) and analysed by flow cytometry. C) The median fluorescent intensity (MFI) is shown for cells transduced as described in B), with the wt L-selectin in black and the ΔM-N L-selectin in red.

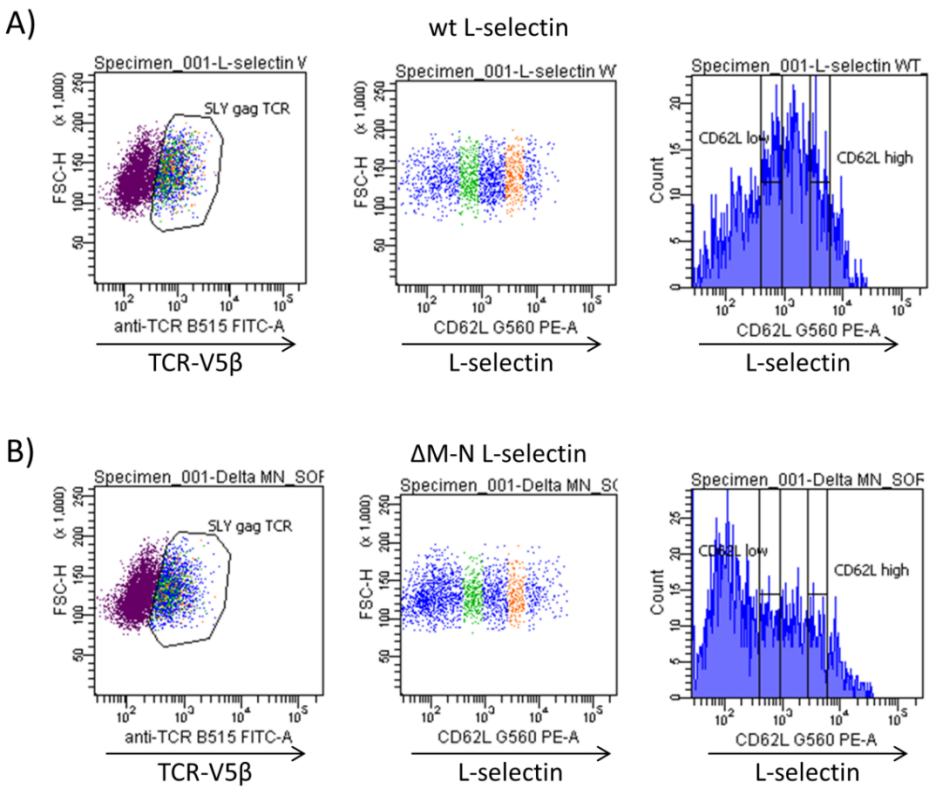

Figure 6.9: Wt or ΔM-N L-selectin LV transduced gag$^+$ MOLT-3 T cells were sorted into L-selectin^{high} and L-selectin^{low} gag$^+$ populations by FACS. Gag$^+$ MOLT-3 T cells transduced with wt (A) and ΔM-N (B) L-selectin LV were stained with anti-TCRV5β and anti-L-selectin Ab, in the presence of Dasatinib and FACS sorted. All cells were gated on FSC/SSC, a single cell gate and expression of the gag TCR. Cells were further sorted for high (orange) or low (green) L-selectin expression.

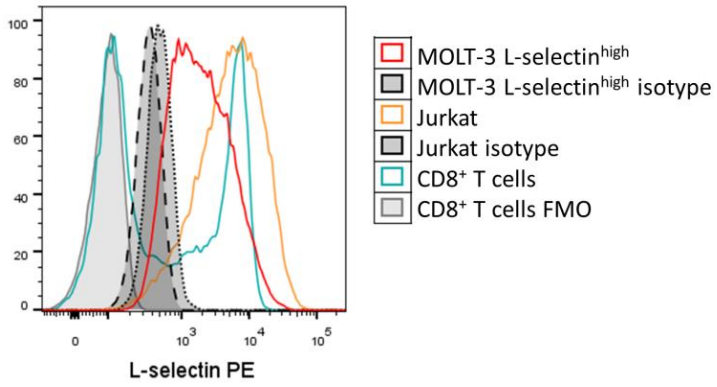

Figure 6.10: L-selectin expression of primary CD8$^+$ T cells, gag$^+$ Jurkat and gag$^+$ MOLT-3 cells. Primary CD8$^+$ T cells (turquoise), gag$^+$ Jurkat cells (orange) and FACS sorted L-selectin^{high} MOLT-3 cells (red) were stained with anti-L-selectin Ab. Jurkat cells (lined) and MOLT-3 cells (dotted) were stained with isotype control. The FMO control is shown for CD8$^+$ T cells (grey filled). PBMCs were freshly isolated from blood, stained with anti-CD8 and anti-L-selectin Ab and gated on FSC/SSC, Pacific blue live/dead and CD8$^+$. Cells were analysed on different days using the same experimental settings.

6.4 The role of ADAM17 in the shedding of L-selectin in T cells

To study the involvement of two metalloproteinases, ADAM10 and ADAM17 in the shedding of L-selectin in human T cells, gag^+ MOLT-3 leukaemic cells were activated with PMA or with cognate peptide in the presence or absence of ADAM10 or ADAM17 specific inhibitors. PMA induced L-selectin shedding has been extensively studied previously (Jung and Dailey 1990; Peschon et al. 1998) and is used here to confirm that lentivirally expressed L-selectin protein behaves in the same manner. Subsequently, gag^+ MOLT-3 cells were activated with cognate peptide pulsed APCs and L-selectin shedding studied.

6.4.1 PMA induced L-selectin shedding and the role of ADAM17

To establish the optimal conditions for PMA induced L-selectin shedding, L-$selectin^{high}$ or L-$selectin^{low}$ wt or ΔM-N gag^+ MOLT-3 cells were activated with a titration of PMA (3-1000 nM) and 300 nM was established as the ideal dose of PMA to induce maximal shedding of 50-60%, without being toxic to the cells (figure 6.11 A-B). As expected, no shedding was observed in the ΔM-N^{high} or ΔM-N^{low} cells. The slight decrease in L-selectin levels at high PMA doses was most likely due to the cells not having been fixed and being analysed last, leading to a certain level of endocytosis of the Ab. To establish the optimal time to incubate cells with PMA, L-$selectin^{high}$ expressing cells were incubated for 1-60 min with the 300 nM PMA and 30 min was established as the ideal duration of PMA exposure as shedding plateaued after this time point (figure 6.11 C).

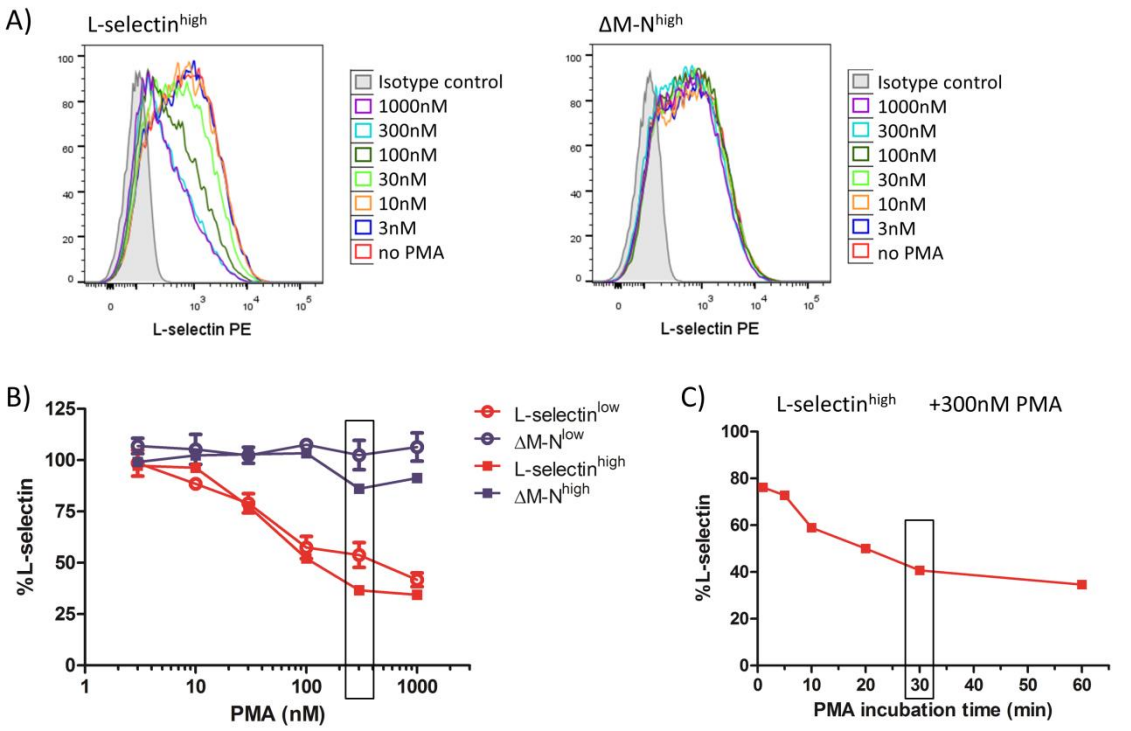

Figure 6.11: Titration and time course of PMA induced L-selectin shedding in gag$^+$ MOLT-3 T cells. FACS sorted L-selectin^{high} or L-selectin^{low} wt or ΔM-N gag$^+$ MOLT-3 were incubated with 0-1000 nM of PMA and L-selectin surface expression analysed by flow cytometry. A) Flow cytometry histograms for L-selectin^{high} wt (left) or ΔM-N (right) gag$^+$ MOLT-3 cells incubated with 3-1000 nM of PMA. B) L-selectin^{high} or L-selectin^{low} wt or ΔM-N gag$^+$ MOLT-3 were incubated for 30 min with 3-1000 nM PMA and the percentage of L-selectin was obtained by subtracting the MFI of the isotype from the MFI of each sample and it was normalised to untreated cells, representing 100% L-selectin. Results show single observations for L-selectin^{low} cells and means from two experiments with single wells for L-selectin^{high} cells. The black box indicates the 300 nM PMA concentration chosen for further experiments. C) Wt L-selectin^{high} MOLT-3 cells were incubated for 1, 5, 10, 20, 30 and 60 min with 300 nM PMA. Each condition was done in single wells. The black box indicates the 30 min incubation period chosen for further PMA induced L-selectin shedding experiments.

Next, L-selectin^{high} wt or ΔM-N MOLT-3 cells were incubated with two metalloproteinase inhibitors, GW and GI, and activated with 300 nM PMA. GW was shown to preferentially inhibit ADAM17 whereas GI is thought to be 100 times more potent at inhibiting ADAM10 than ADAM17 (Hundhausen et al. 2003). Thus both inhibitors are not exclusively inhibitory to one or the other ADAMs. It was shown that 10 μM of GW is sufficient to completely inhibit PMA induced L-selectin shedding whereas GI only inhibited L-selectin shedding by a maximum of 20% at 30 μM (figures 6.12 B and 6.13 B). Additionally, GW also inhibits constitutive L-selectin shedding as levels increased above that of untreated cells for 3 μM or above of GW. No shedding was observed in ΔM-N^{high} L-selectin gag^{+} MOLT-3 cells and neither GW nor GI altered L-selectin levels.

The above results and previous publications (Peschon et al. 1998) indicate that ADAM17 is the main protease involved in PMA induced L-selectin shedding. To confirm this finding, we tested whether the ADAM17 specific cross-domain blocking Ab, D1(A12) (Tape et al. 2011), inhibits PMA induced L-selectin shedding. As shown in figure 6.14 B, complete inhibition of shedding was achieved with 300 nM of the ADAM17 blocking Ab. The control Ab did not inhibit L-selectin shedding.

Overall these results show that PMA induced shedding of L-selectin in the MOLT-3 T cell line is driven by ADAM17 and that ADAM17 also has a role in constitutive L-selectin cleavage.

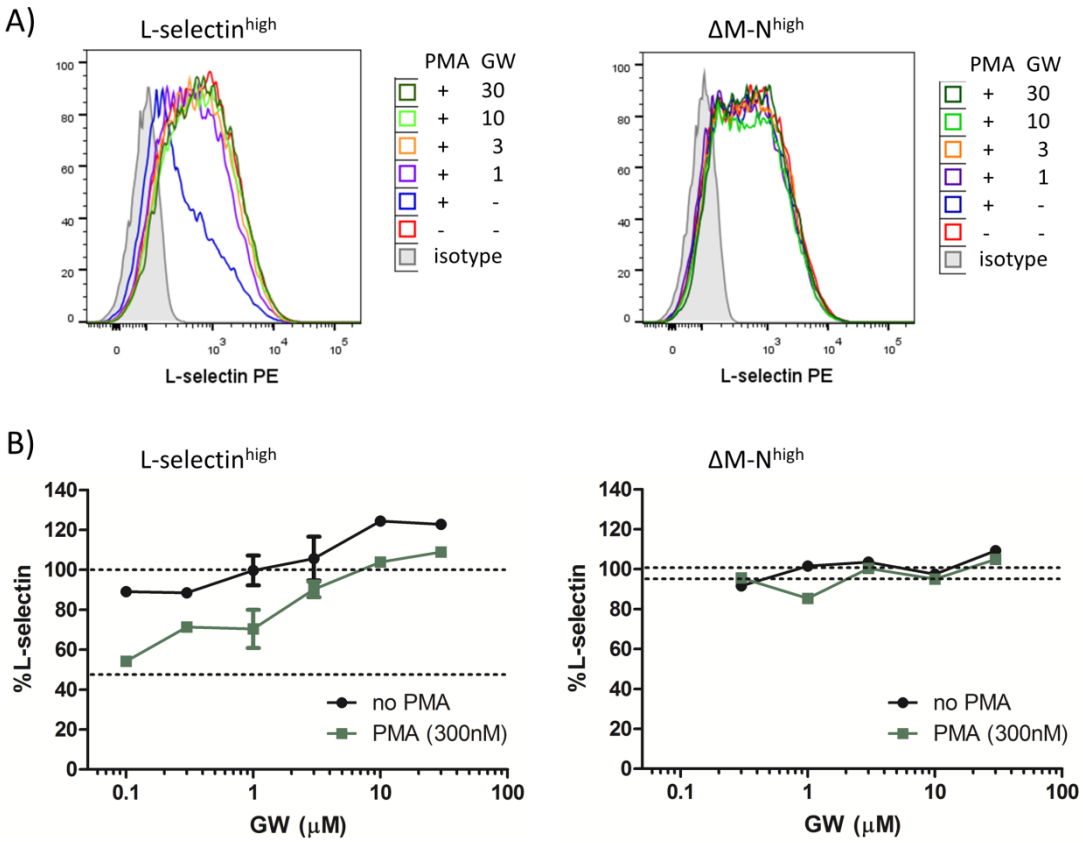

Figure 6.12: Effect of metalloproteinase inhibitors, GW, on PMA induced shedding. L-selectin^{high} wt (left) or ΔM-N (right) gag^{+} MOLT-3 cells were incubated for an h with 0.1-30 µM of the metalloproteinase inhibitor GW before activation with 300 nM PMA for 30 min and analysed of the cells by flow cytometry. A) Flow cytometry histograms showing representative samples incubated with 1-30 µM GW and activated with PMA. B) The percentage of L-selectin was obtained by subtracting the MFI of the isotype from the MFI of each sample and normalising it to the untreated cells, representing 100% L-selectin. Results for single wells are shown for the wt L-selectin^{high} cells at 0.1, 0.3, 10 and 30 µM GW and for all ΔM-N L-selectin^{high} cells. The wt L-selectin^{high} cells at 1 and 3 µM GW show results from two independent experiments with single wells. Dotted lines indicate the levels of L-selectin in the absence of GW with (lower) or without (upper) PMA.

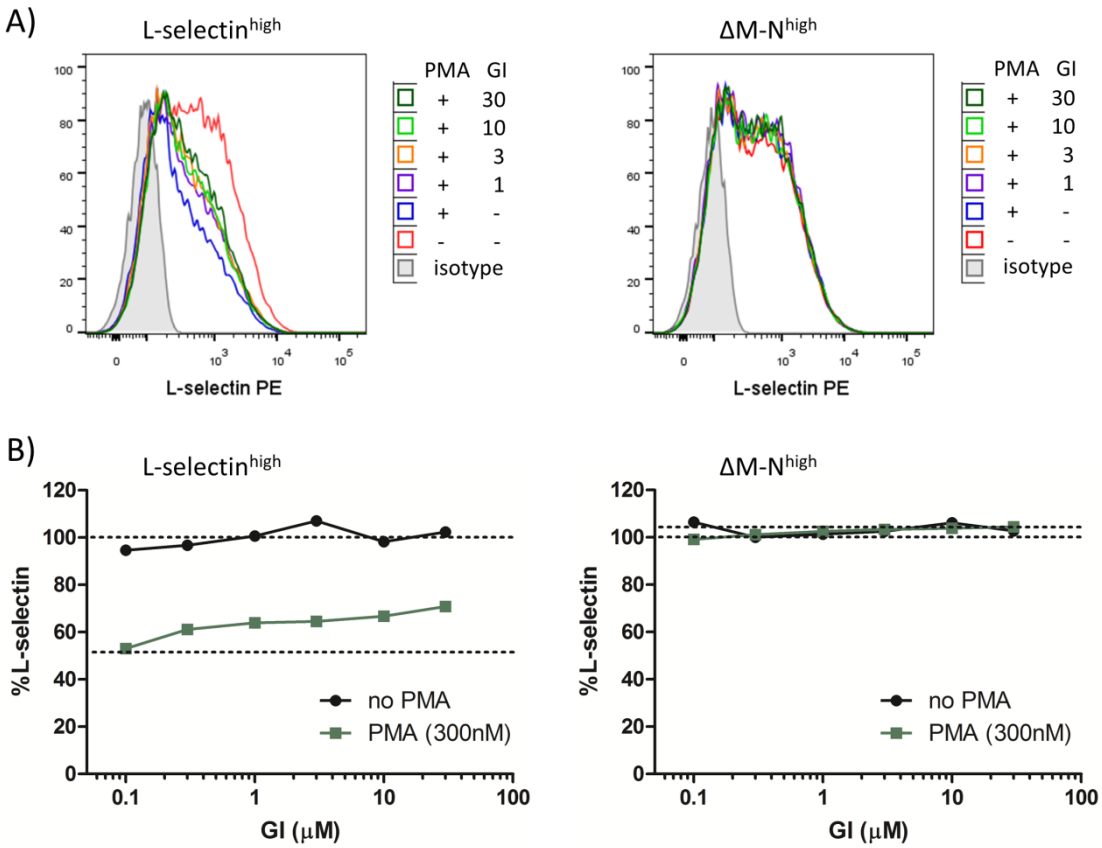

Figure 6.13: Effect of metalloproteinase inhibitors, GI, on PMA induced shedding. L-selectin^{high} wt (left) or ΔM-N (right) gag^{+} MOLT-3 cells were incubated for an h with 0.1-30 μM of the metalloproteinase inhibitor GI before activation with 300 nM PMA for 30 min and analysed of the cells by flow cytometry. A) Flow cytometry histograms showing representative samples incubated with 1-30 μM GI and activated with PMA. B) The percentage of L-selectin was obtained by subtracting the MFI of the isotype from the MFI of each sample and normalising it to the untreated cells, representing 100% L-selectin. Results for single wells are shown. Dotted lines indicate the levels of L-selectin in the absence of GI with (lower) or without (upper) PMA.

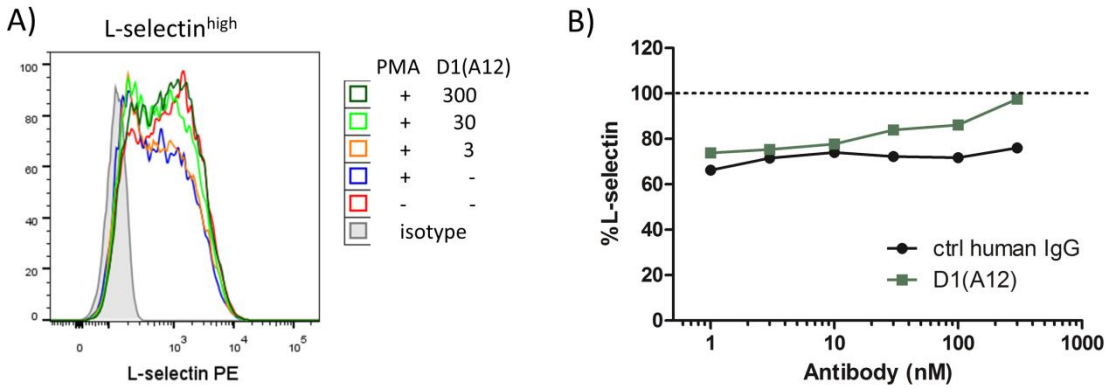

Figure 6.14: Effect of an ADAM17 specific blocking Ab D1(A12) on PMA induced L-selectin shedding. Wt L-selectin^{high} gag^{+} MOLT-3 cells were incubated for 1 h with 1-300 nM of ADAM17 specific inhibiting Ab D1(A12) or control human IgG and activated with 300 nM PMA for 30 min. A) Flow cytometry histograms showing representative samples incubated with 3-300 nM of D1(A12) Ab and activated with PMA. B) The percentage of L-selectin was obtained by subtracting the MFI of the isotype from the MFI of each sample and normalising it to the untreated cells, representing 100% L-selectin. Results for single wells are shown. The dotted line indicates the levels of L-selectin in the absence of Ab and without PMA.

6.4.2 TCR induced L-selectin shedding and the role of ADAM17

Activation of T cells by PMA is via the activation of protein kinase C whereas activation of T cells by the engagement of the TCR and peptide-MHC triggers a signalling cascade initiated by Src family kinases (Brownlie and Zamoyska 2013). Due to the different signalling pathways involved, we wanted to establish whether ADAM17 was also the main protease involved in TCR induced L-selectin shedding or whether the two pathways operated differently. To establish the ideal conditions for TCR induced L-selectin shedding, gag^+ MOLT-3 cells were activated with a titration of cognate SLY peptide (10^{-9}-10^{-4} M) pulsed C1R cells. At 10^{-6} M SLY peptide or higher, 70% of L-selectin was shed from the cell surface of wt L-$selectin^{high}$ gag^+ MOLT-3 cells (figure 6.15 A). No shedding was observed for the ΔM-N L-$selectin^{high}$ gag^+ MOLT-3 cells. To establish the ideal incubation time, wt L-$selectin^{high}$ gag^+ MOLT-3 cells were incubated for 1-120 min with 10^{-4} M peptide pulsed C1R cells and L-selectin and TCR levels analysed (figure 6.15 B). TCR downregulation was used as a control for MOLT-3 cell activation. Both molecules showed a very similar pattern of loss of expression followed by re-expression beyond 60 min; however the underlying mechanisms are distinct. Upon activation, L-selectin undergoes shedding due to cleavage by a metalloproteinase whereas the TCR is internalised (Valitutti et al. 1995). It was established that 60 min was the ideal incubation period for TCR induced L-selectin shedding experiments.

In order to confirm that the TCR activation induced L-selectin shedding observed in gag^+ MOLT-3 cells is physiologically relevant, gag^+ Jurkat cells expressing endogenous L-selectin were stimulated with 10^{-8}-10^{-4} M SLY peptide for either 18 or 24 h and L-selectin and CD69 expression levels analysed (figure 6.15 C). L-selectin shedding occurred in a peptide dose dependent manner alongside increased expression in the activation marker CD69. Overall L-selectin shedding was shown to occur in gag^+ Jurkat and L-$selectin^+$ gag^+ MOLT-3 cells in response to cognate peptide pulsed APCs in a dose dependant manner.

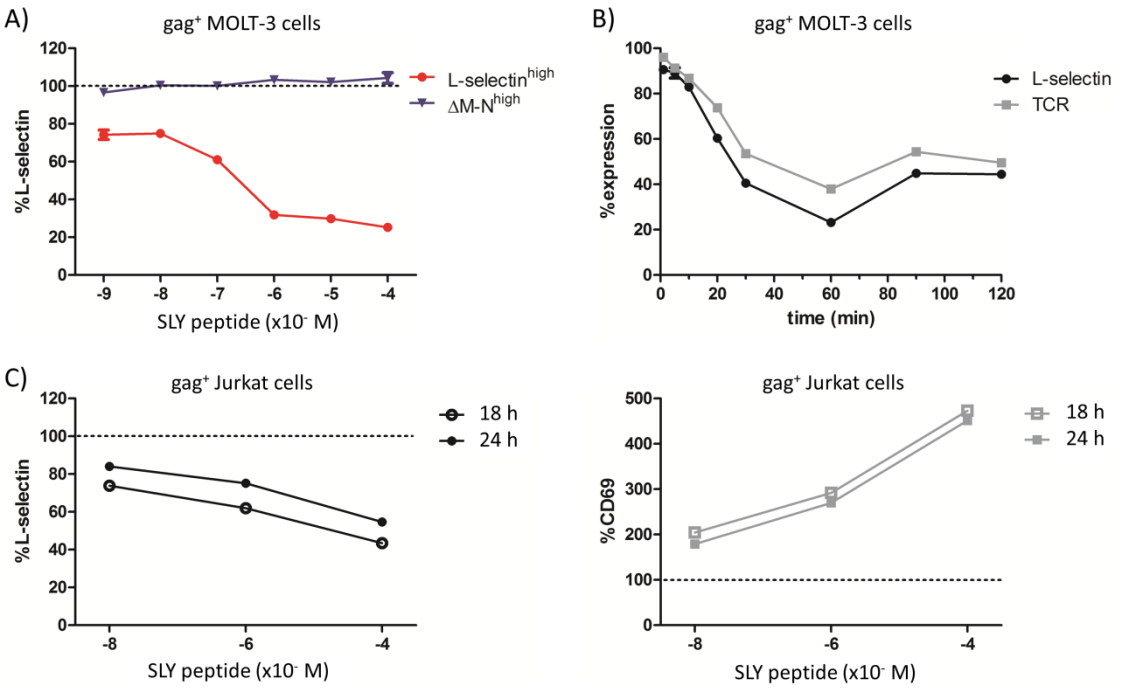

Figure 6.15: Titration and time course of TCR induced L-selectin shedding in gag$^+$ MOLT-3 and gag$^+$ Jurkat T cells. A) FACS sorted wt (red) or ΔM-N (blue) L-selectin^{high} gag$^+$ MOLT-3 cells were incubated for one h with 10^{-9}-10^{-4} M SLY peptide pulsed C1R cells. The APC:T cell ratio was 1:3. L-selectin surface expression analysed by flow cytometry. Triplicate wells are shown and error bars show the SEM. B) L-selectin^{high} gag$^+$ MOLT-3 cells were incubated for 1, 5, 10, 20, 30, 60, 90 and 120 min with 10^{-4} M SLY peptide pulsed C1R cells and levels of L-selectin (black) and TCR (grey) surface expression analysed by flow cytometry. PE anti-L-selectin and FITC-anti-TCRV5β Abs were used to stain the cells. Triplicate wells are shown and error bars show the SEM. C) Gag$^+$ Jurkat cells, expressing endogenous L-selectin, were activated with 10^{-8}-10^{-4} M SLY peptide pulsed C1R cells for either 18 (open symbol) or 24 (filled symbol) h and surface expression of L-selectin (left) and CD69 (right) analysed by flow cytometry. The Abs against L-selectin and CD69 were both PE conjugated, thus these results represent single well experiments and cells were different for the L-selectin and the CD69 staining. All cells were gated on FSC/SSC, AmCyan live/dead negativity, single cells and APC CD19$^-$. The percentages of L-selectin, TCR and CD69 were obtained by subtracting the MFI of the isotype from the MFI of each sample and normalising it to untreated cells, representing 100% L-selectin, TCR or CD69 respectively.

To determine whether TCR induced L-selectin shedding is mediated by ADAM17, gag$^+$ MOLT-3 cells were preincubated with 0.1-30 µM of GI or GW and activated with 10^{-4} M SLY peptide pulsed C1R cells (figure 6.16 A). As with PMA induced L-selectin shedding, at 10 µM, GW

completely inhibited L-selectin shedding whereas GI showed only partial inhibition. At 3 µM or less of GI there is no inhibition of L-selectin shedding, indicating that ADAM10 is not involved and that the inhibition observed is due to inhibition of ADAM17 at high GI doses. For further experiments, GW and GI were used at 30 µM as this concentration showed the highest level of inhibition.

To further study the importance of ADAM17 or ADAM10 for L-selectin shedding, wt or ΔM-N L-selectin^{high} gag^{+} MOLT-3 cells were incubated with GW, GI or no inhibitor and activated with a titration of SLY peptide pulsed C1R cells. In the absence of inhibitors, up to 74% of L-selectin was shed at 10^{-4} M, which was completely blocked by GW and only partially by GI, with 3% and 47% of observed L-selectin shedding respectively (figure 6.16 B). This intermediate level of inhibition by GI was observed at all five peptide doses. Again, GW inhibited constitutive L-selectin shedding, as at low stimulation of 10^{-8}-10^{-6} M peptide, L-selectin levels were above the background. Neither inhibitor affected the expression levels of ΔM-N L-selectin on gag^{+} MOLT-3 cells. As a control for the effects of GW and GI on T cell activation, TCR levels were analysed (figure 6.16 C). Wt and ΔM-N L-selectin^{high} gag^{+} MOLT-3 cells showed matching loss of the TCR in response to activation and the highest peptide dose of 10^{-4} M led to the highest level of TCR endocytosis of 80%. GW or GI did not affect the loss of TCR from the cell surface.

These results indicated that ADAM17 is probably the predominant metalloproteinase controlling L-selectin shedding in response to cognate peptide activation in T cells. To confirm these findings, wt L-selectin^{high} gag^{+} MOLT-3 cells were incubated with 1-300 nM of the ADAM17 specific blocking Ab, D1(A12), and activated with 10^{-4} M SLY peptide (figure 6.17). Control human IgG Ab did not inhibit L-selectin shedding even at the highest dose, whereas the D1(A12) Ab inhibited shedding in a dose-dependent manner, with complete inhibition at 300 nM.

In summary, L-selectin shedding was confirmed to be mediated by ADAM17 either when cells were activated with PMA or by engagement of TCR.

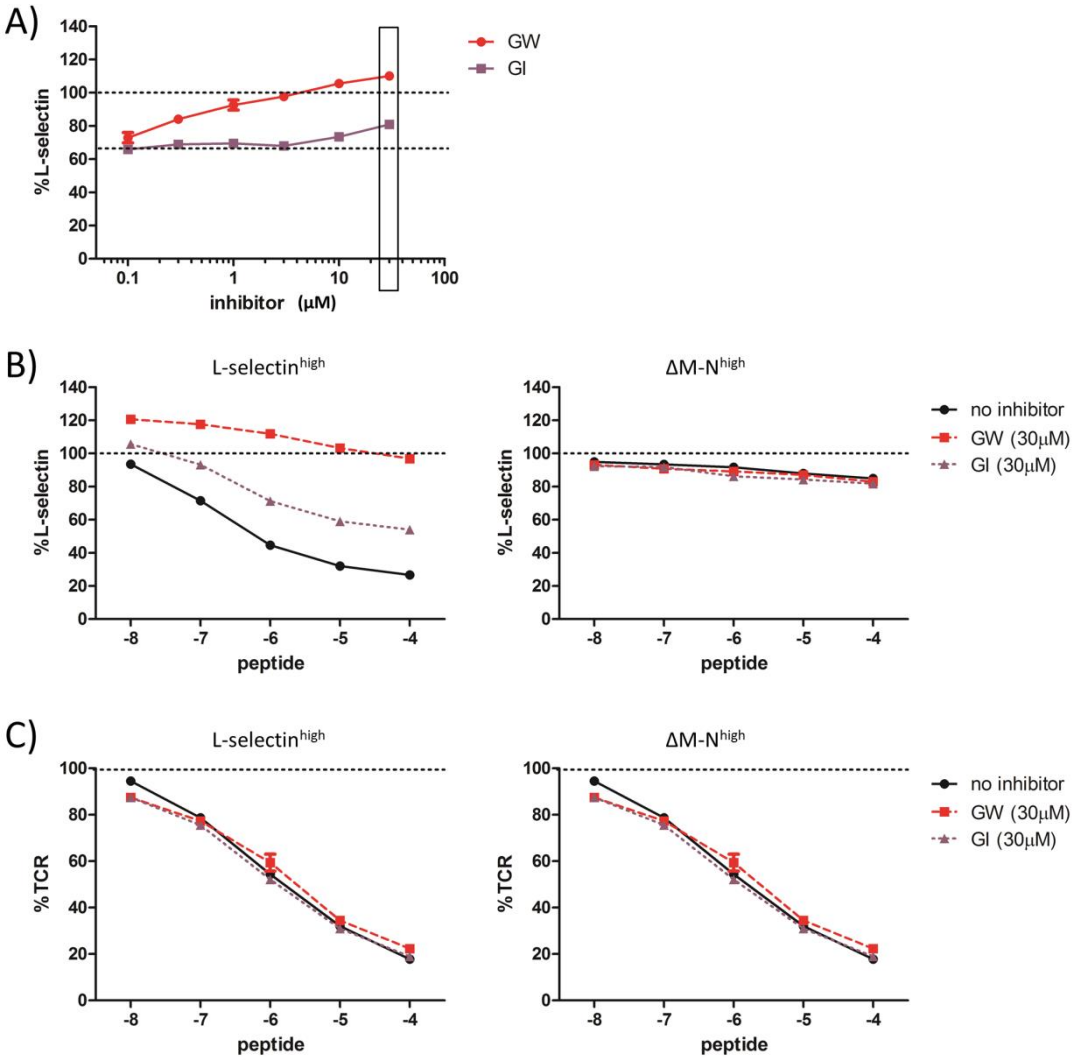

Figure 6.16: Effect of metalloproteinase inhibitors, GW and GI, on TCR induced shedding. A) L-selectin^{high} gag^{+} MOLT-3 cells were incubated with a 0.1-30 μM GI (red) or GW (purple) for 60 min and activated with 10^{-4} M cognate SLY peptide pulsed C1R cells for 60 min. The APC:T cell ratio was 1:3. L-selectin surface expression was analysed by flow cytometry. B) Wt (left) or ΔM-N (right) L-selectin^{high} gag^{+} MOLT-3 cells were incubated for an h with medium alone (black), 30 μM GW (red) or GI (purple) and activated for an h with a 10^{-8}-10^{-4} M SLY peptide pulsed C1R cells. Cells were stained using anti-L-selectin (B) and anti-TCRV5β (C) Ab and flow cytometry analysis was done. The percentage of L-selectin and TCR expression was obtained by subtracting the MFI of the FMO from the MFI of the samples and normalising it to the untreated cells, representing 100% L-selectin expression. All results represent triplicates and the error bars show the SEM. Dotted lines indicate the levels of L-selectin or TCR in the absence of inhibitors with (bottom) or without (top) 10^{-4} M peptide activation. All cells were gated on FSC/SSC, AmCyan live/dead negativity, single cells, and APC CD19^{-}.

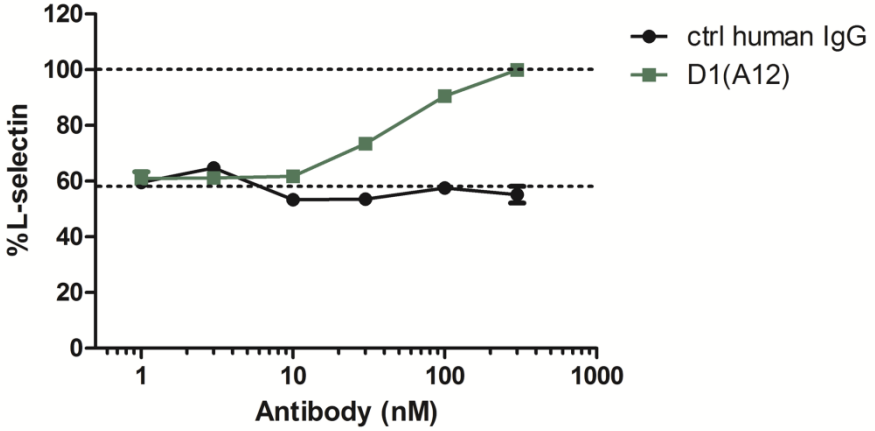

Figure 6.17: Effect of an ADAM17 specific blocking Ab D1(A12) on TCR induced L-selectin shedding. L-selectin^{high} gag^{+} MOLT-3 cells were incubated for an h with 1-300 nM of ADAM17 specific inhibiting Ab D1(A12) or control human IgG and activated with 10^{-4} M SLY peptide pulsed C1R cells for 60 min and analysed by flow cytometry. The APC:T cell ratio was 1:3. The percentage of L-selectin expression was obtained by subtracting the MFI of the isotype from the MFI of each sample and normalising it to the untreated cells, representing 100% L-selectin. All results represent triplicates and the error bars show the SEM. Dotted lines indicate the levels of L-selectin expression in the absence of Ab with (bottom) or without (top) 10^{-4} M peptide activation. All cells were gated on FSC/SSC, AmCyan live/dead negativity, single cells, and APC CD19^{-}.

6.5 The role of γ-secretase in the proteolysis of L-selectin in T cells

After the first proteolytic cleavage of L-selectin by a metalloproteinase, such as ADAM17, the membrane retained fragment (MRF) can be further cleaved, a process called regulated intramembrane proteolysis (RIP). Proteins such as Trop2 undergo cleavage by ADAM17 leaving a MRF that can then be cleaved by the γ-secretase complex (Stoyanova et al. 2012). Here we wanted to investigate whether the same process could be happening for L-selectin.

Initially, gag^{+} Jurkat cells expressing endogenous L-selectin were activated with either PMA or anti-CD3/28 Dynabeads. Dynabeads were used to generate TCR induced L-selectin shedding as peptide pulsed C1R cells could not be used since C1R cells express high levels of L-selectin. This

would interfere with the interpretation of the protein analysis and immunoblotting results. Gag$^+$ Jurkat cells were incubated with either medium alone or DAPT, a γ-secretase inhibitor, and activated with PMA or Dynabeads. As shown in figure 6.18 A, PMA induced very strong L-selectin shedding whereas the Dynabeads gave much weaker shedding. This is reflected by the complete loss of full length L-selectin (68 kDa) in PMA activated groups (lane 3-4) but not in Dynabead activated cells (lanes 5-6). In the absence of γ-secretase activity the MRF accumulates, as there is a clear difference in the quantity of MRF (6 kDa) present in the DAPT treated cells (lanes 4 and 6) compared to the non-treated cells (lanes 3 and 6). This result, although not definitive as no loading control protein was measured, hinted towards γ-secretase as the main candidate involved in further processing of the MRF.

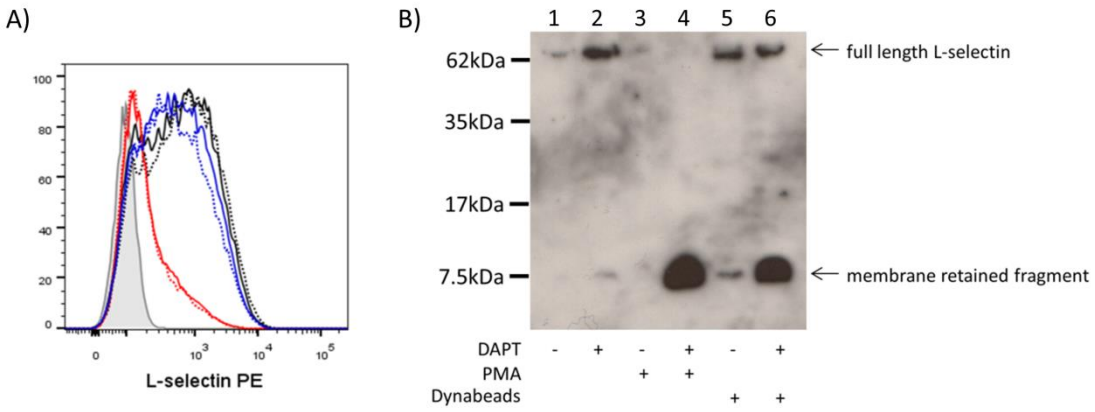

Figure 6.18: L-selectin shedding and further processing in the presence of a γ-secretase inhibitor, DAPT, in gag$^+$ Jurkat cells. A) Gag$^+$ Jurkat cells were incubated without (solid line) or with 5 µM DAPT (dotted lines) for 30 min and activated with either a 1:1 ratio of CD3/28 Dynabeads (blue) or 500 nM PMA (red) for 60 or 30 min, respectively. Control wells were left unstimulated (black). A small fraction of the cells was collected and L-selectin expression was analysed by flow cytometry. Cells were gated on FSC/SSC, single cells and CD19$^-$. B) The remaining cells from A were lysed and the lysate was probed for L-selectin protein by immunoblotting.

Gag^{+} MOLT-3 cells were used to further study the processing of the MRF as these cells do not express endogenous L-selectin and it was possible to transduce them with either wt, ΔM-N or I-K L-selectin LV. To confirm that L-selectin shedding in response to CD3/28 Dynabeads was similar to activation with cognate peptide pulsed APCs, a 1:1 ratio of cells:Dynabeads was compared to 10^{-4} M peptide pulsed C1R activation (figure 6.19). The L-selectin shedding was very similar with the peptide giving 58% and the Dynabeads 55% loss of L-selectin.

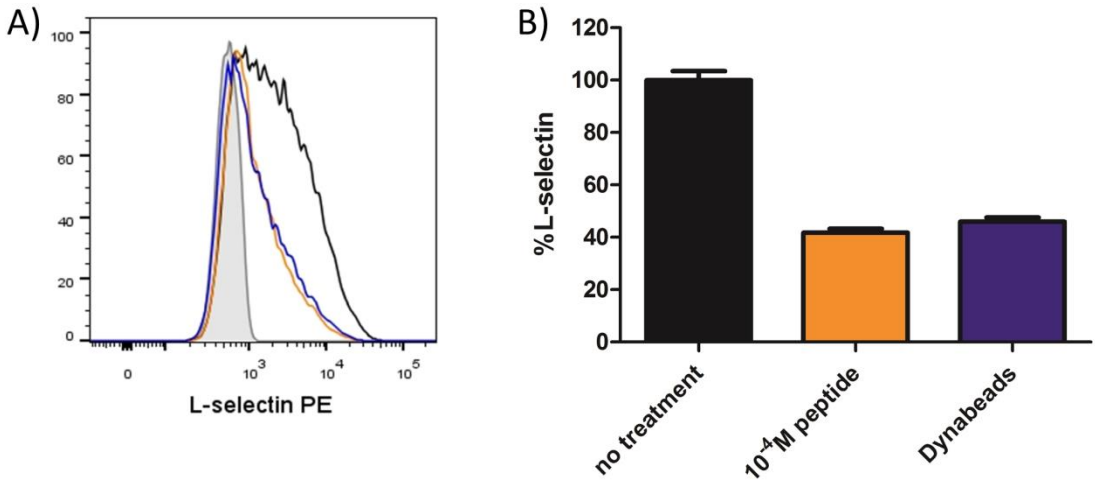

Figure 6.19: Comparison of peptide and Dynabead induced L-selectin shedding in gag^{+} MOLT-3 cells. A) Gag^{+} L-selectin^{high} MOLT-3 cells were incubated for 60 min with medium alone (black), 10^{-4} M SLY peptide pulsed C1R cells (orange) or a 1:1 ratio of CD3/28 Dynabeads (blue) and cells collected for flow cytometry analysis. Representative plots of L-selectin expression for all three treatment samples are shown and the isotype control is shown in grey filled. B) The percentage of L-selectin expression was obtained by subtracting the MFI of the isotype from the MFI of each sample and normalising it to the MFI mean of the untreated cells, representing 100% L-selectin. Triplicates are shown and the error bars show the SEM. All cells were gated on FSC/SSC, Pacific Blue live/dead negativity, single cells, and CD19^{-}.

The expression levels of wt, ΔM-N and I-K L-selectin on gag$^+$ MOLT-3 cells were compared and found to be very similar (figure 6.20 A). These three groups of cells were pre-incubated with DAPT and activated with either PMA or Dynabeads in the presence of DAPT and L-selectin expression analysed by flow cytometry and immunoblotting. In both the wt and I-K expressing cells, PMA induced more shedding than the Dynabeads (figure 6.20 B). There was no shedding in the ΔM-N cells. DAPT did not influence the shedding of the L-selectin ectodomain. Most importantly, the results observed with the gag$^+$ Jurkat cells were reproduced with the wt L-selectin gag$^+$ MOLT-3 cells; inhibition of γ-secretase by DAPT led to an accumulation of the MRF (figure 6.20 C). In addition to a strong MRF signal present for DAPT treated PMA (3.6 fold) or TCR (5.5 fold) stimulated cells, an MRF signal is also observed in cells that were DAPT treated but not activated (1 fold), indicating the role of γ-secretase in constitutive L-selectin processing. The full length L-selectin protein was not observed in some lanes, possibly due to the high threshold of detection for the anti-L-selectin Ab used. No MRF was detected with the ΔM-N gag$^+$ MOLT-3 cells, which was expected considering that the ΔM-N mutant is not cleaved by ADAM17 thus not producing any MRF. The I-K L-selectin mutation was generated to be resistant to γ-secretase lysis; however the results show that this is not the case. There is a very weak signal for the MRF of cells that were stimulated with PMA or Dynabeads but not DAPT (0.2 and 0.1); however this is a much weaker MRF signal than the MRF signal in the DAPT treated and PMA and TCR activated cells (3.7 and 2.2). If the I-K mutant influences γ-secretase activity, it is only slight and might not be an ideal system to take forward.

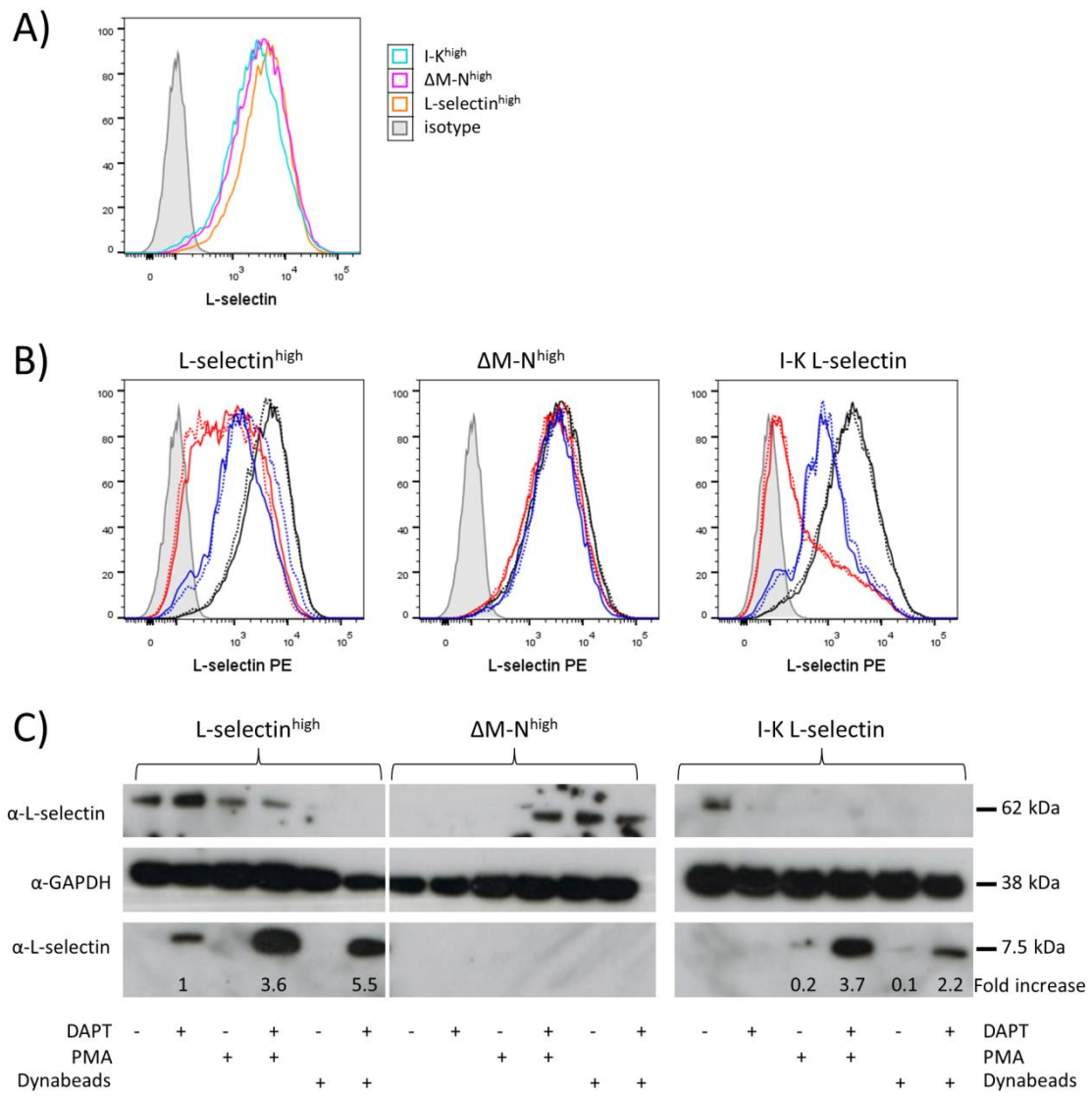

Figure 6.20: L-selectin shedding and further processing in the presence of a γ-secretase inhibitor, DAPT, in wt, ΔM-N and I-K L-selectin^{high} gag^{+} MOLT-3 cells. A) Comparison of L-selectin surface expression for wt (orange), ΔM-N (pink) and I-K (turquoise) L-selectin^{high} gag^{+} MOLT-3 cells. The grey filled cells were stained with an isotype control Ab. B) Wt, ΔM-N and I-K L-selectin^{high} gag^{+} MOLT-3 cells were incubated with medium alone (solid line) or 5 μM DAPT (dotted line) for 30 min and activated with either a 1:1 ratio of CD3/28 Dynabeads (blue) or 300 nM PMA (red) for one or half an h, respectively. L-selectin expression was analysed by flow cytometry and representative plots are shown. Control wells were left unstimulated (black) or stained with isotype control (grey filled). Cells were all gated on FSC/SSC, AmCyan live/dead negativity and CD19^{-}. C) The remaining cells from B were lysed and the lysate was probed for L-selectin protein by doing an immunoblot. The blots were also probed for the housekeeping protein GAPDH as a loading control. Exposure time for the L-selectin probe was 10 min and the GAPDH probe was 30 s. The signal for the MRF was normalised to GAPDH and the fold increase over the DAPT only treated wt L-selectin^{high} cells is shown.

6.6 *In vitro* flow assay of gag$^+$ MOLT-3 cells over TNF-α activated HUVEC cells

To study the role of wt or ΔM-N L-selectin in the tethering, rolling and arrest of T cells on activated endothelial cells, *in vitro* flow experiments were performed in collaboration with Dr Aleksandar Ivetic at King's College London. These assays were performed in London and the details can be found in the 'Materials and Methods'. Briefly, human umbilical vein endothelial cells (HUVECs) were grown on fibronectin covered microscope slides and activated with TNF-α for 4-6 h before the flow chamber was fitted onto the slide and gag$^+$ MOLT-3 cells were added under shear flow. Three different gag$^+$ MOLT-3 cells were used; untransduced cells expressing no L-selectin and transduced cells expressing matched levels of either wt or ΔM-N L-selectin to levels similar to gag$^+$ Jurkat cells (figure 6.22 A). Figure 6.21 shows images captured at the start and at the end (15-21 min) of the flow assay. Representative full movies, made of photographs captured every 15 s, of each of a total of four regions per slide can be found on DVDs attached in the appendix A3. No transendothelial migration (TEM) was observed for any MOLT-3 cells, indicating that either the cells are not capable of TEM or the conditions to trigger TEM are not met. The number of MOLT-3 cells that rolled or arrested on the HUVEC cells was obtained by counting newly attached cells in each frame. No striking differences between cells expressing no, wt or ΔM-N L-selectin were found in the total number of cells attached, in the rate of recruitment or in the % of cells attached at the end of the experiment (figure 6.22 B-D).

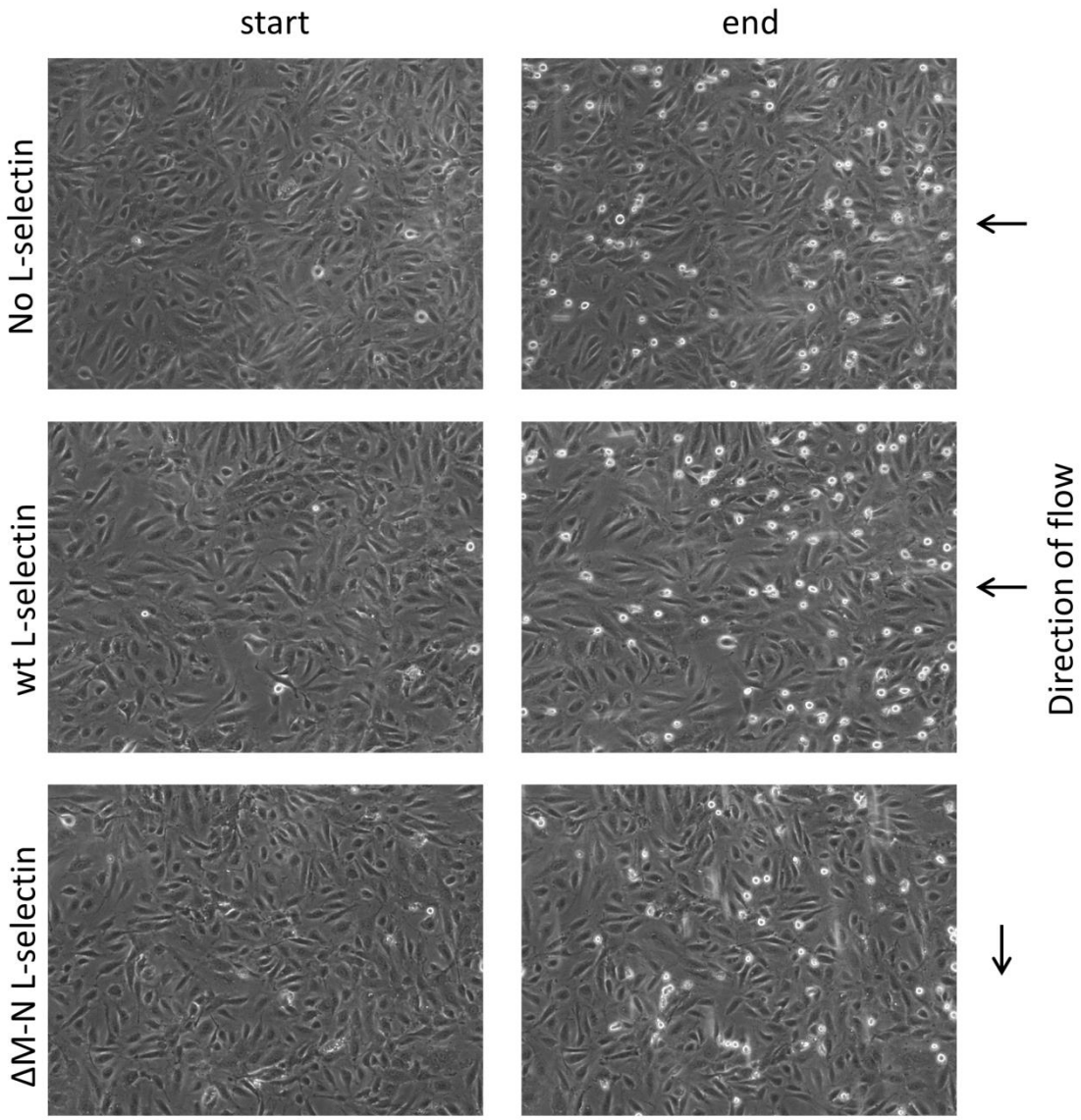

Figure 6.21: Tethering, rolling and adhesion of gag$^+$ MOLT-3 cells expressing no, wt or ΔM-N L-selectin on TNF-α activated HUVEC cells. Gag$^+$ MOLT-3 cells (bright round cells) expressing no, wt or ΔM-N L-selectin were used in an *in vitro* flow assay to look at the impact of L-selectin on adherence to TNF-α activated HUVEC cells (elongated dark cells). Every 15 s, a picture was taken by an inverted bright field microscope of a set region on the coverslip. Four points of view were recorded per assay and one per cell type is shown. The overall period of recording (end) was 15 min for the no and ΔM-N L-selectin cells and 21 min for the wt L-selectin cells. The direction of flow is indicated by an arrow.

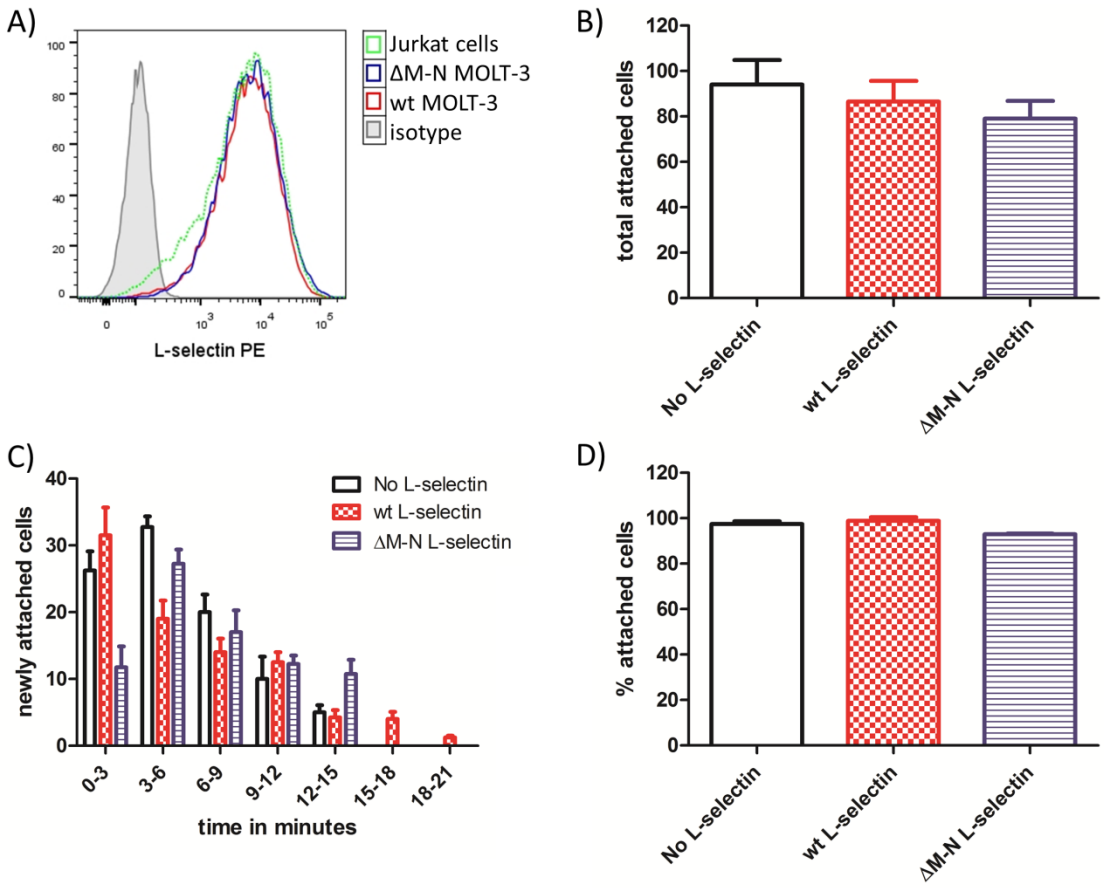

Figure 6.22: Quantification of adhesion of gag$^+$ MOLT-3 cells expressing no, wt or ΔM-N L-selectin on TNF-α activated HUVEC cells under flow. Adhesion of gag$^+$ MOLT-3 cells expressing no (black), wt (red) or ΔM-N (blue) L-selectin to TNF-α activated HUVEC cells under flow was quantified. A) Gag$^+$ MOLT-3 cells were analysed for L-selectin expression by flow cytometry. Wt (red) and ΔM-N (blue) expressing cells were compared to gag$^+$ Jurkat cells (green dotted) Cells stained with an isotype control Ab are shown in grey. B) Adhesion of gag$^+$ MOLT-3 cells from the experiment shown in figure 6.21 was quantified by counting all cells that attached over a 15 min (no L-selectin and ΔM-N) or a 21 min (wt L-selectin) timeframe. C) The number of newly attached cells is shown for 3 min intervals. D) The percentage of attached cells at the end of the assay over the overall attached cells is shown. For each cell type, four points of view from a single coverslip were analysed and the error bars show the SEM.

6.7 Generation of human $CD8^+$ T cells expressing CD2-L-selectin or CD2-ΔM-N

Melanoma-specific $CD8^+$ T cells expressing either wt L-selectin or shedding-resistant ΔM-N L-selectin under a heterologous promoter were generated subsequently with the aim to use these cells in future cytotoxic experiments and *in vitro* flow assays and *in vivo* homing assays. Cells from a HLA-$A2^+$ donor were transduced simultaneously with both the CD2-L-selectin wt or ΔM-N and the Mel LVs (figure 6.23). The CD2-L-selectin LV was used to enable identification of successfully transduced cells, as primary $CD8^+$ T cells express endogenous L-selectin. Cells were sorted by MACS for both Mel TCR and CD2 expression and 60% of the wt L-selectin cells were double positives after 6 stimulation cycles, whereas only 7% of the ΔM-N L-selectin cells were co-expressing the Mel TCR and CD2. It was also observed that the levels of CD2 surface expression were considerably lower in cells transduced with the CD2-L-selectin LV than cells stimulated and sorted identically but transduced with the ZFN2-CD2 and (figure 7.10). Whether this is due to the CD2 being upstream of the 2A sequence in the L-selectin LV or whether there is a level of gene silencing is presently unknown.

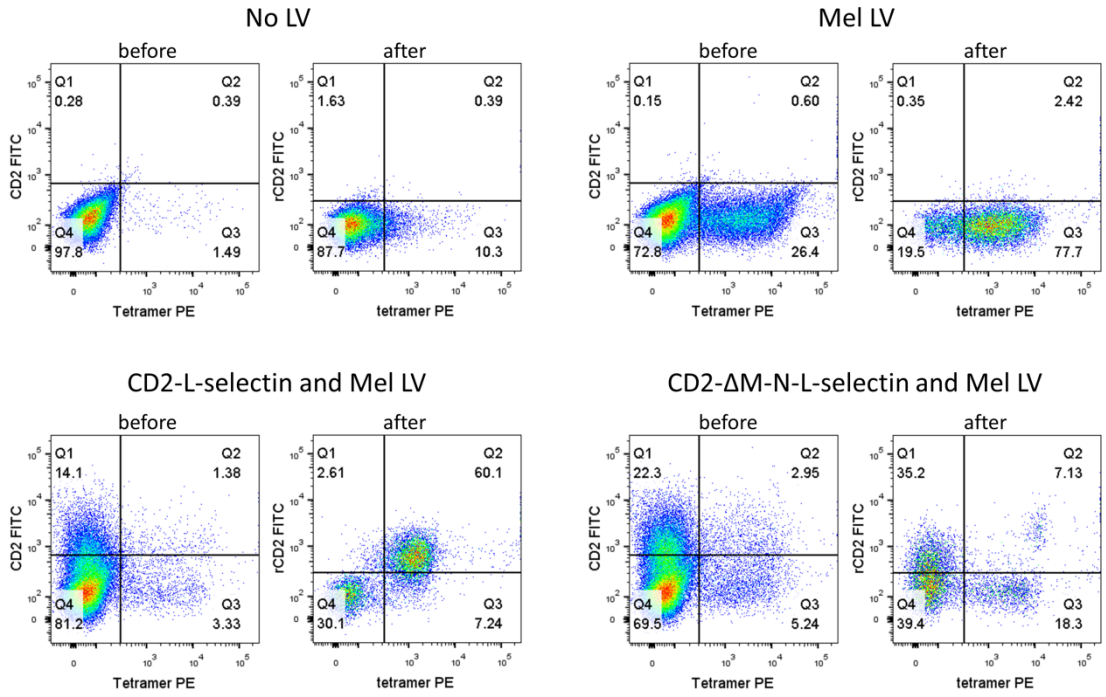

Figure 6.23: Generation of primary CD8$^+$ T cells transduced with CD2-L-selectin wt or ΔM-N. Primary CD8$^+$ T cells were transduced with 100 µl Mel LV or/and 25 µl of CD2-L-selectin wt or ΔM-N. AT day 13 post transduction, cells were analysed by flow cytometry for the surface expression of CD2 and Mel TCR (before). After an expansion of the cells, they were sorted for the expression of tetramer and an expansion cycle later for the expression of CD2 by MACS separation. Cells were analysed again by flow cytometry once they had undergone a total of 6 stimulation cycles (after). Cells were all gated on FSC/SSC, AmCyan live/dead negativity and APC CD8$^+$. The gates for the tetramer and CD2 staining are set in relation to the FMOs and in accordance with cells grown at the same time that were transduced with Mel and ZFN LVs (figure 7.10 B).

6.8 Conclusion

In this chapter, it was confirmed that PMA induced shedding was ADAM17 dependant. Additionally it was found that TCR induced L-selectin shedding is also ADAM17 mediated. L-selectin shedding showed a similar time course and intensity in response to PMA or TCR activation. Additionally, it was established that the MRF was cleaved by γ-secretase after cells were activated by PMA or TCR. Shedding-resistant ΔM-N L-selectin was not shed or further processed, confirming that, similarly to other ADAM17 and γ-secretase substrates, L-selectin ectodomain shedding has to proceed γ-secretase proteolysis. Constitutive L-selectin shedding and further processing was also shown to be ADAM17 and γ-secretase driven.

The I-K mutant, hypothesised to be γ-secretase-resistant only showed a slight increase in the MRF above wt L-selectin. Thus this mutation might not be useful for further studies especially as the I-K mutation might interfere with the binding of calmodulin to the cytoplasmic tail of L-selectin (Gifford et al. 2012). This interference might lead to the spontaneous or premature release of calmodulin and the shedding of L-selectin (figure 1.8 B).

The effect of shedding-resistant ΔM-N L-selectin on the rolling and tethering of T cells on endothelial cells was assessed by doing the *in vitro* flow assay. However, there was no difference in the recruitment of MOLT-3 on TNF-α activated HUVECs between cells expressing no, wt or ΔM-N L-selectin. This could simply be due to the lentivirally delivered L-selectin not being functional, for example due to abnormal glycosylation. However, the shedding in response to PMA in lentivirally transduced MOLT-3 cells did fit with that of cells expressing endogenous L-selectin and previous studies using lentivirally delivered L-selectin. It is possible that MOLT-3 cells use alternative proteins to tether and roll on activated HUVECs, such as LFA-1, which is expressed at high levels in MOLT-3 cells (Phongpradist et al. 2010). Alternatively it has been shown *in vitro* that α4 integrins, such as α4β1 and α4β7, can support tethering and rolling of leucocytes (Berlin et al. 1995) and MOLT-3 cells express α4β1 (Tomczuk et al. 2003).

Additionally, it is possible that L-selectin expression on MOLT-3 cells was not high enough to support tethering and rolling or that TNF-α activated HUVECs do not express L-selectin ligands. For further studies, a different cell line or primary $CD8^+$ T cells should be used. A reason for the absence of TEM in the *in vitro* flow assay might have been the absence of basal membrane, pericytes and chemokine gradients.

Chapter 7: Adoptive transfer of human CD8$^+$ T cells into Mel526 tumour bearing NOD-SCID or NSG mice

7.1 Introduction

The aim of this chapter was to establish an *in vivo* xenograft model to compare the anti-tumour potential of populations of Mel$^+$ CD8$^+$ T cells, sufficient or mutant in SHP-1. Two different types of immunodeficient mice were used; NOD-SCID mice, lacking both functional T and B cells and having a decreased level of NK and myeloid cell activity (Shultz et al. 1995), and NSG mice, lacking functional B, T and NK cells and having a decreased myeloid cell activity (Ishikawa et al. 2005).

Initial tumour cell titration and ACT experiments were done using NOD-SCID mice, due to their local availability. The Mel526 cells used here were generated in Chapter 5, and express the RFP-GLuciferase gene cassette and the RFP expressed is the DsRed protein from the coral of the *Discoma* genus (Matz et al. 1999; Baird et al. 2000). Expression of RFP allowed for the monitoring of tumour growth by non-invasive fluorescence imaging.

Tumour cell titration experiments were based on a study by Liddy *et al.* where they used 2 x 10^6 Mel526 cells to establish tumours in Beige-SCID mice (Liddy et al. 2012). The optimal Mel526 cell number necessary to generate reliable tumour take was established in NOD-SCID mice. Two small T cell transfer experiments were conducted after which it was decided to use NSG mice for further experiments due to their higher level of immunodeficiency. A second Mel526 cell titration experiment was performed in NSG mice, followed by an ACT experiment comparing the anti-tumour potential of wt, Mel$^+$ and a Mel$^+$ population of T cells containing a minority of mutant SHP-1 cells.

7.2 Mel526 tumour cell titration in NOD-SCID mice

The optimal Mel526 cell number for tumour take in male NOD-SCID mice was established by titrating Mel526 cells. One mouse was injected with 2 x 10^6 and a second mouse was injected with 10 x 10^6 and two mice were injected with 15 x 10^6 DsRed labelled Mel526 cells, subcutaneously into the left flank. One mouse did not receive any Mel526 cells and was used as a negative control for tumour imaging. At day 0, the indicated tumour cell number in 200 µl of saline was injected and the mice imaged daily for the first 3 days and twice weekly thereafter (figure 7.1 B). The DsRed signal at day 0 was detected over a large area due to the high volume of injected fluid containing fluorescent cells. At day 2, this area had shrunk and Mel526 cells started forming a more localised tumour; in future experiments imaging of the tumour commenced on day 3. Calliper measurements of the tumour commenced on day 8 and were used to calculate the tumour area and thus obtain a second measurement of tumour growth.

The lowest Mel526 cell dose (2 x 10^6) generated a palpable tumour on day 10 but not thereafter; imaging showed that the tumour shrank after day 8 (figure 7.1 B-D). The mouse injected with 10 x 10^6 Mel526 cells gave a palpable tumour throughout the experiment however the tumour did not grow for 20 days, as shown by the stable tumour size and DsRed intensity, before showing signs of growth. The two mice injected with 15 x 10^6 Mel526 cells showed continual tumour growth from day 3 onwards as shown by DsRed signal and tumour area. Overall, it was decided to inject 15 x 10^6 Mel526 cells in future experiments.

At day 28, tumours were imaged and measured by callipers, mice were sacrificed and tumours excised. When opening the peritoneal cavity, the tumours looked very different between the low and high dose of Mel526 cells (figure 7.2 D). The smallest tumour looked entirely white whereas the bigger tumours were partly red/pink indicating the presence of Mel526 cells. The 15 x 10^6 Mel526 cell tumours were bigger in calliper measured size and in weight than the

lower dose tumours (figure 7.1 C and 7.2 A). The two smaller tumours as well as one of the 15 x 10^6 Mel526 tumours had a layer of white tissue around it possibly indicating a capsular structure formed to segregate the tumour from the rest of the body. The weight of the tumours at the endpoint were plotted against the caliper measurements and the DSRed signal (figure 7.2 B and C).

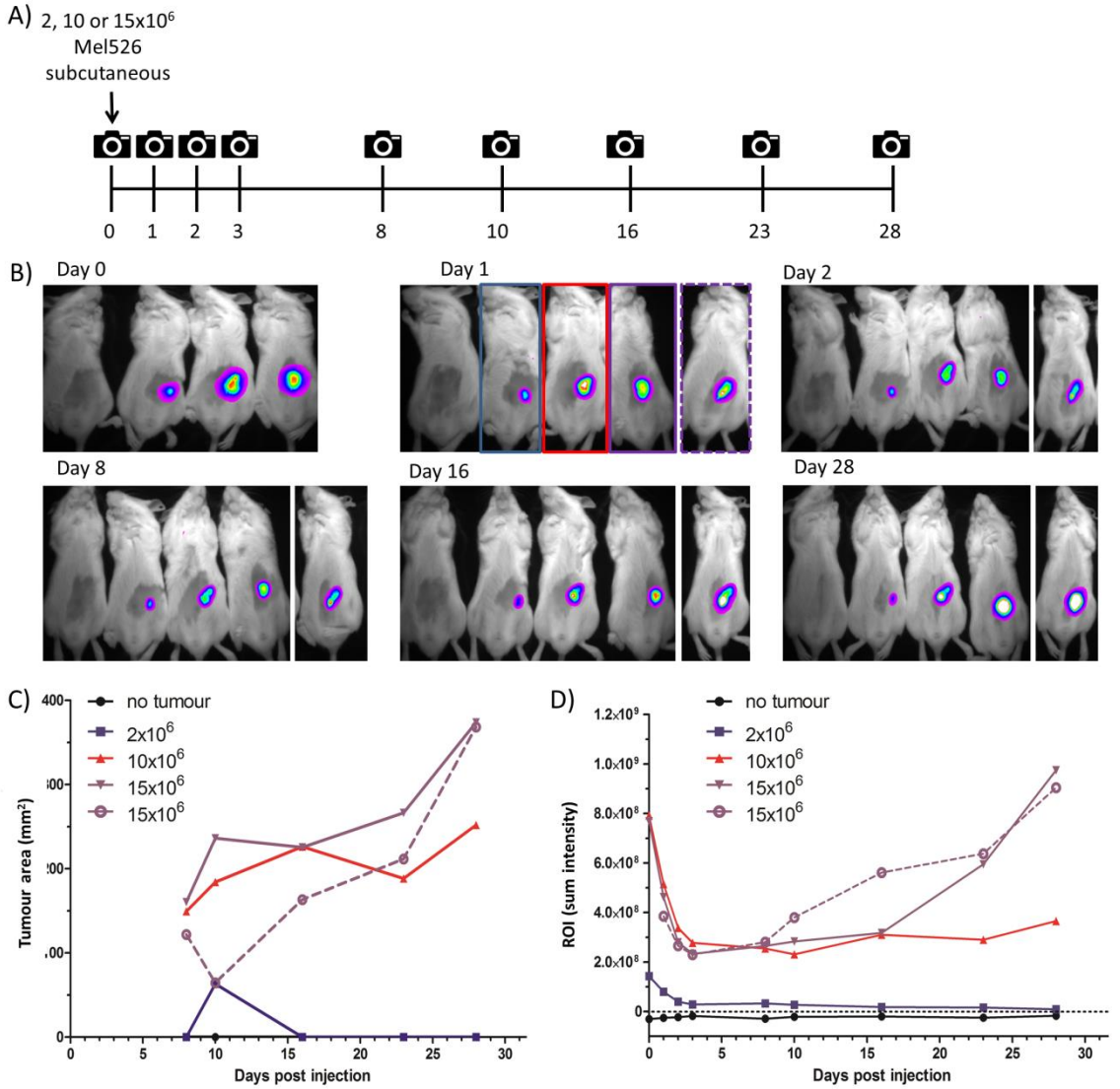

Figure 7.1: Titration of Mel526 tumour cells in NOD-SCID mice. A) Experimental layout for the titration of Mel526 tumour cells in NOD-SCID mice. Single mice were injected subcutaneously with 0, 2 x 10^6 (blue), 10 x 10^6 (red) Mel526 cells and two mice received 15 x 10^6 (purple solid and dotted) Mel526 cells. B) and D) Tumour growth was monitored by imaging and the fluorescence images were superimposed on white light images and the pixel intensity in a defined a region of interest (ROI) around the tumour was quantified by subtracting the pixel intensity of a ROI outside of the tumour. C) Tumour growth was monitored from day 8 onwards by measuring the tumour dimensions using callipers.

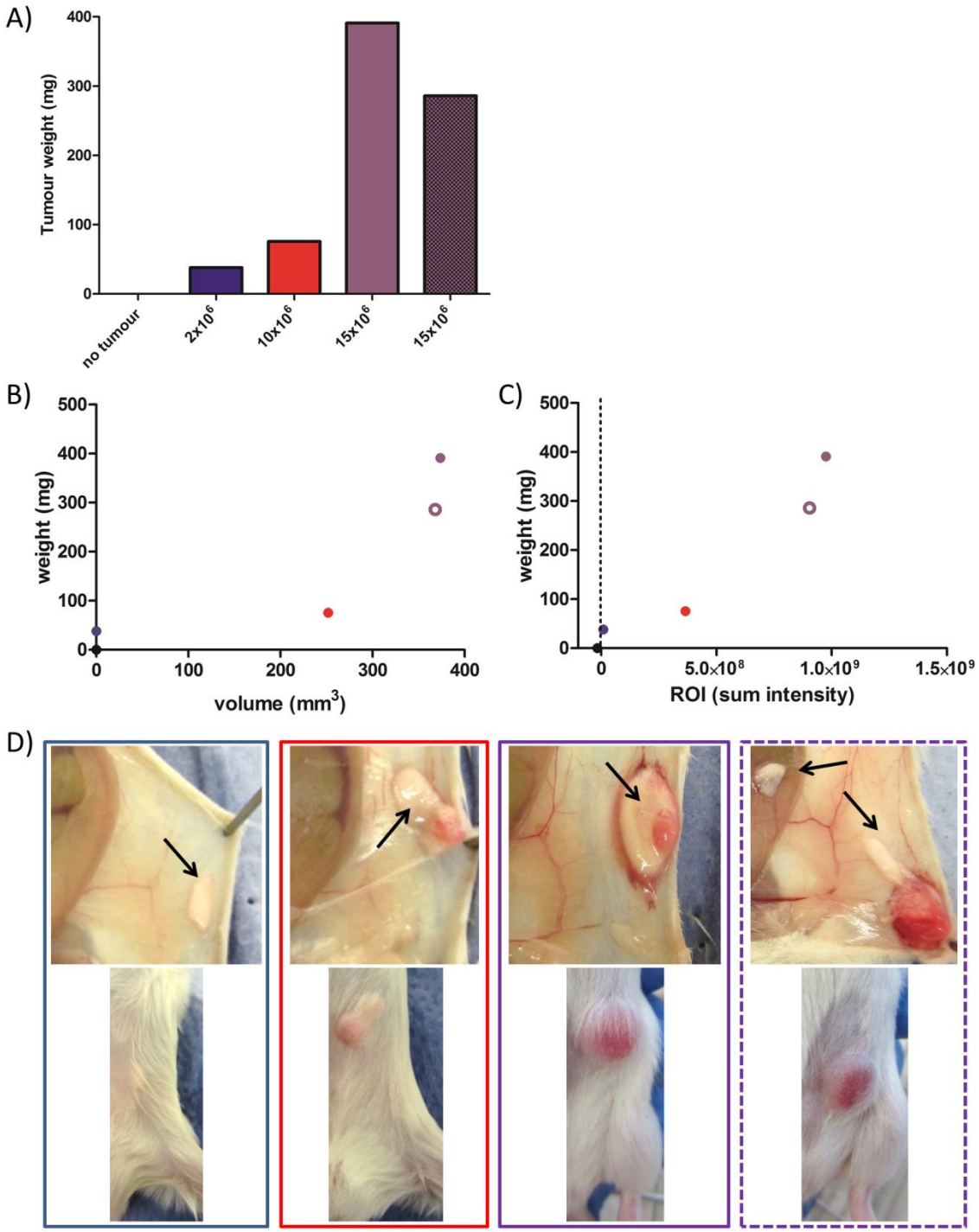

Figure 7.2: Analysis of the Mel526 tumours from NOS-SCID mice at day 28. A) Tumours were weighed after tumour excision. B) Correlation between the tumour area and tumour weight at day 28 is shown. C) Correlation between the sum intensity of the DsRed signal and tumour weight at the day 28 is shown. D) Photographs of tumour before (lower) and after (upper) opening of the peritoneal cavity were taken for mice injected with 2 x 10^6 (blue), 10 x 10^6 (red) or 15 x 10^6 (purple) Mel526 cells. The Mel526 cells are bright red/pink and the white tissue is indicated by arrows.

7.3 Adoptive transfer of human $CD8^+$ T cells into irradiated and non-irradiated NOD-SCID mice

To establish whether human $CD8^+$ T cells can survive and potentially exhibit an anti-tumour effect *in vivo*, two male NOD-SCID mice were injected intravenously (i.v.) with 5.7 x 10^6 human $CD8^+$ T cells. The cells were sorted for CD8 expression and stimulated for three cycles *in vitro* before injection. It was hypothesised that irradiation of the mice could reduce $CD8^+$ T cell rejection by the host's immune cells by reducing the remaining NK cells. Hence, one mouse was irradiated with 2 Gy and the other one left untreated and both mice injected i.v. with 5.7 x 10^6 $CD8^+$ T cells (figure 7.3 A). The injected $CD8^+$ T cells comprised two cell populations that differed in size; a small population of mostly $CCR7^+$ L-$selectin^-$ (70.8%) cells and a larger population of mostly $CCR7^-$ L-$selectin^-$ (73.9%) cells (figure 7.3 B).

Two days post T cell transfer, the mice were culled, their organs collected and single cell suspensions stained for human $CD8^+$ and analysed by flow cytometry. The overall cell numbers of live cells in the spleen, blood and lungs were between 2.3 and 17 times higher in the non-irradiated mouse than the irradiated one (figure 7.4 A and B). This reduced cell number in the irradiated mouse was also seen in samples from the mesenteric LN and the combined axillary, brachial and inguinal LNs. On the other hand, more human $CD8^+$ T cells were recovered from the irradiated mouse with 1.4 to 2.8 fold more human $CD8^+$ T cells in the spleen, blood and lungs of this mouse (figure 7.4 C). Overall this showed that irradiation might enhance human $CD8^+$ T cell survival and irradiation was adopted in the next adoptive T cell transfer experiment.

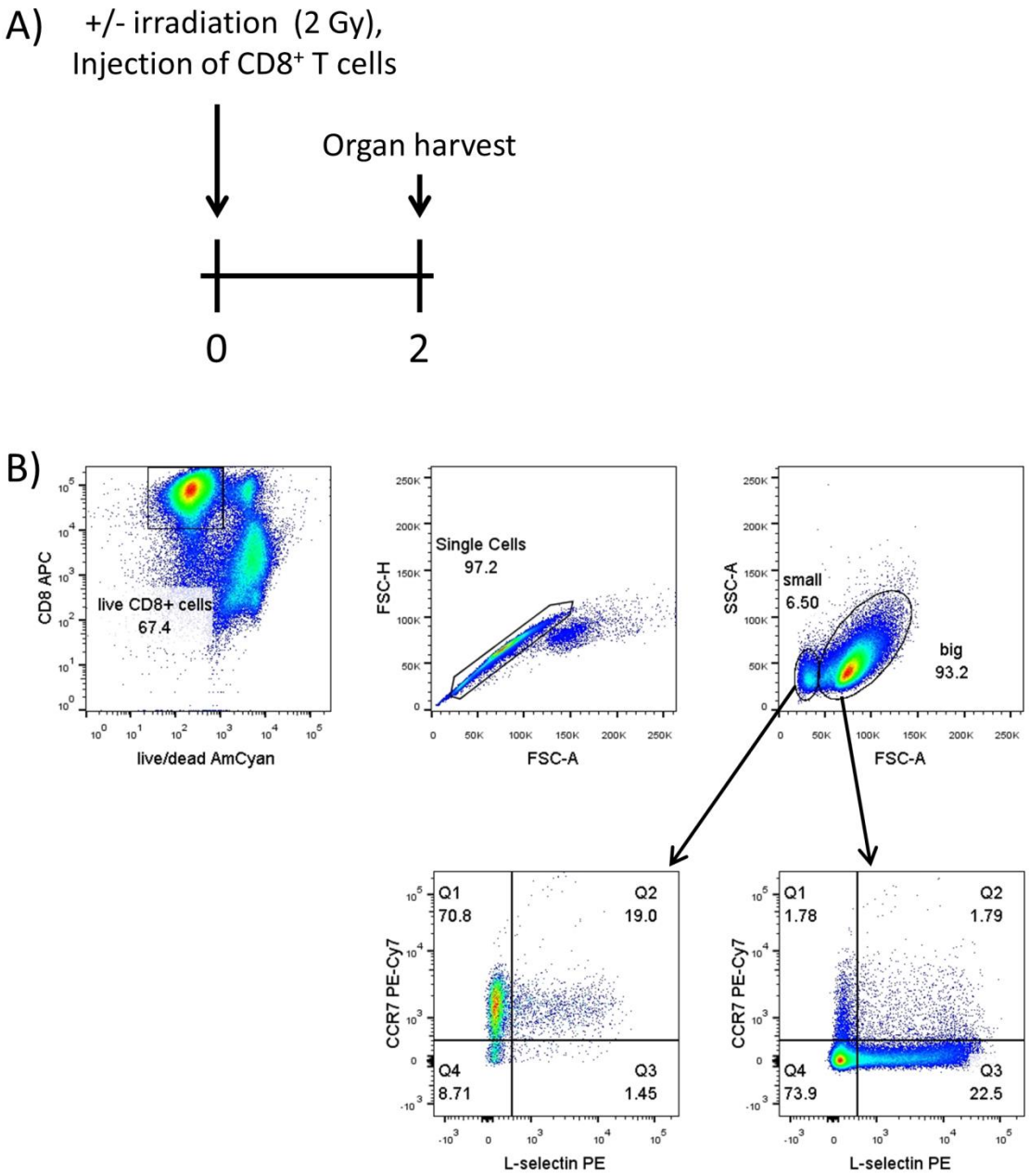

Figure 7.3: Adoptive transfer of human CD8$^+$ T cells into irradiated or non-irradiated NOD-SCID mice. A) Experimental layout for the adoptive transfer of 5.7 x 10^6 human CD8$^+$ T cells into an irradiated (2 Gy) or a non-irradiated NOD-SCID mouse. B) Flow cytometry analysis of the human CD8$^+$ T cells injected. Cells were stained with an anti-CD8, anti-CCR7 and anti-L-selectin Ab and the gating strategy is shown. Two populations of T cells with different SSC/FSC appearances (bottom right) were further analysed for L-selectin and CCR7 expression.

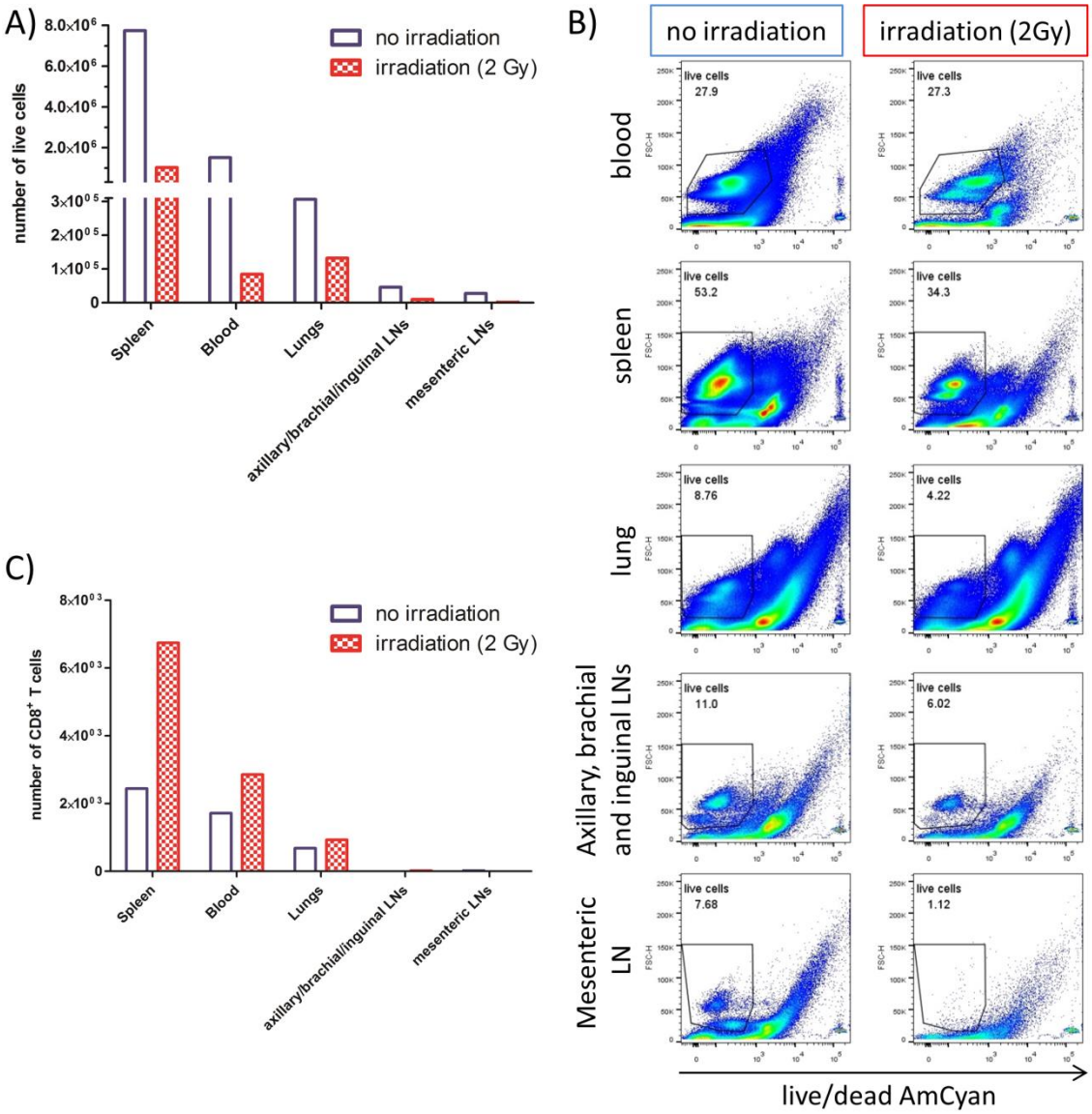

Figure 7.4: Comparison between mouse and human lymphocytes numbers from irradiated and non-irradiated NOD-SCID mice. Non-irradiated (blue) and 2 Gy irradiated (red) NOD-SCID mice were injected i.v. with 5.7 x 10^6 human $CD8^+$ T cells and the spleen, blood, lungs and LNs collected two days later. A) The total number of live cells in each sample was enumerated by flow cytometry using cytocount beads. B) Flow cytometry gating of $AmCyan^-$ live cells in different organs. C) The total number of live human $CD8^+$ T cells in each sample was enumerated by flow cytometry using cytocount beads.

7.4 Adoptive transfer of human wt or Mel$^+$ CD8$^+$ T cells into irradiated Mel526 tumour bearing NOD-SCID mice

Following the two pilot experiments above, a therapeutic adoptive T cell experiment using 13 male NOD-SCID mice was conducted. Mice were injected subcutaneously with 15 x 10^6 Mel526 cells and once tumours had established at day 7, mice were irradiated at 2 Gy and injected i.v. with saline, human wt or Mel$^+$ CD8$^+$ T cells (figure 7.5 A). The human CD8$^+$ T cells injected were enumerated and analysed by flow cytometry as shown in figure 7.5 B and C. Due to a problem with the stimulation cycle of the CD8$^+$ T cells, large numbers of the T cells had died and only 3.8% and 8.6% of the wt respectively Mel$^+$ T cells analysed cells were alive. Therefore the mice were injected with human CD8$^+$ T cells and a large quantity of apoptotic cells and cell debris. The total number of CD8$^+$ T cells available for injection was low and only 1.3 x 10^5 and 1.4 x 10^5 wt or Mel$^+$ live CD8$^+$ T cells respectively were injected (figure 7.5 C). Out of the 1.4 x 10^5 Mel$^+$ T cell population injected, 59.7% were actually Mel$^+$ giving a total of 0.83 x 10^5 tumour-specific CD8$^+$ T cells. It is also of note that 19.2% of Mel$^+$ CD8$^+$ T cells were CCR7$^+$ L-selectin$^+$ whereas the only 3.1% of wt cells were CCR7$^+$ L-selectin$^+$.

Mice were weighed and tumour growth measured by calliper and by imaging for 21 days (figure 7.6 A-C). Mice did not lose weight following irradiation or during the experimental period (figure 7.6 D). Tumour growth was slowest in the saline control group compared to the two groups that received CD8$^+$ T cells. However tumours in the saline group were smaller at the start which could partly explain the observed slower growth. The group of mice that received wt CD8$^+$ T cell was reduced to one mouse by day 21 as two mice were found dead on day 14 and a third mouse had to be culled on day 19 due to sickness. This may have been due to a missing filter on the scantainer cage leading to an infection of these immunodeficient irradiated mice. No statistically significant differences were found between the growth rates of the tumours in the three groups (figure 7.6 E).

At day 21, mice were sacrificed and tumours excised and weighed (figure 7.7 A). Due to the scales not detecting tumours below 10 mg, 3/5 tumours in the saline control group could not be weighed whereas 5/6 tumours from mice that received T cells were large enough to be weighed. The spleen, blood, lungs, draining LNs (dLNs) and non-draining LNs (ndLNs) were collected as well as the tumours. Single cell suspensions were stained for human CD8 and analysed by flow cytometry. The tumour was dissociated and tumour infiltrating lymphocytes (TILs) were isolated by flotation on Ficoll. Human $CD8^+$ T cells were not detected in any organ of any mouse which may simply reflect the low number of $CD8^+$ T cells injected.

Tumour measurement by calliper was compared to DsRed signal and as shown in figure 7.7 B, the two measurements correlated ($r^2 = 0.75$, $p < 0.0001$). However, the correlation between calliper measurements and tumour weight ($r^2 = 0.75$, $p < 0.0001$) was better than that between DsRed intensity and tumour weight ($r^2 = 0.66$, $p < 0.027$) (figure 7.7 C and D).

Overall, Mel^+ $CD8^+$ T cells did not control tumour growth in a superior manner to wt $CD8^+$ T cells. However, tumour growth was increased in mice receiving T cell injections with large amounts of cell debris. One explanation for this could be that the cell debris together with NK recognition of human T cells led to an inflammatory environment enhancing tumour growth. Thus in subsequent adoptive T cell transfer experiments NSG mice were used.

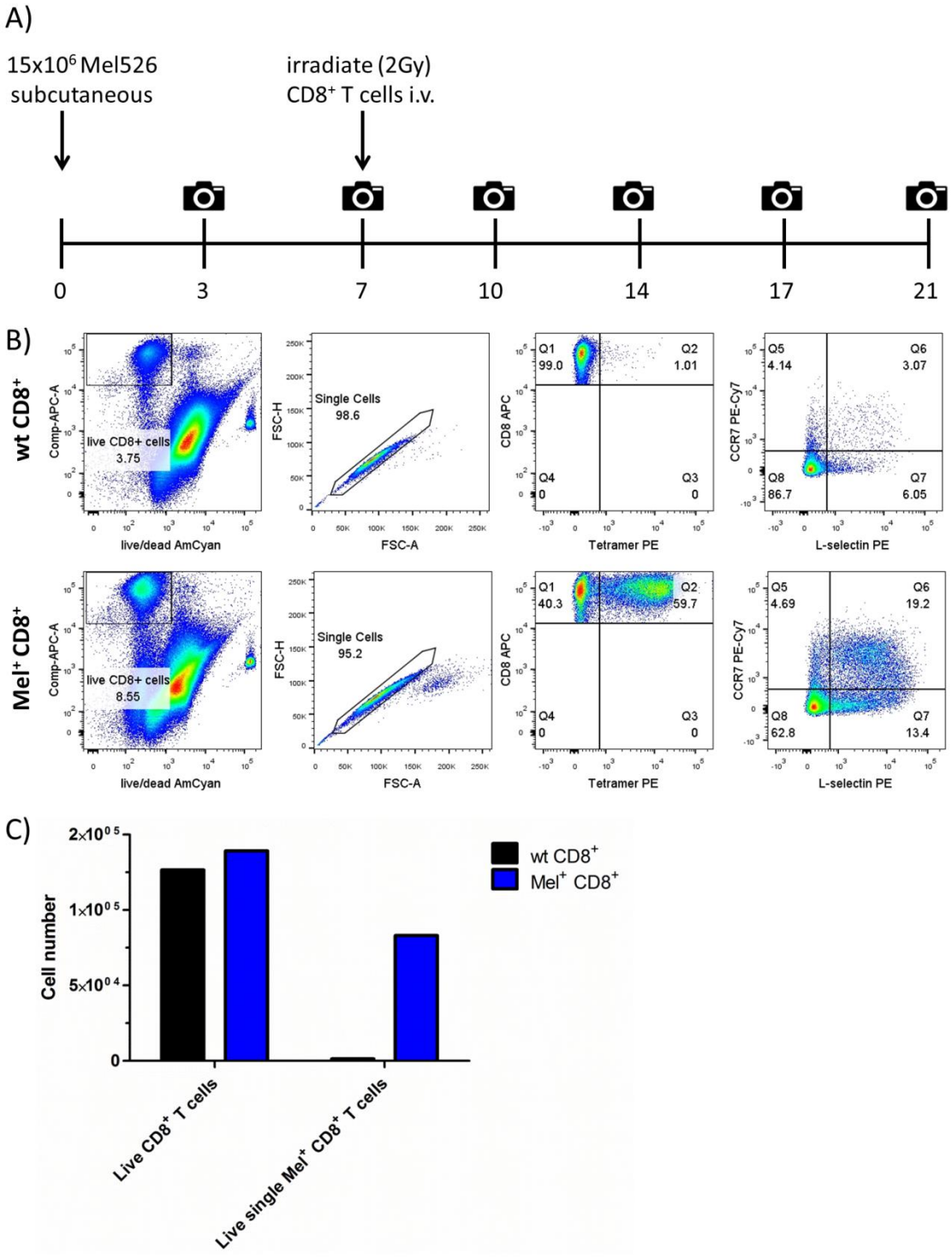

Figure 7.5: Adoptive transfer of human wt or Mel$^+$ CD8$^+$ T cells into irradiated Mel526 tumour bearing NOD-SCID mice. A) Experimental layout for the adoptive transfer of human wt or Mel$^+$ CD8$^+$ T cells into irradiated (2 Gy) NOD-SCID mice 7 days post subcutaneous injection of 15 x 10^6 Mel526 cells. B) Flow cytometry analysis of the human CD8$^+$ T cells used for injection. Cells were stained with an ELA tetramer, anti-CD8, anti-CCR7 and anti-L-selectin Ab and the gating strategy is shown. C) The total number of live human CD8$^+$ T cells injected per mouse was enumerated by flow cytometry using cytocount beads. The number of live Mel$^+$ CD8$^+$ T cells was obtained from the % of tetramer$^+$ cells in B).

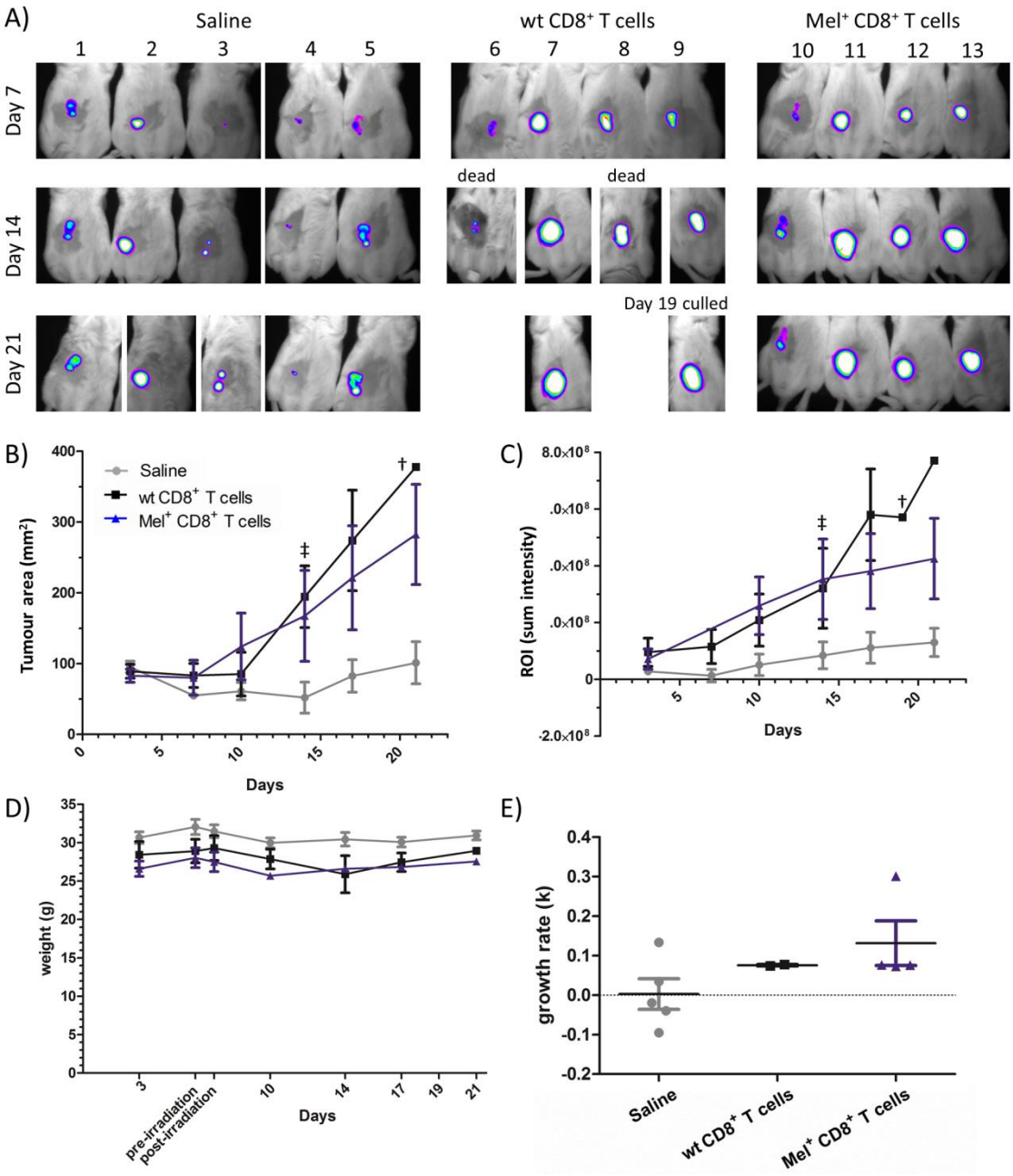

Figure 7.6: Tumour growth in irradiated Mel526 tumour bearing NOD-SCID mice injected with human wt or Mel$^+$ CD8$^+$ T cells. A) and C) Tumour growth was monitored by imaging. The fluorescence images were superimposed on white light images and the pixel intensity in a defined a region of interest (ROI) around the tumour was quantified by subtracting the pixel intensity of a ROI outside of the tumour. Data was grouped into saline (grey), wt (black) or Mel$^+$ (blue) CD8$^+$ T cell groups. Measurements on day 7 were done before T cells were injected. B) Tumour growth was monitored by measuring the tumour dimensions using callipers and data grouped. D) Mice were weighed throughout the experiment and grouped data is shown. E) The tumour growth rate for each group is shown (two mice found dead at day 14 were excluded). No statistically significant differences were observed by a One-way ANOVA with a post-hoc Tukey test. ‡ indicates two mice found dead on day 14 and † indicates the culling of one mouse due to sickness on day 19. Error bars show the SEM.

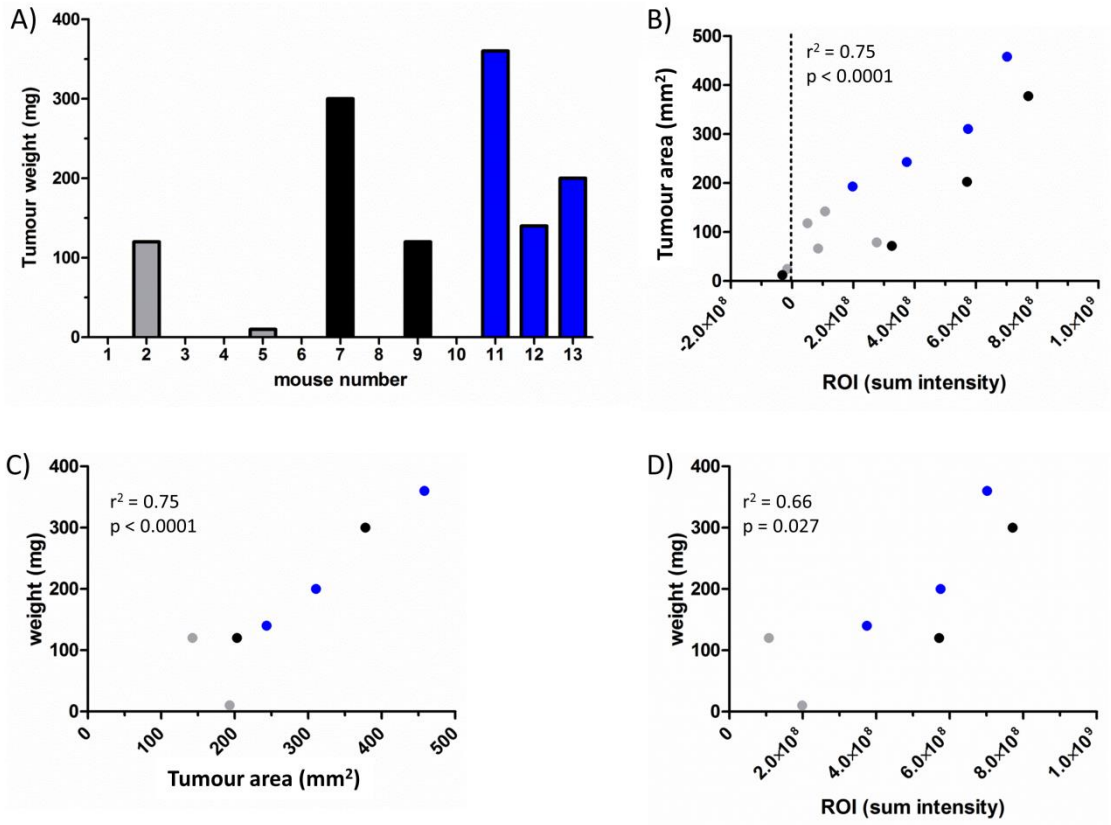

Figure 7.7: Tumour weight at the day 21 and comparison of different methods used to measure tumour growth. A) Tumours were weighed after mice from the saline (grey), wt (black) or Mel^+ (blue) $CD8^+$ T cell groups were culled and tumours excised. B) Correlation of the tumour area measured by calliper and the sum intensity of DsRed signal measured by Kodak imaging of each tumour is shown at the endpoint (day 14, 19 and 21 respectively). C) Correlation between the tumour area and tumour weight at the endpoint (day 19 or 21). D) Correlation between the sum intensity of the DsRed signal and tumour weight at the endpoint (day 19 or 21) for each tumour is shown. The r^2 Pearson's correlation coefficient was calculated for data in B-D.

7.5 Mel526 tumour cell titration in NSG mice

Age-matched female NSG mice were purchased from Charles River (Kent, UK) and mice rested for more than a week after arrival. Mice were not irradiated as NSG mice are more immunodeficient than NOD-SCID mice. A Mel526 tumour cell titration was done to determine the optimal Mel526 cell dose to generate reproducible tumour take in NSG mice.

A total of 9 NSG mice were injected subcutaneously into the left flank with 0.5, 2 or 8 x 10^6 Mel526 cells and tumour growth was measured for 34 days (figure 7.8). At the low dose of 0.5 x 10^6 Mel526 cells, tumours were only visible by day 14 using Kodak imaging and day 21 using callipers. Both the middle and the high tumour cell dose yielded large tumours within 34 days, as shown by calliper and Kodak measurements (figure 7.8 A and D). Both groups showed similar sized tumours and growth curves.

The dissection of the tumours at day 34, or day 28 for mouse number 9, showed that the tumour in mouse number 4 was much bigger than the other tumours (figure 7.9 A). This was not evident from the calliper or Kodak measurements and was due to the tumour growing into the peritoneal cavity as well as subcutaneously. No statistically significant correlation was observed between the tumour weight and area or weight and DsRed signal (figure 7.9 C-D). However the area and DsRed signal measurements correlated (r^2 = 0.76, P = 0.002) (figure 7.9 B).

Overall, the results for the 2 x 10^6 and 8 x 10^6 Mel526 cell doses showed that all 6 mice established growing tumours. It was concluded that a subcutaneous injection of 7.5 fold fewer Mel526 cells in the NSG mice (2 x 10^6) than in the NOD-SCID mice (15 x 10^6) was sufficient to generate established tumours by day 7, the chosen day for adoptive T cell transfers (figure 7.8 E). This tumour cell number was thus chosen for subsequent ACT experiments.

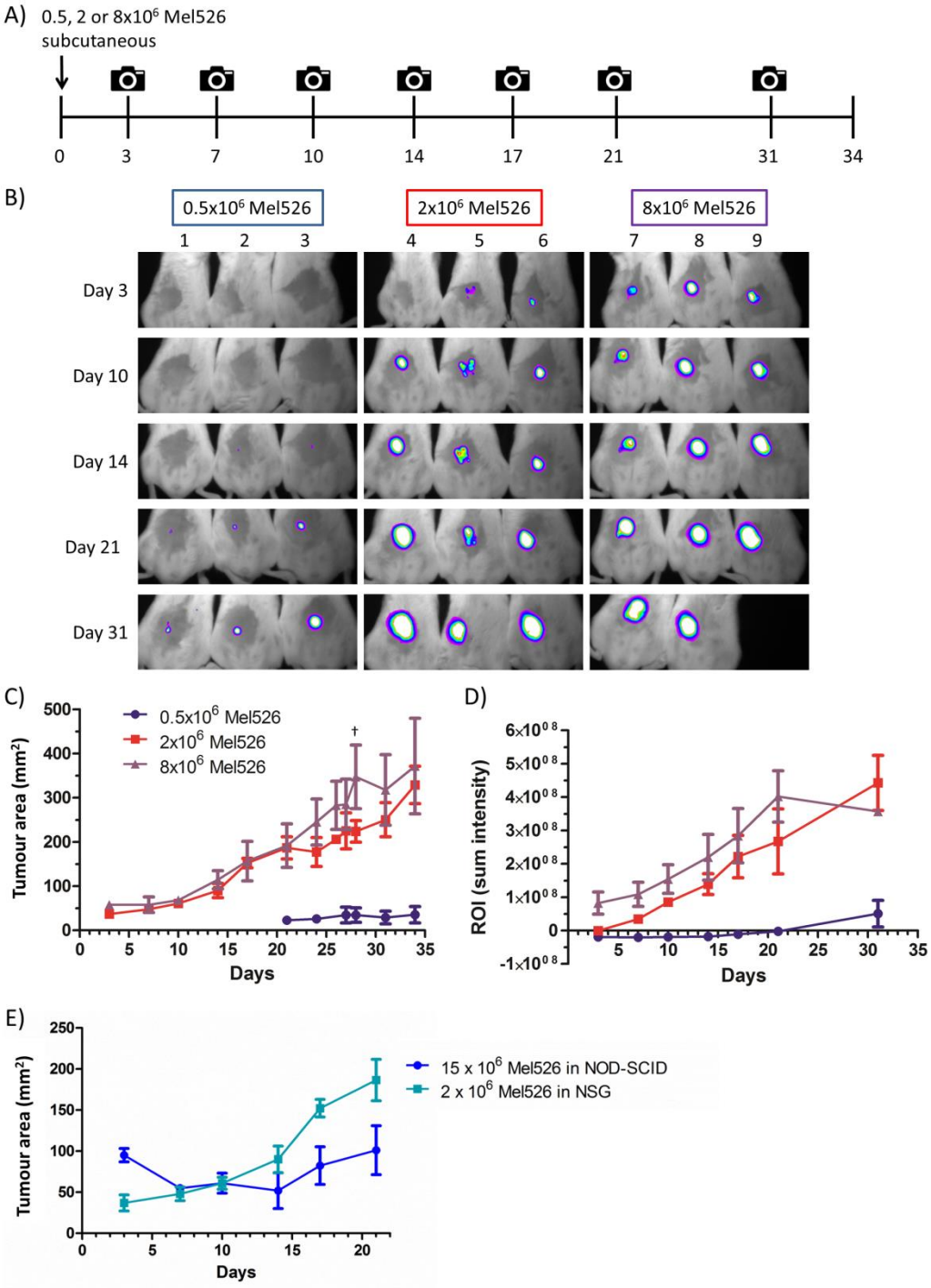

Figure 7.8: Titration of Mel526 tumour cells in NSG mice. A) Experimental layout for the titration of Mel526 tumour cells in NSG mice. Three mice were each injected subcutaneously with 0.5 x 10^6 (blue), 2 x 10^6 (red) or 8 x 10^6 (purple) Mel526 cells. B) and D) Tumour growth was monitored by imaging. The fluorescence images were superimposed on white light images and the pixel intensity in a defined a region of interest (ROI) around the tumour was quantified by subtracting the pixel intensity of a ROI outside of the tumour. C) Tumour growth was monitored by measuring the tumour dimensions using callipers and data grouped. † indicates the culling of mouse number 9 due to a large tumour at day 28. Error bars show the SEM. E) Comparison of tumour growth in NOD-SCID or NSG mice injected with 15 x 10^6 (figure 7.6 B) or 2 x 10^6 Mel526 (C) cells respectively and no human T cells.

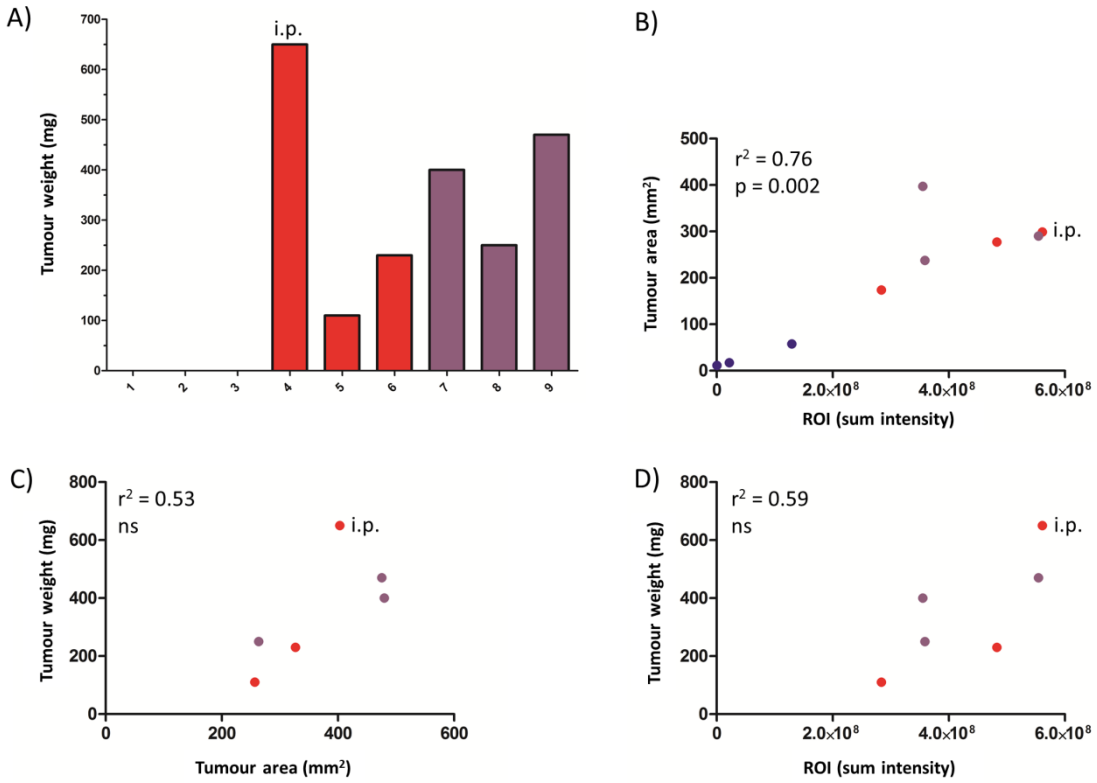

Figure 7.9: Tumour weight and comparison of different methods used to measure tumour growth. A) Tumours were weighed after mice injected with 0.5 x 10^6 (blue), 2 x 10^6 (red) or 8 x 10^6 (purple) Mel526 cells were culled and tumours excised. B) Correlation of the tumour area measured by calliper and the sum intensity of DsRed signal of each tumour is shown at the endpoint (day 28 and 31 respectively). C) Correlation between the tumour area and tumour weight at the endpoint (day 28 and 31). D) Correlation between the sum intensity of the DsRed signal and tumour weight at the endpoint (day 28 and 31) for each tumour is shown. Pearson's correlation coefficient was calculated for data in B-D. The tumour of mouse 4 was found to have grown intraperitoneally (i.p.).

7.6 Adoptive transfer of human wt, Mel$^+$ or mutant SHP-1 Mel$^+$ CD8$^+$ T cells into Mel526 tumour bearing NSG mice

The tumour cell killing potentials of Mel$^+$ SHP-1 sufficient and mutant CD8$^+$ T cells were compared *in vivo* in a therapeutic adoptive T cell experiment. Female NSG mice were injected subcutaneously with 2 x 10^6 Mel526 cells and once tumours had established at day 7, mice were injected i.v. with saline, human wt, Mel$^+$ or mutant SHP-1 Mel$^+$ CD8$^+$ T cells (figure 7.10). The latter being a population encompassing a minority of T cells with SHP-1 mutations. The human CD8$^+$ T cells injected were enumerated and analysed by flow cytometry as shown in figure 7.10 B and C. Groups of 4 mice each received either no T cells or a low number of wt or Mel$^+$ T cells (2.3 and 2.0 x 10^6 cells respectively) and groups of 4, 7 and 5 mice received a high number of wt, Mel$^+$ or mutant SHP-1 Mel$^+$ T cells (3.7, 3.1 and 3.2 x 10^6 cells respectively) (figure 7.10 C). There were insufficient mutant SHP-1 Mel$^+$ T cells to test at the lower dose of T cells.

84.4% of cells in the Mel$^+$ population and 90.5% of cells in the mutant SHP-1 Mel$^+$ population actually expressed tumour-specific TCR measured by ELA tetramer binding. The latter contained 80.5% ZFN2-CD2$^+$ Mel$^+$ cells. A Cel-I assay confirmed the presence of mutant SHP-1 cells and approximately 10.1% of the mutant SHP-1 Mel$^+$ cells were found to contain mutations in the SHP-1 gene (figure 7.10 D).

As shown in figure 7.11 A, tumours formed in all 28 mice and grew up to 747 mm^2 in area (mouse number 3). Overall, the sizes of tumours the day before adoptive T cell transfer (day 6) were largest in the 'high mutant SHP-1 Mel$^+$ CD8$^+$' group and smallest in the 'saline' and the 'low wt CD8$^+$' groups. From day 34 onwards 11/27 mice started to develop necrotic lesions within the tumour as shown in figure 7.11 B. These lesions were independent of the treatment

group. Necrotic tissue covered the DsRed signal of healthy tumour cells as seen in figure 7.11 A for mice numbered 3, 16, 21 and 28 on day 41.

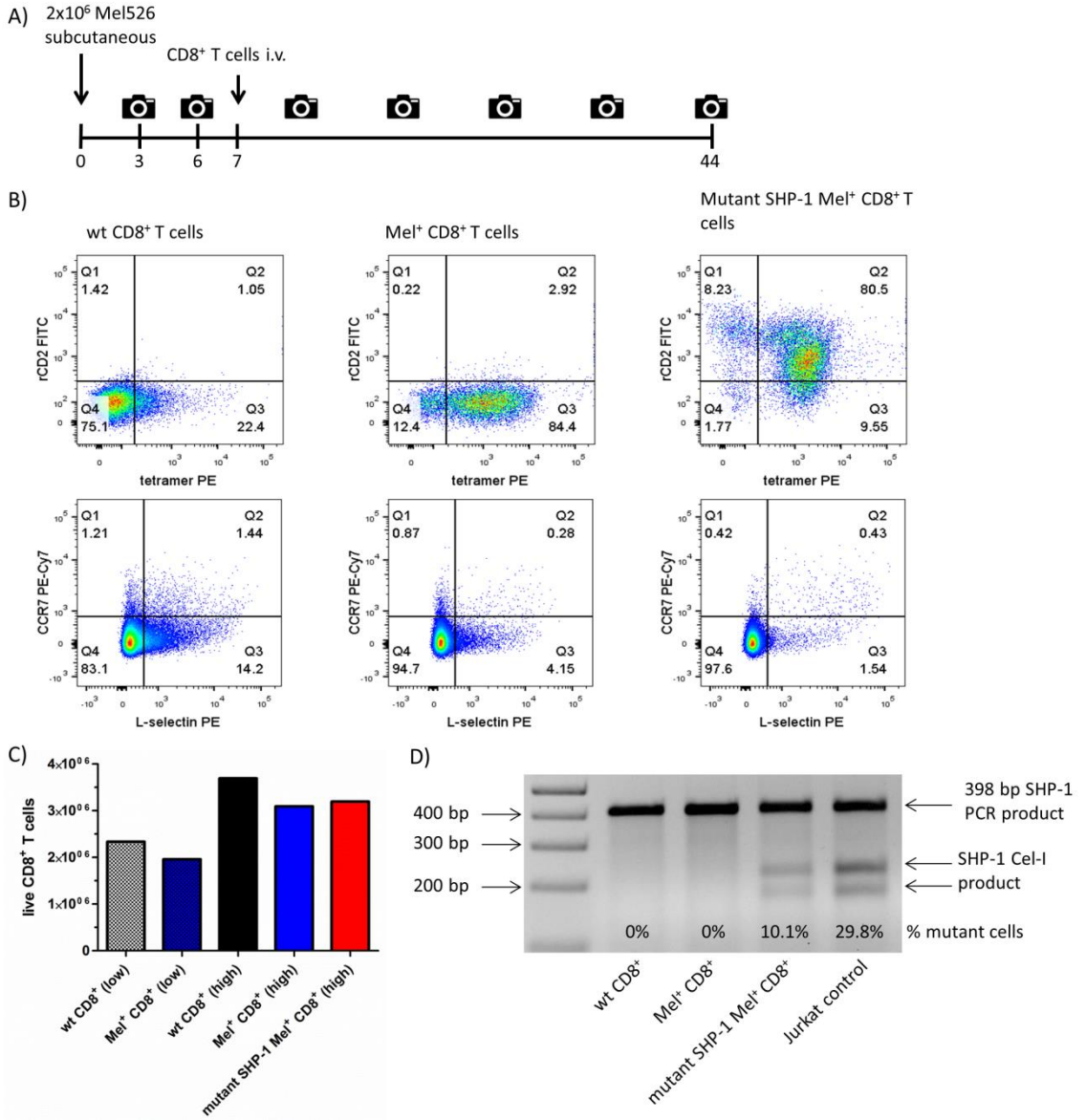

Figure 7.10: Adoptive transfer of human wt, Mel$^+$ or mutant SHP-1 Mel$^+$ CD8$^+$ T cells into Mel526 tumour bearing NSG mice. A) Experimental layout for the adoptive transfer of human wt, Mel$^+$ or mutant SHP-1 Mel$^+$ CD8$^+$ T cells into NSG mice 7 days post subcutaneous injection of 2 x 10^6 Mel526 cells. B) Flow cytometry analysis of the human CD8$^+$ T cells injected. Cells were stained with ELA tetramer, anti-CD8, anti-CCR7 and anti-L-selectin Ab. C) The total number of live human CD8$^+$ T cells injected per mouse was enumerated by flow cytometry using cytocount beads. D) gDNA extracted from wt, Mel$^+$ and mutant SHP-1 Mel$^+$ CD8$^+$ T cells was used to PCR amplify 398 bp SHP-1 genomic segment. After hybridisation of the PCR product and digestion of the DNA with the Cel-I enzyme, mutated SHP-1 DNA is indicated by 178 bp and 220 bp DNA cleavage fragments. Jurkat cells transduced with both ZFN LVs were used as a positive control. The % of cells harbouring SHP-1 mutations was obtained by ImageJ analysis.

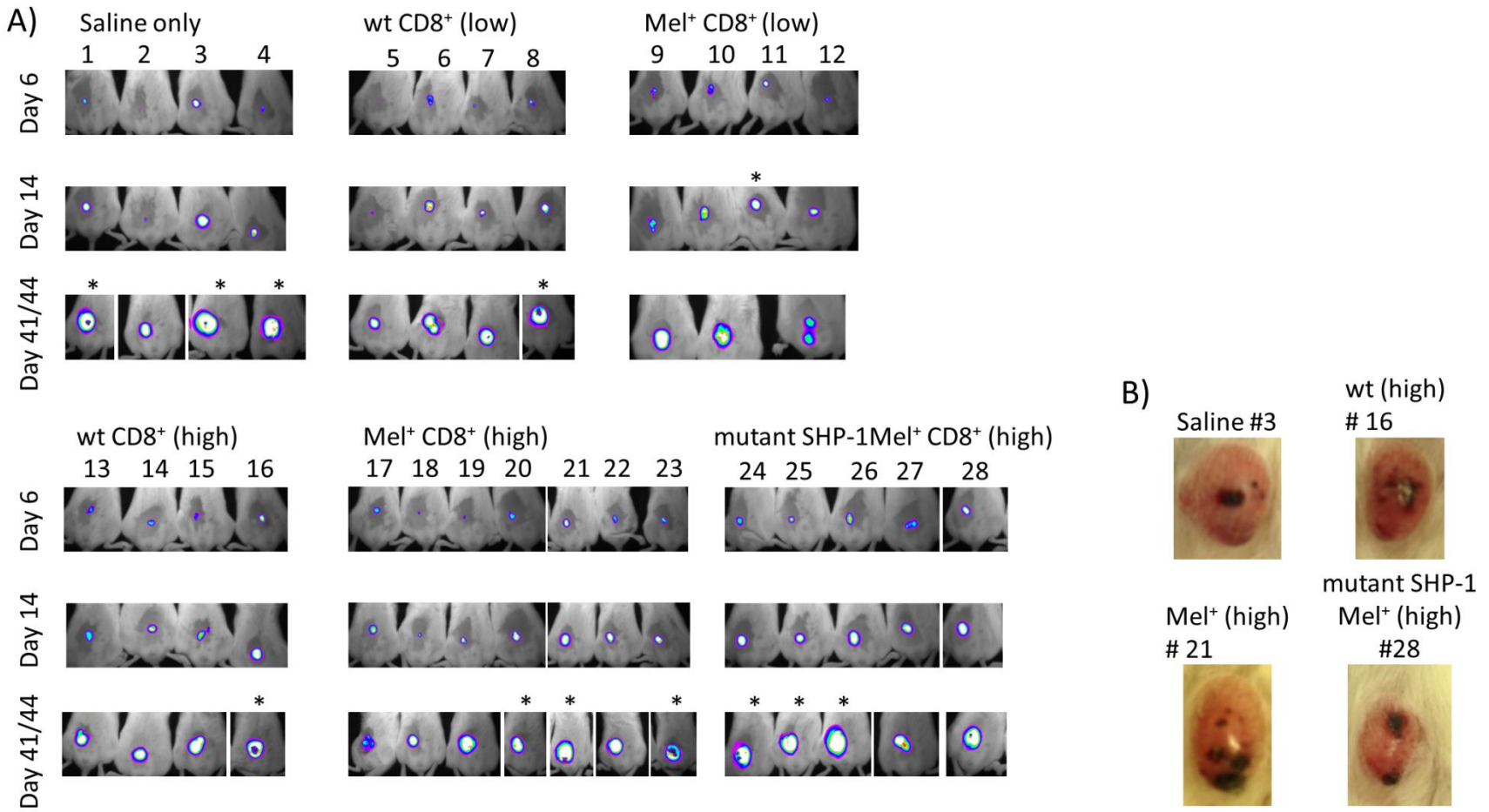

Figure 7.11: Growth of Mel526 tumours in NSG mice injected with human wt, Mel$^+$ or mutant SHP-1 Mel$^+$ CD8$^+$ T cells. A) Tumour growth was monitored by imaging the DsRed signal using the Kodak FX-Pro camera and the signal was analysed using the Carestream software. The fluorescence images were superimposed on white light images. * indicates mice sacrificed on day 41 due to a high level of necrotic lesions, except for mouse number 11 which was culled on day 14 due to sickness. B) Representative images of necrotic lesions within intact tumours of four different groups are shown at day 37.

Looking at the grouped growth curves for mice injected with low (figure 7.12) or high (figure 7.13) doses of $CD8^+$ T cells, no significant differences were found between the groups using either tumour areas or DsRed signals as a readout. There are differences between the growth curves using either the user-dependant or user-independent measuring method but overall the trends of the growth curves look similar (figure 7.12 and 7.13 A and B). The tumour growth curves for each mouse show that the variation between mice in each group is large. For example, tumours in the saline group ranged from 137 to 747 mm^2 at the endpoint (figure 7.12 and 7.13 C).

Mice were sacrificed on day 41 or day 44 and tumours were weighed (figure 7.14 A). The tumour from mouse 17 had grown into the peritoneum and was found to be considerably larger than the others at 107 mg. There was better correlation between the calliper measured area and the tumour weight than the DsRed signal and the tumour weight ($r = 0.66$ vs. $r = 0.46$) (figure 7.14 C and D). There were no statistically significant differences between the growth rates of tumours from all five groups (figure 7.14 E).

Overall this experiment showed that Mel^+ $CD8^+$ T cells were not able to kill Mel526 tumour cells *in vivo* and that mutations in the SHP-1 gene did not overcome this. The absence of an anti-tumour effect could be due to poor survival of the human $CD8^+$ T cells in the mouse host as at the end of this experiment no human $CD8^+$ T cells were found in the spleen, blood, tumour and dLNs (data not shown).

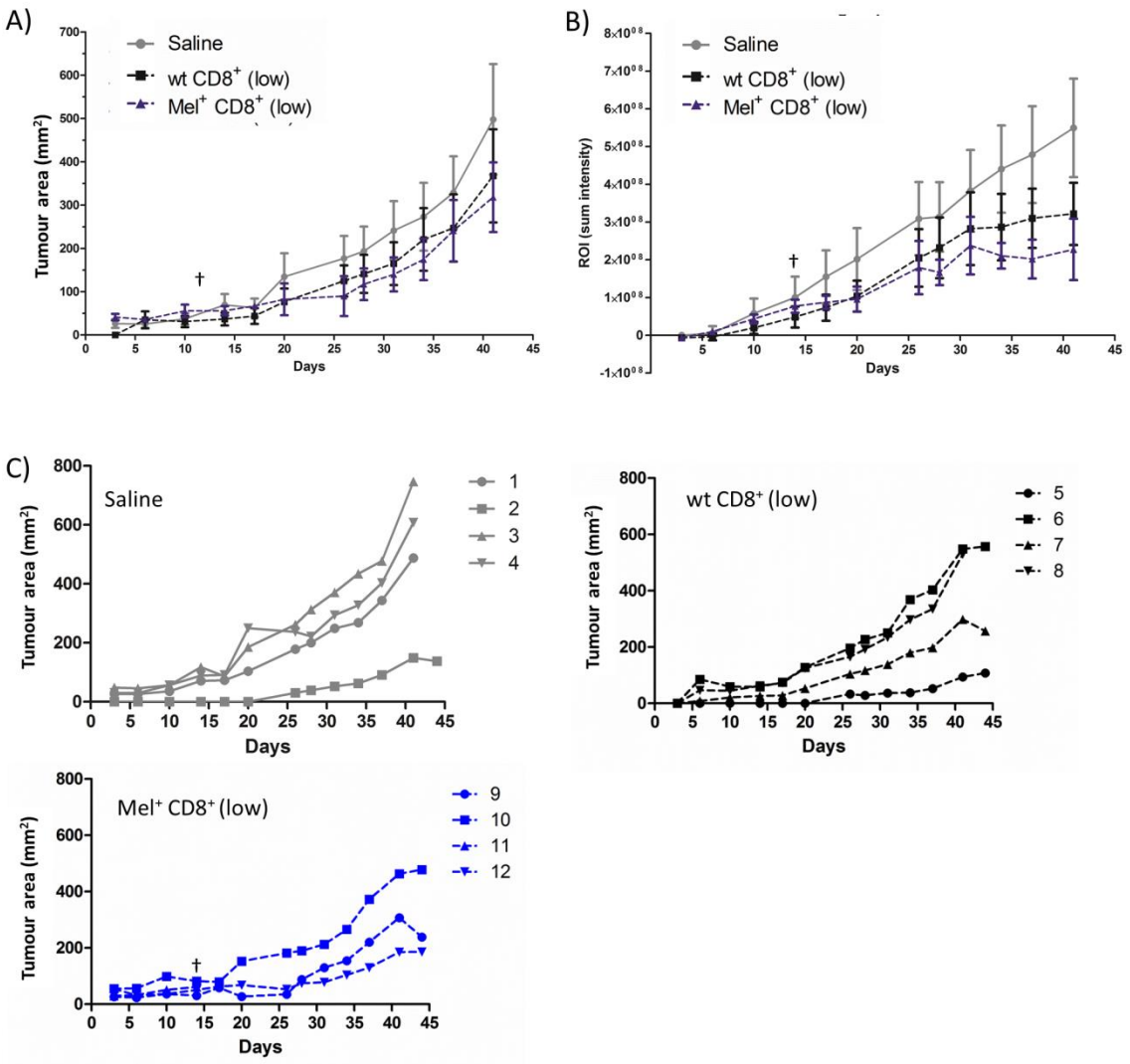

Figure 7.12: Tumour growth in NSG mice that received a low dose of human wt or Mel$^+$ CD8$^+$ T cells. A) Tumour growth of the saline (grey), low wt (black dotted) or low Mel$^+$ (blue dotted) CD8$^+$ T cell groups was monitored by measuring the tumour dimensions using callipers. Individual tumour growth curves are shown in C). B) Tumour growth was monitored by imaging. The fluorescence images were superimposed on white light images and the pixel intensity in a defined a region of interest (ROI) around the tumour was quantified by subtracting the pixel intensity of a ROI outside of the tumour. † indicates the culling of one mouse due to sickness at day 14. The error bars show the SEM. No statistically significant differences were observed.

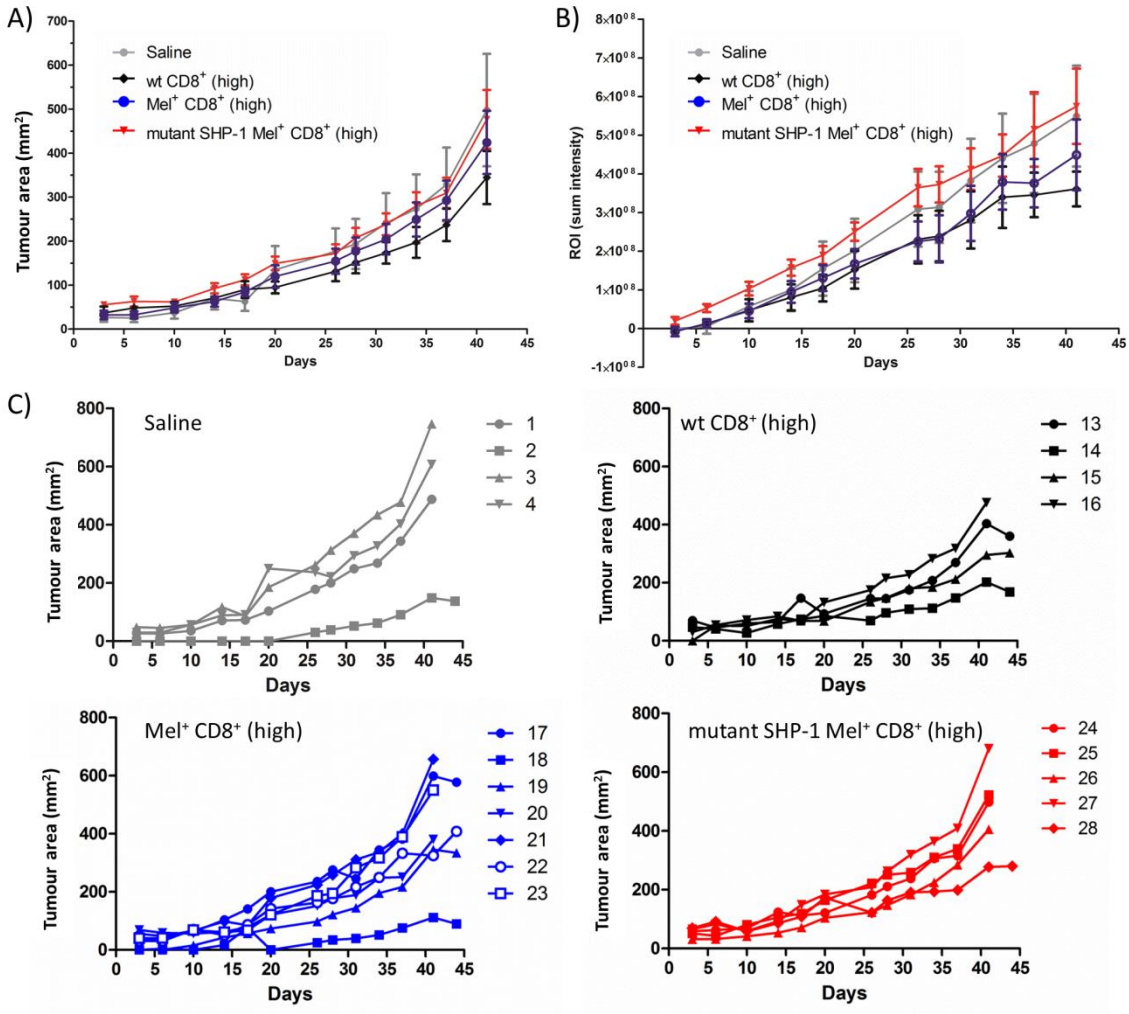

Figure 7.13: Tumour growth in NSG mice that received a high dose human wt, Mel+ or mutant SHP-1 Mel+ CD8+ T cells. A) Tumour growth of the saline (grey), high wt (black), high Mel$^+$ (blue) or mutant SHP-1 Mel$^+$ (red) CD8$^+$ T cell groups was monitored by measuring the tumour dimensions using callipers. Individual tumour growth curves are shown in C). B) Tumour growth was monitored by imaging. The fluorescence images were superimposed on white light images and the pixel intensity in a defined a region of interest (ROI) around the tumour was quantified by subtracting the pixel intensity of a ROI outside of the tumour. The error bars show the SEM. No statistically significant differences were observed.

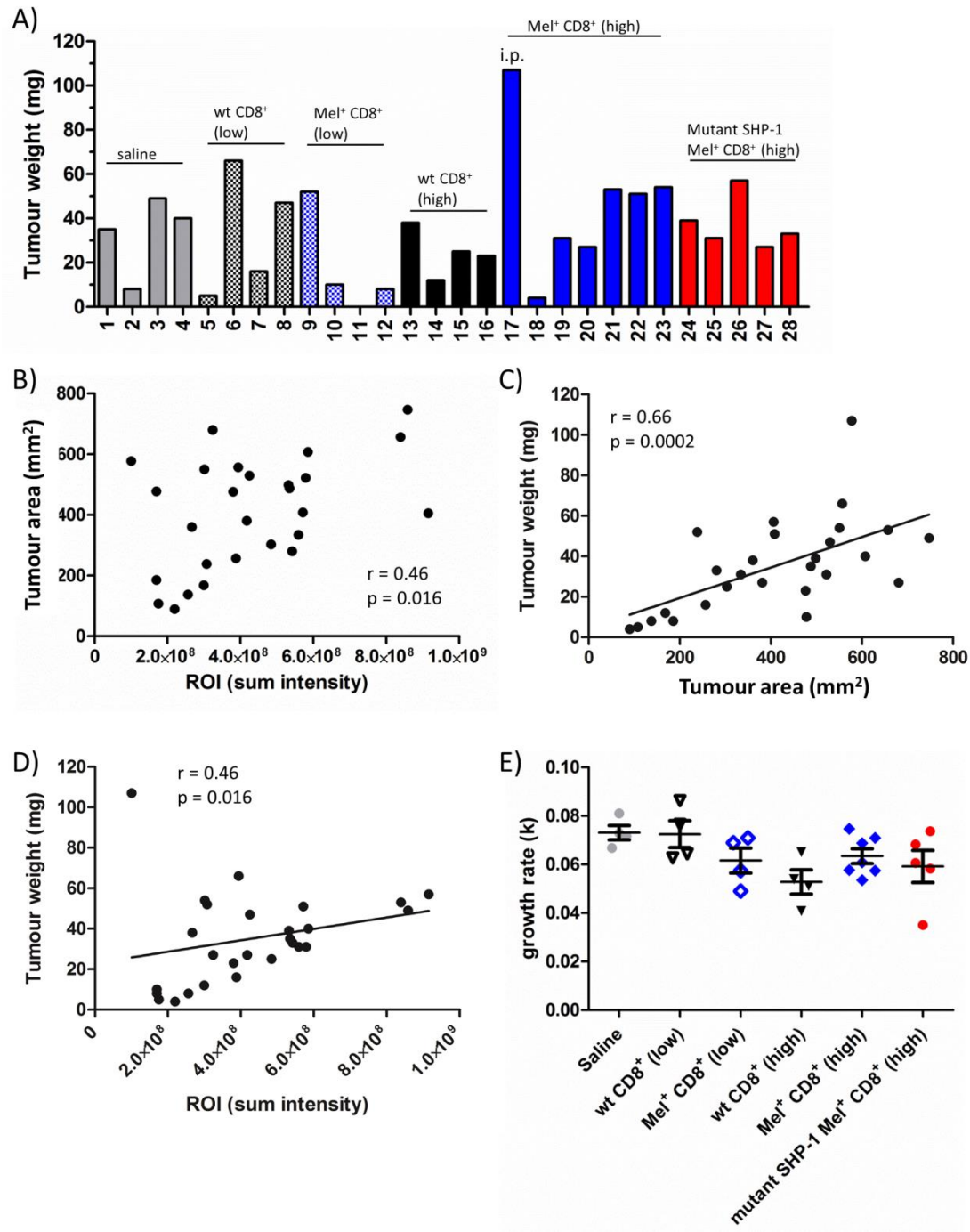

Figure 7.14: Tumour weight at the day 41/44 and comparison of different tumour measuring methods. A) Tumours were weighed after mice from the saline (grey), low wt (black dotted), low Mel$^+$ (blue dotted), high wt (black), high Mel$^+$ (blue) or high mutant SHP-1 Mel$^+$ (red) CD8$^+$ T cell groups were culled and tumours excised. The tumour in mouse 17 had grown into the peritoneum (i.p.). B) Correlation of the tumour area measured by calliper and the sum intensity of DsRed signal of each tumour is shown at the endpoint (day 41 or 44). C) Correlation between the tumour area and tumour weight at the endpoint (day 41 or 44) for each tumour is shown. D) Correlation between the sum intensity of the DsRed signal and tumour weight at the endpoint (day 41 or 44) for each tumour is shown. Spearman correlation coefficient was calculated for data in B, C and D. E) Tumour growth rates for all 5 groups are shown. No statistically significant differences were observed. The error bars show the SEM.

7.7 Conclusion

The finding that 5x greater numbers of Mel526 cells were needed to establish tumours in NOD-SCID mice compared to NSG mice could be explained by the residual NK activity observed in the NOD-SCID mice compared to much less NK activity in the NSG mice (Shultz et al. 1995). It is possible that the white 'capsular' structure around the Mel526 tumour in section 7.2 is part of the rejection of the tumour by host NK and myeloid cells. Graft rejection of both the human tumour and T cells could contribute to suboptimal experimental results in the NOD-SCID model and, although irradiation potentially reduced the NK activity in the short-term, long term tumour regression experiments may require a more robust and long-term immunodeficiency. Due to these concerns, subsequent experiments were done in NSG mice.

It was shown here that the measurement of the tumour by calliper and by DsRed imaging correlated in most instances and both measurement methods have their advantages and disadvantages. The DsRed signal can be covered by necrotic tissue or cells might lose the DsRed transgene expression *in vivo* due to transgene silencing (Ellis 2005), both resulting in an underestimation of the tumour size. Meanwhile, calliper measurements are user-dependant and small tumours, such as those at day 14 in figure 7.8 B), were not detectable by calliper measurement, yet they showed up by imaging.

The lack of anti-tumour effect of the adoptively transferred tumour-specific Mel^{+} T cells could be due to several factors. Firstly, most of the T cells generated here by several rounds of stimulation in IL-2 and IL-15 (3 or 5 cycles) were L-selectin and CCR7 negative, indicating a terminally differentiated effector phenotype. It has been shown by several groups that 'younger' and/or memory T cells are better for therapy rather than effector T cells. This might be due to the prolonged survival of the memory rather than the effector T cells *in vivo*, as shown in NOD-SCID mice (Yang et al. 2011). Altering the cytokines used for T cell culture (e.g.:

IL-15 and IL-7 rather than IL-2) can enhance the formation of memory T cells (Gattinoni et al. 2005; Alcantar-Orozco et al. 2013) and could be considered for future ACT experiments.

Secondly, the lack of cytokines in NSG mice, due to the lack of lymphocytes, can leave the T cells deprived of support for survival and engraftment. Injections of exogenous IL-2 have been shown to correlate with a better outcome in mice (Klebanoff et al. 2011b). IL-15 has also been shown to enhance T cell engraftment in immunodeficient mice (Sun et al. 2006). A superior strategy would have been to inject immunocomplexes of IL-2 and anti-IL-2 monoclonal Ab and/or IL-15 and IL-15α-Fc chimera as they have a longer half-life *in vivo* than the cytokines alone and they promote T cell survival in mice and enhance anti-tumour effects of leucocytes (Votavova et al. 2014). Additionally, the injection of irradiated PBMCs and cognate FLT peptide could possibly have enhanced the anti-tumour effect of the Mel^+ T cells by providing APCs and further support.

Thirdly, the expression of the Mel TCR transgenes in T cells will have led to the mispairing with endogenous TCR α and β chains. Although the Mel^+ T cells showed potent target killing of Mel526 cells at E:T ratios as low as 0.3:1 *in vitro* in Chapter 5, the T cells expressing mispaired TCR might not be potent enough to induce measurable tumour killing *in vivo*. This hypothesis is supported by unpublished data from our group, where T cells from mice hemizygous for a tumour specific transgenic TCR were not able to protect against a B16 tumour when compared to T cells from homozygous transgenic TCR mice.

Overall, future xenograft and ACT experiments in NSG mice should be done with 'younger' T cells and combined with injections of cytokine immunocomplexes and peptide pulsed irradiated PBMCs. However, regardless of how much exogenous support will be provided, NSG mice will always provide very limited lymphoid structures, with only the mesenteric LNs developing properly (Shultz et al. 2012). This, together with the incompatibility of some human

and mouse adhesion molecules and ligands, will be a major problem to study the effect of shedding-resistant L-selectin on the homing of T cells to LNs and to the tumour.

Chapter 8: General discussion and conclusions

Alternative methods of generating SHP-1 deficient T cells

It was demonstrated in this thesis that lentivirally delivered ZFNs can successfully generate mutations in the SHP-1 gene in human primary $CD8^+$ T cells. However, it was not established whether these mutations were mono- or biallelic and whether they resulted in a complete loss of functional SHP-1 protein. For this assessment, T cells would have to be cloned and analysed on a clonal level, as the sorting of potential SHP-1 deficient primary T cells generated in this thesis was not possible. A possible improvement to the current ZFN delivery system would have been the inclusion of a surface marker within the ZFN1 delivery vector such as truncated versions of the nerve growth factor or CD19 receptors (Barese and Dunbar 2011). These two marker proteins have been found to be non-immunogenic and thus suitable for *in vivo* experiments. Double markers, rather than the currently used single rat CD2 marker, could be included into the vectors encoding ZFN1 and ZFN2 respectively, allowing doubly transduced cells to be isolated by FACS.

Cells transduced with integrase proficient LV expressing the ZFNs will only ever be of use for experiments *in vitro* or in mice due to the high risk associated with the stable integration of the ZFNs and resulting possibility of increased off-target mutations and a conceivable risk of mutational integration. For clinical trials, an alternative delivery method where the ZFNs would only be expressed transiently would have to be used. One such method would be to use integrase deficient LVs. However, in this thesis no SHP-1 mutations were observed when employing integrase deficient LVs. As well as adeno-associated viral delivery of ZFNs, non-viral approaches might be used as 'hit-and-run' delivery methods. In the long term, direct protein delivery of ZFNs might be the most straightforward method if preliminary studies prove to be reproducible (Gaj et al. 2012; Liu et al. 2015). Currently, the most easily adoptable non-viral

delivery method would be electroporation of T cells with plasmid DNA or ideally mRNA. The latter eliminates all risk of ZFN genetic material integrating into the host genome and is less toxic than plasmid DNA. However, mRNA is significantly less stable *in vitro* and more elaborate to produce than plasmid DNA. Considerable optimisation would have to be done to establish optimal conditions for electroporation in order to achieve minimal toxicity to primary $CD8^+$ T cells and this was not within the scope of this project.

As well as altering the delivery method, the frequency of ZFN mediated SHP-1 mutations could potentially be increased by cold shocking the $CD8^+$ T cells at 30°C for 2-3 days, as this was shown to increase mutations when cells were electroporated with plasmid DNA or mRNA encoding for a pair of ZFNs (Doyon et al. 2010). It is thought that this is partly due to a decrease in protein and mRNA turnover in cells exposed to mild hypothermia.

Although not of major concern for the *in vitro* functional assays or the *in vivo* experiments performed in this thesis, the specificity of the SHP-1 specific ZFN pair would have to be tested extensively before ZFN modified T cells could be used in a clinical setting. Firstly, the genome can be screened *in silico* for possible off-target DNA sequences, based on the sequence homology with the target sites. These sequences can then be screened for mutations *in vitro* and in cells. In addition, it would be preferable to screen the whole genome in a more unbiased way, as previous studies identified off-target mutations that were not predicted by the above mentioned method (Gabriel et al. 2011). However, the screening methods employed by Gabriel *et al.* are very labour intensive and outside of the scope of this thesis (Mussolino and Cathomen 2011). Since the pair of SHP-1 ZFNs used in this thesis were designed, newer, more specific versions of ZFNs that further enhance the need for dimerization by ZFNs have been described and could be used to reduce the potential of off-target mutations (Doyon et al. 2011).

Newer methods of gene editing have emerged since the start of this project, namely transcription activator-like effector nucleases (TALENs) and RNA-guided nucleases derived from clustered regulatory interspaced short palindromic repeats (CRISPR). Both CRISPR and TALENs have been found to generate higher average mutation rates of approximately 20% compared to 10% for ZFNs (Kim and Kim 2014). A major advantage of the CRISPR system is that only the guide RNA sequence needs to be newly designed for each target whereas new arrays of DNA specific protein domains need to be assembled and tested for each target gene for ZFNs and TALENs. Due to the simplicity of designing short RNA sequences, genome editing using CRISPR has been used for the rapid generation and subsequent screening of large libraries of knockout mouse embryonic stem cells *in vitro* (Koike-Yusa et al. 2014). However, to date CRISPR modified cells have not been used for clinical trials. The DNA sequence encoding for the ZFN pairs (~ 1 kb x 2) is at least two times smaller than that of the CRISPR system (~ 4.3 kb) and TALENs (~ 3kb x 2) and thus the former is preferential for encoding into non-integrating adenoviral based vectors used extensively in clinical settings. A problem with the TALEN DNA sequence, and to a lesser degree with that of ZFNs, is that it is very repetitive, which can lead to recombination between the ZFN pairs or TALENs and the deletion of sequence when packaging into adeno-associated viral vectors and LVs, as observed in this thesis. The CRISPR system does not have this issue.

It is believed that the system with the possibly lowest off-target rate is TALENs, followed by CRISPR and ZFNs (Ain et al. 2014). However, it has been shown that the CRISPR system can tolerate up to 5 nucleotides of mismatch DNA (Fu et al. 2013). Additionally, the study on specificity was performed with non-commercial ZFNs. It is of importance to note that ZFNs which are designed and tested by commercial companies have the advantage of being selected for high efficiency and against off-target mediated toxicity.

An alternative to genome editing is genome silencing. Here, ZFs are not linked to the nuclease domain of FokI but to the catalytic domain of the DNA methyltransferase 3A or to the transcription repressor domain of the Krueppel associated box (KRAB) (Davis and Stokoe 2010). The former has been shown resulting in inheritable epigenetic changes leading to a prolonged silencing of the target gene (Stolzenburg et al. 2015). The use of ZF-KRAB repressors has shown to result in over 50% repression of targeted genes in mammalian cells (Ren et al. 2002). This could be advantageous to ZFNs as the latter potentially introduce mutations that do not lead to the complete loss of target gene expression. Additionally, as opposed to genetic changes, methylation of the gene is reversible provided the engineered genome silencing or repressor protein is only expressed transiently.

Although ZFNs maybe not as efficient at inducing high frequencies of mutations, ZFNs still seem to be the safest option for clinical applications, due to the depth of experience with ZFNs and with the approval of clinical trials using ZFN modified human T cells (Tebas et al. 2014). This might change in the future, once more progress has been made with studying the biosafety of TALENs and CRISPR modified human cells in preclinical studies. For now, ZFNs are still the safest choice.

SHP-1 deficiency and adoptive T cell therapy

In this thesis, a phenotype associated with human SHP-1 deficient primary $CD8^+$ T cells was not detected, possibly due to the low frequency of SHP-1 deficient cells in the studied population. However, the initial hypothesis that a genetic deletion of SHP-1 in human $CD8^+$ T cell is beneficial for ACT, due to an enhanced entrance into proliferation leading to a greater number of tumour-specific T cells, is still valid. Based on mouse data using T cells from motheaten or SHP-1 floxed mice, it was shown that a lack of SHP-1 decreases the activation threshold of T

cells (Kilgore et al. 2003; Fowler et al. 2010) and that SHP-1 deficient T cells are activated by epitopes that induce anergy or tolerance in wt T cells (Schnell et al. 2009). The latter is important for ACT, especially for TIL therapy, as the TAA are often weakly immunogenic and SHP-1 sufficient T cells might not be fully activated. Thus loss of SHP-1 in these TILs could potentially 'unmask' a tumour reactivity of T cells in the tumour environment, where the tumour is employing a multitude of mechanisms to limit T cell activation. It was shown that pharmacological inhibition of SHP-1 in T cells from elderly patients, which generally express increased levels of catalytically active SHP-1 protein, could recover T cell responses in these cells (Le Page et al. 2014). This supports the hypothesis that loss of SHP-1 in T cells can unleash T cell responses and may be especially relevant when conducting ACT in elderly patients, where the T cells are potentially less responsive.

One major concern about genetically deleting SHP-1 in T cells is the potential development of severe autoimmunity. Even though it was shown that the inflammation and autoimmunity observed in motheaten mice was not dependent on T cells (Yu et al. 1996), it is possible that SHP-1 deficient T cells, when injected in large numbers (up to 10^{11}) for ACT, could lead to severe autoimmunity. Contrary to this hypothesis is a study that showed that the transfer of SHP-1 deficient mouse T cells to treat leukaemia in mice did not cause any autoimmunity in the liver which expressed the cognate self-Ag (Stromnes et al. 2012). Although this study showed no autoimmunity, it is possible that cells with different TCR specificities together with different Ags with different patterns of expression could lead to SHP-1 deficient T cells causing autoimmunity where wt T cells would not.

To enhance the safety of SHP-1 deficient $CD8^+$ T cells, suicide genes could be delivered to T cells, alongside other genes such as TCRs or CARs, to enable clinicians to abolish the T cell response if symptoms of autoimmunity or leukaemia were to occur. Leukaemia is a concern as a number of leukaemias have been shown to be SHP-1 deficient, however whether this is

causal or not is not known (Oka et al. 2001). Two such suicide genes that have been used in phase I and II clinical trials of leukaemia patients are the *Herpes simplex* virus thymidine kinase gene and the inducible caspase 9 gene (Ciceri et al. 2007; Di Stasi et al. 2011). Drug induced dimerization of the latter in patients that had received haploidentical hematopoietic stem cells and experienced graft-versus-host disease led to a rapid elimination of 90% of the alloreactive T cells, stopping the most severe symptoms within 24 hours (Di Stasi et al. 2011). A third option is the truncated human epidermal growth factor receptor polypeptide which not only provides rapid elimination of T cells via Ab-dependant cell-mediated cytotoxicity, but also allows for *in vitro* selection of transduced cells and *ex vivo* analysis of cells by flow cytometry (Wang et al. 2011). These suicide genes would be an additional layer of safety if a SHP-1 deficiency (as well as other genetic modifications such as TCRs or CARs) caused unpredicted off-tumour effects, excessive autoimmunity and damage to vital organs. To reduce these risks further, mispairing of the endogenous and exogenous TCR α and β chains could be avoided by deleting the endogenous TCR chains (Provasi et al. 2012), thus eliminating the possible generation of new TCR specificities.

Overall, abolishing SHP-1 expression in human $CD8^+$ T cells is still a valid target for improving ACT as it might release the 'brake' from both low and high affinity tumour specific T cells (Hebeisen et al. 2013). Preclinical studies in mice have shown SHP-1 deficient T cells to be superior at protecting against disseminating leukaemia (Stromnes et al. 2012) and against B16 melanoma in mice (unpublished data from our group, A. Watson). Biochemical SHP-1 inhibition would be the simplest treatment method, however all chemical SHP-1 inhibitors have shown considerable cross-reactivity with SHP-2 and no clinical benefit (Kundu et al. 2010; Naing et al. 2011; Yi et al. 2011). Additionally, systemic inhibition of SHP-1 might lead to an enhanced risk of developing severe neutrophil and myeloid cell driven inflammation and autoimmunity, as observed in motheaten mice (Jiao et al. 1997). Thus the best strategy is to

silence SHP-1 gene expression or mutate the SHP-1 gene *in vitro* in T cells prior to transfer of the T cells into patients.

L-selectin and adoptive T cell therapy

In this thesis, the process of L-selectin shedding in response to cognate peptide was studied in leukaemic T cells and it was determined that the main sheddase responsible for this activity is ADAM17. If time had allowed, the human primary Mel^+ $CD8^+$ T cells transduced with wt or ΔM-N L-selectin, generated in Chapter 6, would have been studied for their lytic activity *in vitro* and *in vivo*. Previous reports showed reduced killing of Mel526 cells by human tumour-specific T cells expressing shedding-resistant L-selectin (Yang et al. 2011). This contrasts with our hypothesis that shedding-resistant L-selectin is beneficial for ACT, however our main hypothesis is that prolonged expression of L-selectin on the cell surface of T cells will enhance the homing of T cells to LNs and possibly to the tumour. Unpublished data from our group have shown no differences in target cell killing by mouse $CD8^+$ T cells expressing wt or shedding-resistant L-selectin. Ideally, *in vivo* ACT experiments would be done in xenograft bearing immunodeficient mice comparing T cells expressing wt and shedding-resistant L-selectin. The major problem with using immunodeficient $IL2r\gamma^{-/-}$ mice is the lack of fully developed lymphoid structures (Shultz et al. 2012). In $IL\text{-}2r\gamma^{-/-}/Rag2^{-/-}$ mice it was shown that IL-7 signalling is needed for the persistence of LN structures after birth and that the transfer of $IL\text{-}7R^+$ NK or T cells into these mice at one week of age rescues LN development (Coles et al. 2006). Another study showed that injection of human IL-7 can enhance the maturation of neonatal LNs (Chappaz and Finke 2010). In addition to altered LN development, mouse and human molecules involved in cell trafficking and adhesion are often not compatible. Two such species specific molecules are LFA-1 and ICAM1 (Johnston et al. 1990), both molecules involved in the leucocyte adhesion cascade. To address this problem, immunodeficient mouse

strains would have to be generated to express the relevant ligands or receptors. However, it is still not fully understood what cell adhesion molecules and chemokine receptors govern T cell recruitment to tumours and it is possible that different combinations are important in different tumours and at different stages of cancer development. Overall, these studies indicate that further optimisation of the existing mouse models is necessary to generate models to study T cell homing and trafficking for ACT and other settings.

There are many more unanswered questions about the biology of L-selectin which our group is currently aiming to address. Firstly, the fate of the cytoplasmic tail, generated upon proteolysis of the MRF by the γ-secretase, is completely unknown and it would be interesting to determine whether it is simply degraded or whether it can act as a transcription factor. Further work should thus focus on imaging the cytoplasmic tail in cells and on generating a γ-secretase-resistant form of L-selectin which can be shed normally via the activation of ADAM17 but the MRF cannot be processed further. This would allow a comparison of the impact of wt, shedding-resistant and γ-secretase-resistant L-selectin expression on $CD8^+$ T cells *in vitro* and *in vivo* and might unveil a new role of L-selectin in cell signalling. Experiments are currently being done to compare the anti-tumour effect of mouse $CD8^+$ T cells expressing wt or shedding-resistant L-selectin in B16 melanoma bearing mice. A crucial difference between the mouse T cells, used in these experiments, and patient T cells is that the mouse T cells are from a L-selectin knockout background and do not express endogenous L-selectin, whereas patient T cells do. It is thus of importance to study the effect of endogenous L-selectin expression in combination with shedding-resistant L-selectin expression in T cells and this can be done in mice.

Mouse xenograft models to study the effect of immunotherapy

Mice have been used extensively to study cancer development, metastasis and cancer treatment. 'Proof of principle' for cancer treatments have often been obtained in mice, prior to clinical trials in humans. Early studies were done in immunodeficient mice lacking T and B cells and having decreased innate immune cell functions and one such mouse is the NOD-SCID mouse, used in this thesis. However it was found that NOD-SCID mice and other strains with similar levels of immunodeficiency, exhibited much lower human tumour take than NSG mice (Quintana et al. 2008). This is probably due to the different levels of xenograft rejecting NK cells in the NOD-SCID and NSG mouse strains. NSG mice lack NK cells, due to a mutation in the IL-2rγ gene whereas NOD-SCID mice have some residual NK activity. NSG mice support metastasis and thus these mice have become the strain of choice to study the development of the metastatic process itself as well as its treatment (Zhou et al. 2014). The latter is important as the life-threatening symptoms of cancer often do not stem from the primary tumour but rather from highly aggressive metastasis. NSG mice, although costly, are thus a popular mouse strain for tumour immunotherapy studies.

Even though NSG mice are permissive to the development of human xenografts, they have considerable drawbacks for analysing the interplay between immune cells and cancer. One such drawback is the lack of fully developed LNs, discussed in the section above. Another disadvantage of NSG mice is the lack of cytokines that support T cell engraftment and development. Two ways to overcome this problem are to either administer exogenous cytokines or immunocomplexes of IL-2 or/and IL-15 (Votavova et al. 2014) or to knock-in human cytokine genes into mouse embryonic stem cells (Shultz et al. 2012). Additionally, NSG and all other mouse strains lack the expression of human HLA, which renders the generation of *de novo* anti-tumour T cell responses following vaccination or other treatments unlikely, unless the mice have been additionally reconstituted with human PBMCs or human haematopoietic

stem cells. Unfortunately, such humanized mice are both labour intensive and expensive and thus not available to most laboratories. To overcome the lack of HLA, HLA-A2 transgenic NSG mice have been generated (Strowig et al. 2009).

In summary, results from studies in mice can only ever be used as an indication for the possible success of a therapy in man. An example of a therapy that was first shown to be beneficial in mice was the anti-CTLA Ab therapy, which provided a well-tolerated, robust antitumour response in mice, but when used in patients caused severe side-effects such as colitis (June 2007). This shows that due to the species specific differences, a certain level of risk will always remain for when a therapy is taken into the first patients. Thus, the most reliable experimental model for all immunotherapies will be human patients.

Future of adoptive T cell therapy and immunotherapy

A major problem with ACT is the cost associated with the production of the personalised T cells and the question arises whether this therapy will ever be cost-efficient and adopted by health services (Kaiser et al. 2015). For it to become more extensively used some issues need to be addressed and these will be discussed below.

ACT requires many hours of skilled labour in sterile conditions and due to the many open handling steps is liable to infections and thus failure. Currently, PBMCs are extracted from patients' blood, T cells selected, activated and transduced to express transgenes, expanded and tested *in vitro* prior to reinfusion into patients. One big advance would be the development of partly or fully automated closed-systems that do the isolation, transduction and expansion steps following standardised protocols (Kaiser et al. 2015). This would allow for a more robust, reproducible and, in the long-term, a more cost-efficient final product. As well as the processing of T cells, the production of clinical-grade transduction agents needs to be

optimised to reduce costs. For this goal, major efforts have been put into developing stable viral packaging systems for large scale clinical-grade production of LVs (Sanber et al. 2015).

Secondly, the selection of the TCR or CAR is crucial for a successful outcome and more research needs to be done to derive new receptors with maximal on-tumour and minimal off-tumour effects. Another strategy is to make ACT less personalised by developing 'universal T cells'. These T cells would ideally be endogenously TCR and HLA negative, express a non-classical HLA to prevent recognition by NK cells and have the potential to be expanded and transduced *in vitro* for many cycles without losing their memory and effector potential (Kaiser et al. 2015). These T cells would be redirected with carefully selected TCRs or CARs that recognise tumour-associated Ags. However, there are still many hurdles to overcome for the development of universal T cells, not the least exhaustion of these T cells following long-term *in vitro* culture.

Thirdly, alternative T cell delivery strategies should be trialled to improve safety and efficiency of ACT. For example, delivering the T cells in several doses of smaller T cell numbers instead of all in one injection could decrease the risk of life-threatening effects such as early cytokine release syndrome to occur (Qasim and Thrasher 2014). Additionally, T cells might be more potent when delivered locally, in the proximity of the tumour, instead of systemically by intravenous injections. This was shown to be the case in a mouse xenograft model where locally delivered T cells outperformed those administered intravenously, possibly due to rapid local Ag-dependant activation of the T cells administered locally (Adusumilli et al. 2014).

ACT and other immunotherapies, such as anti-CTLA-4 and anti-PD-1/PD-L1, have been shown to be successful in a subset of patients (Rosenberg and Restifo 2015; Sharma and Allison 2015). It is thus essential to determine biomarkers associated with successful outcomes to help choose the best therapy for each patient. These biomarkers can be tumour-associated or immune- associated. For example, increased mutation loads in tumours might be an indication

that higher levels of neo-Ag specific T cells are present and that checkpoint inhibitor therapy might be successful. However, it was shown that checkpoint inhibitor therapy did also improve the outcome of low immunogenic kidney tumour patients (Sharma and Allison 2015). Other biomarkers could be molecules within the tumour that inhibit T cell activity, molecules on blood vessels that regulate T cell infiltration into tumours or molecules expressed by T cells within the tumour. Successful ACT might be associated with phenotypic markers on T cells after *in vitro* expansion, such as L-selectin, which has already been shown to be associated with a more favourable outcome in ACT experiments in mice (Gattinoni et al. 2005).

Currently, the field of immunotherapy is showing very encouraging results, possibly the most exciting being checkpoint inhibitor therapies, such as anti-CTLA-4 and anti-PD-1/PD-L1 Abs. The latter are considerably easier to manufacture than T cells and it is thus going to be important to decide when either or both therapies are beneficial. Many more possible targets are being explored for improved immunotherapy and in particular ACT, including both SHP-1 and L-selectin, as discussed in this thesis. As well as the blockade of inhibitory signalling pathways such as PD-1 and CTLA-4, current research also focuses on activating stimulatory pathways (Sharma and Allison 2015). One scenario where ACT might be necessary is in poorly immunogenic tumours with low T cell infiltration, where an injection of a high numbers of tumour-specific T cells could boost the anti-tumour immune response considerably.

Overall, it is likely that the most successful cancer immunotherapies will be combinatorial treatments. For example a patient could undergo a lymphodepleting chemotherapy treatment prior to ACT, followed by a checkpoint inhibitor treatment such as anti-PD-1. To determine optimal combinations, many more trials will have to be done and the complexity and costs of production, especially of the ACT, will have to be reduced.

References

2012. Method of the Year 2011. *Nat Meth* 9(1), pp. 1-1.

Abram, C. L. et al. 2013. Distinct roles for neutrophils and dendritic cells in inflammation and autoimmunity in motheaten mice. *Immunity* 38(3), pp. 489-501.

Adler, M. J. and Dimitrov, D. S. 2012. Therapeutic antibodies against cancer. *Hematol Oncol Clin North Am* 26(3), pp. 447-481, vii.

Adusumilli, P. S. et al. 2014. Regional delivery of mesothelin-targeted CAR T cell therapy generates potent and long-lasting CD4-dependent tumor immunity. *Sci Transl Med* 6(261), p. 261ra151.

Ager, A. 2012. ADAMs and Ectodomain Proteolytic Shedding in Leukocyte Migration: Focus on L-selectin and ADAM17. *Current Immunology Reviews* 8, pp. 103-117.

Ain, Q. U. et al. 2014. Current and future delivery systems for engineered nucleases: ZFN, TALEN and RGEN. *J Control Release*.

Alcantar-Orozco, E. M. et al. 2013. Potential limitations of the NSG humanized mouse as a model system to optimize engineered human T cell therapy for cancer. *Hum Gene Ther Methods* 24(5), pp. 310-320.

Algarra, I. et al. 2004. The selection of tumor variants with altered expression of classical and nonclassical MHC class I molecules: implications for tumor immune escape. *Cancer Immunol Immunother* 53(10), pp. 904-910.

Amirache, F. et al. 2014. Mystery solved: VSV-G-LVs do not allow efficient gene transfer into unstimulated T cells, B cells, and HSCs because they lack the LDL receptor. *Blood* 123(9), pp. 1422-1424.

Arbones, M. L. et al. 1994. Lymphocyte homing and leukocyte rolling and migration are impaired in L-selectin-deficient mice. *Immunity* 1(4), pp. 247-260.

Baird, G. S. et al. 2000. Biochemistry, mutagenesis, and oligomerization of DsRed, a red fluorescent protein from coral. *Proc Natl Acad Sci U S A* 97(22), pp. 11984-11989.

Banville, D. et al. 1995. Human protein tyrosine phosphatase 1C (PTPN6) gene structure: alternate promoter usage and exon skipping generate multiple transcripts. *Genomics* 27(1), pp. 165-173.

Barese, C. N. and Dunbar, C. E. 2011. Contributions of gene marking to cell and gene therapies. *Hum Gene Ther* 22(6), pp. 659-668.

Barry, M. and Bleackley, R. C. 2002. Cytotoxic T lymphocytes: all roads lead to death. *Nat Rev Immunol* 2(6), pp. 401-409.

Bendle, G. M. et al. 2010. Lethal graft-versus-host disease in mouse models of T cell receptor gene therapy. *Nat Med* 16(5), pp. 565-570, 561p following 570.

Berlin, C. et al. 1995. alpha 4 integrins mediate lymphocyte attachment and rolling under physiologic flow. *Cell* 80(3), pp. 413-422.

Besser, M. J. et al. 2010. Clinical responses in a phase II study using adoptive transfer of short-term cultured tumor infiltration lymphocytes in metastatic melanoma patients. *Clin Cancer Res* 16(9), pp. 2646-2655.

Betts, M. R. et al. 2003. Sensitive and viable identification of antigen-specific CD8+ T cells by a flow cytometric assay for degranulation. *J Immunol Methods* 281(1-2), pp. 65-78.

Bibikova, M. et al. 2001. Stimulation of homologous recombination through targeted cleavage by chimeric nucleases. *Mol Cell Biol* 21(1), pp. 289-297.

Bibikova, M. et al. 2002. Targeted chromosomal cleavage and mutagenesis in Drosophila using zinc-finger nucleases. *Genetics* 161(3), pp. 1169-1175.

Binstadt, B. A. et al. 1998. SLP-76 is a direct substrate of SHP-1 recruited to killer cell inhibitory receptors. *J Biol Chem* 273(42), pp. 27518-27523.

Bitinaite, J. et al. 1998. FokI dimerization is required for DNA cleavage. *Proc Natl Acad Sci U S A* 95(18), pp. 10570-10575.

Blaese, R. M. et al. 1995. T lymphocyte-directed gene therapy for ADA- SCID: initial trial results after 4 years. *Science* 270(5235), pp. 475-480.

Boshoff, C. and Weiss, R. 2002. AIDS-related malignancies. *Nat Rev Cancer* 2(5), pp. 373-382.

Bouchard, P. et al. 1994. Phosphorylation and identification of a major tyrosine phosphorylation site in protein tyrosine phosphatase 1C. *J Biol Chem* 269(30), pp. 19585-19589.

Brinkman, C. C. et al. 2013. Peripheral tissue homing receptor control of naive, effector, and memory CD8 T cell localization in lymphoid and non-lymphoid tissues. *Front Immunol* 4, p. 241.

Brockdorff, J. et al. 1999. Dephosphorylation of ZAP-70 and inhibition of T cell activation by activated SHP1. *Eur J Immunol* 29(8), pp. 2539-2550.

Brown, S. D. et al. 2014. Neo-antigens predicted by tumor genome meta-analysis correlate with increased patient survival. *Genome Res* 24(5), pp. 743-750.

Brownlie, R. J. and Zamoyska, R. 2013. T cell receptor signalling networks: branched, diversified and bounded. *Nat Rev Immunol* 13(4), pp. 257-269.

Burns, S. O. et al. 2010. A congenital activating mutant of WASp causes altered plasma membrane topography and adhesion under flow in lymphocytes. *Blood* 115(26), pp. 5355-5365.

Burshtyn, D. N. et al. 1997. A novel phosphotyrosine motif with a critical amino acid at position -2 for the SH2 domain-mediated activation of the tyrosine phosphatase SHP-1. *J Biol Chem* 272(20), pp. 13066-13072.

Callahan, M. K. et al. 2014. CTLA-4 and PD-1 Pathway Blockade: Combinations in the Clinic. *Front Oncol* 4, p. 385.

Carreno, B. M. et al. 2015. A dendritic cell vaccine increases the breadth and diversity of melanoma neoantigen-specific T cells. *Science*.

Carroll, D. 2011. Genome engineering with zinc-finger nucleases. *Genetics* 188(4), pp. 773-782.

Carter, J. D. et al. 1999. The tyrosine phosphatase SHP-1 influences thymocyte selection by setting TCR signaling thresholds. *International Immunology* 11(12), pp. 1999-2014.

Cebrián, M. et al. 1988. Triggering of T cell proliferation through AIM, an activation inducer molecule expressed on activated human lymphocytes. *The Journal of Experimental Medicine* 168(5), pp. 1621-1637.

Chalaris, A. et al. 2010. ADAM17-mediated shedding of the IL6R induces cleavage of the membrane stub by gamma-secretase. *Biochim Biophys Acta* 1803(2), pp. 234-245.

Chao, C. C. et al. 1997. Mechanisms of L-selectin regulation by activated T cells. *J Immunol* 159(4), pp. 1686-1694.

Chappaz, S. and Finke, D. 2010. The IL-7 signaling pathway regulates lymph node development independent of peripheral lymphocytes. *J Immunol* 184(7), pp. 3562-3569.

Cheadle, E. J. et al. 2014. CAR T cells: driving the road from the laboratory to the clinic. *Immunol Rev* 257(1), pp. 91-106.

Chemnitz, J. M. et al. 2004. SHP-1 and SHP-2 associate with immunoreceptor tyrosine-based switch motif of programmed death 1 upon primary human T cell stimulation, but only receptor ligation prevents T cell activation. *J Immunol* 173(2), pp. 945-954.

Chen, A. et al. 1995. Structural requirements regulate endoproteolytic release of the L-selectin (CD62L) adhesion receptor from the cell surface of leukocytes. *J Exp Med* 182(2), pp. 519-530.

Chen, D. S. and Mellman, I. 2013. Oncology meets immunology: the cancer-immunity cycle. *Immunity* 39(1), pp. 1-10.

Chen, Z. et al. 2008. Carcinoembryonic antigen-related cell adhesion molecule 1 inhibits proximal TCR signaling by targeting ZAP-70. *J Immunol* 180(9), pp. 6085-6093.

Chia, J. et al. 2009. Temperature sensitivity of human perforin mutants unmasks subtotal loss of cytotoxicity, delayed FHL, and a predisposition to cancer. *Proc Natl Acad Sci U S A* 106(24), pp. 9809-9814.

Christophi, G. P. et al. 2008. SHP-1 deficiency and increased inflammatory gene expression in PBMCs of multiple sclerosis patients. *Lab Invest* 88(3), pp. 243-255.

Ciceri, F. et al. 2007. Antitumor effects of HSV-TK-engineered donor lymphocytes after allogeneic stem-cell transplantation. *Blood* 109(11), pp. 4698-4707.

Clemente, C. G. et al. 1996. Prognostic value of tumor infiltrating lymphocytes in the vertical growth phase of primary cutaneous melanoma. *Cancer* 77(7), pp. 1303-1310.

Cole, D. K. et al. 2009. Germ line-governed recognition of a cancer epitope by an immunodominant human T-cell receptor. *J Biol Chem* 284(40), pp. 27281-27289.

Coles, M. C. et al. 2006. Role of T and NK cells and IL7/IL7r interactions during neonatal maturation of lymph nodes. *Proc Natl Acad Sci U S A* 103(36), pp. 13457-13462.

Criswell, L. A. et al. 2005. Analysis of families in the multiple autoimmune disease genetics consortium (MADGC) collection: the PTPN22 620W allele associates with multiple autoimmune phenotypes. *Am J Hum Genet* 76(4), pp. 561-571.

Croker, B. A. et al. 2008. Inflammation and autoimmunity caused by a SHP1 mutation depend on IL-1, MyD88, and a microbial trigger. *Proceedings of the National Academy of Sciences* 105(39), pp. 15028-15033.

Crompton, J. G. et al. 2015. Akt inhibition enhances expansion of potent tumor-specific lymphocytes with memory cell characteristics. *Cancer Res* 75(2), pp. 296-305.

Curiel, T. J. et al. 2004. Specific recruitment of regulatory T cells in ovarian carcinoma fosters immune privilege and predicts reduced survival. *Nat Med* 10(9), pp. 942-949.

Davis, D. and Stokoe, D. 2010. Zinc finger nucleases as tools to understand and treat human diseases. *BMC Med* 8, p. 42.

de Felipe, P. et al. 2006. E unum pluribus: multiple proteins from a self-processing polyprotein. *Trends Biotechnol* 24(2), pp. 68-75.

De Meyer, S. F. et al. 2006. Phenotypic correction of von Willebrand disease type 3 blood-derived endothelial cells with lentiviral vectors expressing von Willebrand factor. *Blood* 107(12), pp. 4728-4736.

de Saint Basile, G. et al. 2010. Molecular mechanisms of biogenesis and exocytosis of cytotoxic granules. *Nat Rev Immunol* 10(8), pp. 568-579.

Delviks, K. A. and Pathak, V. K. 1999. Effect of distance between homologous sequences and 3' homology on the frequency of retroviral reverse transcriptase template switching. *J Virol* 73(10), pp. 7923-7932.

Demaison, C. et al. 2002. High-level transduction and gene expression in hematopoietic repopulating cells using a human immunodeficiency [correction of imunodeficiency] virus type 1-based lentiviral vector containing an internal spleen focus forming virus promoter. *Hum Gene Ther* 13(7), pp. 803-813.

Deng, C. et al. 2002. Expression of the tyrosine phosphatase SRC homology 2 domain-containing protein tyrosine phosphatase 1 determines T cell activation threshold and severity of experimental autoimmune encephalomyelitis. *J Immunol* 168(9), pp. 4511-4518.

Di Stasi, A. et al. 2011. Inducible apoptosis as a safety switch for adoptive cell therapy. *N Engl J Med* 365(18), pp. 1673-1683.

Dickie, M. M. et al. 1969. Two unusual dominant mutations in the mouse. *J Hered* 60(2), pp. 84-86.

Dovey, H. F. et al. 2001. Functional gamma-secretase inhibitors reduce beta-amyloid peptide levels in brain. *J Neurochem* 76(1), pp. 173-181.

Doyon, Y. et al. 2010. Transient cold shock enhances zinc-finger nuclease-mediated gene disruption. *Nat Methods* 7(6), pp. 459-460.

Doyon, Y. et al. 2011. Enhancing zinc-finger-nuclease activity with improved obligate heterodimeric architectures. *Nat Methods* 8(1), pp. 74-79.

Dudley, M. E. et al. 2002. Cancer regression and autoimmunity in patients after clonal repopulation with antitumor lymphocytes. *Science* 298(5594), pp. 850-854.

Dudley, M. E. et al. 2008. Adoptive cell therapy for patients with metastatic melanoma: evaluation of intensive myeloablative chemoradiation preparative regimens. *J Clin Oncol* 26(32), pp. 5233-5239.

Ekeruche-Makinde, J. et al. 2012. T-cell receptor-optimized peptide skewing of the T-cell repertoire can enhance antigen targeting. *J Biol Chem* 287(44), pp. 37269-37281.

Ellis, J. 2005. Silencing and variegation of gammaretrovirus and lentivirus vectors. *Hum Gene Ther* 16(11), pp. 1241-1246.

Evans, M. E. et al. 2014. TRIM5[alpha] Variations Influence Transduction Efficiency With Lentiviral Vectors in Both Human and Rhesus CD34+ Cells In Vitro and In Vivo. *Mol Ther* 22(2), pp. 348-358.

Fabre, S. et al. 2008. FOXO1 regulates L-Selectin and a network of human T cell homing molecules downstream of phosphatidylinositol 3-kinase. *J Immunol* 181(5), pp. 2980-2989.

Faveeuw, C. et al. 2001. Transendothelial migration of lymphocytes across high endothelial venules into lymph nodes is affected by metalloproteinases. *Blood* 98(3), pp. 688-695.

Fawcett, V. C. and Lorenz, U. 2005. Localization of Src homology 2 domain-containing phosphatase 1 (SHP-1) to lipid rafts in T lymphocytes: functional implications and a role for the SHP-1 carboxyl terminus. *J Immunol* 174(5), pp. 2849-2859.

Finger, E. B. et al. 1996. Adhesion through L-selectin requires a threshold hydrodynamic shear. *Nature* 379(6562), pp. 266-269.

Fors, B. P. et al. 2001. L-selectin shedding is independent of its subsurface structures and topographic distribution. *J Immunol* 167(7), pp. 3642-3651.

Fowler, C. C. et al. 2010. SHP-1 in T Cells Limits the Production of CD8 Effector Cells without Impacting the Formation of Long-Lived Central Memory Cells. *The Journal of Immunology* 185(6), pp. 3256-3267.

Frank, C. et al. 2004. Effective dephosphorylation of Src substrates by SHP-1. *J Biol Chem* 279(12), pp. 11375-11383.

Fu, Y. et al. 2013. High-frequency off-target mutagenesis induced by CRISPR-Cas nucleases in human cells. *Nat Biotechnol* 31(9), pp. 822-826.

Gabriel, R. et al. 2011. An unbiased genome-wide analysis of zinc-finger nuclease specificity. *Nat Biotechnol* 29(9), pp. 816-823.

Gaj, T. et al. 2012. Targeted gene knockout by direct delivery of zinc-finger nuclease proteins. *Nat Methods* 9(8), pp. 805-807.

Galkina, E. et al. 2007. T lymphocyte rolling and recruitment into peripheral lymph nodes is regulated by a saturable density of L-selectin (CD62L). *Eur J Immunol* 37(5), pp. 1243-1253.

Galkina, E. et al. 2003. L-selectin shedding does not regulate constitutive T cell trafficking but controls the migration pathways of antigen-activated T lymphocytes. *J Exp Med* 198(9), pp. 1323-1335.

Galon, J. et al. 2006. Type, density, and location of immune cells within human colorectal tumors predict clinical outcome. *Science* 313(5795), pp. 1960-1964.

Gattinoni, L. et al. 2005. Acquisition of full effector function in vitro paradoxically impairs the in vivo antitumor efficacy of adoptively transferred CD8+ T cells. *J Clin Invest* 115(6), pp. 1616-1626.

Geling, A. et al. 2002. A gamma-secretase inhibitor blocks Notch signaling in vivo and causes a severe neurogenic phenotype in zebrafish. *EMBO Rep* 3(7), pp. 688-694.

Giblin, P. A. et al. 1997. Ligation of L-selectin on T lymphocytes activates beta1 integrins and promotes adhesion to fibronectin. *J Immunol* 159(7), pp. 3498-3507.

Gifford, J. L. et al. 2012. Structural Insights into Calmodulin-regulated L-selectin Ectodomain Shedding. *J Biol Chem* 287(32), pp. 26513-26527.

Girard, J. P. et al. 2012. HEVs, lymphatics and homeostatic immune cell trafficking in lymph nodes. *Nat Rev Immunol* 12(11), pp. 762-773.

Govers, C. et al. 2011. T Cell Receptor Fused to CD3ζ: Transmembrane Domain of CD3ζ Prevents TCR Mis-Pairing, Whereas Complete CD3ζ Directs Functional TCR Expression. *The Open Gene Therapy Journal* 4, pp. 11-22.

Green, M. C. and Shultz, L. D. 1975. Motheaten, an immunodeficient mutant of the mouse. I. Genetics and pathology. *J Hered* 66(5), pp. 250-258.

Guarda, G. et al. 2007. L-selectin-negative CCR7- effector and memory CD8+ T cells enter reactive lymph nodes and kill dendritic cells. *Nat Immunol* 8(7), pp. 743-752.

Guntermann, C. and Alexander, D. R. 2002. CTLA-4 suppresses proximal TCR signaling in resting human CD4(+) T cells by inhibiting ZAP-70 Tyr(319) phosphorylation: a potential role for tyrosine phosphatases. *J Immunol* 168(9), pp. 4420-4429.

Hacein-Bey-Abina, S. et al. 2003. LMO2-associated clonal T cell proliferation in two patients after gene therapy for SCID-X1. *Science* 302(5644), pp. 415-419.

Hafezi-Moghadam, A. et al. 2001. L-selectin shedding regulates leukocyte recruitment. *J Exp Med* 193(7), pp. 863-872.

Hanahan, D. and Weinberg, R. A. 2011. Hallmarks of cancer: the next generation. *Cell* 144(5), pp. 646-674.

Handel, E. M. et al. 2009. Expanding or restricting the target site repertoire of zinc-finger nucleases: the inter-domain linker as a major determinant of target site selectivity. *Mol Ther* 17(1), pp. 104-111.

Haque, T. et al. 2007. Allogeneic cytotoxic T-cell therapy for EBV-positive posttransplantation lymphoproliferative disease: results of a phase 2 multicenter clinical trial. *Blood* 110(4), pp. 1123-1131.

Hasslen, S. et al. 1995. Spatial distribution of L-selectin (CD62L) on human lymphocytes and transfected murine L1-2 cells. *The Histochemical Journal* 27(7), pp. 547-554.

He, D. et al. 2005. EGF-stimulation activates the nuclear localization signal of SHP-1. *J Cell Biochem* 94(5), pp. 944-953.

He, Q. et al. 1988. A role in transmembrane signaling for the cytoplasmic domain of the CD2 T lymphocyte surface antigen. *Cell* 54(7), pp. 979-984.

Hebeisen, M. et al. 2013. SHP-1 phosphatase activity counteracts increased T cell receptor affinity. *J Clin Invest*.

Higashimoto, T. et al. 2007. The woodchuck hepatitis virus post-transcriptional regulatory element reduces readthrough transcription from retroviral vectors. *Gene Ther* 14(17), pp. 1298-1304.

Holkers, M. et al. 2013. Differential integrity of TALE nuclease genes following adenoviral and lentiviral vector gene transfer into human cells. *Nucleic Acids Res* 41(5), p. e63.

Holt, N. et al. 2010. Human hematopoietic stem/progenitor cells modified by zinc-finger nucleases targeted to CCR5 control HIV-1 in vivo. *Nat Biotechnol* 28(8), pp. 839-847.

http://www.abedia.com/wiley/indications.php. 2015. *The Journal of Gene Medicine*.

http://www.abedia.com/wiley/vectors.php. 2015. *The Journal of Gene Medicine*.

Huang, X. et al. 2008. Sleeping Beauty transposon-mediated engineering of human primary T cells for therapy of CD19+ lymphoid malignancies. *Mol Ther* 16(3), pp. 580-589.

Hundhausen, C. et al. 2003. The disintegrin-like metalloproteinase ADAM10 is involved in constitutive cleavage of CX3CL1 (fractalkine) and regulates CX3CL1-mediated cell-cell adhesion. *Blood* 102(4), pp. 1186-1195.

Hunter, T. and Sefton, B. M. 1980. Transforming gene product of Rous sarcoma virus phosphorylates tyrosine. *Proc Natl Acad Sci U S A* 77(3), pp. 1311-1315.

Isalan, M. 2012. Zinc-finger nucleases: how to play two good hands. *Nat Methods* 9(1), pp. 32-34.

Ishikawa, F. et al. 2005. Development of functional human blood and immune systems in NOD/SCID/IL2 receptor {gamma} chain(null) mice. *Blood* 106(5), pp. 1565-1573.

Ivetic, A. 2013. Signals regulating L-selectin-dependent leucocyte adhesion and transmigration. *Int J Biochem Cell Biol*.

Ivetic, A. et al. 2002. The cytoplasmic tail of L-selectin interacts with members of the Ezrin-Radixin-Moesin (ERM) family of proteins: cell activation-dependent binding of Moesin but not Ezrin. *J Biol Chem* 277(3), pp. 2321-2329.

Ivetic, A. et al. 2004. Mutagenesis of the ezrin-radixin-moesin binding domain of L-selectin tail affects shedding, microvillar positioning, and leukocyte tethering. *J Biol Chem* 279(32), pp. 33263-33272.

Jantz, D. et al. 2004. The design of functional DNA-binding proteins based on zinc finger domains. *Chem Rev* 104(2), pp. 789-799.

Jiao, H. et al. 1997. Macrophages from motheaten and viable motheaten mutant mice show increased proliferative responses to GM-CSF: detection of potential HCP substrates in GM-CSF signal transduction. *Exp Hematol* 25(7), pp. 592-600.

Johnson, D. J. et al. 2013. Shp1 regulates T cell homeostasis by limiting IL-4 signals. *J Exp Med*.

Johnson, K. G. et al. 1999. TCR signaling thresholds regulating T cell development and activation are dependent upon SHP-1. *J Immunol* 162(7), pp. 3802-3813.

Johnston, S. C. et al. 1990. On the species specificity of the interaction of LFA-1 with intercellular adhesion molecules. *J Immunol* 145(4), pp. 1181-1187.

June, C. H. 2007. Principles of adoptive T cell cancer therapy. *J Clin Invest* 117(5), pp. 1204-1212.

Jung, T. M. and Dailey, M. O. 1990. Rapid modulation of homing receptors (gp90MEL-14) induced by activators of protein kinase C. Receptor shedding due to accelerated proteolytic cleavage at the cell surface. *J Immunol* 144(8), pp. 3130-3136.

Kaech, S. M. and Cui, W. 2012. Transcriptional control of effector and memory CD8+ T cell differentiation. *Nat Rev Immunol* 12(11), pp. 749-761.

Kahn, J. et al. 1994. Membrane proximal cleavage of L-selectin: identification of the cleavage site and a 6-kD transmembrane peptide fragment of L-selectin. *J Cell Biol* 125(2), pp. 461-470.

Kahn, J. et al. 1998. Calmodulin regulates L-selectin adhesion molecule expression and function through a protease-dependent mechanism. *Cell* 92(6), pp. 809-818.

Kaiser, A. D. et al. 2015. Towards a commercial process for the manufacture of genetically modified T cells for therapy. *Cancer Gene Ther* 22(2), pp. 72-78.

Kalos, M. et al. 2011. T cells with chimeric antigen receptors have potent antitumor effects and can establish memory in patients with advanced leukemia. *Sci Transl Med* 3(95), p. 95ra73.

Kebriaei, P. et al. 2012. Infusing CD19-directed T cells to augment disease control in patients undergoing autologous hematopoietic stem-cell transplantation for advanced B-lymphoid malignancies. *Hum Gene Ther* 23(5), pp. 444-450.

Kenneth Murphy, P. T., Mark Walport. 2008. *Janeway's Immunobiology*. Garland Science.

Kerdiles, Y. M. et al. 2009. Foxo1 links homing and survival of naive T cells by regulating L-selectin, CCR7 and interleukin 7 receptor. *Nat Immunol* 10(2), pp. 176-184.

Kilgore, N. E. et al. 2003. Cutting edge: dependence of TCR antagonism on Src homology 2 domain-containing protein tyrosine phosphatase activity. *J Immunol* 170(10), pp. 4891-4895.

Killock, D. J. et al. 2009. In Vitro and in Vivo Characterization of Molecular Interactions between Calmodulin, Ezrin/Radixin/Moesin, and L-selectin. *J Biol Chem* 284(13), pp. 8833-8845.

Kim, C. H. et al. 1999. Abnormal chemokine-induced responses of immature and mature hematopoietic cells from motheaten mice implicate the protein tyrosine phosphatase SHP-1 in chemokine responses. *J Exp Med* 190(5), pp. 681-690.

Kim, H. and Kim, J. S. 2014. A guide to genome engineering with programmable nucleases. *Nat Rev Genet* 15(5), pp. 321-334.

Kim, H. J. et al. 2009. Targeted genome editing in human cells with zinc finger nucleases constructed via modular assembly. *Genome Res* 19(7), pp. 1279-1288.

Kim, Y. G. et al. 1996. Hybrid restriction enzymes: zinc finger fusions to Fok I cleavage domain. *Proc Natl Acad Sci U S A* 93(3), pp. 1156-1160.

Kim, Y. G. and Chandrasegaran, S. 1994. Chimeric restriction endonuclease. *Proc Natl Acad Sci U S A* 91(3), pp. 883-887.

Klebanoff, C. A. et al. 2011a. Therapeutic cancer vaccines: are we there yet? *Immunol Rev* 239(1), pp. 27-44.

Klebanoff, C. A. et al. 2011b. Determinants of successful CD8+ T-cell adoptive immunotherapy for large established tumors in mice. *Clin Cancer Res* 17(16), pp. 5343-5352.

Klinger, A. et al. 2009. Cyclical expression of L-selectin (CD62L) by recirculating T cells. *Int Immunol* 21(4), pp. 443-455.

Koike-Yusa, H. et al. 2014. Genome-wide recessive genetic screening in mammalian cells with a lentiviral CRISPR-guide RNA library. *Nat Biotechnol* 32(3), pp. 267-273.

Kon-Kozlowski, M. et al. 1996. The tyrosine phosphatase PTP1C associates with Vav, Grb2, and mSos1 in hematopoietic cells. *J Biol Chem* 271(7), pp. 3856-3862.

Kundu, S. et al. 2010. Novel SHP-1 inhibitors tyrosine phosphatase inhibitor-1 and analogs with preclinical anti-tumor activities as tolerated oral agents. *J Immunol* 184(11), pp. 6529-6536.

Kung, C. et al. 2000. Mutations in the tyrosine phosphatase CD45 gene in a child with severe combined immunodeficiency disease. *Nat Med* 6(3), pp. 343-345.

Lamers, C. H. et al. 2013. Treatment of metastatic renal cell carcinoma with CAIX CAR-engineered T cells: clinical evaluation and management of on-target toxicity. *Mol Ther* 21(4), pp. 904-912.

Lawrence, M. S. et al. 2013. Mutational heterogeneity in cancer and the search for new cancer-associated genes. *Nature* 499(7457), pp. 214-218.

Le Gall, S. M. et al. 2009. ADAMs 10 and 17 represent differentially regulated components of a general shedding machinery for membrane proteins such as transforming growth factor alpha, L-selectin, and tumor necrosis factor alpha. *Mol Biol Cell* 20(6), pp. 1785-1794.

Le Page, A. et al. 2014. Downregulation of inhibitory SRC homology 2 domain-containing phosphatase-1 (SHP-1) leads to recovery of T cell responses in elderly. *Cell Commun Signal* 12, p. 2.

Leavitt, A. D. et al. 1996. Human immunodeficiency virus type 1 integrase mutants retain in vitro integrase activity yet fail to integrate viral DNA efficiently during infection. *J Virol* 70(2), pp. 721-728.

Ley, K. et al. 2007. Getting to the site of inflammation: the leukocyte adhesion cascade updated. *Nat Rev Immunol* 7(9), pp. 678-689.

Li, H. et al. 2011. In vivo genome editing restores haemostasis in a mouse model of haemophilia. *Nature* 475(7355), pp. 217-221.

Li, L. et al. 1992. Functional domains in Fok I restriction endonuclease. *Proc Natl Acad Sci U S A* 89(10), pp. 4275-4279.

Liddy, N. et al. 2012. Monoclonal TCR-redirected tumor cell killing. *Nat Med* 18(6), pp. 980-987.

Linette, G. P. et al. 2013. Cardiovascular toxicity and titin cross-reactivity of affinity-enhanced T cells in myeloma and melanoma. *Blood* 122(6), pp. 863-871.

Lissina, A. et al. 2009. Protein kinase inhibitors substantially improve the physical detection of T-cells with peptide-MHC tetramers. *J Immunol Methods* 340(1), pp. 11-24.

Liu, J. et al. 2015. Improved cell-penetrating zinc-finger nuclease proteins for precision genome engineering. *Mol Ther Nucleic Acids* 4, p. e232.

Loi, S. et al. 2013. Prognostic and predictive value of tumor-infiltrating lymphocytes in a phase III randomized adjuvant breast cancer trial in node-positive breast cancer comparing the addition of docetaxel to doxorubicin with doxorubicin-based chemotherapy: BIG 02-98. *J Clin Oncol* 31(7), pp. 860-867.

Lombardo, A. et al. 2007. Gene editing in human stem cells using zinc finger nucleases and integrase-defective lentiviral vector delivery. *Nat Biotechnol* 25(11), pp. 1298-1306.

Long, E. O. 1999. Regulation of immune responses through inhibitory receptors. *Annu Rev Immunol* 17, pp. 875-904.

Lorenz, U. 2009. SHP-1 and SHP-2 in T cells: two phosphatases functioning at many levels. *Immunol Rev* 228(1), pp. 342-359.

Lorenz, U. et al. 1996. Lack of SHPTP1 results in src-family kinase hyperactivation and thymocyte hyperresponsiveness. *Proc Natl Acad Sci U S A* 93(18), pp. 9624-9629.

Lorenz, U. et al. 1994. Lck-dependent tyrosyl phosphorylation of the phosphotyrosine phosphatase SH-PTP1 in murine T cells. *Mol Cell Biol* 14(3), pp. 1824-1834.

Lou, J. et al. 2006. Flow-enhanced adhesion regulated by a selectin interdomain hinge. *J Cell Biol* 174(7), pp. 1107-1117.

Marini, B. et al. 2015. Nuclear architecture dictates HIV-1 integration site selection. *Nature*.

Martinet, L. et al. 2011. Human solid tumors contain high endothelial venules: association with T- and B-lymphocyte infiltration and favorable prognosis in breast cancer. *Cancer Res* 71(17), pp. 5678-5687.

Martinet, L. et al. 2012. High endothelial venules (HEVs) in human melanoma lesions: Major gateways for tumor-infiltrating lymphocytes. *Oncoimmunology* 1(6), pp. 829-839.

Massa, P. T. and Wu, C. 1996. The role of protein tyrosine phosphatase SHP-1 in the regulation of IFN-gamma signaling in neural cells. *J Immunol* 157(11), pp. 5139-5144.

Matthews, R. J. et al. 1992. Characterization of hematopoietic intracellular protein tyrosine phosphatases: description of a phosphatase containing an SH2 domain and another enriched in proline-, glutamic acid-, serine-, and threonine-rich sequences. *Mol Cell Biol* 12(5), pp. 2396-2405.

Matz, M. V. et al. 1999. Fluorescent proteins from nonbioluminescent Anthozoa species. *Nat Biotechnol* 17(10), pp. 969-973.

Mauldin, I. S. et al. 2012. The tyrosine phosphatase SHP-1 dampens murine Th17 development. *Blood* 119(19), pp. 4419-4429.

McCarthy, E. F. 2006. The toxins of William B. Coley and the treatment of bone and soft-tissue sarcomas. *Iowa Orthop J* 26, pp. 154-158.

McEver, R. P. 2005. A sulfated address for lymphocyte homing. *Nat Immunol* 6(11), pp. 1067-1069.

Medema, J. P. et al. 2001. Blockade of the granzyme B/perforin pathway through overexpression of the serine protease inhibitor PI-9/SPI-6 constitutes a mechanism for immune escape by tumors. *Proc Natl Acad Sci U S A* 98(20), pp. 11515-11520.

Merling, R. K. et al. 2015. An AAVS1-targeted minigene platform for correction of iPSCs from all five types of chronic granulomatous disease. *Mol Ther* 23(1), pp. 147-157.

Migone, T. S. et al. 1998. Recruitment of SH2-containing protein tyrosine phosphatase SHP-1 to the interleukin 2 receptor; loss of SHP-1 expression in human T-lymphotropic virus type I-transformed T cells. *Proc Natl Acad Sci U S A* 95(7), pp. 3845-3850.

Miller, J. C. et al. 2007. An improved zinc-finger nuclease architecture for highly specific genome editing. *Nat Biotechnol* 25(7), pp. 778-785.

Minoo, P. et al. 2004. A novel SHP-1/Grb2-dependent mechanism of negative regulation of cytokine-receptor signaling: contribution of SHP-1 C-terminal tyrosines in cytokine signaling. *Blood* 103(4), pp. 1398-1407.

Moore, M. et al. 2001. Improved DNA binding specificity from polyzinc finger peptides by using strings of two-finger units. *Proc Natl Acad Sci U S A* 98(4), pp. 1437-1441.

Morgan, R. A. et al. 2006. Cancer regression in patients after transfer of genetically engineered lymphocytes. *Science* 314(5796), pp. 126-129.

Mussolino, C. and Cathomen, T. 2011. On target? Tracing zinc-finger-nuclease specificity. *Nat Methods* 8(9), pp. 725-726.

Nagaishi, T. et al. 2006. SHP1 phosphatase-dependent T cell inhibition by CEACAM1 adhesion molecule isoforms. *Immunity* 25(5), pp. 769-781.

Naing, A. et al. 2011. Phase I Dose Escalation Study of Sodium Stibogluconate (SSG), a Protein Tyrosine Phosphatase Inhibitor, Combined with Interferon Alpha for Patients with Solid Tumors. *J Cancer* 2, pp. 81-89.

Oka, T. et al. 2001. Reduction of hematopoietic cell-specific tyrosine phosphatase SHP-1 gene expression in natural killer cell lymphoma and various types of lymphomas/leukemias : combination analysis with cDNA expression array and tissue microarray. *Am J Pathol* 159(4), pp. 1495-1505.

Palucka, K. and Banchereau, J. 2012. Cancer immunotherapy via dendritic cells. *Nat Rev Cancer* 12(4), pp. 265-277.

Pani, G. et al. 1996. Signaling capacity of the T cell antigen receptor is negatively regulated by the PTP1C tyrosine phosphatase. *J Exp Med* 184(3), pp. 839-852.

Papayannakos, C. and Daniel, R. 2013. Understanding lentiviral vector chromatin targeting: working to reduce insertional mutagenic potential for gene therapy. *Gene Ther* 20(6), pp. 581-588.

Parkhurst, M. R. et al. 2011. T cells targeting carcinoembryonic antigen can mediate regression of metastatic colorectal cancer but induce severe transient colitis. *Mol Ther* 19(3), pp. 620-626.

Pavalko, F. M. et al. 1995. The cytoplasmic domain of L-selectin interacts with cytoskeletal proteins via alpha-actinin: receptor positioning in microvilli does not require interaction with alpha-actinin. *J Cell Biol* 129(4), pp. 1155-1164.

Pavletich, N. P. and Pabo, C. O. 1991. Zinc finger-DNA recognition: crystal structure of a Zif268-DNA complex at 2.1 A. *Science* 252(5007), pp. 809-817.

Pei, D. et al. 1996. Differential functions of the two Src homology 2 domains in protein tyrosine phosphatase SH-PTP1. *Proc Natl Acad Sci U S A* 93(3), pp. 1141-1145.

Perez, E. E. et al. 2008. Establishment of HIV-1 resistance in CD4+ T cells by genome editing using zinc-finger nucleases. *Nat Biotechnol* 26(7), pp. 808-816.

Peschon, J. J. et al. 1998. An essential role for ectodomain shedding in mammalian development. *Science* 282(5392), pp. 1281-1284.

Phongpradist, R. et al. 2010. LFA-1 on leukemic cells as a target for therapy or drug delivery. *Curr Pharm Des* 16(21), pp. 2321-2330.

Pilon-Thomas, S. et al. 2012. Efficacy of adoptive cell transfer of tumor-infiltrating lymphocytes after lymphopenia induction for metastatic melanoma. *J Immunother* 35(8), pp. 615-620.

Plas, D. R. et al. 1996. Direct regulation of ZAP-70 by SHP-1 in T cell antigen receptor signaling. *Science* 272(5265), pp. 1173-1176.

Pluskey, S. et al. 1995. Potent stimulation of SH-PTP2 phosphatase activity by simultaneous occupancy of both SH2 domains. *J Biol Chem* 270(7), pp. 2897-2900.

Plutzky, J. et al. 1992a. Isolation of a src homology 2-containing tyrosine phosphatase. *Proc Natl Acad Sci U S A* 89(3), pp. 1123-1127.

Plutzky, J. et al. 1992b. Chromosomal localization of an SH2-containing tyrosine phosphatase (PTPN6). *Genomics* 13(3), pp. 869-872.

Poole, A. W. and Jones, M. L. 2005. A SHPing tale: perspectives on the regulation of SHP-1 and SHP-2 tyrosine phosphatases by the C-terminal tail. *Cell Signal* 17(11), pp. 1323-1332.

Poznansky, M. et al. 1991. Gene transfer into human lymphocytes by a defective human immunodeficiency virus type 1 vector. *J Virol* 65(1), pp. 532-536.

Preece, G. et al. 1996. Metalloproteinase-mediated regulation of L-selectin levels on leucocytes. *J Biol Chem* 271(20), pp. 11634-11640.

Preston, G. C. et al. 2013. The impact of KLF2 modulation on the transcriptional program and function of CD8 T cells. *PLoS One* 8(10), p. e77537.

Provasi, E. et al. 2012. Editing T cell specificity towards leukemia by zinc finger nucleases and lentiviral gene transfer. *Nat Med* 18(5), pp. 807-815.

Purbhoo, M. A. et al. 2004. T cell killing does not require the formation of a stable mature immunological synapse. *Nat Immunol* 5(5), pp. 524-530.

Qasim, W. and Thrasher, A. J. 2014. Progress and prospects for engineered T cell therapies. *Br J Haematol* 166(6), pp. 818-829.

Qu, C. K. et al. 2001. Requirement of Shp-2 tyrosine phosphatase in lymphoid and hematopoietic cell development. *Blood* 97(4), pp. 911-914.

Quintana, E. et al. 2008. Efficient tumour formation by single human melanoma cells. *Nature* 456(7222), pp. 593-598.

Ren, D. et al. 2002. PPARgamma knockdown by engineered transcription factors: exogenous PPARgamma2 but not PPARgamma1 reactivates adipogenesis. *Genes Dev* 16(1), pp. 27-32.

Rhee, I. and Veillette, A. 2012. Protein tyrosine phosphatases in lymphocyte activation and autoimmunity. *Nat Immunol* 13(5), pp. 439-447.

Richards, H. et al. 2008. CD62L (L-selectin) down-regulation does not affect memory T cell distribution but failure to shed compromises anti-viral immunity. *J Immunol* 180(1), pp. 198-206.

Richardson, M. W. et al. 2008. Mode of transmission affects the sensitivity of human immunodeficiency virus type 1 to restriction by rhesus TRIM5alpha. *J Virol* 82(22), pp. 11117-11128.

Rieux-Laucat, F. et al. 2003. Cell-death signaling and human disease. *Curr Opin Immunol* 15(3), pp. 325-331.

Robbins, P. F. et al. 2011. Tumor regression in patients with metastatic synovial cell sarcoma and melanoma using genetically engineered lymphocytes reactive with NY-ESO-1. *J Clin Oncol* 29(7), pp. 917-924.

Rosenberg, S. A. et al. 1990. Gene transfer into humans--immunotherapy of patients with advanced melanoma, using tumor-infiltrating lymphocytes modified by retroviral gene transduction. *N Engl J Med* 323(9), pp. 570-578.

Rosenberg, S. A. et al. 1988. Use of tumor-infiltrating lymphocytes and interleukin-2 in the immunotherapy of patients with metastatic melanoma. A preliminary report. *N Engl J Med* 319(25), pp. 1676-1680.

Rosenberg, S. A. and Restifo, N. P. 2015. Adoptive cell transfer as personalized immunotherapy for human cancer. *Science* 348(6230), pp. 62-68.

Ryan, M. D. et al. 1991. Cleavage of foot-and-mouth disease virus polyprotein is mediated by residues located within a 19 amino acid sequence. *J Gen Virol* 72 (Pt 11), pp. 2727-2732.

Sanber, K. S. et al. 2015. Construction of stable packaging cell lines for clinical lentiviral vector production. *Sci Rep* 5, p. 9021.

Sander, J. D. et al. 2011. Selection-free zinc-finger-nuclease engineering by context-dependent assembly (CoDA). *Nat Methods* 8(1), pp. 67-69.

Sankarshanan, M. et al. 2007. Identification of a novel lipid raft-targeting motif in Src homology 2-containing phosphatase 1. *J Immunol* 179(1), pp. 483-490.

Sathish, J. G. et al. 2007. Loss of Src homology region 2 domain-containing protein tyrosine phosphatase-1 increases CD8+ T cell-APC conjugate formation and is associated with enhanced in vivo CTL function. *J Immunol* 178(1), pp. 330-337.

Sathish, J. G. et al. 2001a. Constitutive association of SHP-1 with leukocyte-associated Ig-like receptor-1 in human T cells. *J Immunol* 166(3), pp. 1763-1770.

Sathish, J. G. et al. 2001b. Requirement for CD28 co-stimulation is lower in SHP-1-deficient T cells. *Eur J Immunol* 31(12), pp. 3649-3658.

Sato, E. et al. 2005. Intraepithelial CD8+ tumor-infiltrating lymphocytes and a high CD8+/regulatory T cell ratio are associated with favorable prognosis in ovarian cancer. *Proc Natl Acad Sci U S A* 102(51), pp. 18538-18543.

Schleiffenbaum, B. et al. 1992. Soluble L-selectin is present in human plasma at high levels and retains functional activity. *J Cell Biol* 119(1), pp. 229-238.

Schnell, F. J. et al. 2009. CD8+ T cell responses to a viral escape mutant epitope: active suppression via altered SHP-1 activity. *J Immunol* 182(4), pp. 1829-1835.

Sharma, P. and Allison, J. P. 2015. The future of immune checkpoint therapy. *Science* 348(6230), pp. 56-61.

Shimada, T. et al. 1991. Targeted and highly efficient gene transfer into CD4+ cells by a recombinant human immunodeficiency virus retroviral vector. *J Clin Invest* 88(3), pp. 1043-1047.

Shimizu, Y. et al. 2009. Restricted spacer tolerance of a zinc finger nuclease with a six amino acid linker. *Bioorg Med Chem Lett* 19(14), pp. 3970-3972.

Shultz, L. D. et al. 2012. Humanized mice for immune system investigation: progress, promise and challenges. *Nat Rev Immunol* 12(11), pp. 786-798.

Shultz, L. D. et al. 1984. "Viable motheaten," a new allele at the motheaten locus. I. Pathology. *Am J Pathol* 116(2), pp. 179-192.

Shultz, L. D. et al. 1995. Multiple defects in innate and adaptive immunologic function in NOD/LtSz-scid mice. *J Immunol* 154(1), pp. 180-191.

Shultz, L. D. et al. 1993. Mutations at the murine motheaten locus are within the hematopoietic cell protein-tyrosine phosphatase (Hcph) gene. *Cell* 73(7), pp. 1445-1454.

Smalley, D. M. and Ley, K. 2005. L-selectin: mechanisms and physiological significance of ectodomain cleavage. *J Cell Mol Med* 9(2), pp. 255-266.

Smith, F. O. et al. 2009. Impact of a recombinant fowlpox vaccine on the efficacy of adoptive cell therapy with tumor infiltrating lymphocytes in a patient with metastatic melanoma. *J Immunother* 32(8), pp. 870-874.

Smith, J. et al. 2000. Requirements for double-strand cleavage by chimeric restriction enzymes with zinc finger DNA-recognition domains. *Nucleic Acids Res* 28(17), pp. 3361-3369.

Steeber, D. A. et al. 1997. Ligation of L-selectin through conserved regions within the lectin domain activates signal transduction pathways and integrin function in human, mouse, and rat leukocytes. *J Immunol* 159(2), pp. 952-963.

Stefanova, I. et al. 2003. TCR ligand discrimination is enforced by competing ERK positive and SHP-1 negative feedback pathways. *Nat Immunol* 4(3), pp. 248-254.

Stoddart, J. H., Jr. et al. 1996. Protease-resistant L-selectin mutants. Down-modulation by cross-linking but not cellular activation. *J Immunol* 157(12), pp. 5653-5659.

Stolzenburg, S. et al. 2015. Stable oncogenic silencing in vivo by programmable and targeted de novo DNA methylation in breast cancer. *Oncogene*.

Stoyanova, T. et al. 2012. Regulated proteolysis of Trop2 drives epithelial hyperplasia and stem cell self-renewal via beta-catenin signaling. *Genes Dev* 26(20), pp. 2271-2285.

Strauss, D. C. and Thomas, J. M. 2010. Transmission of donor melanoma by organ transplantation. *Lancet Oncol* 11(8), pp. 790-796.

Stromnes, I. M. et al. 2012. Abrogation of SRC homology region 2 domain-containing phosphatase 1 in tumor-specific T cells improves efficacy of adoptive immunotherapy by enhancing the effector function and accumulation of short-lived effector T cells in vivo. *J Immunol* 189(4), pp. 1812-1825.

Strowig, T. et al. 2009. Priming of protective T cell responses against virus-induced tumors in mice with human immune system components. *J Exp Med* 206(6), pp. 1423-1434.

Subramanian, H. et al. 2012. Signaling through L-selectin mediates enhanced chemotaxis of lymphocyte subsets to secondary lymphoid tissue chemokine. *J Immunol* 188(7), pp. 3223-3236.

Sun, A. et al. 2006. Human interleukin-15 improves engraftment of human T cells in NOD-SCID mice. *Clin Vaccine Immunol* 13(2), pp. 227-234.

Surh, C. D. and Sprent, J. 2008. Homeostasis of naive and memory T cells. *Immunity* 29(6), pp. 848-862.

Tape, C. J. et al. 2011. Cross-domain inhibition of TACE ectodomain. *Proc Natl Acad Sci U S A* 108(14), pp. 5578-5583.

Tebas, P. et al. 2014. Gene editing of CCR5 in autologous CD4 T cells of persons infected with HIV. *N Engl J Med* 370(10), pp. 901-910.

Tomczuk, M. et al. 2003. Role of multiple beta1 integrins in cell adhesion to the disintegrin domains of ADAMs 2 and 3. *Exp Cell Res* 290(1), pp. 68-81.

Uchida, T. et al. 1994. Insulin stimulates the phosphorylation of Tyr538 and the catalytic activity of PTP1C, a protein tyrosine phosphatase with Src homology-2 domains. *J Biol Chem* 269(16), pp. 12220-12228.

Unsoeld, H. and Pircher, H. 2005. Complex memory T-cell phenotypes revealed by coexpression of CD62L and CCR7. *J Virol* 79(7), pp. 4510-4513.

Urnov, F. D. et al. 2005. Highly efficient endogenous human gene correction using designed zinc-finger nucleases. *Nature* 435(7042), pp. 646-651.

Valitutti, S. et al. 1995. Serial triggering of many T-cell receptors by a few peptide-MHC complexes. *Nature* 375(6527), pp. 148-151.

Van Maele, B. et al. 2003. Impact of the central polypurine tract on the kinetics of human immunodeficiency virus type 1 vector transduction. *J Virol* 77(8), pp. 4685-4694.

Varela-Rohena, A. et al. 2008. Control of HIV-1 immune escape by CD8 T cells expressing enhanced T-cell receptor. *Nat Med* 14(12), pp. 1390-1395.

Veillette, A. et al. 1988. The CD4 and CD8 T cell surface antigens are associated with the internal membrane tyrosine-protein kinase p56lck. *Cell* 55(2), pp. 301-308.

Vely, F. et al. 1997. Differential association of phosphatases with hematopoietic co-receptors bearing immunoreceptor tyrosine-based inhibition motifs. *Eur J Immunol* 27(8), pp. 1994-2000.

Victor, C. T.-S. et al. 2015. Radiation and dual checkpoint blockade activate non-redundant immune mechanisms in cancer. *Nature* advance online publication.

Votavova, P. et al. 2014. Increasing the biological activity of IL-2 and IL-15 through complexing with anti-IL-2 mAbs and IL-15Ralpha-Fc chimera. *Immunol Lett* 159(1-2), pp. 1-10.

Walcheck, B. et al. 2003. ADAM-17-independent shedding of L-selectin. *J Leukoc Biol* 74(3), pp. 389-394.

Wang, W. et al. 2011. Crystal Structure of Human Protein Tyrosine Phosphatase SHP-1 in the Open Conformation. *Journal of Cellular Biochemistry* 112(8), pp. 2062-2071.

Wanisch, K. and Yanez-Munoz, R. J. 2009. Integration-deficient lentiviral vectors: a slow coming of age. *Mol Ther* 17(8), pp. 1316-1332.

Wasserman, H. A. et al. 2008. MHC variant peptide-mediated anergy of encephalitogenic T cells requires SHP-1. *J Immunol* 181(10), pp. 6843-6849.

Wyman, C. and Kanaar, R. 2006. DNA double-strand break repair: all's well that ends well. *Annu Rev Genet* 40, pp. 363-383.

Yago, T. et al. 2004. Catch bonds govern adhesion through L-selectin at threshold shear. *J Cell Biol* 166(6), pp. 913-923.

Yanez-Munoz, R. J. et al. 2006. Effective gene therapy with nonintegrating lentiviral vectors. *Nat Med* 12(3), pp. 348-353.

Yang, J. et al. 2003. Crystal structure of human protein-tyrosine phosphatase SHP-1. *J Biol Chem* 278(8), pp. 6516-6520.

Yang, S. et al. 2011. In vitro generated anti-tumor T lymphocytes exhibit distinct subsets mimicking in vivo antigen-experienced cells. *Cancer Immunol Immunother* 60(5), pp. 739-749.

Yang, W. et al. 2002. A bipartite NLS at the SHP-1 C-terminus mediates cytokine-induced SHP-1 nuclear localization in cell growth control. *Blood Cells Mol Dis* 28(1), pp. 63-74.

Yi, T. et al. 2011. Phosphatase inhibitor, sodium stibogluconate, in combination with interferon (IFN) alpha 2b: phase I trials to identify pharmacodynamic and clinical effects. *Oncotarget* 2(12), pp. 1155-1164.

Yi, T. et al. 2002. Anticancer activity of sodium stibogluconate in synergy with IFNs. *J Immunol* 169(10), pp. 5978-5985.

Yi, T. L. et al. 1992. Protein tyrosine phosphatase containing SH2 domains: characterization, preferential expression in hematopoietic cells, and localization to human chromosome 12p12-p13. *Mol Cell Biol* 12(2), pp. 836-846.

Yokosuka, T. et al. 2010. Spatiotemporal basis of CTLA-4 costimulatory molecule-mediated negative regulation of T cell activation. *Immunity* 33(3), pp. 326-339.

Yokosuka, T. et al. 2012. Programmed cell death 1 forms negative costimulatory microclusters that directly inhibit T cell receptor signaling by recruiting phosphatase SHP2. *The Journal of Experimental Medicine* 209(6), pp. 1201-1217.

Yu, C. C. et al. 1996. B and T cells are not required for the viable motheaten phenotype. *J Exp Med* 183(2), pp. 371-380.

Yusa, K. et al. 2011. Targeted gene correction of alpha1-antitrypsin deficiency in induced pluripotent stem cells. *Nature* 478(7369), pp. 391-394.

Zhang, N. and Bevan, M. J. 2011. CD8(+) T cells: foot soldiers of the immune system. *Immunity* 35(2), pp. 161-168.

Zhang, Q. et al. 2000. Lack of phosphotyrosine phosphatase SHP-1 expression in malignant T-cell lymphoma cells results from methylation of the SHP-1 promoter. *Am J Pathol* 157(4), pp. 1137-1146.

Zhang, Z. Y. 2002. Protein tyrosine phosphatases: structure and function, substrate specificity, and inhibitor development. *Annu Rev Pharmacol Toxicol* 42, pp. 209-234.

Zhang, Z. Y. et al. 1994. The Cys(X)5Arg catalytic motif in phosphoester hydrolysis. *Biochemistry* 33(51), pp. 15266-15270.

Zhao, L. C. et al. 2001. Characterization of the rapid proteolytic shedding of murine L-selectin. *Dev Immunol* 8(3-4), pp. 267-277.

Zhou, Q. et al. 2014. Humanized NOD-SCID IL2rg-/- mice as a preclinical model for cancer research and its potential use for individualized cancer therapies. *Cancer Lett* 344(1), pp. 13-19.

Zitvogel, L. et al. 2006. Cancer despite immunosurveillance: immunoselection and immunosubversion. *Nat Rev Immunol* 6(10), pp. 715-727.

Zufferey, R. et al. 1998. Self-inactivating lentivirus vector for safe and efficient in vivo gene delivery. *J Virol* 72(12), pp. 9873-9880.

Appendix

Appendix A1: Primers

Primer number	Primer sequence		Reference to figure or assay
9	*ATTCGGATCC*TCTAGAGCCGCCACC**ATG**GACTACAAAGACCATGACGG	F	3.2.2
10	*CGCTGCCG*CTCTCGAGAGATCTGAAGTTGATCTCGCCGTTG	R	
17	ATCCACGGGGTTCCCGCCGCTAT	F	3.2.3
18	ATAGCGGCGGGAACCCCGTGGAT	R	
19	*ACCCTGGCCCGCGC*GGTACC**ATG**AGATCTGACTACAAAGACCATGAC	F	3.2.4
20	*CTTGGATCC*GCGGCCGCGAAGTTGATCTCGCCGTTGTTGAAC	R	
57	*ATCAACTTC*GCGGCCGCAAGCGGCTCCGGTGCCA	F	3.2.5
30	*TTGGATCC*GCGGCCGC**TTA**CCGTTTTTTCCTCTTGCAG	R	
52	*CGCCCGGGGG*GGATCCGCCGCCACC**ATG**GACTACAA	F	3.2.6
32	*CTCGAGCCC*GGGATCC**TTA**CCGTTTTTTCCTCTTGCAG	R	
60	*CGCCCGGGGG*GGATCCGCCGCCACC**ATG**GACTACAAAGACCATGACG	F	3.3.1
61	*CTCGAGCCC*GGGATCCTCAAGATCTGAAGTTGATCTCGC	R	
55	GAGTCCGAGGATACAGCCAA	F	Cel-I assay
56	GAGGGTGGAGACCTGTGAGA	R	398bp SHP-1
58	GGCACACAGTAGGTGCTTGA	F	3.2.10
59	CCTAGCAGCTGGTTCTGGAC	R	1733bp SHP-1
62	*CGCCCGGGGG*GGATCCGCCGCCACC**ATG**GGTAAGCCTATCCCTAACCCTCTCCTCGGTCTCGATTCTACG**ATG**GCCCCCAAGAAGAAGAGGA	F	3.3.2
63	*CTCGAGCCC*GGGATCCTCAGAAGTTGATCTCGCCGTTG	R	
66	*CGCCCGGGGG*GGATCCGCCGCCACC**ATG**GCCCCCAAGAAGAAGA	F	3.3.3
32	*CTCGAGCCC*GGGATCC**TTA**CCGTTTTTTCCTCTTGCAG	R	
68	GCCGCCACC**ATG**GTGAGGTGGTTTCACCGAGACCTC	F	3.8.1 A)
69	**TCA**CTTCCTCTTGAGGGAAC	R	
70	*CGCCCGGGGG*GGATCCGCCGCCACC**ATG**GTGA	F	3.8.1 B)
71	*CTCGAGCCC*GGGATCC**TCA**CTTCCTCTTGAGGGAACCC	R	
80	GTGTACGGCTACAGGGGAAA	F	FokI domain
81	TGGGGTTGAGGTGCTTATTC	R	not used

Table A1: Primers used for cloning in Chapter 3. Numbered forward (F) and reverse (R) primers for In-Fusion reactions (orange), site-directed mutagenesis (red) or other uses (magenta) are shown. For In-Fusion reactions, primer sequence homology with the vector backbone is indicated in italics followed by the underlined sequence of the restriction enzyme sites utilised (BamHI=GGATCC, KpnI=GGTACC, NotI=GCGGCCGC, XbaI=TCTAGA and XhoI=CTCGAG). Start (ATG) and stop (TAA, TGA, TAG) codons are indicated in bold and the Kozak consensus sequence is shown in green. The red nucleotide either indicates an altered nucleotide for site-directed mutagenesis or an introduction of additional nucleotide. The V5 tag sequence highlighted in green.

Primer number	Primer sequence		Binding site of primer
4	AGATCTCAAATGCTCCCGAT	R	CD2 219
5	ATCGGGAGCATTTGAGATCT	F	CD2 219
6	GCTGACCCTGTTTACCGCCT	R	CD2 539
7	AGGCGGTAAACAGGGTCAGC	F	CD2 539
8	GAAACAGCTATGACCATGTT	R	pUC19 downstream of stop codon
11	CTGCAAGGCGATTAAGTTGGG	F	pUC19 75 upstream of start codon
12	CGACACTGGAAGGGCCGTTG	R	ZFN1 298
13	CAACGGCCCTTCCAGTGTCG	F	ZFN1 298
14	CCAGGTGCTTTCCCCTGTAG	R	ZFN1 717
15	CTACAGGGGAAAGCACCTGG	F	ZFN1 717
16	ATCGCCCTCGCCCTCGCCGG	R	within GFP
21	CACATCACCAACTGCAATGGC	F	ZFN1 1015
22	AGGTGGCCGGACTGACTGAA	R	ZFN2 253
23	TTCAGTCAGTCCGGCCACCT	F	ZFN2 253
24	CTGCCCACTGTATAGATGGC	R	ZFN2 766
25	GCCATCTATACAGTGGGCAG	F	ZFN2 766
26	GCAGTGAGCGCAACGCAATT	R	pUC reverse
33	AATCAGCCTGCTTCTCGCT	F	pSxW
34	GCGTATCCACATAGCGTAAA	R	pSxW
53	AGATCTCTCGAGAGCGGCAG	F	within T2A
54	CTGCCGCTCTCGAGAGATCT	R	within T2A
72	GGGCGAGCCCTGGACGT	F	SHP-1 381
73	GGTCCGACTACATCAATGCC	F	SHP-1 893
74	CCAAGGGCCTGGACTGTG	F	SHP-1 1424
75	CAGCCTTGGGCTGGTCA	R	SHP-1 453
76	TGACCGTGGCCTCCAGACA	R	SHP-1 979
77	ACTTGTACTGCGCCTCCG	R	SHP-1 1502
T7	TAATACGACTCACTATAGGG	F	TA cloning
SP6	CTATAGTGTCACCTAAATA	R	TA cloning

Table A2: Primers used for sequencing. Numbered forward (F) and reverse (R) primers used for sequencing are shown and the binding site within a gene is indicated.

Primer number	Primer sequence		Reference to figure
45	*CGCCCGGGGG*GGATCCGCCGCCACC**ATG**GGCTGC AGAAGAACTAGAG	F	6.2
46	*CTCGAGCCCG*GGATCC**TTA**ATATGGGTCATTCATAC TTCTC	R	6.2 and 6.6
47	AGAATCCAGGCCCCATGCATATGGGCTGCAGAAGA ACTAGAG	F	6.4
48	*TATCTTATTA*GTCGAC**TTA**ATATGGGTCATTCATAC TTCTC	R	6.4
49	*ATTTAATTAA*TCTAGAGCCGCCACCATGAGATGTAA ATTCCTAGGGAG	F	6.5
50	*CGGAGCCGCT*CTCGAGCCGTTTTTTCCTCTTGCAGA TAC	R	6.5
51	*CGCCCGGGGG*GGATCCGCCGCCACCATGAGAT	F	6.6
64	GGGTTGGCATTTATCA**AG**TGGCTGGCAAGGAGA	F	6.2
65	TCTCCTTGCCAGCCA**CT**TGATAAATGCCAACCC	R	6.2
Primer number	**Primer sequence**		**Binding site of primer**
37	ATGGGCTGCAGAAGAACTAG	F	L-selectin start codon
38	CTGTGTAATTGTCTCGGCAG	R	L-selectin 206
39	TACACAGCTTCTTGCCAGCC	F	L-selectin 504
40	CCTCCAAAGGCTCACACTGA	R	L-selectin 623
41	GCATGTACCTTCATCTGCTCAG	F	L-selectin 888
42	ATATGGGTCATTCATACTTC	R	L-selectin stop codon
33	AATCAGCCTGCTTCTCGCT	F	pSxW
34	GCGTATCCACATAGCGTAAA	R	pSxW
4	AGATCTCAAATGCTCCCGAT	R	CD2 219
5	ATCGGGAGCATTTGAGATCT	F	CD2 219
6	GCTGACCCTGTTTACCGCCT	R	CD2 539
7	AGGCGGTAAACAGGGTCAGC	F	CD2 539
8	GAAACAGCTATGACCATGTT	R	pUC19 downstream of stop codon

Table A3: Primers used for cloning and sequencing in Chapter 6. Numbered forward (F) and reverse (R) primers for In-Fusion reactions (orange), site-directed mutagenesis (red) and sequencing (blue) are shown. For In-Fusion reactions, primer sequence homology with the vector backbone is indicated in italics followed by the underlined sequence of the restriction enzyme sites utilised (BamHI=GGATCC, NsiI=ATGCAT, SalI=GTCGAC, KpnI=GGTACC, XbaI=TCTAGA and XhoI=CTCGAG). Start (ATG) and stop (TAA, TGA, TAG) codons are indicated in bold and the Kozak consensus sequence is shown in green. For the sequencing primers the binding site within a gene is indicated.

Appendix A2: DNA sequences of plasmids generated in chapter 3 and 6

All sequences below were inserted into the BamHI site in the lentiviral transfer pSxW plasmid. Kozak consensus sequences are shown in green letters, ZFN and L-selectin sequences are highlighted in grey, the CD2 sequence is highlighted in green and the T2A and P2A sequences are highlighted in turquoise. The 3xFlag or V5 tags are highlighted in pink. Unlabelled sequences correspond to restriction sites.

pLenti-ZFN1-T2A-ZFN2-P2A-CD2 (from figure 3.2 and 3.7)

GCCGCCACCATGGACTACAAAGACCATGACGGTGATTATAAAGATCATGACATCGATTACAAGGATGA
CGATGACAAGATGGCCCCCAAGAAGAAGAGGAAGGTGGGCATCCACGGGGTTCCCGCCGCTATGGCT
GAGAGGCCCTTCCAGTGTCGAATCTGCATGCGTAACTTCAGTCGCTCCGACCACCTGTCCCGCCACATC
CGCACCCACACCGGCGAGAAGCCTTTTGCCTGTGACATTTGTGGGAGGAAATTTGCCACCTCCGGCCAC
CTGTCCCGCCATACCAAGATACACACGGGCGGACAACGGCCCTTCCAGTGTCGAATCTGCATGCGTAAC
TTCAGTCGTAGTGACAGCCTGAGCGTACACATCCGCACCCACACAGGCGAGAAGCCTTTTGCCTGTGAC
ATTTGTGGGAGGAAATTTGCCACCAACCACAACCGCAAAACGCATACCAAGATACACACGGGCGAGAA
GCCCTTCCAGTGTCGAATCTGCATGCGTAAGTTTGCCCAGAACGCCCACCGCAAGACCCATACCAAGAT
ACACCTGCGGGGATCCCAGCTGGTGAAGAGCGAGCTGGAGGAGAAGAAGTCCGAGCTGCGGCACAA
GCTGAAGTACGTGCCCCACGAGTACATCGAGCTGATCGAGATCGCCAGGAACAGCACCCAGGACCGCA
TCCTGGAGATGAAGGTGATGGAGTTCTTCATGAAGGTGTACGGCTACAGGGGAAAGCACCTGGGCGG
AAGCAGAAAGCCTGACGGCGCCATCTATACAGTGGGCAGCCCCATCGATTACGGCGTGATCGTGGACA
CAAAGGCCTACAGCGGCGGCTACAATCTGCCTATCGGCCAGGCCGACGAGATGGAGAGATACGTGGA
GGAGAACCAGACCCGGAATAAGCACCTCAACCCCAACGAGTGGTGGAAGGTGTACCCTAGCAGCGTG
ACCGAGTTCAAGTTCCTGTTCGTGAGCGGCCACTTCAAGGGCAACTACAAGGCCCAGCTGACCAGGCT
GAACCACATCACCAACTGCAATGGCGCCGTGCTGAGCGTGGAGGAGCTGCTGATCGGCGGCGAGATG
ATCAAAGCCGGCACCCTGACACTGGAGGAGGTGCGGCGCAAGTTCAACAACGGCGAGATCAACTTCA
GATCTCTCGAGAGCGGCAGCGGGCGCAGCGGCAGCGGCGAAGGCCGCGGCAGCCTGCTGACCTGCG
GCGATGTGGAAGAAAACCCTGGCCCGCGCGGTACCATGAGATCTGACTACAAAGACCATGACGGTGAT
TATAAAGATCATGACATCGATTACAAGGATGACGATGACAAGATGGCCCCCAAGAAGAAGAGGAAGG
TGGGCATTCATGGGGTACCCGCCGCTATGGCTGAGAGGCCCTTCCAGTGTCGAATCTGCATGCGTAAG
TTTGCCACCTCCGGCCACCTGTCCCGCCATACCAAGATACACACGGGCGAGAAGCCCTTCCAGTGTCGA
ATCTGCATGCGTAACTTCAGTCAGTCCGGCCACCTGCAGCGCCACATCCGCACCCACACCGGCGAGAAG
CCTTTTGCCTGTGACATTTGTGGGAGGAAATTTGCCCAGTCCGGCGACCTGACCCGCCATACCAAGATA
CACACGGGATCTCAGAAGCCCTTCCAGTGTCGAATCTGCATGCGTAACTTCAGTCAGTCCGGCAACCTG
GCCCGCCACATCCGCACCCACACCGGCGAGAAGCCTTTTGCCTGTGACATTTGTGGGAGGAAATTTGCC
CAGTCCGGCGACCTGACCCGCCATACCAAGATACACCTGCGGGGATCCCAGCTGGTGAAGAGCGAGCT
GGAGGAGAAGAAGTCCGAGCTGCGGCACAAGCTGAAGTACGTGCCCCACGAGTACATCGAGCTGATC
GAGATCGCCAGGAACAGCACCCAGGACCGCATCCTGGAGATGAAGGTGATGGAGTTCTTCATGAAGG
TGTACGGCTACAGGGGAAAGCACCTGGGCGGAAGCAGAAAGCCTGACGGCGCCATCTATACAGTGGG
CAGCCCCATCGATTACGGCGTGATCGTGGACACAAAGGCCTACAGCGGCGGCTACAATCTGCCTATCG

GCCAGGCCGACGAGATGCAGAGATACGTGAAGGAGAACCAGACCCGGAATAAGCACATCAACCCCAA
CGAGTGGTGGAAGGTGTACCCTAGCAGCGTGACCGAGTTCAAGTTCCTGTTCGTGAGCGGCCACTTCA
AGGGCAACTACAAGGCCCAGCTGACCAGGCTGAACCACAAAACCAACTGCAATGGCGCCGTGCTGAGC
GTGGAGGAGCTGCTGATCGGCGGCGAGATGATCAAAGCCGGCACCCTGACACTGGAGGAGGTGCGG
CGCAAGTTCAACAACGGCGAGATCAACTTCGCGGCCGCAAGCGGCTCCGGTGCCACCAACTTCTCTCTG
CTGAAGCAGGCCGGGGATGTCGAAGAGAATCCAGGCCCCATGCATATGAGATGTAAATTCCTAGGGA
GTTTCTTTCTGCTCTTCAGCCTGTCCAGCAAAGGAGCAGACTGCAGAGACAGTGGGACCGTCTGGGGT
GCCCTGGGTCATGGCATCAACCTGAACATCCCTAACTTTCAAATGACTGATGATATTGATGAGGTGCGA
TGGGAGAGGGGGAGCACCCTGGTTGCCGAGTTTAAAAGGAAGATGAAGCCTTTTTTGAAATCGGGAG
CATTTGAGATCTTAGCAAATGGAGACTTGAAGATAAAGAATCTGACAAGAGATGACAGTGGCACCTAT
AATGTAACGGTATACAGCACAAATGGGACACGTATCCTGAACAAGGCACTGGACTTGAGGATTCTGGA
GATGGTCTCAAAGCCGATGATCTACTGGGAGTGCAGCAACGCAACCCTGACCTGTGAGGTCTTGGAAG
GAACAGATGTTGAACTAAAGCTGTACCAAGGAAAGGAGCATCTCAGGAGCCTCCGTCAGAAGACCATG
AGTTACCAGTGGACCAACCTGAGAGCACCGTTTAAGTGCAAGGCGGTAAACAGGGTCAGCCAGGAGT
CTGAGATGGAAGTTGTCAACTGTCCAGAGAAAGGTCTGCCCCTCTATCTCATAGTGGGGGTCAGTGCA
GGAGGACTCCTCTTGGTGTTCTTTGGGGCGCTGTTTATTTTCTGTATCTGCAAGAGGAAAAAACGGTAA

pLenti-3xFlag-ZFN1 (from figure 3.15)

GCCGCCACCATGGACTACAAAGACCATGACGGTGATTATAAAGATCATGACATCGATTACAAGGATGA
CGATGACAAGATGGCCCCCAAGAAGAAGAGGAAGGTGGGCATCCACGGGGTACCCGCCGCTATGGCT
GAGAGGCCCTTCCAGTGTCGAATCTGCATGCGTAACTTCAGTCGCTCCGACCACCTGTCCCGCCACATC
CGCACCCACACCGGCGAGAAGCCTTTTGCCTGTGACATTTGTGGGAGGAAATTTGCCACCTCCGGCCAC
CTGTCCCGCCATACCAAGATACACACGGGCGGACAACGGCCCTTCCAGTGTCGAATCTGCATGCGTAAC
TTCAGTCGTAGTGACAGCCTGAGCGTACACATCCGCACCCACACAGGCGAGAAGCCTTTTGCCTGTGAC
ATTTGTGGGAGGAAATTTGCCACCAACCACAACCGCAAAACGCATACCAAGATACACACGGGCGAGAA
GCCCTTCCAGTGTCGAATCTGCATGCGTAAGTTTGCCCAGAACGCCCACCGCAAGACCCATACCAAGAT
ACACCTGCGGGGATCCCAGCTGGTGAAGAGCGAGCTGGAGGAGAAGAAGTCCGAGCTGCGGCACAA
GCTGAAGTACGTGCCCCACGAGTACATCGAGCTGATCGAGATCGCCAGGAACAGCACCCAGGACCGCA
TCCTGGAGATGAAGGTGATGGAGTTCTTCATGAAGGTGTACGGCTACAGGGGAAAGCACCTGGGCGG
AAGCAGAAAGCCTGACGGCGCCATCTATACAGTGGGCAGCCCCATCGATTACGGCGTGATCGTGGACA
CAAAGGCCTACAGCGGCGGCTACAATCTGCCTATCGGCCAGGCCGACGAGATGGAGAGATACGTGGA
GGAGAACCAGACCCGGAATAAGCACCTCAACCCCAACGAGTGGTGGAAGGTGTACCCTAGCAGCGTG
ACCGAGTTCAAGTTCCTGTTCGTGAGCGGCCACTTCAAGGGCAACTACAAGGCCCAGCTGACCAGGCT
GAACCACATCACCAACTGCAATGGCGCCGTGCTGAGCGTGGAGGAGCTGCTGATCGGCGGCGAGATG
ATCAAAGCCGGCACCCTGACACTGGAGGAGGTGCGGCGCAAGTTCAACAACGGCGAGATCAACTTCA
GATCTTGA

pLenti-V5-ZFN2 (from figure 3.16)

GCCGCCACCATGGGTAAGCCTATCCCTAACCCTCTCCTCGGTCTCGATTCTACGATGGCCCCCAAGAAG
AAGAGGAAGGTGGGCATTCATGGGGTACCCGCCGCTATGGCTGAGAGGCCCTTCCAGTGTCGAATCTG
CATGCGTAAGTTTGCCACCTCCGGCCACCTGTCCCGCCATACCAAGATACACACGGGCGAGAAGCCCTT
CCAGTGTCGAATCTGCATGCGTAACTTCAGTCAGTCCGGCCACCTGCAGCGCCACATCCGCACCCACAC
CGGCGAGAAGCCTTTTGCCTGTGACATTTGTGGGAGGAAATTTGCCCAGTCCGGCGACCTGACCCGCC
ATACCAAGATACACACGGGATCTCAGAAGCCCTTCCAGTGTCGAATCTGCATGCGTAACTTCAGTCAGT
CCGGCAACCTGGCCCGCCACATCCGCACCCACACCGGCGAGAAGCCTTTTGCCTGTGACATTTGTGGGA
GGAAATTTGCCCAGTCCGGCGACCTGACCCGCCATACCAAGATACACCTGCGGGGATCCCAGCTGGTG
AAGAGCGAGCTGGAGGAGAAGAAGTCCGAGCTGCGGCACAAGCTGAAGTACGTGCCCCACGAGTACA
TCGAGCTGATCGAGATCGCCAGGAACAGCACCCAGGACCGCATCCTGGAGATGAAGGTGATGGAGTT
CTTCATGAAGGTGTACGGCTACAGGGGAAAGCACCTGGGCGGAAGCAGAAAGCCTGACGGCGCCATC
TATACAGTGGGCAGCCCCATCGATTACGGCGTGATCGTGGACACAAAGGCCTACAGCGGCGGCTACAA
TCTGCCTATCGGCCAGGCCGACGAGATGCAGAGATACGTGAAGGAGAACCAGACCCGGAATAAGCAC
ATCAACCCCAACGAGTGGTGGAAGGTGTACCCTAGCAGCGTGACCGAGTTCAAGTTCCTGTTCGTGAG
CGGCCACTTCAAGGGCAACTACAAGGCCCAGCTGACCAGGCTGAACCACAAAACCAACTGCAATGGCG
CCGTGCTGAGCGTGGAGGAGCTGCTGATCGGCGGCGAGATGATCAAAGCCGGCACCCTGACACTGGA
GGAGGTGCGGCGCAAGTTCAACAACGGCGAGATCAACTTCTGA

pLenti-ZFN2-P2A-CD2 (from figure 3.17)

GCCGCCACCATGGCCCCCAAGAAGAAGAGGAAGGTGGGCATTCATGGGGTACCCGCCGCTATGGCTG
AGAGGCCCTTCCAGTGTCGAATCTGCATGCGTAAGTTTGCCACCTCCGGCCACCTGTCCCGCCATACCA
AGATACACACGGGCGAGAAGCCCTTCCAGTGTCGAATCTGCATGCGTAACTTCAGTCAGTCCGGCCACC
TGCAGCGCCACATCCGCACCCACACCGGCGAGAAGCCTTTTGCCTGTGACATTTGTGGGAGGAAATTTG
CCCAGTCCGGCGACCTGACCCGCCATACCAAGATACACACGGGATCTCAGAAGCCCTTCCAGTGTCGAA
TCTGCATGCGTAACTTCAGTCAGTCCGGCAACCTGGCCCGCCACATCCGCACCCACACCGGCGAGAAGC
CTTTTGCCTGTGACATTTGTGGGAGGAAATTTGCCCAGTCCGGCGACCTGACCCGCCATACCAAGATAC
ACCTGCGGGGATCCCAGCTGGTGAAGAGCGAGCTGGAGGAGAAGAAGTCCGAGCTGCGGCACAAGC
TGAAGTACGTGCCCCACGAGTACATCGAGCTGATCGAGATCGCCAGGAACAGCACCCAGGACCGCATC
CTGGAGATGAAGGTGATGGAGTTCTTCATGAAGGTGTACGGCTACAGGGGAAAGCACCTGGGCGGAA
GCAGAAAGCCTGACGGCGCCATCTATACAGTGGGCAGCCCCATCGATTACGGCGTGATCGTGGACACA
AAGGCCTACAGCGGCGGCTACAATCTGCCTATCGGCCAGGCCGACGAGATGCAGAGATACGTGAAGG
AGAACCAGACCCGGAATAAGCACATCAACCCCAACGAGTGGTGGAAGGTGTACCCTAGCAGCGTGACC
GAGTTCAAGTTCCTGTTCGTGAGCGGCCACTTCAAGGGCAACTACAAGGCCCAGCTGACCAGGCTGAA
CCACAAAACCAACTGCAATGGCGCCGTGCTGAGCGTGGAGGAGCTGCTGATCGGCGGCGAGATGATC
AAAGCCGGCACCCTGACACTGGAGGAGGTGCGGCGCAAGTTCAACAACGGCGAGATCAACTTCGCGG
CCGCAAGCGGCTCCGGTGCCACCAACTTCTCTCTGCTGAAGCAGGCCGGGGATGTCGAAGAGAATCCA
GGCCCCATGCATATGAGATGTAAATTCCTAGGGAGTTTCTTTCTGCTCTTCAGCCTGTCCAGCAAAGGA
GCAGACTGCAGAGACAGTGGGACCGTCTGGGGTGCCCTGGGTCATGGCATCAACCTGAACATCCCTAA
CTTTCAAATGACTGATGATATTGATGAGGTGCGATGGGAGAGGGGGAGCACCCTGGTTGCCGAGTTTA
AAAGGAAGATGAAGCCTTTTTTGAAATCGGGAGCATTTGAGATCTTAGCAAATGGAGACTTGAAGATA

AAGAATCTGACAAGAGATGACAGTGGCACCTATAATGTAACGGTATACAGCACAAATGGGACACGTAT
CCTGAACAAGGCACTGGACTTGAGGATTCTGGAGATGGTCTCAAAGCCGATGATCTACTGGGAGTGCA
GCAACGCAACCCTGACCTGTGAGGTCTTGGAAGGAACAGATGTTGAACTAAAGCTGTACCAAGGAAAG
GAGCATCTCAGGAGCCTCCGTCAGAAGACCATGAGTTACCAGTGGACCAACCTGAGAGCACCGTTTAA
GTGCAAGGCGGTAAACAGGGTCAGCCAGGAGTCTGAGATGGAAGTTGTCAACTGTCCAGAGAAAGGT
CTGCCCCTCTATCTCATAGTGGGGGTCAGTGCAGGAGGACTCCTCTTGGTGTTCTTTGGGGCGCTGTTT
ATTTTCTGTATCTGCAAGAGGAAAAAACGGTAA

pLenti-L-selectin wt (from figure 6.2)

GCCGCCACCATGGGCTGCAGAAGAACTAGAGAAGGACCAAGCAAAGCCATGATATTTCCATGGAAATG
TCAGAGCACCCAGAGGGACTTATGGAACATCTTCAAGTTGTGGGGGTGGACAATGCTCTGTTGTGATTT
CCTGGCACATCATGGAACCGACTGCTGGACTTACCATTATTCTGAAAAACCCATGAACTGGCAAAGGGC
TAGAAGATTCTGCCGAGACAATTACACAGATTTAGTTGCCATACAAAACAAGGCGGAAATTGAGTATCT
GGAGAAGACTCTGCCTTTCAGTCGTTCTTACTACTGGATAGGAATCCGGAAGATAGGAGGAATATGGA
CGTGGGTGGGAACCAACAAATCTCTCACTGAAGAAGCAGAGAACTGGGGAGATGGTGAGCCCAACAA
CAAGAAGAACAAGGAGGACTGCGTGGAGATCTATATCAAGAGAAACAAAGATGCAGGCAAATGGAAC
GATGACGCCTGCCACAAACTAAAGGCAGCCCTCTGTTACACAGCTTCTTGCCAGCCCTGGTCATGCAGT
GGCCATGGAGAATGTGTAGAAATCATCAATAATTACACCTGCAACTGTGATGTGGGGTACTATGGGCC
CCAGTGTCAGTTTGTGATTCAGTGTGAGCCTTTGGAGGCCCCAGAGCTGGGTACCATGGACTGTACTCA
CCCTTTGGGAAACTTCAGCTTCAGCTCACAGTGTGCCTTCAGCTGCTCTGAAGGAACAAACTTAACTGG
GATTGAAGAAACCACCTGTGGACCATTTGGAAACTGGTCATCTCCAGAACCAACCTGTCAAGTGATTCA
GTGTGAGCCTCTATCAGCACCAGATTTGGGGATCATGAACTGTAGCCATCCCCTGGCCAGCTTCAGCTT
TACCTCTGCATGTACCTTCATCTGCTCAGAAGGAACTGAGTTAATTGGGAAGAAGAAAACCATTTGTGA
ATCATCTGGAATCTGGTCAAATCCTAGTCCAATATGTCAAAAATTGGACAAAAGTTTCTCAATGATTAAG
GAGGGTGATTATAACCCCCTCTTCATTCCAGTGGCAGTCATGGTTACTGCATTCTCTGGGTTGGCATTTA
TCATTTGGCTGGCAAGGAGATTAAAAAAAGGCAAGAAATCCAAGAGAAGTATGAATGACCCATATTAA

pLenti-L-selectin ΔM-N (from figure 6.2)

GCCGCCACCATGGGCTGCAGAAGAACTAGAGAAGGACCAAGCAAAGCCATGATATTTCCATGGAAATG
TCAGAGCACCCAGAGGGACTTATGGAACATCTTCAAGTTGTGGGGGTGGACAATGCTCTGTTGTGATTT
CCTGGCACATCATGGAACCGACTGCTGGACTTACCATTATTCTGAAAAACCCATGAACTGGCAAAGGGC
TAGAAGATTCTGCCGAGACAATTACACAGATTTAGTTGCCATACAAAACAAGGCGGAAATTGAGTATCT
GGAGAAGACTCTGCCTTTCAGTCGTTCTTACTACTGGATAGGAATCCGGAAGATAGGAGGAATATGGA
CGTGGGTGGGAACCAACAAATCTCTCACTGAAGAAGCAGAGAACTGGGGAGATGGTGAGCCCAACAA
CAAGAAGAACAAGGAGGACTGCGTGGAGATCTATATCAAGAGAAACAAAGATGCAGGCAAATGGAAC
GATGACGCCTGCCACAAACTAAAGGCAGCCCTCTGTTACACAGCTTCTTGCCAGCCCTGGTCATGCAGT
GGCCATGGAGAATGTGTAGAAATCATCAATAATTACACCTGCAACTGTGATGTGGGGTACTATGGGCC
CCAGTGTCAGTTTGTGATTCAGTGTGAGCCTTTGGAGGCCCCAGAGCTGGGTACCATGGACTGTACTCA
CCCTTTGGGAAACTTCAGCTTCAGCTCACAGTGTGCCTTCAGCTGCTCTGAAGGAACAAACTTAACTGG

GATTGAAGAAACCACCTGTGGACCATTTGGAAACTGGTCATCTCCAGAACCAACCTGTCAAGTGATTCA
GTGTGAGCCTCTATCAGCACCAGATTTGGGGATCATGAACTGTAGCCATCCCCTGGCCAGCTTCAGCTT
TACCTCTGCATGTACCTTCATCTGCTCAGAAGGAACTGAGTTAATTGGGAAGAAGAAAACCATTTGTGA
ATCATCTGGAATCTGGTCAAATCCTAGTCCAATATGTCAAAAATTGGACAAAAGCTTCTCACCCCTCTTC
ATTCCAGTGGCAGTCATGGTTACTGCATTCTCTGGGTTGGCATTTATCATTTGGCTGGCAAGGAGATTA
AAAAAAGGCAAGAAATCCAAGAGAAGTATGAATGACCCATATTAA

pLenti-CD2-P2A-L-selectin wt (from figure 6.3)

GCCGCCACCATGAGATGTAAATTCCTAGGGAGTTTCTTTCTGCTCTTCAGCCTGTCCAGCAAAGGAGCA
GACTGCAGAGACAGTGGGACCGTCTGGGGTGCCCTGGGTCATGGCATCAACCTGAACATCCCTAACTT
TCAAATGACTGATGATATTGATGAGGTGCGATGGGAGAGGGGGAGCACCCTGGTTGCCGAGTTTAAA
AGGAAGATGAAGCCTTTTTTGAAATCGGGAGCATTTGAGATCTTAGCAAATGGAGACTTGAAGATAAA
GAATCTGACAAGAGATGACAGTGGCACCTATAATGTAACGGTATACAGCACAAATGGGACACGTATCC
TGAACAAGGCACTGGACTTGAGGATTCTGGAGATGGTCTCAAAGCCGATGATCTACTGGGAGTGCAGC
AACGCAACCCTGACCTGTGAGGTCTTGGAAGGAACAGATGTTGAACTAAAGCTGTACCAAGGAAAGGA
GCATCTCAGGAGCCTCCGTCAGAAGACCATGAGTTACCAGTGGACCAACCTGAGAGCACCGTTTAAGT
GCAAGGCGGTAAACAGGGTCAGCCAGGAGTCTGAGATGGAAGTTGTCAACTGTCCAGAGAAAGGTCT
GCCCCTCTATCTCATAGTGGGGGTCAGTGCAGGAGGACTCCTCTTGGTGTTCTTTGGGGCGCTGTTTAT
TTTCTGTATCTGCAAGAGGAAAAAACGGCTCGAGAGCGGCTCCGGTGCCACCAACTTCTCTCTGCTGAA
GCAGGCCGGGGATGTCGAAGAGAATCCAGGCCCCATGCATATGGGCTGCAGAAGAACTAGAGAAGG
ACCAAGCAAAGCCATGATATTTCCATGGAAATGTCAGAGCACCCAGAGGGACTTATGGAACATCTTCAA
GTTGTGGGGGTGGACAATGCTCTGTTGTGATTTCCTGGCACATCATGGAACCGACTGCTGGACTTACCA
TTATTCTGAAAAACCCATGAACTGGCAAAGGGCTAGAAGATTCTGCCGAGACAATTACACAGATTTAGT
TGCCATACAAAACAAGGCGGAAATTGAGTATCTGGAGAAGACTCTGCCTTTCAGTCGTTCTTACTACTG
GATAGGAATCCGGAAGATAGGAGGAATATGGACGTGGGTGGGAACCAACAAATCTCTCACTGAAGAA
GCAGAGAACTGGGGAGATGGTGAGCCCAACAACAAGAAGAACAAGGAGGACTGCGTGGAGATCTAT
ATCAAGAGAAACAAAGATGCAGGCAAATGGAACGATGACGCCTGCCACAAACTAAAGGCAGCCCTCT
GTTACACAGCTTCTTGCCAGCCCTGGTCATGCAGTGGCCATGGAGAATGTGTAGAAATCATCAATAATT
ACACCTGCAACTGTGATGTGGGGTACTATGGGCCCCAGTGTCAGTTTGTGATTCAGTGTGAGCCTTTGG
AGGCCCCAGAGCTGGGTACCATGGACTGTACTCACCCTTTGGGAAACTTCAGCTTCAGCTCACAGTGTG
CCTTCAGCTGCTCTGAAGGAACAAACTTAACTGGGATTGAAGAAACCACCTGTGGACCATTTGGAAACT
GGTCATCTCCAGAACCAACCTGTCAAGTGATTCAGTGTGAGCCTCTATCAGCACCAGATTTGGGGATCA
TGAACTGTAGCCATCCCCTGGCCAGCTTCAGCTTTACCTCTGCATGTACCTTCATCTGCTCAGAAGGAAC
TGAGTTAATTGGGAAGAAGAAAACCATTTGTGAATCATCTGGAATCTGGTCAAATCCTAGTCCAATATG
TCAAAAATTGGACAAAAGTTTCTCAATGATTAAGGAGGGTGATTATAACCCCCTCTTCATTCCAGTGGC
AGTCATGGTTACTGCATTCTCTGGGTTGGCATTTATCATTTGGCTGGCAAGGAGATTAAAAAAAGGCAA
GAAATCCAAGAGAAGTATGAATGACCCATATTAA

pLenti-CD2-P2A-L-selectin ΔM-N (from figure 6.3)

GCCGCCACCATGAGATGTAAATTCCTAGGGAGTTTCTTTCTGCTCTTCAGCCTGTCCAGCAAAGGAGCA
GACTGCAGAGACAGTGGGACCGTCTGGGGTGCCCTGGGTCATGGCATCAACCTGAACATCCCTAACTT
TCAAATGACTGATGATATTGATGAGGTGCGATGGGAGAGGGGGAGCACCCTGGTTGCCGAGTTTAAA
AGGAAGATGAAGCCTTTTTTGAAATCGGGAGCATTTGAGATCTTAGCAAATGGAGACTTGAAGATAAA
GAATCTGACAAGAGATGACAGTGGCACCTATAATGTAACGGTATACAGCACAAATGGGACACGTATCC
TGAACAAGGCACTGGACTTGAGGATTCTGGAGATGGTCTCAAAGCCGATGATCTACTGGGAGTGCAGC
AACGCAACCCTGACCTGTGAGGTCTTGGAAGGAACAGATGTTGAACTAAAGCTGTACCAAGGAAAGGA
GCATCTCAGGAGCCTCCGTCAGAAGACCATGAGTTACCAGTGGACCAACCTGAGAGCACCGTTTAAGT
GCAAGGCGGTAAACAGGGTCAGCCAGGAGTCTGAGATGGAAGTTGTCAACTGTCCAGAGAAAGGTCT
GCCCCTCTATCTCATAGTGGGGGTCAGTGCAGGAGGACTCCTCTTGGTGTTCTTTGGGGCGCTGTTTAT
TTTCTGTATCTGCAAGAGGAAAAAACGGCTCGAGAGCGGCTCCGGTGCCACCAACTTCTCTCTGCTGAA
GCAGGCCGGGGATGTCGAAGAGAATCCAGGCCCCATGCATATGGGCTGCAGAAGAACTAGAGAAGG
ACCAAGCAAAGCCATGATATTTCCATGGAAATGTCAGAGCACCCAGAGGGACTTATGGAACATCTTCAA
GTTGTGGGGGTGGACAATGCTCTGTTGTGATTTCCTGGCACATCATGGAACCGACTGCTGGACTTACCA
TTATTCTGAAAAACCCATGAACTGGCAAAGGGCTAGAAGATTCTGCCGAGACAATTACACAGATTTAGT
TGCCATACAAAACAAGGCGGAAATTGAGTATCTGGAGAAGACTCTGCCTTTCAGTCGTTCTTACTACTG
GATAGGAATCCGGAAGATAGGAGGAATATGGACGTGGGTGGGAACCAACAAATCTCTCACTGAAGAA
GCAGAGAACTGGGGAGATGGTGAGCCCAACAACAAGAAGAACAAGGAGGACTGCGTGGAGATCTAT
ATCAAGAGAAACAAAGATGCAGGCAAATGGAACGATGACGCCTGCCACAAACTAAAGGCAGCCCTCT
GTTACACAGCTTCTTGCCAGCCCTGGTCATGCAGTGGCCATGGAGAATGTGTAGAAATCATCAATAATT
ACACCTGCAACTGTGATGTGGGGTACTATGGGCCCCAGTGTCAGTTTGTGATTCAGTGTGAGCCTTTGG
AGGCCCCAGAGCTGGGTACCATGGACTGTACTCACCCTTTGGGAAACTTCAGCTTCAGCTCACAGTGTG
CCTTCAGCTGCTCTGAAGGAACAAACTTAACTGGGATTGAAGAAACCACCTGTGGACCATTTGGAAACT
GGTCATCTCCAGAACCAACCTGTCAAGTGATTCAGTGTGAGCCTCTATCAGCACCAGATTTGGGGATCA
TGAACTGTAGCCATCCCCTGGCCAGCTTCAGCTTTACCTCTGCATGTACCTTCATCTGCTCAGAAGGAAC
TGAGTTAATTGGGAAGAAGAAAACCATTTGTGAATCATCTGGAATCTGGTCAAATCCTAGTCCAATATG
TCAAAAATTGGACAAAAGCTTCTCACCCCTCTTCATTCCAGTGGCAGTCATGGTTACTGCATTCTCTGGG
TTGGCATTTATCATTTGGCTGGCAAGGAGATTAAAAAAAGGCAAGAAATCCAAGAGAAGTATGAATGA
CCCATATTAA

pLenti-L-selectin I-K (from figure 6.7)

GCCGCCACCATGGGCTGCAGAAGAACTAGAGAAGGACCAAGCAAAGCCATGATATTTCCATGGAAATG
TCAGAGCACCCAGAGGGACTTATGGAACATCTTCAAGTTGTGGGGGTGGACAATGCTCTGTTGTGATTT
CCTGGCACATCATGGAACCGACTGCTGGACTTACCATTATTCTGAAAAACCCATGAACTGGCAAAGGGC
TAGAAGATTCTGCCGAGACAATTACACAGATTTAGTTGCCATACAAAACAAGGCGGAAATTGAGTATCT
GGAGAAGACTCTGCCTTTCAGTCGTTCTTACTACTGGATAGGAATCCGGAAGATAGGAGGAATATGGA
CGTGGGTGGGAACCAACAAATCTCTCACTGAAGAAGCAGAGAACTGGGGAGATGGTGAGCCCAACAA
CAAGAAGAACAAGGAGGACTGCGTGGAGATCTATATCAAGAGAAACAAAGATGCAGGCAAATGGAAC
GATGACGCCTGCCACAAACTAAAGGCAGCCCTCTGTTACACAGCTTCTTGCCAGCCCTGGTCATGCAGT
GGCCATGGAGAATGTGTAGAAATCATCAATAATTACACCTGCAACTGTGATGTGGGGTACTATGGGCC

CCAGTGTCAGTTTGTGATTCAGTGTGAGCCTTTGGAGGCCCCAGAGCTGGGTACCATGGACTGTACTCA
CCCTTTGGGAAACTTCAGCTTCAGCTCACAGTGTGCCTTCAGCTGCTCTGAAGGAACAAACTTAACTGG
GATTGAAGAAACCACCTGTGGACCATTTGGAAACTGGTCATCTCCAGAACCAACCTGTCAAGTGATTCA
GTGTGAGCCTCTATCAGCACCAGATTTGGGGATCATGAACTGTAGCCATCCCCTGGCCAGCTTCAGCTT
TACCTCTGCATGTACCTTCATCTGCTCAGAAGGAACTGAGTTAATTGGGAAGAAGAAAACCATTTGTGA
ATCATCTGGAATCTGGTCAAATCCTAGTCCAATATGTCAAAAATTGGACAAAAGTTTCTCAATGATTAAG
GAGGGTGATTATAACCCCCTCTTCATTCCAGTGGCAGTCATGGTTACTGCATTCTCTGGGTTGGCATTTA
TCA**AG**TGGCTGGCAAGGAGATTAAAAAAAGGCAAGAAATCCAAGAGAAGTATGAATGACCCATATTA
A

Appendix A3: *In vitro* flow assay of gag^{+} MOLT-3 cells over TNF-α activated HUVEC cells

Please find attached a DVD with a representative movie of each MOLT-3 cell type (no, wt or ΔM-N L-selectin).